

NORTHWESTERN UNIVERSITY

New Lewis Bases for Enantioselective Catalysis

A DISSERTATION

SUBMITTED TO THE GRADUATE SCHOOL
IN PARTIAL FULFILLMENT OF THE REQUIREMENTS

for the degree

DOCTOR OF PHILOSOPHY

Field of Chemistry

By

Charles Benjamin Schwamb

EVANSTON, ILLINOIS

March 2018

© Copyright by Charles Schwamb 2017

All Rights Reserved

Abstract

New Lewis Bases for Enantioselective Catalysis

Charles Schwamb

The discovery and tailoring of new useful organic molecules for applications such as medicine and materials science is highly driven by meaningful developments in chemical methodology, and some of the most impactful advances have invoked catalysis to increase efficiency and specificity. *N*-heterocyclic carbenes (NHCs) have continuously occupied a prominent space in catalytic methodology due to their unique steric features, electronic properties, and versatility as both metal ligands and organocatalysts. This thesis describes our efforts to invoke unusual molecular topology in extending the value of this ligand class in enantioselective catalysis. The first chapter details our initial attempts to incorporate metallocenes as effective control units in NHC-mediated asymmetric catalysis. The unique product of these efforts is employed in chapter two for the asymmetric synthesis of the privileged, but challenging α -aminoboronate motif. Lastly, chapter three briefly describes our initial foray into the development of exotic NHC precursors which incorporate a metal atom at the “wingtip *N*” position.

Thesis Advisor: Professor Karl A. Scheidt

Acknowledgements

First and foremost, I'm indebted to my parents who started this little chain reaction that is myself and never stopped rooting for it. Never ever. Ma and Dad, I know you would give the world for me, and never think for a second that I don't know how insanely, impossibly fortunate I am. Through the thick and thin chronicled in pages beyond, I was empowered, heartened, and ultimately carried through by your love and support. I am here because of you, so please take a bow. My pride is yours.

My advisor, Dr. Karl Scheidt, will forever epitomize the sacrifice and drive that both sustain this extraordinarily well-equipped lab and exemplify the resolve needed to successfully take the weed-whacker to the extraneous vocabulary in anything I write. I would be unfathomably lucky if I could pull off the insane feat of emulating just a small fraction of his determination and acuity.

Dr. Regan Thomson: I have many, many things I am in your debt for, and it's impossible to fully articulate how instrumental you've been in all your various capacities in getting me through my degree. I was very lucky to have you as a resource. Thank you for your patience and support. Dr. Michael Wang: You are simultaneously the D11 bulldozer and DaVinci surgery robot of organic chemistry. You are the enviable paradox that can approach a workload with detail and care while simultaneously crushing it into oblivion. Seriously man, what do you eat, and where can I find it? (The scavenger diet isn't working for me!) I wish nothing but the best for you in Midland!

(Pretty much Dr.) Ben McDonald: Thank you for your unremitting generosity at every turn. Thanks for bringing me to Ohio and meeting your interesting, amazing family, and offering

me a place to stay when life got hectic. Thanks for giving me advice I didn't want to hear but needed to. Thanks for being the unsung hero of lab morale. Thanks for being impossibly clever. Thank you for helping me discover my strange addiction to Trident Salmon Burgers. I'm grateful that I've been your labmate throughout my tenure here and your roommate for a considerable part of it. I was going to say that my only regret was never solving that whodunit scenario in Bilbao on that groggy morning, but honestly, do we really want to know?

Dr. Kris Deibler: Kris and I weren't always on the same wavelength, but quiet people have a special connection. The rest of you loudmouths wouldn't understand. Best of luck in Seattle, Kris! Dr. Eric Lee: I wish I got to know you a bit better. Hope you're in your element in Boston. Dr. Todd Hovey: One of the most comforting things is knowing that somewhere out there, at least one person is truly where they belong. I feel the logic of synthetic chemistry can very much be perceived as a language, both visual and verbal, and you were the best example of what true, natural fluency looks like. I think I speak for everyone when I say that I'm stoked about where you ended up, and I hope you make a lot of waves. Dr. Bi-Shun Zeng: I know we never chatted much, maybe because I'm a bit of a dork and you were probably harnessing every little fiber of patience you could to restrain yourself from breaking my hands so I couldn't fidget anymore. I am so sorry. Four years is a long, long time.

Dr. Chris Check: You were my sherpa for organometallic chemistry, and man did I need you because I had no idea what I was doing and would have definitely croaked on that mountain. Hope we can laugh about all the stupid crap I did over a few beers in the future. Dr. Paul Siu: Thank you for steering me straight, making me discover a cool coordination polymer, and being unfailingly calm and rational. See you on Ingress? Dr. Anna Lee: I really need to take you up on

that offer and pay you a visit, Professor. Maybe the best way to do that would be to actually send you a message rather than talking about it here. So yeah. I'll get on that. Dr. Matthew O'Connor: You were the veteran, grizzled, wise postdoc on a mission who could have easily been way too busy to listen to my nonsense, but you always made the time to lend an ear. Notwithstanding all that, you still laughed at my jokes, so automatic awesome points for you. Or at least you tried to. Just do me a favor and don't tell me which it was.

Mark Maskeri: I've been vicariously experiencing delusions of grandeur on your behalf where I revolutionize computerized structure drawing and eat ChemDraw's lunch. Use your powers, Mark. And never stop yankin' those chains, buddy. :D Alison Bailly: One day I hope I'll be able to harness the huge amounts of energy that do in the course of taking life on. I'll be rooting for you. Best of luck. Eric Miller: Poor, poor Eric. You've had both the misfortunes of discovering how much I talk to myself in the office and having the habit rub off on you. Good news is you'll soon have the seniority to rudely encroach on someone else's desk space. Enjoy that power carefully, grasshopper.

Rick Betori: The most remarkable thing that your scientific productivity has been so impressively large, it rightfully overshadows your productivity in ~~breaking~~ stress testing equipment. Who could really say this isn't a net-successful approach? If it ain't broke, don't fix it. David Barsoum: Emeritus GC acolyte, photochemistranaut, Se master, cool dude, much missed lab member. Jake Collins: Man, you're sneaky. If you ever end up reading this thing, don't feel afraid to drop a line and say hi. Or bye, even. ;/

Dalton Kim: If you keep on making Alison laugh like that no one will pay attention when she's walked into a cloud of HCl and is gasping for air. Please be careful; we like Alison.

Keegan Fitzpatrick: It's a privilege to have an experienced student inheriting your work. It's my sincerest hope you find success with it and make my accomplishments look meager in comparison. Dr. Brice Uno: Eyyy buddy. Wish we overlapped at Grinnell. Those would have been good times. Never stop drawing, okay? Former lab members Chris Price, Rachel Dicken, and Louis Redfern: we were all sad to see you go and happier to see you find a place where you thrived. Enjoy your new gigs!

Dr. Susana Lopez: Thanks for your generosity and constant willingness to help me out when I was pulling my hair out. Also, you are a GOD for taking over inventory as smoothly as you did. Dr. Katie Murauski: You may not have laughed at my jokes like Matthew, but maybe at my dumb quirks. I'll still interpret that as a success. Best of luck at AbbVie! Drs. Javi Izquierdo, Atul Jain, Rama Mishra, and Master Purav Vagadia: I'll miss all of you. If you'll miss me more than you'll miss McDonald, you don't have to tell me. I know. ;] Drs. Ash Younai, Eddie Hall, Lizzie McCusker, Dmitrijs Cernaks, Robert Chapman, Kun Liu, Gerri Hutson, Neha Malik, Vince Lombardo, Kipo Jang, Ansoo Lee, Adam Csakai and Yubai Zhou: Without exception, *every* postdoc in this lab was willing to go out of their way to help a feckless grad student out no matter how much it put them behind for the day. The amounts of self-sacrifice, humility, and generosity that I've had the privilege of seeing come to Evanston from all corners of the world is nothing short of astounding.

Dr. Daniel Cohen: We only overlapped for a few months, but your positivity and constant reassurance really gave me a boost. I'm happy I got to know you early on. Colin Sugalski: Best friend of fifteen years, fellow workaholic, restaurant savant. You embody so many qualities I aspire to, and I hope I can reciprocate on your merciless kindness in the years to come. Thank

you for letting me live in your hotel for a month. Also, thank you for reading this. (Why are you reading this?) Miss you, man. Brandon Rugg: We must stay in touch. We must. Thank you for being the most entertaining roommate in existence and not letting me be a stick in the mud. You are insanely perceptive and clever, and humble to a fault. I've learned quite a bit from you, and I hope others realize how much you bring to the table. Ashley Jaworski: Chatting with you has always been a super grounding, reassuring thing and I'll miss having someone with their head so securely fixed on their shoulders to confide in, as well as someone to tactfully tell me I'm being a bonehead. Please send me pictures of your dog often.

To my network of friends who are somehow always happy to see me after long stretches of me disappearing off the face of the planet, I love you all. Jon Lee, I hope I'll be seeing you around. Thanks for helping me meet so many great folks.

Lastly, I'd like to thank my extended family for spoiling me rotten with oversized doses of support and good vibes.

List of Abbreviations

| | |
|----------------|---|
| 4 Å MS | 4 angstrom molecular sieves |
| AcOH | Acetic acid |
| Ar | aryl |
| Ac | acetyl |
| Bp | boiling point |
| BINAP | 2,2'-bis(diphenylphosphino)-1,1'-binaphthyl |
| BINOL | 1,1'-bi(2-naphthol) |
| Boc | <i>tert</i> -butyloxycarbonyl |
| Bu | butyl |
| <i>n</i> -BuLi | <i>n</i> -butyl lithium |
| Bz | benzoyl |
| δ | chemical shift (parts per million) |
| COSY | correlation spectroscopy |
| dba | dibenzylidene acetone |
| DBN | 1,5-diazabicyclo[4.3.0]non-5-ene |
| DBU | 1,8-diazabicyclo[5.4.0]undec-7-ene |
| DCE | 1,2-dichloroethane |
| DEAD | diethylazodicarboxylate |
| DFT | density functional theory |
| DIBAL | diisobutyl aluminum hydride |
| DIPEA | diisopropylethylamine |

| | |
|----------|---|
| DKR | dynamic kinetic resolution |
| DMSO | dimethylsulfoxide |
| dr | diastereomeric ratio |
| ee | enantiomeric excess |
| er | enantiomeric ratio |
| eq | equation |
| equiv | equivalents |
| er | enantiomeric ratio |
| EI | electron impact |
| ESI | electrospray ionization mass spectrometry |
| EtOAc | ethyl acetate |
| GC | gas chromatography |
| HBD | hydrogen bond donor |
| HOMO | highest occupied molecular orbital |
| HPLC | high-performance liquid chromatography |
| HRMS | high-resolution mass spectrometry |
| IMES | 2,4,6-trimethylphenylimidazole |
| IPA | isopropanol |
| IR | infrared |
| <i>J</i> | coupling constant |
| KHMDS | potassium hexamethyldisilazane |
| KOtBu | potassium <i>tert</i> -butoxide |

| | |
|-------------------|--|
| LA | Lewis acid |
| LDA | Lithium diisopropylamide |
| LRMS | low-resolution mass spectroscopy |
| LUMO | lowest unoccupied molecular orbital |
| MALDI-TOF | matrix-assisted laser desorption ionization time-of-flight |
| Me | methyl |
| MeOH | methanol |
| Mes | 2,4,6-trimethylphenyl |
| mg | milligram |
| Mp | melting point |
| Ms | mesylate |
| NHC | <i>N</i> -heterocyclic carbene |
| NMR | nuclear magnetic resonance |
| NOE | nuclear Overhauser effect |
| NR | no reaction |
| ORTEP | Oak Ridge thermal ellipsoid plot |
| Ph | phenyl |
| PhCH ₃ | toluene |
| PCC | pyridinium chlorochromate |
| PPTS | pyridinium <i>p</i> -toluenesulfonate |
| R _f | response factor |
| Rt | room temperature |

| | |
|--------------------|---|
| <i>s</i> factor | selectivity factor |
| TBS | <i>tert</i> -butyldimethylsilyl |
| TBDPS | <i>tert</i> -butyldiphenylsilyl |
| TES | triethylsilyl |
| TEP | Tolman electronic parameter |
| THF | tetrahydrofuran |
| TLC | thin layer chromatography |
| TMS | trimethylsilyl |
| Ts | <i>p</i> -toluene sulfonyl |
| <i>p</i> -TsOH | <i>para</i> -toluenesulfonic acid |
| TsNBr ₂ | <i>N,N</i> -dibromo- <i>p</i> -toluenesulfonamide |
| UV | ultraviolet |
| %V _{bur} | Percent buried volume |

Dedication

To my parents

Table of Contents

| | |
|---|----|
| Abstract | 3 |
| Acknowledgements..... | 4 |
| List of Abbreviations | 9 |
| List of Figures | 17 |
| List of Schemes..... | 19 |
| List of Tables | 20 |
| Chapter 1: Development of Planar Chiral Imidazopyridinium Salts for Asymmetric Catalysis.. | 22 |
| 1.1 Introduction to N-Heterocyclic Carbenes | 23 |
| 1.1.1 Axial chirality and its implementation in metallocenes..... | 23 |
| 1.1.2 Historical use of metallocenes in phosphines and NHCs | 25 |
| 1.2 Early attempts at ligand design..... | 27 |
| 1.2.1 Alternate strategy towards a 6,5,6,5 system | 28 |
| 1.3 Building upon the Fu DMAP metallocene | 29 |
| 1.3.1 Development of a diastereomeric resolution | 30 |
| 1.3.2 Multicomponent synthesis of the azolium motif | 33 |
| 1.3.3 Efforts towards (bis)NHC multidentate systems | 36 |
| 1.3.4 An analogous Co(I) sandwich complex..... | 37 |
| 1.3.5 Generation of d-block complexes | 38 |
| 1.4 Spectroscopic and X-ray Diffraction Analysis of Structural and Electronic Properties..... | 40 |
| 1.4.1 Comparison of ⁷⁷ Se NMR and TEP-derived parameters | 41 |
| 1.4.2 Structural characterization via X-ray diffraction | 45 |

| | |
|--|-----|
| | 15 |
| 1.4.3 Analysis of steric parameters via buried volume calculations | 48 |
| 1.5 Applications in Transition-Metal and Lewis Base Catalysis | 52 |
| 1.5.1 Use with metals possessing nonlinear coordination geometries | 53 |
| 1.5.2 Use as Lewis-basic organocatalysts | 54 |
| 1.6 Conclusion | 56 |
| 1.7 Experimental Section | 57 |
| 1.7.1 Experimental Procedures For Synthesis of Enantiopure Imizadopyridinium Salts | 58 |
| 1.7.2 Synthesis of copper(I) chloride complexes | 80 |
| 1.7.3 Synthesis of Rhodium Carbonyl Complexes | 83 |
| 1.7.4 Calculation of Tolman Electronic Parameter | 87 |
| 1.7.5 General Synthesis of Selenourea Compounds | 88 |
| 1.7.6 Selected NMR Spectra | 91 |
| 1.7.7 X-Ray Crystal Structure Data | 124 |
| 1.7.8 Extended Details for Buried Volume Calculations | 147 |
| Chapter 2: Enantioselective Synthesis of α -amidoboronates Mediated by Planar-Chiral NHC- | |
| Cu(I) Complexes | 152 |
| 2.1 Introduction | 153 |
| 2.1.1 α -aminoboronic acids in medicinal chemistry | 154 |
| 2.1.2 Synthetic challenges | 155 |
| 2.1.3 Matteson homologation | 156 |
| 2.1.4 Substrate-directed stereoselective synthesis | 157 |
| 2.1.5 Catalytic enantioselective methods | 158 |

| | |
|--|-----|
| | 16 |
| 2.1.6 Aliphatic α -aminoboronates..... | 160 |
| 2.2 Catalytic borylation of aldimines with planar chiral NHC-Cu(I) complexes..... | 161 |
| 2.2.1 In-situ generation of aldimines from inert α -tosyl precursors | 162 |
| 2.2.2 Optimization of enantioselectivity | 163 |
| 2.2.3 Isolation via precipitation of BF ₃ K salts | 166 |
| 2.3 Intramolecular Suzuki coupling of α -benzamidoboronates..... | 167 |
| 2.3.1 NHC-Cu(I)-mediated tandem borylation-Suzuki coupling | 168 |
| 2.4 Determination of absolute stereochemistry | 170 |
| 2.5 Mechanism and proposed DFT computational studies..... | 171 |
| 2.5.1 Proposed stereoinduction model | 172 |
| 2.6 Conclusion | 174 |
| 2.7 Experimental Section..... | 175 |
| 2.7.1 General Procedure for the Synthesis of α -tosyl Benzamides..... | 177 |
| 2.7.2 Synthesis of Catalyst (–)-G | 186 |
| 2.7.3 General Procedure for the Enantioselective Synthesis of α -amidoboronates | 187 |
| 2.7.4 Selected NMR Spectra..... | 198 |
| 2.7.5 HPLC and SFC Traces of Racemic and Enantioenriched Compounds | 220 |
| 2.7.6 X-Ray Structure Data..... | 229 |
| Chapter 3: Modular Synthesis of Amido Azoles | 233 |
| 3.1 Introduction..... | 234 |
| 3.2 Metal-amido azoles and N-heterocyclic carbenes | 234 |
| 3.3 Square planar complexes of Cu(II) and Co(II) | 236 |

| | |
|---|-----|
| | 17 |
| 3.4 Zn(II) coordination polymers..... | 237 |
| 3.5 Cu-Cu bimetallic coordination polymer | 238 |
| 3.6 η_2 -bound Cu(I) imidazolylidene complex | 241 |
| 3.7 Conclusion | 243 |
| 3.8 Experimental Section..... | 244 |
| 3.8.1 Experimental Procedures | 245 |
| 3.8.2 Selected NMR Spectra..... | 254 |
| 3.8.3 X-ray Crystal Structure Data | 258 |
| References:..... | 263 |

List of Figures

| | |
|---|----|
| Figure 1-1. General NHC anatomy and imidazol-2-ylidene applications..... | 24 |
| Figure 1-2. Selected examples of higher-order chirality in NHC design..... | 25 |
| Figure 1-3. Metallocene asymmetry and its translation to NHC-containing compounds..... | 25 |
| Figure 1-4. Selected examples of chiral ferrocenyl NHCs, pyridines, and phosphines..... | 26 |
| Figure 1-5. General synthetic strategy for imidazopyridinium synthesis..... | 30 |
| Figure 1-6. Compatible and incompatible amines and anilines for azolium synthesis..... | 34 |
| Figure 1-7. Rh(I) dimer I-69 . Thermal ellipsoids are shown at 50% probability. | 39 |
| Figure 1-8. X-ray structures of selected Rh(I) carbonyl and selenium complexes..... | 40 |
| Figure 1-9. TEP and ^{77}Se NMR spectroscopic approaches towards characterization of ligand electronics. | 41 |
| Figure 1-10. Plot of ^{77}Se chemical shift vs. TEP for compounds a-d and several other NHCs... | 43 |

| | |
|--|-----|
| | 18 |
| Figure 1-11. Larger scale plot of ⁷⁷ Se chemical shift vs. TEP data. | 44 |
| Figure 1-12. X-ray structures of analogous metallocene complexes I-48 (left) and I-55 (right). | 47 |
| Figure 1-13. Selected geometric parameters of complexes I-48 and I-55 | 48 |
| Figure 1-14. Application of buried volume concept to NHC ligands. | 49 |
| Figure 1-15. Steric contour maps of ligands analyzed in buried volume calculations. | 51 |
| Figure 2-1. PheProArg and associated peptidomimetics. | 153 |
| Figure 2-2. Approved drugs containing the α -aminoboronate motif. | 154 |
| Figure 2-3. Inhibitory mechanism of the α -aminoboronate motif against serine proteases. | 155 |
| Figure 2-4. Synthesis and application of α -aminoboronates. | 155 |
| Figure 2-5. Postulated mode of α -aminoboronate decomposition. | 156 |
| Figure 2-6. Chiral ligands employed in α -aminoboronate synthesis. | 159 |
| Figure 2-7. Our approach towards alkyl α -aminoboronate synthesis. | 161 |
| Figure 2-8. Crystal structure of compound II-33 | 171 |
| Figure 2-9. Proposed major and minor pathways. | 173 |
| Figure 3-1. Arduengo carbene wingtip substituents. | 234 |
| Figure 3-2. General approach towards modular ligand diversification. | 235 |
| Figure 3-3. X-ray structures of compounds III-7 (left) and III-8 (right). | 237 |
| Figure 3-4. X-ray structure of coordination polymer of tetrahedral Zn(II) (III-9). | 238 |
| Figure 3-5. X-ray structure of coordination polymer of pentacoordinate Zn(II) (III-10). | 238 |
| Figure 3-6. Coordination polymer III-11 | 240 |
| Figure 3-7. Coordination polymer III-11 , rotated 90° about long axis relative to figure 3-5. | 240 |
| Figure 3-8. X-ray structure of compound III-12 | 242 |

List of Schemes

| | |
|--|----|
| Scheme 1-1. Attempted synthesis of a 6, 5, 5, 5 system | 28 |
| Scheme 1-2. Attempted synthesis of a 6, 5, 6, 5 system | 29 |
| Scheme 1-3. Screen of chiral auxiliaries for diastereomeric resolution | 31 |
| Scheme 1-4. Original strategy for pseudoephedrine amide synthesis | 31 |
| Scheme 1-5. Direct amidation of the Fu ferrocene | 32 |
| Scheme 1-6. Synthesis of enantiopure azolium salts from pseudoephedrine amides | 33 |
| Scheme 1-7. Overall strategy for the synthesis of enantiopure azolium salts | 34 |
| Scheme 1-8. Attempted synthesis of a bidentate ligand | 35 |
| Scheme 1-9. Reductive amination approach towards bidentate system | 36 |
| Scheme 1-10. Approaches towards bis(ferrocenyl) system via anhydrous formaldehyde sources | 36 |
| Scheme 1-11. Attempted synthesis of an analogous Co(I) metallocene | 37 |
| Scheme 1-12. Preparation of Cu(I)Cl complexes | 38 |
| Scheme 1-13. Preparation of Rh(COD)Cl and Rh(CO) ₂ Cl complexes | 39 |
| Scheme 1-14. Preparation of selenoureas for NMR spectroscopic analysis of ligand electronic properties | 39 |
| Scheme 1-15. Cu(I)-mediated borylations and Ni(0) reductive couplings surveyed in this study | 52 |
| Scheme 1-16. Performance of catalysts with nonlinear metals | 53 |
| Scheme 1-17. Top: NHC-catalyzed homoenolate additions to ketoesters (eq. 1) and trifluoroacetophenone (eq 2). Bottom: Stereochemical model for reactions (1) and (2) | 55 |

| | |
|---|-----|
| Scheme 2-1. Matteson method of enantiopure α -aminoboronate synthesis..... | 156 |
| Scheme 2-2. Diastereoselective methods of α -aminoboronate synthesis..... | 157 |
| Scheme 2-3. Catalytic enantioselective strategies for α -aminoboronate synthesis..... | 158 |
| Scheme 2-4. Approaches not utilizing Cu(I) or hydroboration of a C=N bond..... | 160 |
| Scheme 2-5. Product isolation via precipitation as BF_3K salt..... | 166 |
| Scheme 2-6. Inter- and intramolecular Cu(I) catalyzed Suzuki reactions disclosed by Dumas. | 168 |
| Scheme 2-7. Postulated catalytic cycle | 172 |
| Scheme 3-1. Azole ligand synthesis..... | 236 |
| Scheme 3-2. Synthesis of Cu(II) and Co(II) triazolylcarboxylate complexes..... | 236 |
| Scheme 3-3. Synthesis of dinuclear Cu(I) complex III-12 | 241 |

List of Tables

| | |
|--|-----|
| Table 1-1. Screen of reductants for the direct conversion of the pseudoephedrine amides to aldehyde I-14 | 33 |
| Table 1-2. NMR spectroscopic and geometrical data of Se and $\text{Rh}(\text{CO})_2\text{Cl}$ complexes of a-d and selected examples from the literature. | 45 |
| Table 1-3. Selected measurements of heterobimetallic compounds analyzed via XRD..... | 47 |
| Table 1-4. $\%V_{\text{Bur}}$ calculated for selected planar Cu(I)Cl complexes and compounds from literature..... | 50 |
| Table 2-1. Initial optimization of yield..... | 162 |
| Table 2-2. Optimization of enantioselectivity..... | 164 |
| Table 2-3. Substrate scope..... | 165 |

| | |
|---|-----|
| Table 2–4. Products isolated via precipitation. | 167 |
| Table 2–5. Control studies on One-pot Borylation-Suzuki coupling sequence | 169 |
| Table 2–6. Direct Suzuki coupling of the isolated enantioenriched boronate. | 170 |

Chapter 1: Development of Planar Chiral Imidazopyridinium Salts for Asymmetric Catalysis

Portions of this chapter appear in the following publication: Check, C. T.; Jang, K. P.; Schwamb, C. B.; Wong, A. S.; Wang, M. H.; Scheidt, K. A. “Ferrocene-Based Planar Chiral Imidazopyridinium Salts for Catalysis,” *Angew. Chem. Int. Ed.* **2015**, *54*, 4264–4268.

1.1 Introduction to N-Heterocyclic Carbenes

The efficient synthesis of enantiopure substances is a crucial enterprise for the production of pharmaceuticals, agrochemicals and other fine chemicals. The continued expansion of the asymmetric chemical space available to chemists relies upon the construction of new catalysts. As a foundation for this goal, established achiral catalyst motifs can serve as highly effective templates for new chiral scaffolds, provided that their integration in a chiral framework does not detract from their desired reactivity, stability, and synthetic accessibility. One such achiral archetype, the N,N'-diaryl imidazol-2-ylidene (IMes-type) motif, constitutes a widely used class of N-heterocyclic carbenes (NHCs) that have been extensively applied as robust, highly σ -donating ligands for metal catalysis.¹⁻⁵ Unlike their saturated imidazoline congeners, IMes-type have also been employed as Lewis bases for organocatalytic transformations (**Figure 1-1**).^{6-10,11-20} Given this versatility as ligands or standalone catalysts, successful implementations of this archetype within a chiral framework could be highly impactful in diverse areas of chemical methodology. However, the planar aromatic structure inherent to this class severely limits how central chirality derived from sp_3 -hybridized carbon can be emplaced. Consequently, examples of *chiral* carbenes which retain this defining aromatic framework remain comparatively scarce.

1.1.1 Axial chirality and its implementation in metallocenes

One valid approach towards attaining chirality without sp_3 carbon can use the hindered relative orientations of two or more functional groups such as aromatic rings and polycyclic structures to impart chirality in the overall structure. Given that this higher-order mode of asymmetry can be propagated by purely aromatic functionality and is defined by a chiral *axis* rather than center, this can eliminate the need for sp_3 carbon as a stereogenic source. Early

examples of NHCs with “axial chirality” include Rajanbabu’s bisamidazolium and Hoyveda’s olefin metathesis catalyst, where the well-known atropisomeric 1,1'-binaphthyl moiety was used in both cases as a bridging structure in a multidentate ligand (**Figure 1-2**).²¹

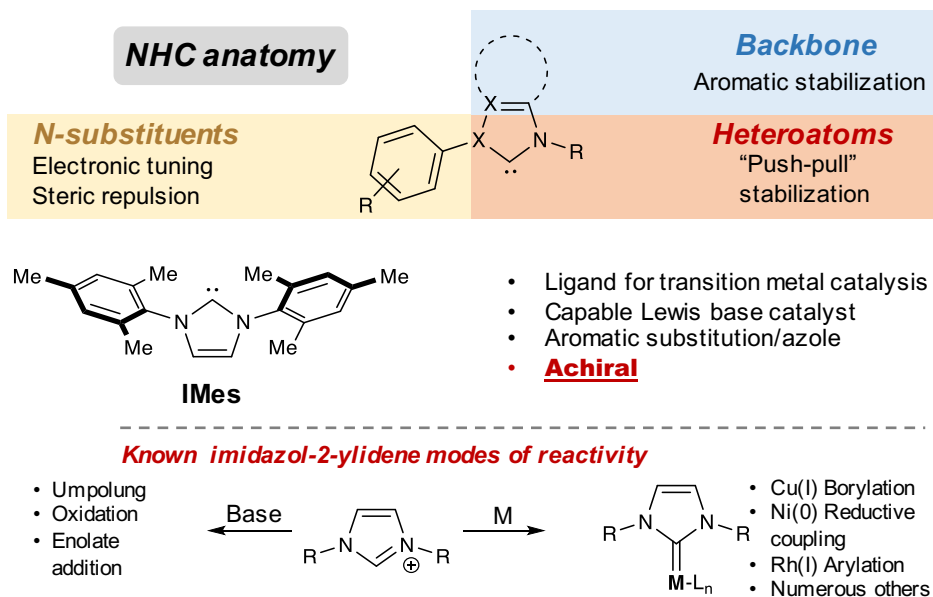


Figure 1-1. General NHC anatomy and imidazol-2-ylidene applications.

A special case of axial chirality, termed planar chirality, can be propagated by two dissymmetric rings fixed in a non-coplanar, but nominally parallel orientation.²²⁻²⁹ Most examples of planar chiral structures employed in asymmetric catalysis are templated on the classical metallocene motif,^{30-34,35-46} which consists of a metal center in complexation with two η^5 -cyclopentadienyl (Cp) rings (**Figure 1-3**). In this case, chirality is generated by coordination of a metal center to at least one Cp ring that (i) cannot be bisected by an orthogonal mirror plane and (ii) is either not identical to its counterpart ring, or is identical but coordinated to the metal via the opposite prochiral face. It should be emphasized that planar chirality does not emerge from hindered *rotation* about a hypothetical axis proceeding through the centroids of both Cp

rings. Thus, any mode of racemization would necessarily involve the migration of a coordinate metal and ring to the opposite face of their dissymmetric counterpart cyclopentadiene.

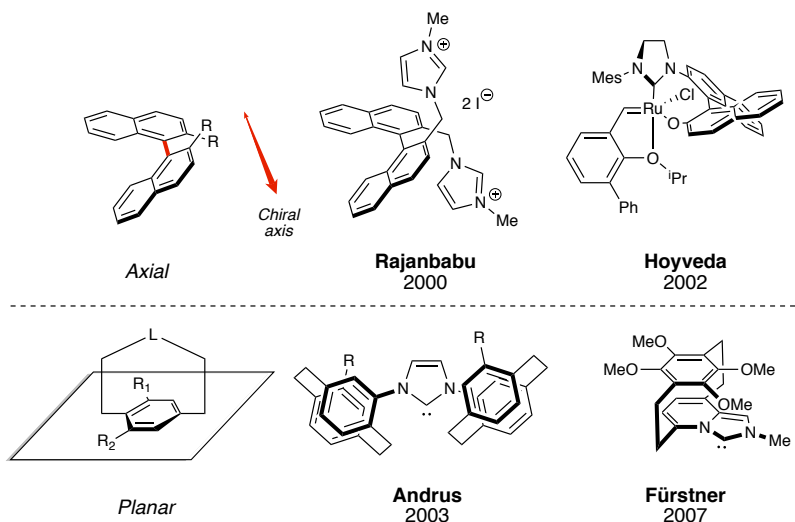


Figure 1-2. Selected examples of higher-order chirality in NHC design

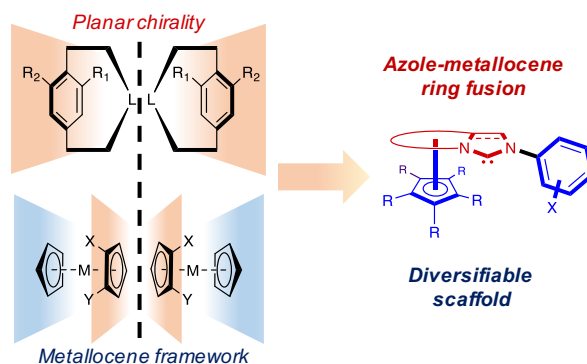


Figure 1-3. Metallocene asymmetry and its translation to NHC-containing compounds

1.1.2 Historical use of metallocenes in phosphines and NHCs

The ten functionalizable sites in the basic ferrocene template allows for great flexibility in crafting metallocenes purposed towards materials design and catalysis.⁴⁷⁻⁵¹ Our particular interest in this motif was initiated by the hypothesis that the considerable size and stability of

ferrocene could be better leveraged as a chiral control element in NHC catalysis through *fusion* of a cyclopentadienyl ring with an imidazole core, as opposed to the numerous designs which feature stereogenic ferrocene as a pendant, rotatable motif relative to the carbene ring.^{1,31,52-58} While contributions to the growing pool of planar chiral ferrocene-derived phosphines are numerous, there is a comparative paucity of N-heterocyclic carbenes which incorporate this motif for stereocontrol. For example, while the Josiphos class of diphosphines⁵⁹⁻⁶¹ has been referenced in over 3500 publications⁶² since its introduction in 1994 by Tongi,⁶³ it was only until 2002 that a chiral NHC-ferrocene hybrid was known to the community with Bolm's disclosure of a silyl imidazolylidene in 2002 (**Figure 1-4**).⁶⁴ This report was shortly followed by publications of similar ligands which were successfully employed in asymmetric catalysis, such as Tongi's bisferrocenyl NHC.⁶⁵ Nevertheless, amongst these few examples, there remains a near-absence of those which do not feature free rotation of the ferrocenyl motif relative to the plane of the NHC.

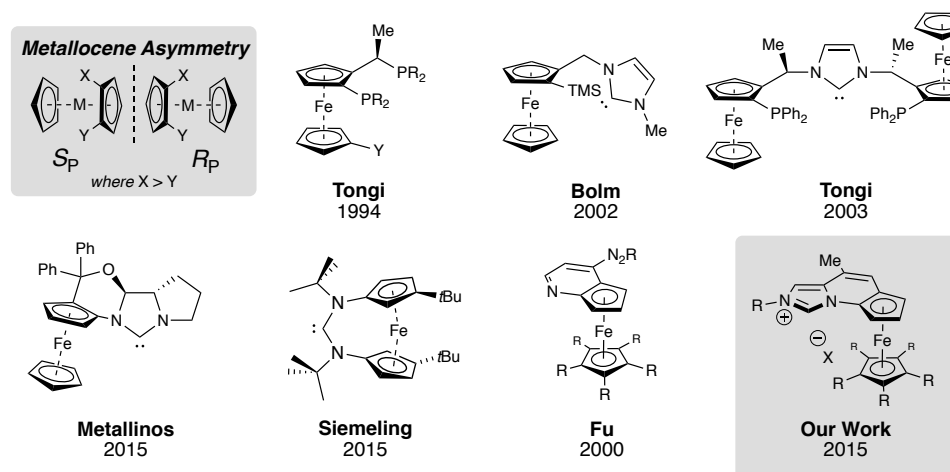


Figure 1-4. Selected examples of chiral ferrocenyl NHCs, pyridines, and phosphines.

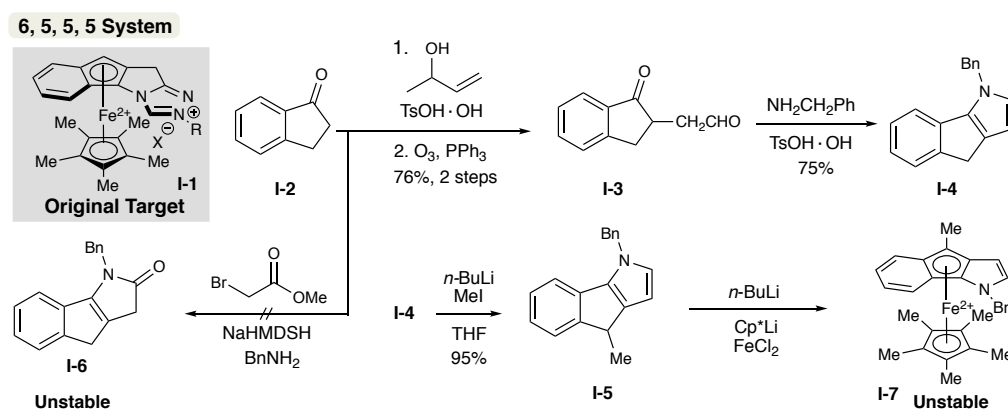
With the aim to enrich the pool of chiral IMes-like carbenes through a metallocene based design, we have designed a class of chiral ferrocenyl IMes-type NHCs which were demonstrated to be highly selective in several Cu(I), Ni(0), and free-carbene catalyzed processes.⁶⁶ This chapter will detail (i) our initial efforts towards construction of a planar chiral azolium salt and the ensuing evolution of our preliminary designs, (ii) an expanded account on the development of a practical synthesis for our new compounds, (iii) efforts towards further diversification of this scaffold and the resulting performance in selected reactions, and (iv) a more robust characterization of NHC electronics through NMR spectroscopic studies of ⁷⁷Se complexes.

1.2 Early attempts at ligand design

Our initial efforts towards achieving a viable synthesis of a conformationally rigid planar chiral ligand were undertaken by postdoctoral researcher Dr. Kipo Jang, who first pursued the construction of a vaulted 6, 5, 5, 5 scaffold, whereby the crucial cyclopentadienyl motif would be positioned within the center of the polycycle (**Scheme 1-1**). It was thought that construction of **I-1** would ultimately allow for the synthesis of the corresponding triazolium through established methods for 1,2,4-triazole synthesis.⁶⁷⁻⁶⁹ However, multiple attempts to synthesize intermediate **I-6** failed, which led us to suspect that the high degree of ring strain engendered in the lactam rendered the compound prone to decomposition. To circumvent this issue, pyrrole **I-4** was targeted as the immediate precursor to its corresponding ferrocene complex. While the pyrrole (**I-4**) was highly sensitive towards oxidation at the benzylic carbon, we found that protection of this position with methyl iodide sufficiently resolved this problem (**I-5**). Subsequent addition of the lithiates of the cyclopentadiene and **I-5** to a suspension of FeCl₂ produced product **I-7** which

could be observed by LCMS-ESI+, however, the resulting ferrocene was found to completely decompose in air and on silica.

Scheme 1-1. Attempted synthesis of a 6, 5, 5, 5 system

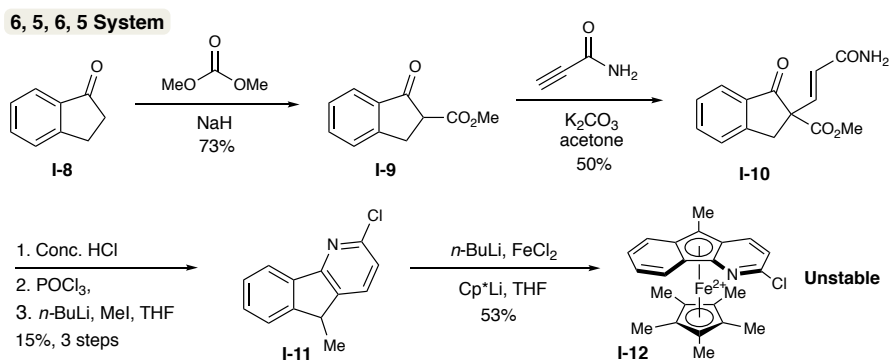


1.2.1 Alternate strategy towards a 6,5,6,5 system

We reasoned that revision of the ferrocene precursor to a 6, 5, 6 polycycle from a 6, 5, 5, system would more closely resemble known, robust scaffolds.⁷⁰⁻⁷⁴ The pyrindenyl motif of the ferrocenyl DMAP-analogues first developed by Fu were identified as ideal templates of precursors for synthesis of an imidazolium salt due to their well-precedented stability.⁷⁰⁻⁷² While we originally attempted to preserve the vaulted character of the polycyclic azolium through inclusion of an additional phenyl ring to produce the 6, 5, 6 derived ferrocene (**I-12**, **Scheme 1-2**), the resulting complex underwent an incomplete, but still significant degree of decomposition during purification. The predisposition of metallocene complexes containing indenyl and fluorenyl systems to readily undergo haptotropic rearrangements via a $\eta^5 \rightarrow \eta^6$ process (formally termed the indenyl effect) and their susceptibility to protonation is well documented, and we attribute the observed instability of our compounds to this known trend.⁷⁵⁻⁸⁰ Given that this degree of sensitivity would certainly render any subsequent functionalization of the compound

infeasible, the simplified pyridenyl 6, 5 motif (**I-15**, **Figure 1-5**) was chosen for further elaboration to the imidazolium salt.

Scheme 1-2. Attempted synthesis of a 6, 5, 6, 5 system



1.3 Building upon the *Fu* DMAP metallocene

Having identified an appropriate ferrocenyl scaffold, the multicomponent annulation disclosed by Hutt and Aron in 2011 was identified as a means for an expedient synthesis of a family of imidazopyridinium-based NHC salts provided that **I-13** (**Figure 1-5**) could be elaborated to the corresponding aldehyde (**I-14**).⁸¹ Given the abundance of methodology pertaining to the metal-catalyzed carbonylation of aromatic systems, we reasoned that this crucial aldehyde could be delivered by the reduction of the carbonylation product of **I-13**.⁸²⁻⁸³ We found that a palladium-mediated conversion of **I-13** to **I-20** proceeded in good yield under one atmosphere of CO gas, and subsequent reduction to the aldehyde **I-14** with DIBAL-H proceeded smoothly without significant overreduction (**Scheme 1-4**).

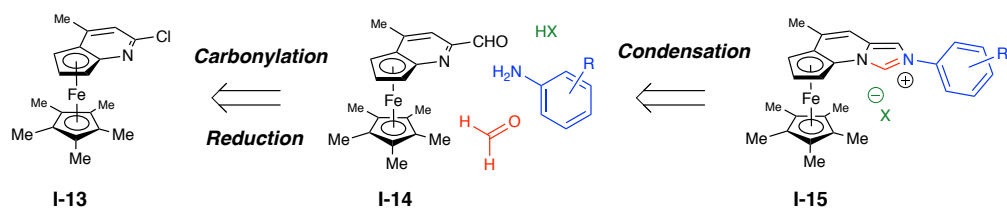
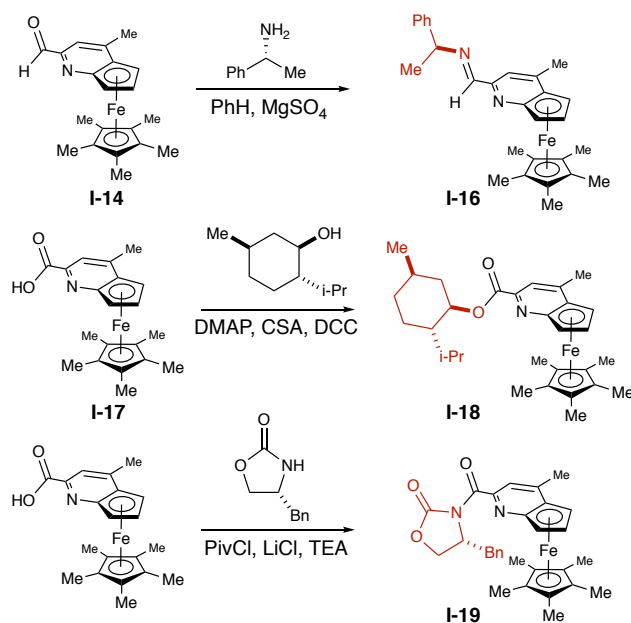


Figure 1-5. General synthetic strategy for imidazopyridinium synthesis.

1.3.1 Development of a diastereomeric resolution

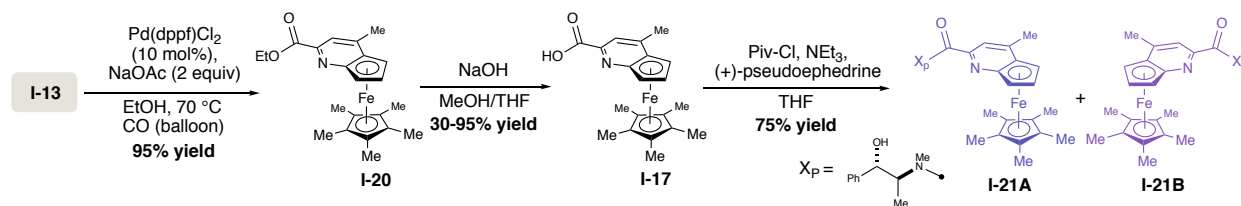
As our initial method of obtaining enantiopure aldehyde **I-14** relied upon chiral preparative HPLC, development of an approach which could obviate this dependence on time and resource-intensive instrumentation was viewed as necessary for an accessible catalyst synthesis. Given the synthetic versatility of the aldehyde and ester functional groups and their facile derivatization with common chiral auxiliaries, we sought a strategy which could enable a practical, gram-scale diastereomeric resolution using only flash column chromatography (**Scheme 1-3**). While the syntheses of menthol ester **I-18** could be attained through standard transesterification conditions, no useful degree of diastereomeric separation could be attained on flash column silica. A similar outcome was observed for aldimine **I-16**, although this adduct was additionally plagued by its susceptibility to hydrolysis on SiO₂. While oxazolidinone **I-19** provided for a detectable, but nevertheless partial degree of separation on TLC,⁸⁴⁻⁸⁵ poor yields observed in its construction rendered this adduct unsuitable for a practical catalyst synthesis. In light of the insufficient degrees of separation observed with **I-16**, **I-18**, and **I-19**, it was thought that pseudoephedrine amides **I-21A** and **I-21B** (**Scheme 1-4**) would provide improved resolution due to its heightened degree of polarity.⁸⁶ To our elation, complete separation was observed ($\Delta r_f = 0.1$) with a standard ethyl acetate/hexanes binary mobile phase.

Scheme 1-3. Screen of chiral auxiliaries for diastereomeric resolution



1.3.1.1 Improving amide synthesis and reduction to enantiopure aldehyde

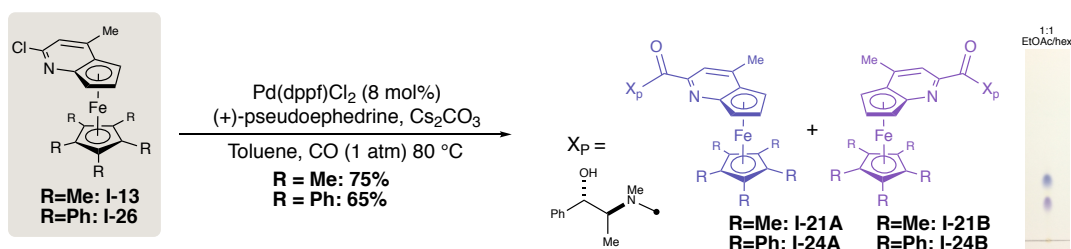
Scheme 1-4. Original strategy for pseudoephedrine amide synthesis.



The synthesis of the amide initially proved problematic due to the low yields associated with the conversion of ester **I-20** to the unstable acid **I-17** (Scheme 1-4), which we reasoned would undergo amide coupling via the procedure described by Myers et al (Route 1).⁸⁶ Disappointingly, efforts to bypass the acid and directly convert ester **I-20** to the corresponding amide delivered lower yields than what was provided by the aforementioned two-step sequence. Gratifyingly, much like the synthesis of the racemic ester (**I-17**), it was found that the palladium

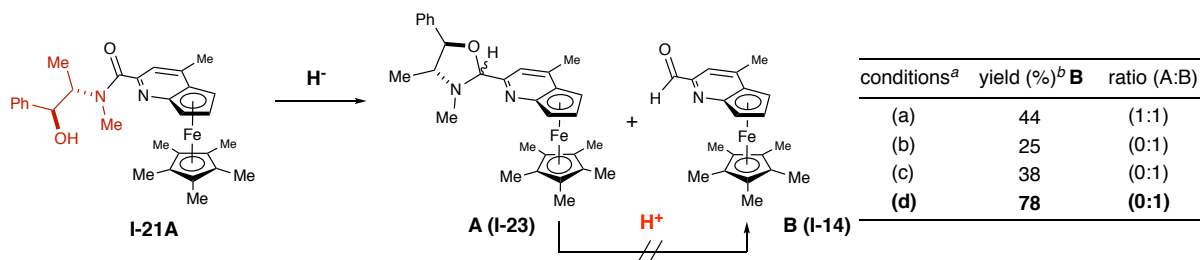
catalyzed amidation of chloride **I-13** could provide the amide in excellent yield, thus circumventing the intermediacy of both ester and acid (**Scheme 1-5**).

Scheme 1-5. Direct amidation of the Fu ferrocene.



With a viable resolution strategy in hand, several strategies of reduction of the amide to the requisite aldehyde were explored (**Table 1-1**). The conditions most directly associated with the reduction of pseudoephedrine amides as developed by Myers and coworkers utilizes LiAlH(OEt)_3 , which often delivers a mixture of aldehyde and the corresponding pseudoephedrine aminal upon pH-neutral aqueous workup. The residual aminal can typically be converted to the aldehyde by treatment with aqueous HCl and TFA to effect complete hydrolysis, however we found that the established procedure significantly decomposed the aldehyde and was not sufficient for complete conversion.⁸⁶ Although the overreduced primary alcohol was not observed upon treatment with an excess of LiAlH_4 , the persistence of incomplete conversion upon the addition of further equivalents of reductant led to poor yields. While Schwartz's reagent typically is an effective solution for the reduction of amides to aldehydes,⁸⁷⁻⁸⁸ significant decomposition of the ferrocene and incomplete conversion were observed in our application of this reagent. We ultimately found that treatment of the amide with four equivalents of DIBAL-H conferred comparatively excellent yields of aldehyde (> 75%). Moreover, aminal formation could be completely suppressed provided that quenching with wet methanol was carefully conducted at -78 °C.

Table 1–1. Screen of reductants for the direct conversion of the pseudoephedrine amides to aldehyde **I-14**.

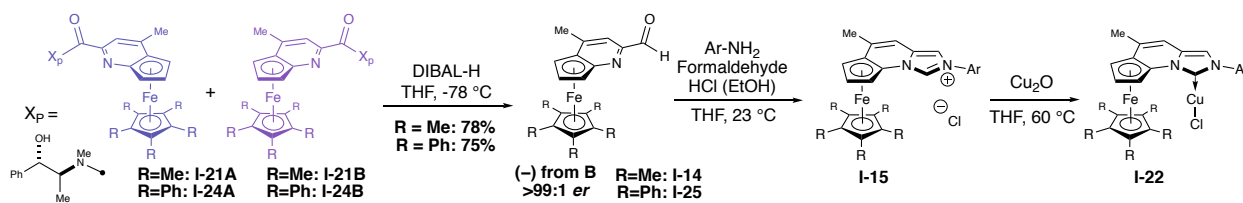


^aConditions: (a) LiAlH(OEt)₃, THF (b) LiAlH₄ (2.3 eq.), EtOAc, THF, -78-0 °C (c) Cp₂ZrHCl (2.5 equiv.), THF, 23 °C (d) DIBAL-H (4 equiv.), THF, -78 °C. ^bIsolated yields.

1.3.2 Multicomponent synthesis of the azolium motif

Initial experiments with the racemic aldehyde obtained from ester **I-20** revealed that a modification of methodology disclosed by Aron and coworkers readily provided the corresponding series of N-aryl azolium chloride salts which could be purified by a relatively simple chromatography protocol (**Scheme 1-6**). The tetrafluoroborate salts could then be obtained by simple anion metathesis with AgBF₄.

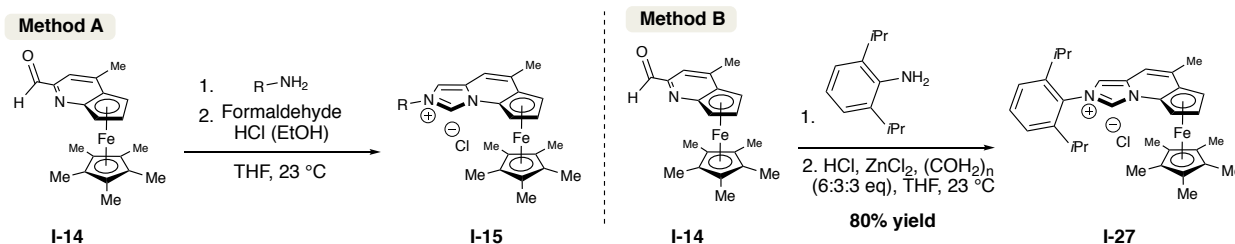
Scheme 1-6. Synthesis of enantiopure azolium salts from pseudoephedrine amides.



We additionally found that the pentaphenylcyclopentadienyl-derived ferrocene^{71,73-74} could be elaborated to the azolium salt with nearly identical synthetic protocols. Effective chromatic resolution of these diastereomers was attained by using a different mobile phase (See Supporting Information). While we found that treatment of **I-24** with 4 equivalents of DIBAL-H

delivered a roughly 1:1 mixture of the pentaphenyl aldehyde (**I-25**) and aminal, the apparent increased robustness of **I-24** to acidic conditions allowed us to use the hydrolytic protocol developed by Myers⁸⁶ with no significant penalty in yield.

Scheme 1-7. Overall strategy for the synthesis of enantiopure azolium salts.



1.3.2.1 Late-stage catalyst diversification via azolium synthesis

Although highly hindered anilines expectedly could not be converted to their respective azolium salts via our standard conditions (**Scheme 1-7, Method A**), we found that conditions developed by Berthon-Gellos et al. for the synthesis of extremely hindered imidazolium salts delivered the 2,6-diisopropylaniline-derived product **I-27** in excellent yield (**Method B**).⁸⁹ Unfortunately, these conditions, as well as those disclosed by Aron, were not tolerant of most anilines which contained an auxiliary Lewis basic functionality such as pyridines and phosphines, with the exceptions of phenol **I-34** and thioanisole **I-35** (**Figure 1-6**).

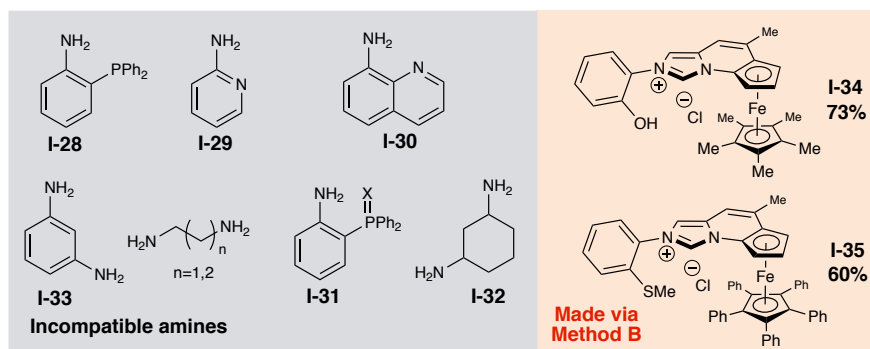
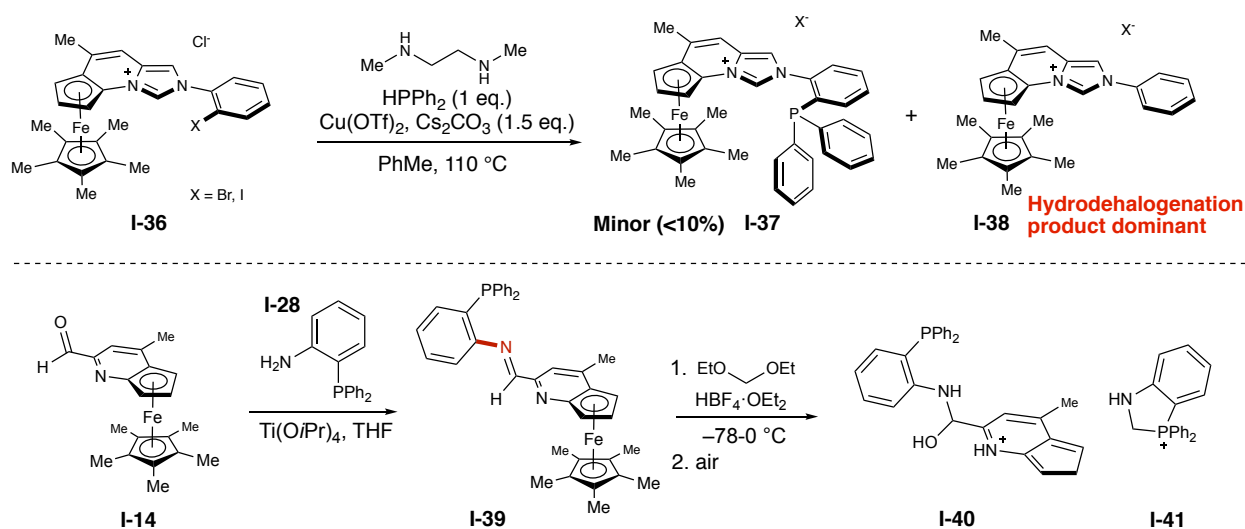


Figure 1-6. Compatible and incompatible amines and anilines for azolium synthesis

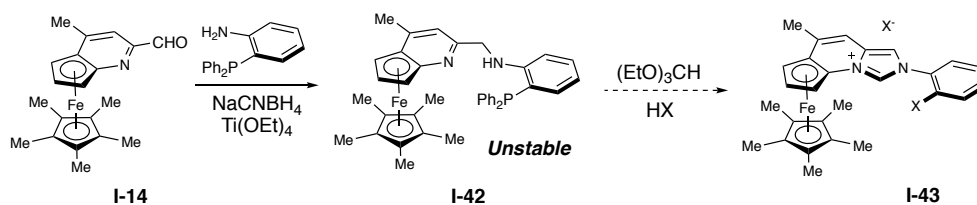
Attempts incorporate phosphine **I-28** through protection as the oxide and sulfide (**I-31**) also failed, as did attempts to couple diphenylphosphine to iodoazolium **I-36** (Scheme 1-8). While a solution of imine **I-39** could be formed using $\text{Ti}(\text{O}i\text{Pr})_4$, subsequent reaction with aqueous and non-aqueous sources of formaldehyde yielded a complex mixture of inseparable products, which predominantly consisted of **I-40** and **I-41** upon exposure to atmosphere.

Scheme 1-8. Attempted synthesis of a bidentate ligand.



Given that Aron's simpler substrates showed a broad tolerance to polyamines, anilines, and alcohols, we can only attribute the failure to either diminished solubility or electronic factors related to the increased nucleophilicity of our pyridenyl aldehyde (**I-14**). As an alternative to these methods, we reasoned that **I-39** could be reduced to amine **I-42** through standard reductive amination conditions and exposed to carbon in the orthoester oxidation state. However, **I-42** demonstrated extreme sensitivity to air, protic additives, and mild heat, and the corresponding azolium could not be observed in any reaction which included these factors (Scheme 1-9).

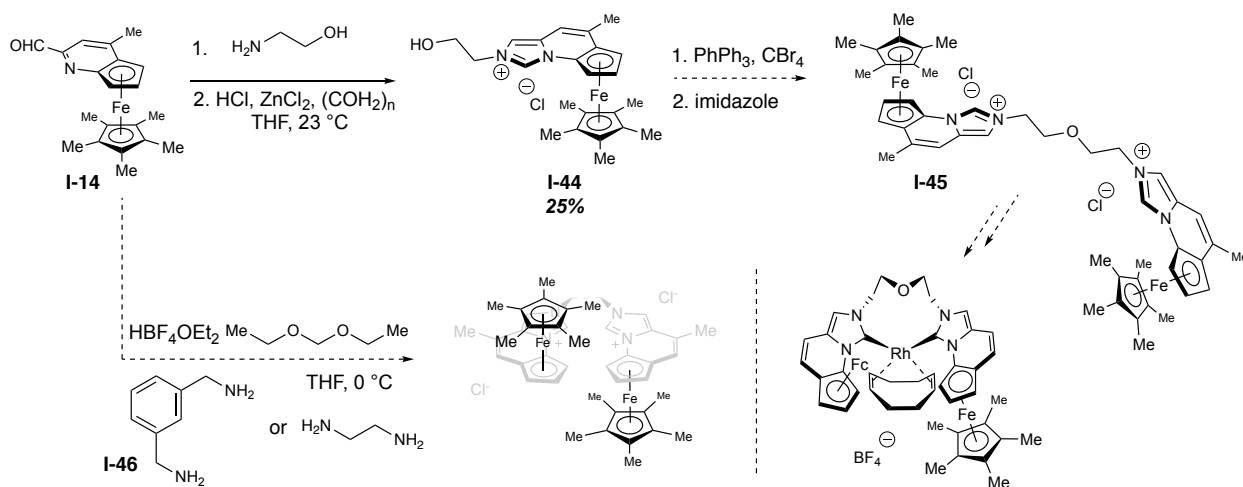
Scheme 1-9. Reductive amination approach towards bidentate system



1.3.3 Efforts towards (bis)NHC multidentate systems

This incompatibility extended to both alkyl and aryl diamines and alcohols, frustrating our attempts to generate a pincer system (**Scheme 1-10**). For example, although alcohol **I-44** could be formed in low yield through reaction with aminoethanol, it could not be separated from numerous other ionic impurities. Exposure of this complex mixture to standard Appel conditions did not yield the desired ether, although a more thorough evaluation of etherification conditions is warranted if a suitable purification strategy for **I-44** is identified. Likewise, application of anhydrous conditions to both aryl and alkyl diamines embodying varying degrees of steric congestion did not form any observable product. In the case of diaminoxylylene **I-46**, a trace amount of monoferrocene complex could be observed by LCMS.

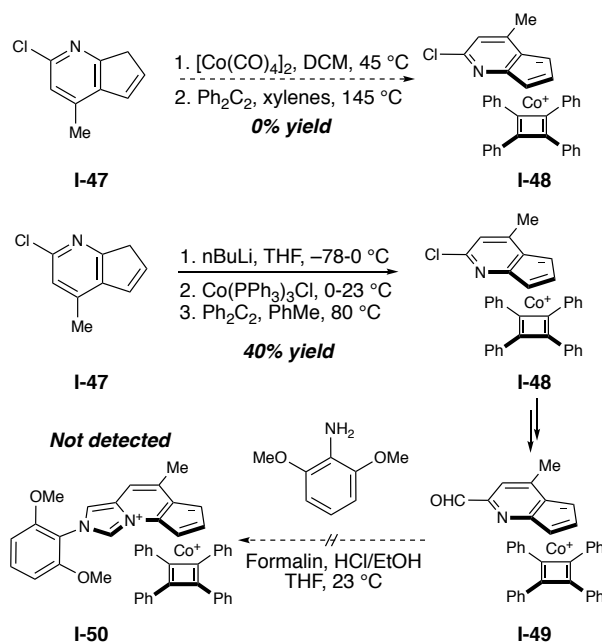
Scheme 1-10. Approaches towards bis(ferrocenyl) system via anhydrous formaldehyde sources



1.3.4 An analogous Co(I) sandwich complex

Inspired by recent reports of the robustness of several Co-butadienyl complexes and their employment in asymmetric catalysis,^{44,90-94} we additionally initiated an attempt to synthesize a related NHC complex with this metal to explore the possibility of further diversifying the topological profile of the metallocene region. Attempts to synthesize **I-48** by heating the pyridene **I-47** in the presence of $[\text{Co}(\text{CO})_4]_2$ followed by the addition of dimethylacetylene failed to deliver product,⁹⁵⁻⁹⁶ although we found that lithiation of diene **I-47** followed by addition of CoPPh_3Cl and diphenylacetylene delivered the corresponding metallocene in modest yield (**Scheme 1-11**). While the complex tolerated elaboration to the ethyl ester (**I-48**) and aldehyde **I-49** using identical methods to the corresponding ferrocenes, complete decomposition was observed upon exposure of the aldehyde to several conditions^{81,89,97-98} for azolium synthesis.

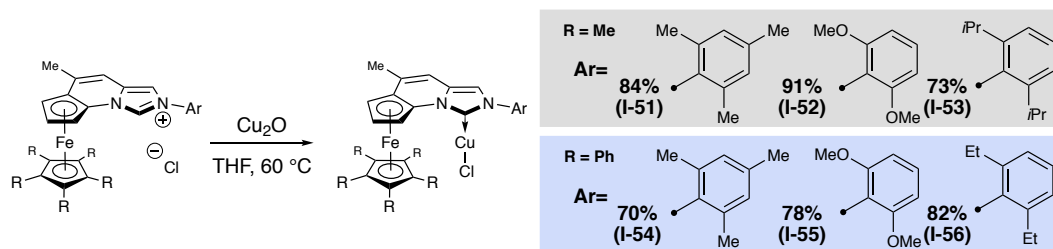
Scheme 1-11. Attempted synthesis of an analogous Co(I) metallocene.

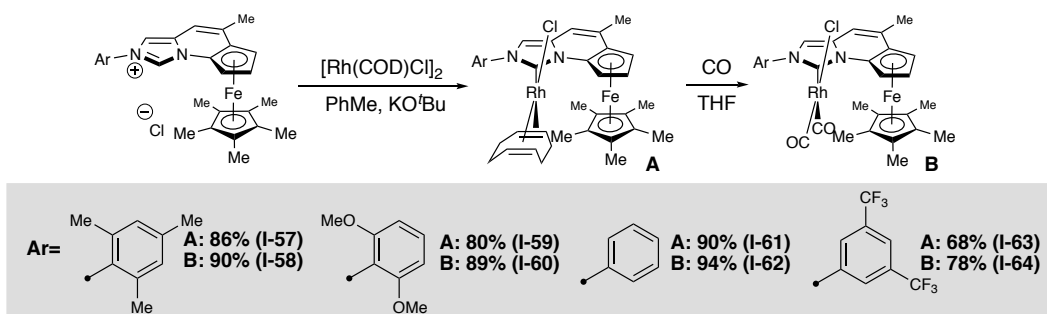


1.3.5 Generation of d-block complexes

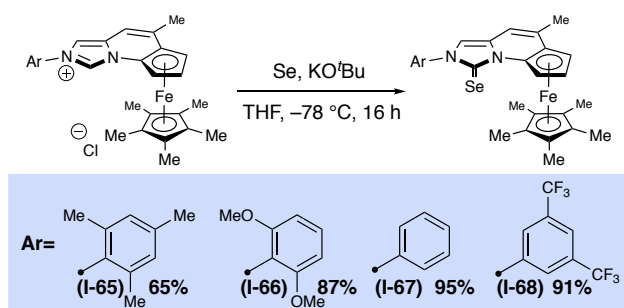
To evaluate the performance of these compounds as ligands for transition metal catalysis, several metal complexes of Cu(I) and Rh(I) were prepared (**Figure 1-8**). Heating of the azolium chlorides in THF in the presence of Cu_2O to generate copper(I) chloride complexes was found to be broadly applicable for this class (**Scheme 1-12**).⁹⁹ The elution of the unpurified reaction mixtures with CH_2Cl_2 through a plug of silica yielded pure copper complexes, which were then precipitated from dichloromethane to afford crystals suitable for x-ray diffraction. Exposure of the azolium salts to alkoxide base and $[\text{Rh}(\text{cod})\text{Cl}]_2$ yielded the corresponding diene complexes which could be employed in catalysis (Section 1.5) or be directly converted to carbonyl complexes via bubbling of CO gas in THF at room temperature for the purposes of TEP (Tolman electronic parameter) analysis (**Scheme 1-13**). Of note, the exposure of an azolium bearing *para*-OMe functionality on its pendant aryl ring to these conditions delivered $[\text{NHC}]_2\text{RhCl}_2$ complex **I-69**, rendering Tolman analysis impractical for this compound (**Figure 1-7**). An additional subset of selenoureas for NMR spectroscopic analysis were prepared by exposure to elemental Se and base at cryogenic temperatures (**Scheme 1-14**).

Scheme 1-12. Preparation of Cu(I)Cl complexes.





Scheme 1-13. Preparation of Rh(COD)Cl and Rh(CO)₂Cl complexes.



Scheme 1-14. Preparation of selenoureas for NMR spectroscopic analysis of ligand electronic properties.

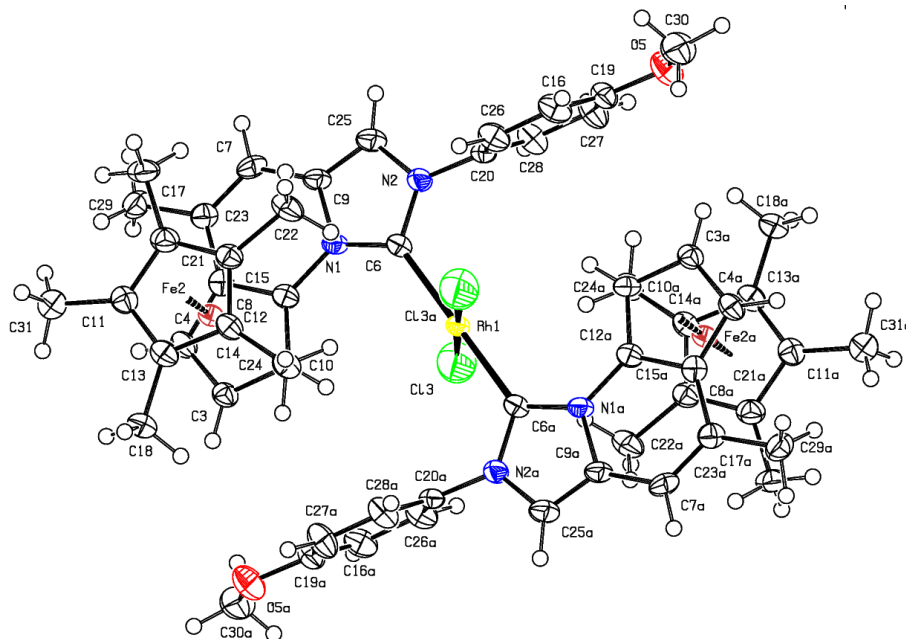
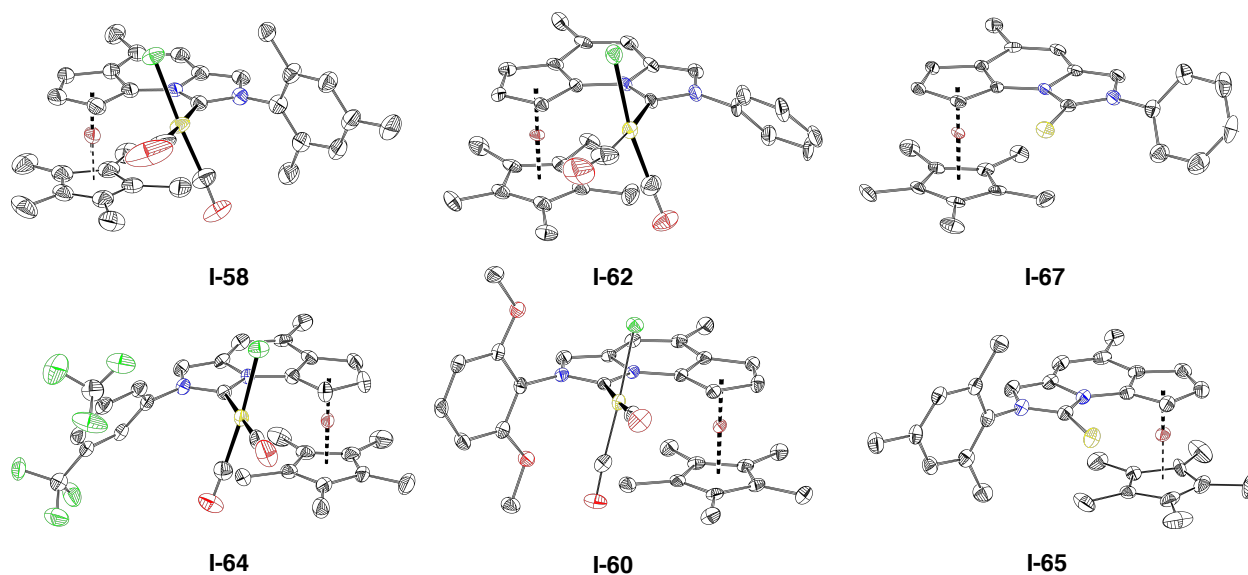


Figure 1-7. Rh(I) dimer I-69. Thermal ellipsoids are shown at 50% probability.



Hydrogens are omitted for clarity.

Figure 1-8. X-ray structures of selected Rh(I) carbonyl and selenium complexes.

1.4 Spectroscopic and X-ray Diffraction Analysis of Structural and Electronic Properties

In our analysis of the electronic properties of this ligand class,⁶⁶ we first used the Tolman electronic parameter (TEP), a widely utilized metric for the degree to which a NHC ligand influences electron density on a metal center (**Figure 1-9**).¹⁰⁰⁻¹⁰² However, recent experimental and theoretical analysis of NHC-metal π -bonding has challenged the longstanding belief that NHC-metal electronic properties are principally governed through σ -donor interactions. While TEP can only measure the net effect of π -acidity and σ -donicity between a NHC and a metal, a method which could selectively measure the magnitude of π -acidity would enable a greater understanding of how a NHC π -system contributes to its interactions with a metal. In addressing this challenge, Bertrand has recently disclosed a ³¹P NMR- based methodology which allows for

the accurate profiling of NHC π -acidity.¹⁰³ Likewise, Ganter has recently described an analogous ^{77}Se NMR-based method which simplifies this process due to the high stability of Se-NHC adducts and their facile preparation (**Figure 1-9**).¹⁰⁴⁻¹⁰⁶ We therefore elected to supplement our TEP analysis with this latter technique.

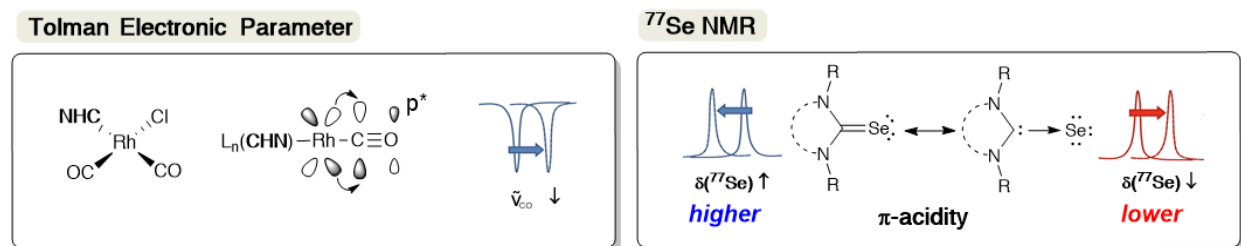


Figure 1-9. TEP and ^{77}Se NMR spectroscopic approaches towards characterization of ligand electronics.

1.4.1 Comparison of ^{77}Se NMR and TEP-derived parameters

After collecting TEP and ^{77}Se NMR data for a range of planar chiral catalysts with electron-donating and electron-withdrawing substitution, it was found that while NHC **a** (**Table 1-2, Figure 1-10**) possessed the highest TEP by an appreciable margin relative to **b**, both exhibited a similar ^{77}Se chemical shift. Despite their similar degrees of π -acidity, TEP indicates that **a** maintains a higher level of electron density on a given host metal than **b**, which further implies that **a** is a substantially stronger σ -donor. Similarly, while **c** and **d** exhibited highly contrasting TEP values relative to one another due to the disparate $-I$ effects of their N-aryl rings, both demonstrated similar ^{77}Se shifts which were distinct from **a** and **b**.

It is unclear whether conformational effects on overall ligand electronic properties (opposed to those which are purely functional) significantly contribute to the parameters observed in this analysis. It has been long established through both theoretical and experimental

work that the degree of coplanarity of two conjugated systems significantly affects conductivity between them,¹⁰⁷⁻¹⁰⁹ however little work has been completed to elucidate how this effect intersects with the behavior of a ligand in catalysis. While the relative clustering of **a/b** vs. **c/d** on the ⁷⁷Se scale can be rationalized in part the nature of substituent *I* effects, an equally conspicuous differentiating factor between these two groupings is the relative ability of their *N*-aryl rings to rotate in plane with their imidazopyridyl cores. In other words, this additional distinction suggests that the ability of the wingtip *N*-aryl ring to rotate in-plane with the carbene and maximize conjugation may serve as a differentiating factor in the π -acidities of these systems. For example, the crystal structure of rhodium complex **I-58** (**Figure 1-8**) reveals the presence of short contacts between the nearly orthogonal mesityl ring and both CO_{cis} and Cl 1 of the metal center, thus constraining it in an orientation where π -delocalization into the aryl ring is completely suppressed. In contrast, the more π -acidic ligands **c** and **d** (**I-62** and **I-64**, **Figure I-8**) demonstrate much more acute interplanar angles relative to their wingtip aryl ring and azole polycycle (**Table 1-2**), although it is unknown how much of this difference in ⁷⁷Se shift is due to this lower rotational barrier. While their precise solid state conformations can offer only limited insight on this effect due to the interfering perturbation from crystal packing and the inherent dynamic nature of a rotatable bond in solution, the increased disparity in torsional strain between **a/b** and **c/d** when the carbene bears large functionality is apparent.

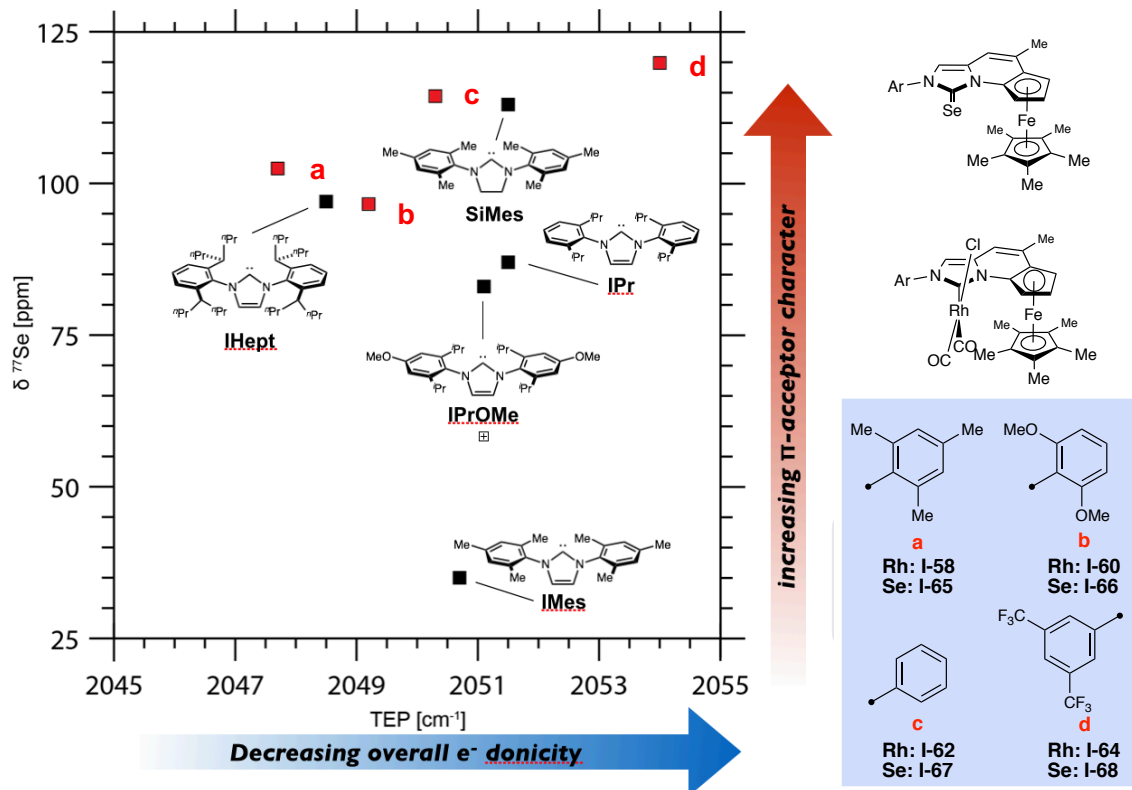
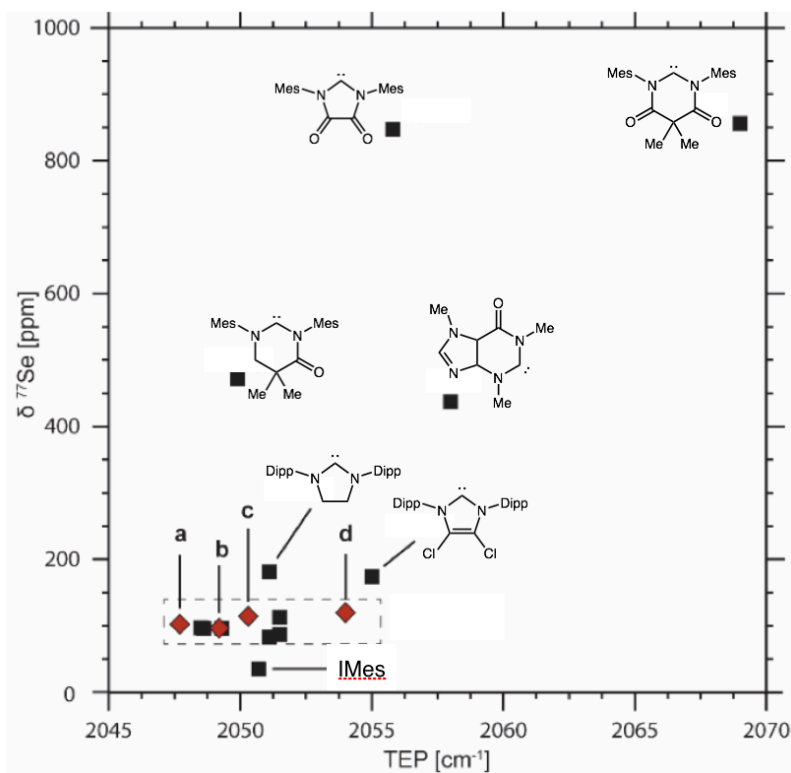


Figure 1-10. Plot of ^{77}Se chemical shift vs. TEP for compounds a-d and several other NHCs.

The placement of planar chiral ligands **a-d** on the ^{77}Se NMR suggests a general level of π -acidity comparable to SiMes, IPent, IHept, and INon. Surprisingly, the location of IMes on this scale is somewhat incongruously situated upfield of this cluster. While the TEP of IMes is comparable to **b** and **c**, its ^{77}Se shift implies a substantially diminished degree of π -acidity, and thus a much smaller magnitude of σ -donicity when compared to **a-c**. In the aim of profiling this latter property using NMR spectroscopy, Ganter et al. have additionally proposed the use of $^1J_{\text{CH}}$ values of the azolium C-2 atom as a direct metric of carbene s-character, analogous to prior

efforts which have used $^1J_{\text{PSe}}$ values to profile phosphine basicity.¹⁰⁵ In our analysis, we found that $^1J_{\text{CH}}$ values were closest to those of IMes and IPr rather than SiMes. Surprisingly, **a-d** displayed very little variation in this metric, which suggests that π -acidity serves as a more important factor in modulating net the electron donicity of our ligands.

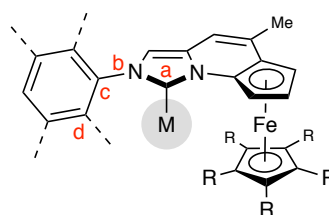


Dotted line represents boundaries of Fig. 1-10.

Figure 1-11. Larger scale plot of ^{77}Se chemical shift vs. TEP data.

Table 1–2. NMR spectroscopic and geometrical data of Se and Rh(CO)₂Cl complexes of **a–d** and selected examples from the literature.

| NHC | NHC-Se | NHC HCl | NHC-Rh(CO) ₂ Cl |
|-------------|---|---|--|
| | $\delta^{77}\text{Se}$ (ppm) ^a | $\delta^{13}\text{C}$ (ppm) ^b $^1J_{\text{CH}}$ (Hz) ^c | TEP (cm ⁻¹) <i>a-b-c-d</i> torsion (°) ^d |
| a | 97 | 129.14 227.60 | 2049.2 82.48 |
| b | 102 | 130.27 228.85 | 2047.7 96.2 |
| c | 114 | 127.00 227.50 | 2050.3 48.64 |
| d | 120 | 128.10 227.40 | 2054.0 60.78 |
| I-84 | - | 132.20 228.20 | - - |
| SIMes | 116 | 160.2 206 | 2051.5 - |
| IPr | 87 | 139.4 224 | 2051.5 - |
| IMes | 35 | 139.9 225 | 2050.7 - |



(a) ⁷⁷Se chemical shift of selenium bound to the carbene carbon. (b) Taken in acetone-*d*₆. (c) Obtained from the hydrochloride azolium precursors. (d) See right structure for atom labels.

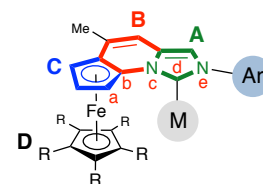
1.4.2 Structural characterization via X-ray diffraction

A subset of the Rh(I), Cu(I), and Se complexes were crystallized and analyzed via X-ray diffraction. All Rh(I) and Cu(I) complexes exhibited features characteristic of the considerable intramolecular between the ferrocene and metal substituent. All metal centers of CuCl and Rh(cod)Cl complexes displayed a marked degree of out-of-plane distortion ranging between 9° to 22°. In the Rh(cod)Cl series of compounds, a moderate degree of torsion of azolium ring A

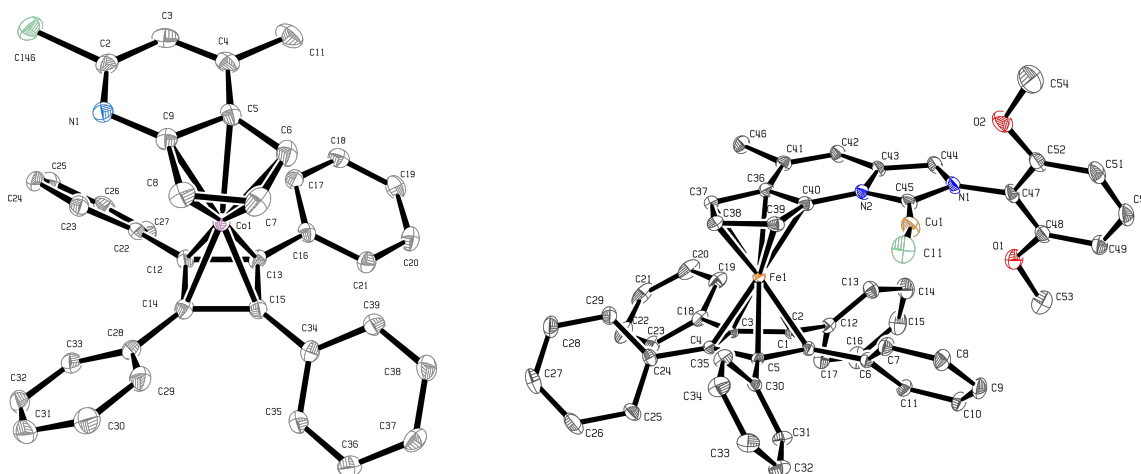
relative to dieny ring **C** was also apparent (**Table 1-3**). For complexes bearing a Cp* ring, rings **C** and **D** did not exhibit any measureable deviation from a parallel orientation, although this was present in pentaphenyl comopund **I-55** and its corresponding azolium salt, as well as in cobalt complex **I-48** in magnitudes up to 5.5° (**Figure 1-13**). While this is attributable to the increased bulk of the pentaphenylcyclopentadienyl and tetraphenylcyclobutadiene ligands, in both cases ¹H NMR spectra reveal coalescence of each set of phenyl ring proton signals at 23 °C, implying that their solution-phase rotation is not significantly inhibited at room temperature. Metal-carbene compounds of all compounds characterized lied in ranges typical for Arguengo-type carbene complexes.¹¹⁰ All ferrocene moieties bearing Cp* ligands were found to crystallize in the eclipsed conformation relative to the pyrindene Cp ring with the exceptions of the mesityl-functionalized complexes of Se and Rh(CO)₂Cl. Pentaphenylcyclodienyl complex **I-55** (**Figure 1-12**) and its azolium precursor conversely exhibited staggered conformations. NCN angles of all compounds were typical for metal-carbene complexes, although in almost all cases, resolution limitations did not permit meaningful comparisons of this angle between the compounds analyzed.

Table 1–3. Selected measurements of heterobimetallic compounds analyzed via XRD.

| M | Ar | d-M (Å) | c-d-e (°) | b-c-d-M tors. (°) | a-b-c-d tors. (°) |
|-----------|-------------------------------------|----------|-----------|-------------------|-------------------|
| Rh(cod)Cl | Mes (I-57) | 2.055(6) | 103.6(6) | 15(1) | 7(1) |
| | 2,6-OMe (I-59) | 2.044(3) | 103.0(2) | 14.5(4) | 4.3(5) |
| | 3,5-CF ₃ (I-63) | 2.036(2) | 102.7(1) | 21.8(3) | 3.0(3) |
| RhCO | Mes (I-58) | 2.08(1) | 104.1(8) | 6(2) | - |
| | 2,6-OMe (I-60) | 2.061(3) | 104.0(3) | 9.6(5) | - |
| | Ph (I-62) | 2.00(1) | 102.8(9) | 6(2) | - |
| | 3,5-CF ₃ (I-64) | 2.058(3) | 103.6(3) | 6.7(5) | - |
| CuCl | Mes (I-51) | 1.877(2) | 103.0(2) | -11.3(3) | - |
| | 2,6-OMe (I-52) | 1.889(2) | 103.4(2) | -12.4(4) | - |
| | 2-OMe-4-Ph (I-70) | 1.84(1) | 102.8(9) | - | - |
| | *2,6-OMe (I-55) | 1.878(3) | 103.5(3) | 9.3(5) | - |
| Se | Mes (I-65) | 1.834(2) | 104.5(2) | - | - |
| | Ph (I-67) | 1.837(5) | 104.5(4) | - | - |

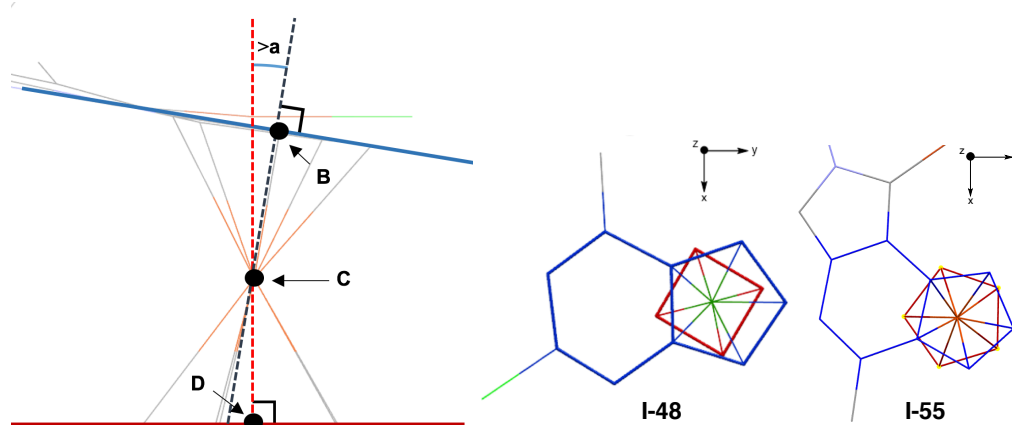


Key (right): Rings are labeled in uppercase. Atoms are labeled in lowercase.



Hydrogens are omitted for clarity. Thermal ellipsoids shown at 50% probability.

Figure 1-12. X-ray structures of analogous metallocene complexes **I-48** (left) and **I-55** (right).



(left) Cartoon of x-axis projections of **I-48** and **I-55**. (right) Actual XRD z-axis projections. Measurements from XRD: (ii) $\angle a = 5.46^\circ$. $CB = 1.700 \text{ \AA}$. $CD = 1.696$. (iii) $\angle a = 4.44^\circ$. $CB = 1.692 \text{ \AA}$. $CD = 1.669 \text{ \AA}$.

Figure 1-13. Selected geometric parameters of complexes **I-48** and **I-55**.

1.4.3 Analysis of steric parameters via buried volume calculations

We additionally examined percent buried volume ($\%V_{\text{Bur}}$) as a means of assessing the overall steric encumbrance around a hypothetical metal center for a set of ligands (**Figure 1-14**).¹¹¹⁻¹¹² In general, buried volume can serve as a valuable metric for a given structure's competency in promoting processes accelerated by a highly encumbered catalytic center (e.g. reductive elimination vs. β -hydride elimination, precatalyst activation).¹¹²⁻¹¹⁵ Additionally, $\%V_{\text{Bur}}$ allows for a quantitative assessment of occupancy in each quadrant, thus allowing a degree of objective insight into the ability of a ligand to project an asymmetric environment around its key reactive space (e.g. a metal center). Calculations performed on the series of Cu(I) complexes **I-51**, **I-52**, **I-55**, and **I-70** reveal that functionalization of the pendant Cp ring (i.e. pentaphenyl vs pentamethyl) unsurprisingly has the greatest effect on total buried volume, where

51.6% of simulated coordination sphere (see SI for calculation details) was occupied by pentaphenyl ligand **I-55** (Table 1-4). This value is extremely large for Arduengo-type NHCs, which typically range between 20-35% $\%V_{\text{Bur}}$. Among carbenes, the large $\%V_{\text{Bur}}$ of **I-55** is only approached by Bertrand's CAAC-type ligands (**I-71**), which possess quarternary carbon vicinal to the carbene, and Glorius's (-)-menthone-derived IBiox NHC.¹¹⁶

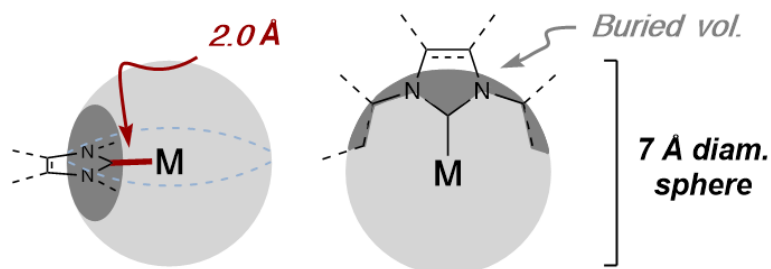
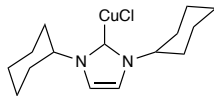


Figure 1-14. Application of buried volume concept to NHC ligands.

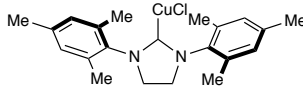
Ligands bearing the Cp* functionality exhibited little variation, with %V_{bur} ranging between 38.5 and 39.5%. All complexes examined are characterized by having the greatest occupancy in quadrant SE where the bulky Cp rings are positioned. Although complex **I-55** significantly differs in structure from others in the set only by its Cp ring, the occupancy of the area in **I-55** not containing this differentiating feature—quadrant NW—still diverges from others in the set. The occupancy of this remote quadrant is still highly altered due to the protrusion of the 2-OMe substituent of the pendant aromatic ring into this quadrant, promoted in turn by the large degree of repulsion between the pentaphenyl Cp ring and the 6-OMe substituent (**Figure 1-15, I-55**). A more in-depth discussion of ligand topology and its effect on Cu(I) mediated enantioselective borylation can be found in chapter 2.

Table 1-4. %V_{Bur} calculated for selected planar Cu(I)Cl complexes and compounds from literature.

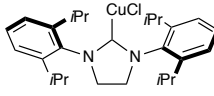
| NHC | Total | SW | NW | NE | SE |
|--------------|-------------|------|------|------|------|
| I-51 | 38.7 | 39.5 | 30.7 | 33.3 | 51.5 |
| I-55 | 51.3 | 58.2 | 46.3 | 31.9 | 68.8 |
| I-52 | 39.5 | 45.3 | 28.0 | 33.2 | 51.5 |
| I-70 | 38.5 | 38.2 | 28.9 | 32.5 | 54.6 |
| Icy | 28.8 | - | - | - | - |
| SIMes | 36.9 | - | - | - | - |
| SIPr | 46.4 | - | - | - | - |
| I-71 | 51.2 | - | - | - | - |
| IBiox | 47.8 | - | - | - | - |



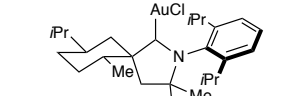
ICy



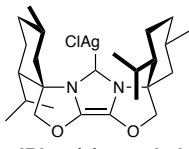
SiMes



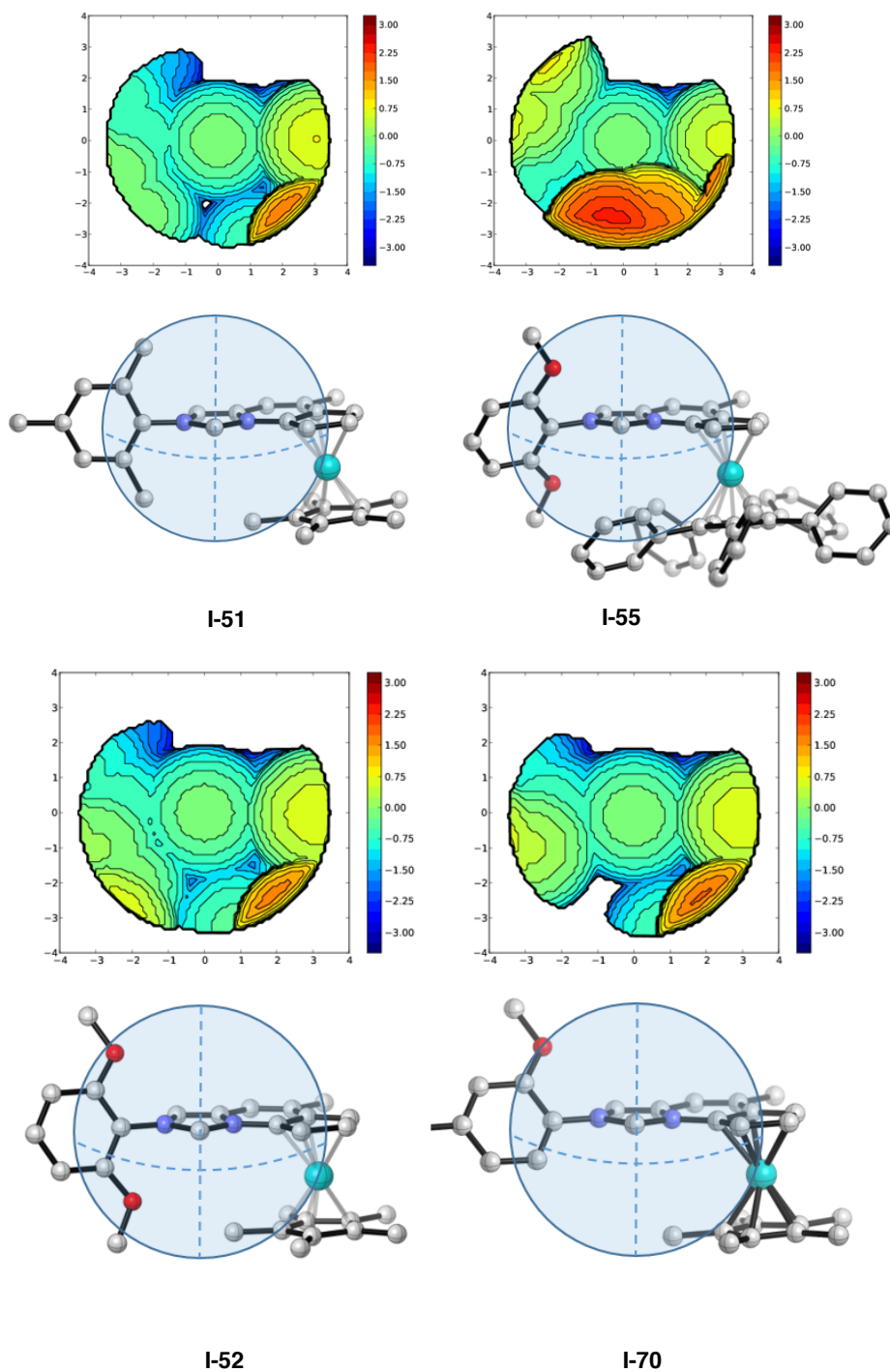
SIPr



I-71



IBiox(-)-menthyl



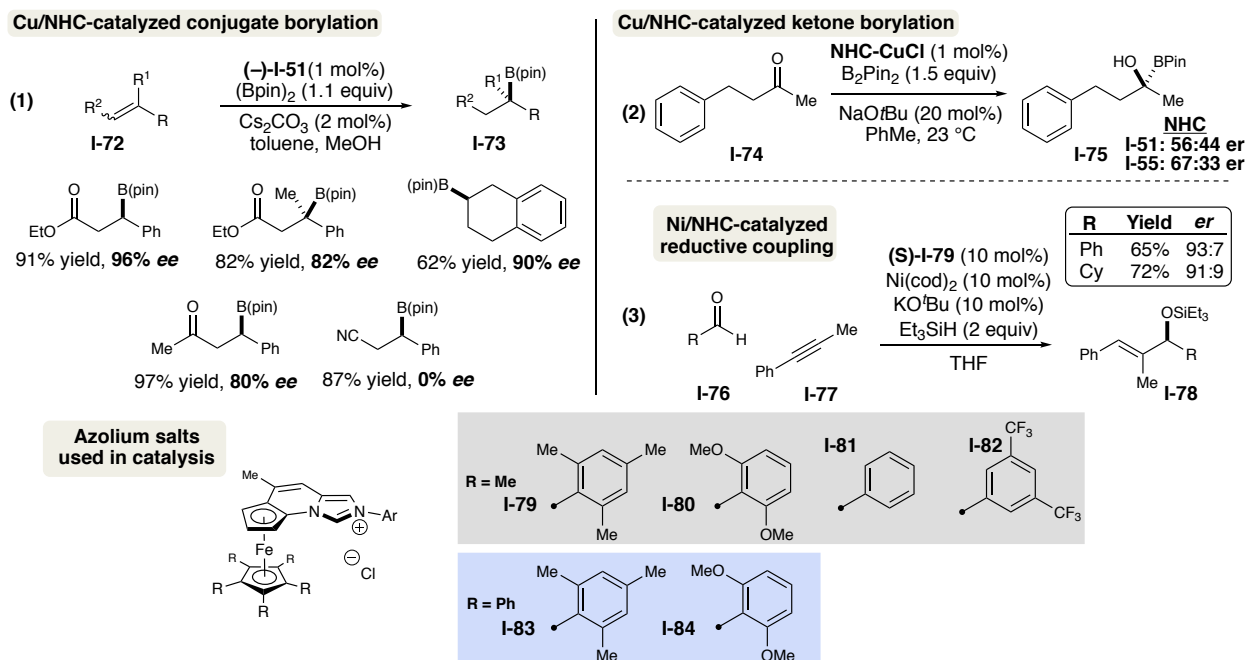
Blue-shaded areas represent 7.0 Å diameter spherical volume centered 2.0 Å from the carbene carbon. Contour maps and V_{bur} calculations generated by SambVca 2.0.¹¹¹ Axes and legend units are Angstroms. See supporting information for calculation details.

Figure 1-15. Steric contour maps of ligands analyzed in buried volume calculations.

1.5 Applications in Transition-Metal and Lewis Base Catalysis

There are few studies concerning imidazopyridinium-based ligands for transition metal catalysis.¹¹⁷⁻¹¹⁸ Consequently, we were eager to further explore the applicability of this class of carbene towards a wider variety of transformations. We have previously disclosed the highly successful application compound **I-51** towards conjugate borylations and reductive couplings (Scheme 1-15).⁶⁶ In applying our copper complexes towards this reaction, we observed several limitations, such as the necessity of either a carbonyl system or restricted rotation of the α,β double bond relative to the aromatic functionality of the substrate for adequate stereoselectivity. Likewise, our attempt to selectively borylate the carbonyl of propiophenone delivered a poor level of selectivity, although a small improvement could be attained with the use of pentaphenyl complex **I-55**.

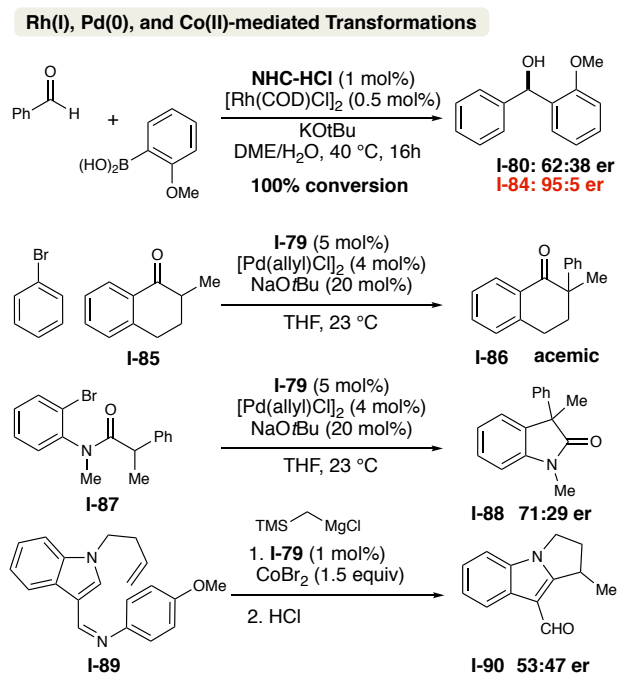
Scheme 1-15. Cu(I)-mediated borylations and Ni(0) reductive couplings surveyed in this study



1.5.1 Use with metals possessing nonlinear coordination geometries

The use of our planar chiral ligands with metals which bind substituents in a nonlinear geometry was met with limited success. While square-planar NHC-rhodium complex, formed *in-situ* with azolium **I-80**, was found to arylate *o*-anisaldehyde with excellent enantioselectivity, the palladium mediated arylation of α -methyltetralone (**I-85**) using azolium **I-80** produced the racemate (**Scheme 1-16**). An intramolecular variant of this transformation conferred a moderate level of selectivity, but was nevertheless vastly outperformed by other ligand systems.¹¹⁶ Attempting the Co-catalyzed intramolecular reductive cyclization of indole **I-89** delivered only a slight enantiomeric excess of **I-90**. We attribute this marked lack of selectivity provided by our complexes in this case due to the insufficiency of a monodentate system for adequate stereocontrol for metals with nonlinear geometries.

Scheme 1-16. Performance of catalysts with nonlinear metals.



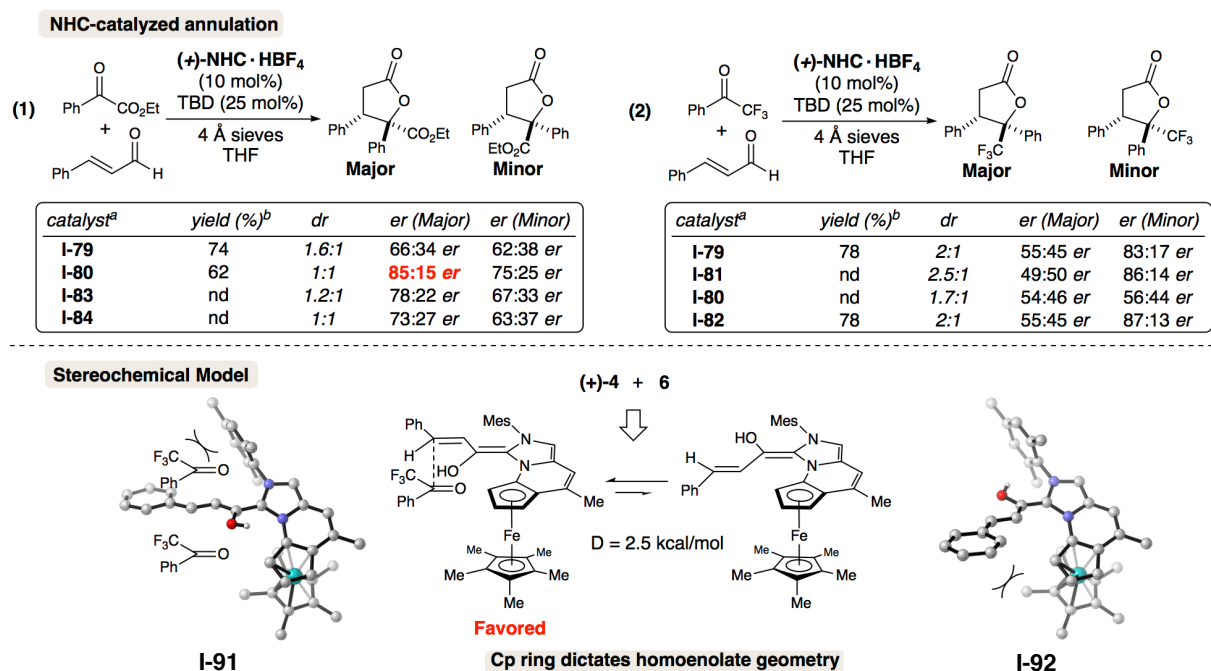
1.5.2 Use as Lewis-basic organocatalysts

We additionally sought to profile the selectivity of these compounds as Lewis base organocatalysts in the homoenolate addition of cinnamaldehyde to α -ketoesters and trifluoroacetophenone (**Scheme 1-17**). These annulations remain considerably challenging, presumably to the remoteness of the nucleophilic β -carbon relative to the catalyst and the more subtle differences in bulk between both α -positions of a ketone carbonyl as opposed to those of an aldehyde or a β -monosubstituted conjugate acceptor.¹¹⁹⁻¹²⁰ Application of the tetrafluoroborate salts of several planar chiral azoliums to annulations of ethyl ketoesters (eq. 1) revealed consistently poor diastereoselectivity, although catalyst **I-80** was able to promote a fair level of enantioselectivity. Interestingly, azolium **I-79** provided the poorest levels of enantioselectivity, yet the highest level of diastereoselectivity of the series.

Although yield was extremely poor for transformations catalyzed by **I-83** and **I-84**, the effect of the pentaphenyl functionality on stereoselectivity was mixed. In comparing mesityl azoliums **I-79** and **I-83**, pentaphenyl derivative (**I-83**) demonstrated decreased diastereoselectivity but moderately higher enantioselectivity. Conversely, (bis)methoxyl azolium **I-84** provided lower enantioselectivity compared to its pentamethyl counterpart (**I-80**). Enantioselectivities obtained in additions to trifluoroacetophenone (eq. 2) were found to be typically higher in the *cis* product (as was observed for ketoesters), although in this case the *cis* product was consistently obtained as the minor diastereomer. The discrepancies in enantioselectivities between the *cis* and *trans* products of eq. 2 may suggest that a certain approach of the ketone relative to the homoenolate (e.g., top vs bottom approach in TS **I-91**) is correlated with selectivity for a certain face of the ketone (e.g. Ph vs. CF₃ projecting out of page

towards viewer in TS **I-91**). Calculations which compare the relative energies of the E and Z isomers of the homoenolate (see experimental section for details) imply an approximate 2.5 kcal/mol difference in energy, which corresponds to a homoenolate population which consists of over 90% **I-91**. Elucidating how this distribution correlates with the observed selectivities necessitates a more thorough quantitative understanding of the relative energies of ketone orientation and attack trajectory.

Scheme 1-17. Top: NHC-catalyzed homoenolate additions to ketoesters (eq. 1) and trifluoroacetophenone (eq. 2). Bottom: Stereochemical model for reactions (1) and (2).



^aAll reactions utilized the BF_4 salts of the azolium precatalyst. ^bIsolated yields.

1.6 Conclusion

In summary, this work provides a practical strategy for the construction of a family of ferrocene-based planar chiral carbenes which have been shown to be useful for a variety of metal- and organocatalyzed transformations. Nevertheless, an intriguing challenge lies within the task of further extending the current scope of coplanar NHC-ferrocene structures to additional metallocene cores and chelating auxiliary functionality, which we expect will enhance its performance as a chiral control element with other metal centers, such as Rh(I) and Pd(0). This effort will correspondingly depend on the successful development of methodology which can achieve the synthesis of an azolium precursor without inducing significant decay of the organometallic core or promoting the formation of unwanted side-products. The characterization of these compounds with TEP and ^{77}Se NMR spectroscopy has revealed an interesting divergence from the electronic characteristics exhibited from IMes: while TEP indicates an overall electron donation capacity on par with IMes for ligands **I-79** and **I-80**, our ligands possess a considerably higher level of π -acidity which is compensated for by their markedly larger level of σ -donicity. Catalysts such as **I-79** and **I-80** show striking similarities with imidazoline-type NHCs such as SiMes or IMes-type carbenes functionalized with large long-chain aliphatics, such as IHept, IPent, and INon. The discrepancy in overall electron donicity observed between **I-79/I-80** and **I-81/I-82** suggests that consideration of structural characteristics such as torsional strain in rotatable aromatic rings when evaluating carbene electronic characteristics may be of high importance, although a more thorough evaluation of this effect will be needed to establish its importance as it relates to π and σ acidities and donicities.

1.7 Experimental Section

All reactions were carried out under a nitrogen atmosphere in oven-dried glassware with magnetic stirring. THF, toluene, and DMF were purified by passage through a bed of activated alumina.¹²¹ Reagents were purified prior to use unless otherwise stated following the guidelines of Perrin and Armarego.¹²² Silica gel used in flash chromatography using Silicycle SiliaFlash P60 silica gel 60 (230-400 mesh). Analytical thin layer chromatography was performed on EM Reagent 0.25 mm silica gel 60-F plates. Visualization was accomplished with UV light and ceric ammonium nitrate stain or potassium permanganate stain followed by heating. Infrared spectra were recorded on a Bruker Tensor 37 FT-IR spectrometer. ¹H NMR spectra were recorded on AVANCE III 500 MHz w/ direct cryoprobe (500 MHz) spectrometer and are reported in ppm using solvent as an internal standard (CDCl₃ at 7.26 ppm, (CD₃)₂SO at 2.50 ppm). Data are reported as (ap = apparent, s = singlet, d = doublet, t = apparent triplet, q = quartet, m = multiplet, b = broad; coupling constant(s) in Hz; integration.) Proton-decoupled ¹³C NMR spectra were recorded on an AVANCE III 500 MHz w/ direct cryoprobe (125 MHz) spectrometer and are reported in ppm using solvent as an internal standard (CDCl₃ at 77.16 ppm, (CD₃)₂SO at 39.52 ppm). ⁷⁷Se spectra were acquired at 26 °C on a 400 MHz Agilent 400MR-DD2 spectrometer equipped with a OneNMR probe and a 7600AS autosampler; this system was funded by NSF CRIF grant CHE-104873. Optical rotations were measured on a Perkin Elmer Model 341 Polarimeter with a sodium lamp. Mass spectra were obtained on a WATERS Acquity-H UPLC-MS with a single quad detector (ESI) or an Agilent 7890 gas chromatograph equipped with a 5975C single quadrupole EI-MS detector.

1.7.1 Experimental Procedures For Synthesis of Enantiopure Imizadopyridinium Salts

Standardization of ^{11}B and ^{19}F Spectra

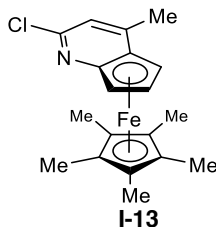
Standardization of all heteronuclear spectra was conducted using the unified scale according to eqn. (1) as described in *Pure Appl. Chem.* **2008**, *80*, 59-84.

$$(1) \quad E_X = 100 \times (\nu_X / \nu_o)$$

where ν_o = the absolute ^1H frequency of 0.00 ppm (δ_{TMS}) for experiments conducted in CDCl_3 ; OR $\nu_o = \delta_{\text{TMS}} + 0.062$ ppm for DMSO, OR $\delta_{\text{TMS}} - 0.160$ for acetone- d_6 , taken consecutively with heteronuclear experiments.

$$E_{77\text{Se}} = 19.071513$$

and ν_x = absolute frequency of the 0 ppm position for isotope x .

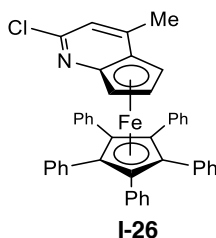


Pentamethyl- η^5 -cyclopentadienyl (3-chloro-1-methyl- η^5 -cyclopenta[b]pyridinyl)iron (I-13)

n-Butyl lithium in hexanes (1.52 M, 21.9 mL, 33.2 mmol) was added dropwise to a 0 °C solution of 1,2,3,4,5-pentamethylcyclopentadiene (5.47 mL, 33.2 mmol) in THF (170 mL), resulting in a milky-white solution. This slurry was stirred for 1 h at 0 °C, and added by cannula to a slurry of iron(II) chloride (4.21 g, 33.2 mmol) in THF (140 mL) at 0 °C (The FeCl₂ had been suspended in THF by sonication at 40 °C for 3 h or until the brown solids changed to a uniform white slurry). Additional portions of THF (2 x 20 mL) were added to completely transfer the white lithiate slurry. Upon completion of the addition, the resulting green solution was stirred at 0 °C for 1 h and at room temperature for 1 h. To a separate round bottom flask, n-Butyl lithium in hexanes (1.52 M, 19.9 mL, 30.2 mmol) was added dropwise to a solution of 2-chloro-4-methyl-5H-cyclopenta[b]pyridine⁷⁰ (5.00 g, 30.2 mmol) in THF (160 mL) at -78 °C and stirred for 1 h at -78 °C and then warmed to 0 °C and stirred an additional 10 min. This solution was then transferred by cannula the stirring solution of Cp*FeCl in THF at 0 °C. After completion of the addition, the reaction mixture was allowed to slowly warm from 0 °C to ambient temperature and stirred for 5-8 h (The reaction was monitored by TLC analysis (20% EtOAc/Hexanes) product appears as dark purple spot). The reaction mixture was filtered through a short silica pad, rinsing with DCM and then concentrated under vacuum. The product was purified by flash chromatography on silica gel (5 to 10% EtOAc/Hexanes) to afford the corresponding ferrocenyl chloride (9.15 g, 25.7 mmol, 85% yield). *Note: Bench stable intermediate. A 20-30% decrease in yield was*

observed when the reaction time was prolonged well past completion (additional 6-12 h).

Analytical data for **1**: ^1H NMR (500 MHz, CDCl_3) δ 6.71 (d, $J = 1.19$ Hz, 1H), 4.70 (dd, $J = 1.14, 2.64$ Hz, 1H), 4.24 (d, $J = 1.14, 2.76$ Hz, 1H), 3.88 (t, $J = 2.72$ Hz, 1H), 2.39 (d, $J = 1.17$ Hz, 3H), 1.69 (s, 15H); ^{13}C NMR (126 MHz, CDCl_3) δ 154.83, 149.26, 116.54, 108.45, 80.81, 79.13, 76.57, 67.43, 62.08, 19.43, 10.17. IR (ATR, neat) 2905, 1699, 1653, 1571, 1559, 1523, 1507, 1457, 1379, 1246, 1096, 1065, 1027, 891 cm^{-1} . LCMS (ESI): Mass calcd for $\text{C}_{19}\text{H}_{22}\text{ClFeN}$ $[\text{M}]^+$, 355.1, 356.1, 357.1; found 355.2, 356.2, 357.2.

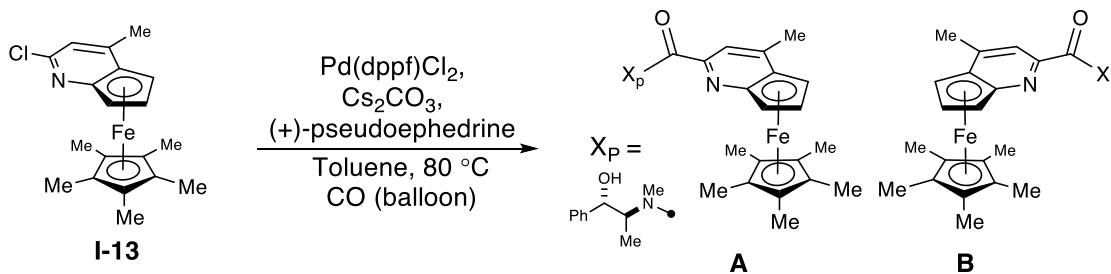


Pentaphenyl- η^5 -cyclopentadienyl (3-chloro-1-methyl- η^5 -cyclopenta[b]pyridinyl)iron (I-26)

n-Butyl lithium in hexanes (1.85 M, 4.96 mL, 8.62 mmol) was added dropwise to a 0 °C solution of 1,2,3,4,5-pentaphenylcyclopentadiene (3.90 mL, 8.72 mmol) in THF (60 mL), resulting in a red-orange solution. This slurry was stirred for 2 h at 0 °C, and added by cannula to a slurry of iron(II) chloride (1.07 g, 8.43 mmol) in THF (20 mL) at 0 °C (The FeCl_2 had been suspended in THF by sonication at 40 °C for 3 h or until the brown solids changed to a uniform white slurry). Additional portions of THF (2 x 20 mL) were added to completely transfer the red-orange lithiate slurry. Upon completion of the addition, the resulting green solution was stirred at 0 °C for 1 h and at room temperature for 1 h. To a separate round bottom flask, n-Butyl lithium in hexanes (1.85 M, 4.13 mL, 7.27 mmol) was added dropwise to a solution of 2-chloro-4-methyl-5H-cyclopenta[b]pyridine⁷⁰ (1.20 g, 7.27 mmol) in THF (30 mL) at -78 °C and stirred for 1 h at -78 °C and then warmed to 0 °C and stirred an additional 10 min. This solution was then

transferred by cannula the stirring solution of Cp*FeCl in THF at 0 °C. After completion of the addition, the reaction mixture was allowed to slowly warmed from 0 °C to 60 °C and stirred for 12 h (The reaction was monitored by TLC analysis (20% EtOAc/Hexanes) product appears as dark purple spot). The reaction mixture was filtered through a short silica pad, rinsing with DCM and then concentrated under vacuum. The product was purified by flash chromatography on silica gel (20 to 30% EtOAc/Hexanes) to afford the corresponding ferrocenyl chloride (3.14 g, 4.71 mmol, 65% yield). *Note: Bench stable intermediate. Product readily crystallizes out of solution; therefore it is recommended that column chromatography be carried out rapidly.*

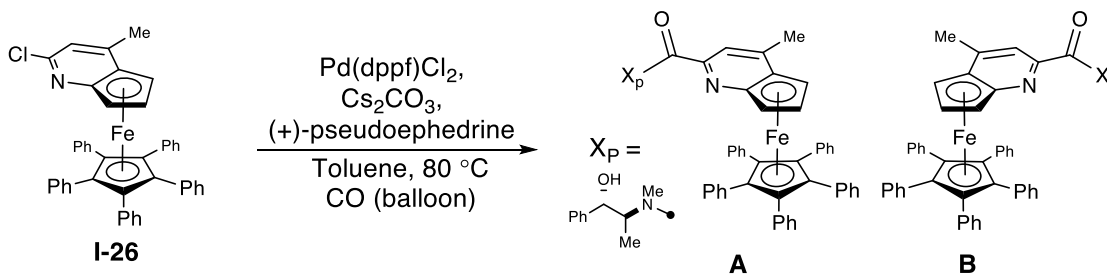
Analytical data for **n**: ¹H NMR (500 MHz, CDCl₃) δ 9.55 (s, 1H), 7.38 (d, *J* = 1.3 Hz, 1H), 7.20 – 7.12 (m, 5H), 7.06 (t, *J* = 7.6 Hz, 10H), 6.97 – 6.85 (m, 10H), 5.37 (dd, *J* = 2.6, 1.2 Hz, 1H), 5.13 (dd, *J* = 2.8, 1.2 Hz, 1H), 4.65 (t, *J* = 2.8 Hz, 1H), 2.41 (d, *J* = 1.1 Hz, 3H). ¹³C NMR (126 MHz, CDCl₃) δ 193.66, 156.23, 150.90, 134.33, 132.10, 127.40, 126.75, 115.40, 109.30, 88.70, 86.18, 82.11, 71.22, 65.19, 20.72. IR (TR, neat): 3055, 2922, 2852, 1250, 896 cm⁻¹.



Pentamethyl- η^5 -cyclopentadienyl-(N-((1*S*,2*S*)-1-hydroxy-1-phenylpropan-2-yl)-N,1-dimethyl- η^5 -cyclopenta[*b*]pyridinyl-3-carboxamide)iron (I-21A/B)

CAUTION: Carbon Monoxide is toxic, all reactions using carbon monoxide should be done in a well-ventilated fume hood, and the use of a CO detector is highly recommended for additional safety. A flame dried round-bottom flask equipped with a stirbar was charged with Pentamethyl- η^5 -cyclopentadienyl (3-chloro-1-methyl- η^5 -cyclopenta[*b*]pyridinyl)iron (**I-13**) (1.50 g, 4.22 mmol) and (1*S*, 2*S*)-(+)-pseudoephedrine (1.39 g, 8.43 mmol). The flask was then taken into the glovebox where Pd(dppf)Cl₂ (241 mg, 0.295 mmol) and cesium carbonate (2.06 g, 6.33 mmol) were added and the flask was then sealed with a teflon septum. After taking the flask out of the glovebox, Toluene (42.0 mL) was added and then carbon monoxide was bubbled through the solution for 10 min. The reaction mixture was then heated to 80 °C under carbon monoxide (1 atm, balloon). After the reaction was deemed complete by TLC analysis (50% EtOAc/Hexanes, 6-8 h, R_f~0.25 (dark blue, no stain), R_f~0.15 (lavender, no stain)) the reaction mixture was allowed to cool to ambient temperature, opened to air, and stirred for 10 min. The reaction mixture was then directly loaded onto a column of silica gel (40-90% EtOAc/Hexanes) to afford the pure diastereomers (1.40 g, 65% combined yield) as dark, foamy purple solids. Absolute configurations were determined from the crystal structure of the NHC prepared from the corresponding material. Note: The amide decomposes at ambient temperature, but can be stored

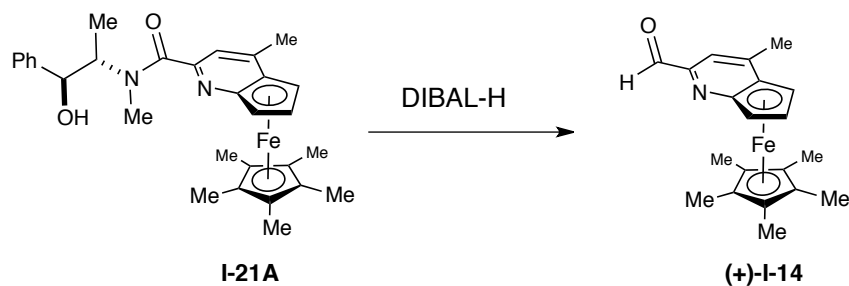
at -30 °C >2 months. Analytical data for the (+)-amide (**I-21A**) Rf~0.25: ^1H NMR (500 MHz, C_6D_6) δ 8.10 (d, $J = 7.5$ Hz, 1H), 7.38 (d, $J = 7.5$ Hz, 2H), 7.32 (s, 1H), 7.07 (d, $J = 7.4$ Hz, 1H), 4.89 (d, $J = 2.7$ Hz, 1H), 4.59 (m, 2H), 4.07 (d, $J = 2.8$ Hz, 1H), 3.78 (m, 1H), 3.10 (s, 3H), 2.06 (s, 3H), 1.51 (s, 15H), 0.58 (d, $J = 5.4$ Hz, 3H); ^{13}C NMR (126 MHz, CD_2Cl_2) δ 168.86, 155.14, 153.91, 144.23, 128.34, 127.41, 127.03, 116.90, 105.89, 83.38, 79.06, 78.17, 75.59, 66.61, 62.42, 58.56, 26.80, 19.55, 16.19, 9.78. IR (ATR, neat) 3233, 2905, 2361, 1698, 1635, 1559, 1473, 1456, 1381, 1285, 1054, 1027, 768, 729, 702 cm^{-1} . LCMS (ESI): Mass calcd for $\text{C}_{30}\text{H}_{37}\text{FeN}_2\text{O}_2$ $[\text{M}+\text{H}]^+$, 513.2; found 513.3.



Pentaphenyl- η^5 -cyclopentadienyl-(N-((1S,2S)-1-hydroxy-1-phenylpropan-2-yl)-N,1-dimethyl- η^5 -cyclopenta[b]pyridinyl-3-carboxamide)iron

A flame dried 2 dram vial equipped with a stir bar was charged with Pentaphenyl- η^5 -cyclopentadienyl (3-chloro-1-methyl- η^5 -cyclopenta[b]pyridinyl)iron (1.1 g, 1.652 mmol) and (1S, 2S)-(+)-pseudoephedrine (0.546 g, 3.30 mmol). The vial was then taken into the glovebox where Pd(dppf)Cl_2 (0.202 g, 0.248 mmol) and Cs_2CO_3 (807 mg, 2.47 mmol) was added. The vial was then sealed with a screwcap with a teflon septa and the vial was taken out of the glovebox. Toluene (Volume: 33.0 ml) was then added to the reaction mixture under nitrogen and carbon monoxide was then bubbled through the solution for 15 min. The reaction mixture was then heated at 80 °C under a balloon of CO. After the reaction was deemed complete by TLC analysis

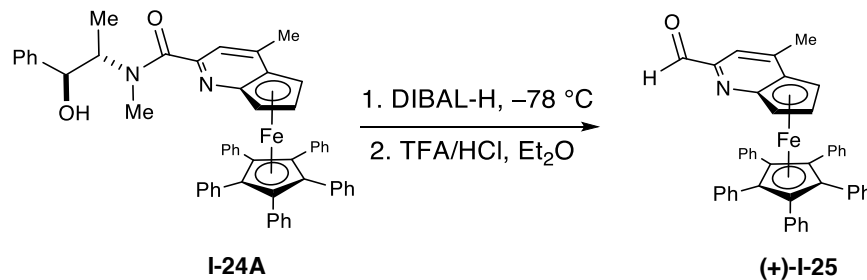
((+, Rf ~0.2; (-) Rf ~0.15; 10:10:80 DCM:Acetone:hexanes) the reaction was filtered through celite, concentrated and purified by column chromatography (loaded with DCM, eluted with 5:5:90 DCM:Acetone:Hexanes) to provide the two separate diastereomers (470 mg, 37% combined yield). Analytical data for **I-24A**: ^1H NMR (500 MHz, CDCl_3) δ 7.51 (s, 1H), 7.46 – 7.33 (m, 3H), 7.33 – 7.26 (m, 1H), 7.17 (t, $J = 7.2$ Hz, 6H), 7.08 (t, $J = 7.6$ Hz, 10H), 6.96 (d, $J = 7.6$ Hz, 10H), 5.29 (s, 1H), 5.15 – 5.01 (m, 1H), 4.71 (s, 1H), 4.55 – 4.46 (m, 2H), 4.20 (s, 1H), 2.43 (s, 3H), 2.35 (s, 3H), 1.02 (d, $J = 6.9$ Hz, 3H). ^{13}C NMR (126 MHz, CDCl_3) δ 170.55, 156.20, 150.48, 142.49, 134.72, 132.23, 128.57, 127.97, 127.43, 127.08, 126.79, 120.85, 109.28, 86.98, 86.34, 80.12, 77.16, 69.91, 63.87, 58.44, 32.75, 20.73, 14.75. IR (ATR, neat): 3568, 3084, 3055, 2924, 2854, 1620, 1483, 1073, 740, 699 cm^{-1} .



(+)-Pentamethyl- η^5 -cyclopentadienyl (1-methyl- η^5 -cyclopenta[b]pyridinyl-3-carbaldehyde)iron (I-14)

Diisobutylaluminum hydride (0.9 M in hexane, 0.43 mL, 0.39 mmol) was added dropwise to a solution of pseudoephedrine amide **I-21A** (50 mg, 0.10 mmol) in THF (2 mL) at -78 °C (acetone/ $\text{CO}_2(\text{s})$) and the reaction mixture was allowed to stir at -78 °C for 2 h; the reaction was monitored by TLC analysis (50% EtOAc/Hex, reaction quenched with methanol in spotter). Once the reaction was deemed complete it was carefully quenched with wet MeOH at -78 °C.

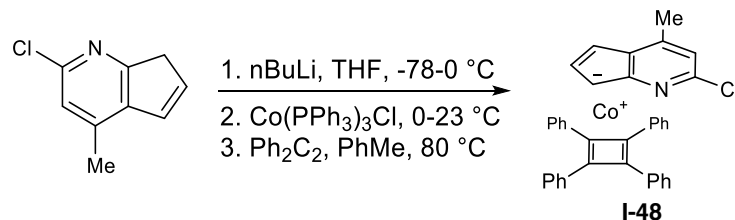
The reaction mixture was then diluted with diethyl ether and a saturated solution of potassium sodium tartrate was added. The reaction mixture was then warmed to ambient temperature and stirred for 4 h. The organic layer was then separated and the aqueous layer was extracted with diethyl ether (3 x 10 mL). The combined organic layers were then washed with brine, dried over MgSO₄, and concentrated *in vacuo*. The product was purified by flash chromatography on silica gel (10-20% EtOAc/Hex, green band) to afford the corresponding ferrocenyl aldehyde as a green solid (27 mg, 78% yield). Note: The aldehyde is bench stable (>2 months). Analytical data: ¹H NMR (500 MHz, CDCl₃) δ 9.97 (s, 1H), 7.33 (d, *J* = 1.24 Hz, 1H), 4.92 (dd, *J* = 1.03, 2.85 Hz, 1H), 4.54 (dd, *J* = 1.09, 2.88 Hz, 1H), 4.20 (t, *J* = 2.77 Hz, 1H), 2.47 (d, *J* = 1.16 Hz, 3H), 1.59 (s, 15H); ¹³C NMR (126 MHz, CDCl₃) δ 193.56, 155.00, 151.67, 111.70, 107.90, 85.39, 79.98, 78.98, 68.57, 63.87, 19.84, 9.91. IR (neat) ν 2923, 2854, 1693, 1539, 1457, 1375, 1309, 1147, 1027, 851, 773, 700 cm⁻¹. LCMS (ESI): Mass calcd for C₂₀H₂₄FeNO [M+H]⁺, 350.1; found 350.2. Enantiomeric ratio was measured by chiral phase HPLC (Regis (*S,S*)-Whelk-01, 25 cm x 4.6 mm; 5% IPA/hexanes 0.7 mL/min, 254 nm), Rt₁(-) = 25.1 min, Rt₂(+) = 27.5 min; >99% *ee*. Rt₂(+) [α]_D²⁰ = +22.4° (c = 0.005, MeOH).



(+)-Pentaphenyl- η^5 -cyclopentadienyl (1-methyl- η^5 -cyclopenta[b]pyridinyl-3-carbaldehyde)iron ((+)-I-25)

To a stirring solution of iron(II) 1,2,3,4,5-pentaphenylcyclopenta-2,4-dien-1-ide 2-(((1S,2S)-1-hydroxy-1-phenylpropan-2-yl)(methyl)carbamoyl)-4-methyl-5H-cyclopenta[b]pyridin-5-ide (325 mg, 0.395 mmol) in DCM (2 mL) at $-78\text{ }^{\circ}\text{C}$ was slowly added DIBAL-H (in Toluene, 1 M) (1.185 mL, 1.185 mmol). The reaction mixture was then allowed to stir at $-78\text{ }^{\circ}\text{C}$ for 1 h and monitored by TLC analysis (30 mol% EtOAc/Hex, observed both aldehyde $R_f \sim 0.5$ and aminal $R_f \sim 0.4$ on TLC). The reaction was allowed to stir another hour at $-78\text{ }^{\circ}\text{C}$ and then the reaction was quenched with Rochelle's salt and extracted with ether. To the combined ethereal layers was then added a solution of TFA (1 mL) in 1M HCl (30 mL), and the biphasic solution was stirred or shaken in a separatory funnel until no aminal was present by TLC analysis (pink spot, 30% EtOAc/Hex). The ethereal layer was then separated, washed with sat. NaHCO_3 , brine, dried over MgSO_4 , and concentrated. The crude reaction mixture was then purified by column chromatography on silica gel (20% EtOAc/Hex) to yield the product (104 mg, 0.158 mmol, 40% yield) as a dark-green solid. Analytical data: ^1H NMR (500 MHz, CDCl_3) δ 7.37 – 7.29 (m, 4H), 7.29 – 7.24 (m, 1H), 7.23 – 7.15 (m, 5H), 7.14 (s, 3H), 7.09 (dd, $J = 7.3, 1.6$ Hz, 1H), 6.99 (ddd, $J = 8.8, 7.3, 1.6$ Hz, 1H), 6.65 (td, $J = 7.4, 1.2$ Hz, 1H), 6.29 (d, $J = 8.1$ Hz, 1H), 5.49 (brs, 1H), 4.52 (d, $J = 3.8$ Hz, 1H), 4.29 (d, $J = 3.9$ Hz, 1H), 2.78 (q, $J = 7.6$ Hz, 4H), 1.36 (t, $J = 7.6$ Hz,

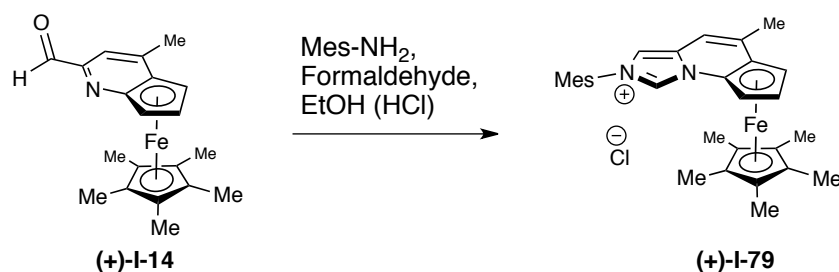
6H); ^{13}C NMR (126 MHz, CDCl_3) δ 144.74, 144.16, 142.68, 141.51, 139.61, 129.96, 128.67, 128.33, 128.30, 128.22, 127.34, 127.32, 127.06, 126.90, 126.53, 126.46, 116.39, 111.38, 63.60, 61.06, 29.12, 15.90. IR (ATR, neat): 3054, 2917, 2849, 1710, 1224, 743, 699 cm^{-1} .



(η^4 -tetraphenylcyclobutadiene)-[η^5 -(2-chloro-4-methylcyclopenta[b]pyridin-7-yl)]cobalt (I-48**)**

To a stirring solution of 2-chloro-4-methyl-7H-cyclopenta[b]pyridine (0.25 g, 1.51 mmol) cooled to $-78\text{ }^\circ\text{C}$ was added 2.17 M *n*-BuLi in cyclohexane (0.70 mL, 1.51 mmol) in 2 mL of THF, and the mixture was stirred for 30 min. The cooling bath was then replaced with ice and stirred for an additional 30 min. $\text{Co}(\text{PPh}_3)_3\text{Cl}$ (1.56 g, 1.31 mmol) in 5 mL toluene was then added to the resultant solution at $0\text{ }^\circ\text{C}$ and stirred for 10 min, whereupon diphenylacetylene (0.54 g, 3.02 mmol) in 5 mL toluene was added, and the mixture was refluxed for 5 h. The reaction mixture was cooled, solvent was evaporated off, and the residue was chromatographed on a silica column. 3 CV of hexanes were passed through to elute PPh_3 . The mobile phase was then gradually ramped to 100% DCM. A light yellow band was observed to elute first, followed by the product as red band. Evaporation of the solvent gave 0.305 g (1.31 mmol, 40% yield) of a red orange solid. Analytical data for **I-48**: ^1H NMR (500 MHz, Chloroform-*d*) δ 7.35 – 7.30 (m, 8H), 7.30 – 7.27 (m, 3H), 7.27 – 7.21 (m, 10H), 6.36 (d, $J = 1.3$ Hz, 1H), 5.28 (dd, $J = 2.9, 1.4$ Hz, 1H), 5.13 (dd, $J = 3.0, 1.4$ Hz, 1H), 4.86 (t, $J = 3.0$ Hz, 1H), 1.91 (s, 3H). ^{13}C NMR (126 MHz,

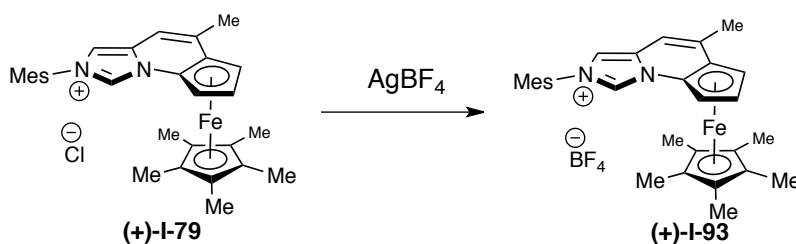
CDCl₃) δ 150.36, 148.79, 134.85, 128.72, 128.28, 126.90, 118.73, 117.28, 91.25, 88.84, 77.82, 77.16, 75.46, 71.02, 18.80. IR (TR, neat): 3058, 2917, 2850, 1532, 1254, 896, 731, 697 cm⁻¹. X-ray quality crystals were obtained by precipitation with n-pentane from a saturated chloroform solution at 23 °C.



(+)-Ferrocenyl mesityl imidazolium chloride ((+)-I-79)

Our NHCs were prepared by a modified literature procedure.⁸¹ A 2 dram vial equipped with a stir bar was charged with formaldehyde (37%, 181 mg, 2.23 mmol), THF (5 mL), and 2,4,6-trimethylaniline (166 mg, 1.23 mmol). The mixture was stirred at ambient temperature for 20 min. and then HCl (3.0 M in EtOH, 0.457 mL, 1.34 mmol) was added and the mixture was stirred for 30 min. Pentamethyl- η^5 -cyclopentadienyl (1-methyl- η^5 -cyclopenta[b]pyridinyl-3-carbaldehyde)iron (**3**) (390 mg, 1.1 mmol) was then added, and the reaction was allowed to stir at ambient temperature for 3 h and then concentrated. The residue was purified by flash chromatography on neutral alumina (Acetone to 5:1, acetone:EtOH), and then the residue was then washed with 5:1 Et₂O:EtOAc to afford the NHC as an orange solid (398 mg, 69%). Note: On occasion the reaction does not go to completion, in these cases the S.M. is isolated and resubjected to the reaction conditions. Note: The NHCs are bench stable, but hygroscopic and should be stored in a desiccator or glovebox. Analytical data: ¹H NMR (500 MHz, CDCl₃) δ 12.28 (s, 1H), 7.18 (s, 1H), 7.03 (d, J = 14.7 Hz, 2H), 7.00 (s, 1H), 6.82 (s, 1H), 6.29 (s, 1H),

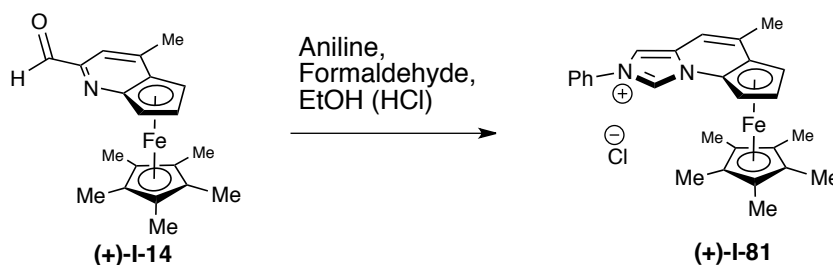
4.16 (d, $J = 2.60$ Hz, 1H), 3.99 (m, 1H), 2.37 (s, 3H), 2.34 (s, 3H), 2.23 (s, 3H), 2.08 (s, 3H), 1.62 (s, 15H); ^{13}C NMR (126 MHz, CDCl_3) δ 141.18, 141.09, 134.68, 133.78, 131.57, 130.59, 130.14, 130.05, 113.89, 105.16, 90.14, 81.46, 77.36, 76.98, 76.61, 73.63, 65.76, 64.94, 21.24, 19.51, 18.15, 17.96, 10.01. IR (neat) ν 3296, 3061, 2969, 2910, 1699, 1629, 1568, 1498, 1479, 1379, 1259, 1218, 1031 cm^{-1} . LCMS (ESI): Mass calcd for $\text{C}_{30}\text{H}_{35}\text{FeN}_2$ $[\text{M}]^+$, 479.4; found 479.5.



(+)-Ferrocenyl mesityl imidazolium tetrafluoroborate ((+)-I-93)

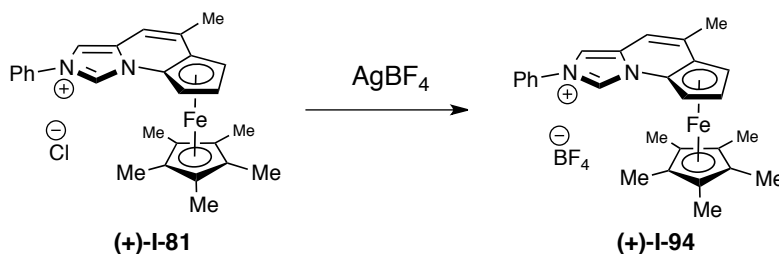
A flame-dried 2 dram vial equipped with a stirbar was charged with the ferrocenyl imidazolium chloride (150 mg, 0.29 mmol). The solid was then dissolved in acetonitrile (2.9 mL) and then silver tetrafluoroborate (68 mg, 0.35 mmol) was added. The reaction mixture was allowed to stir at ambient temperature under nitrogen for 16 h. The reaction mixture was then concentrated in vacuo and the residue was purified by flash chromatography on neutral alumina (CH_2Cl_2 :EtOH, 7:1) to afford the pure tetrafluoroborate salt of the NHC (5) as an orange/red solid (149 mg, 90% yield). Analytical data for 5: ^1H NMR (500 MHz, CDCl_3) δ 10.10 (s, 1H), 7.24 (d, $J = 1.48$ Hz, 1H), 7.05 (s, 1H), 7.02 (s, 1H), 6.86 (s, 1H), 5.60 (m, 1H), 4.20 (m, 1H), 4.04 (q, $J = 2.55$ Hz, 1H), 2.39 (s, 3H), 2.36 (s, 3H), 2.18 (s, 3H), 2.01 (s, 3H), 1.66 (s, 15H); ^{13}C NMR (126 MHz, CDCl_3) δ 141.46, 141.37, 134.68, 133.77, 131.33, 131.06, 130.14, 130.03, 129.92, 114.57, 105.25, 89.81, 81.56, 73.86, 66.04, 63.31, 21.31, 19.54, 17.78, 17.51, 9.84. IR (ATR, neat) 3118,

2909, 1628, 1569, 1457, 1383, 1062 cm^{-1} . LCMS (ESI): Mass calcd for $\text{C}_{30}\text{H}_{35}\text{FeN}_2$ $[\text{M}]^+$, 479.4; found 479.5. $[\alpha]_{\text{D}}^{20} = +38.5^\circ$ ($c = 0.01$, MeOH).



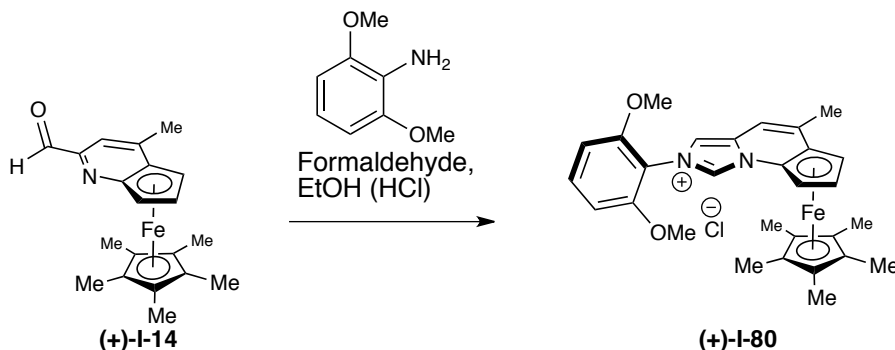
(+)-Ferrocenyl phenyl imidazolium chloride ((+)-I-81)

A 2 dram vial equipped with a stir bar was charged with formaldehyde (37%, 23.2 mg, 0.286 mmol), THF (1.5 mL), and aniline (16.0 mg, 0.17 mmol). The mixture was stirred at ambient temperature for 30 min. and then HCl (3.0 M in EtOH, 0.110 mL, 0.329 mmol) was added and the mixture was stirred for 30 min. (+)-Pentamethyl- η^5 -cyclopentadienyl (1-methyl- η^5 -cyclopenta[b]pyridinyl-3-carbaldehyde)iron ((+)-I-14) (50 mg, 0.143 mmol) was then added, and the reaction was allowed to stir at ambient temperature for 3 h while monitoring by TLC analysis (90:10:1, CH_2Cl_2 :MeOH:AcOH, $R_f \sim 0.25$). The residue was purified by flash chromatography on neutral alumina (Acetone to 5:1, acetone:EtOH), and then the residue was then washed with 5:1 Et_2O :EtOAc to afford the NHC as an orange solid (47.2 mg, 70%). Analytical data: ^1H NMR (500 MHz, CDCl_3) δ 12.76 (s, 1H), 8.08 (s, 2H), 7.74 (s, 1H), 7.60 (s, 2H), 7.47 (s, 1H), 6.82 (s, 1H), 6.21 (s, 1H), 4.15 (s, 1H), 3.99 (s, 1H), 2.34 (s, 3H), 1.63 (s, 17H); ^{13}C NMR (126 MHz, CDCl_3) δ 141.46, 134.98, 131.09, 130.90, 130.00, 121.56, 110.65, 105.22, 89.42, 81.58, 73.75, 65.98, 65.03, 19.56, 9.84. IR (ATR, neat) 3060, 2908, 1629, 1598, 1570, 1467, 1381, 1276, 1073, 1031, 829, 802 cm^{-1} . LCMS (ESI): Mass calcd for $\text{C}_{27}\text{H}_{29}\text{FeN}_2$ $[\text{M}]^+$, 437.2; found 437.3.



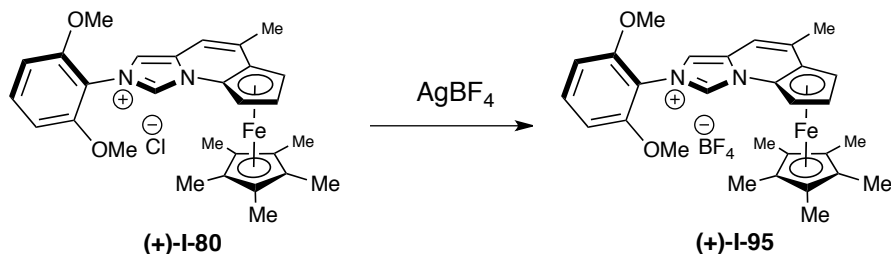
(+)-Ferrocenyl phenyl imidazolium tetrafluoroborate ((+)-I-94)

A flame-dried 2 dram vial equipped with a stirbar was charged with the ferrocenyl imidazolium chloride (35 mg, 0.074 mmol). The solid was then dissolved in acetonitrile (1 mL) and then silver tetrafluoroborate (17.3 mg, 0.089 mmol) was added. The reaction mixture was allowed to stir at ambient temperature under nitrogen for 16 h. The reaction mixture was then concentrated in vacuo and the residue was purified by flash chromatography on neutral alumina (CH_2Cl_2 :EtOH, 7:1) to afford the pure tetrafluoroborate salt of the NHC as an orange/red solid (34 mg, 88% yield). Analytical data: ^1H NMR (500 MHz, CDCl_3) δ 10.78 (s, 1H), 7.86, 7.80 (m, 2H), 7.78 (d, $J = 3.8$ Hz, 1H), 7.48 (m, 2H), 7.40 (t, $J = 7.5$ Hz, 1H), 6.84 (d, $J = 1.6$ Hz, 1H), 5.61 (s, 1H), 4.19 (s, 1H), 4.10 (m, 1H), 3.99 (d, $J = 2.7$ Hz, 1H), 2.31 (s, 3H), 1.58 (d, $J = 1.4$ Hz, 16H); ^{13}C NMR (126 MHz, CDCl_3) δ 141.25, 134.65, 131.33, 130.82, 130.19, 126.86, 121.53, 111.68, 105.44, 88.93, 81.58, 77.36, 73.74, 66.11, 63.43, 19.48, 9.61. IR (ATR, neat) 3060, 2908, 2854, 2360, 1630, 1383, 1072, 690, 589 cm^{-1} . LCMS (ESI): Mass calcd for $\text{C}_{27}\text{H}_{29}\text{FeN}_2 [\text{M}]^+$, 437.2; found 437.3. $[\alpha]_D^{20} = +53.5^\circ$ ($c = 0.01$, MeOH).



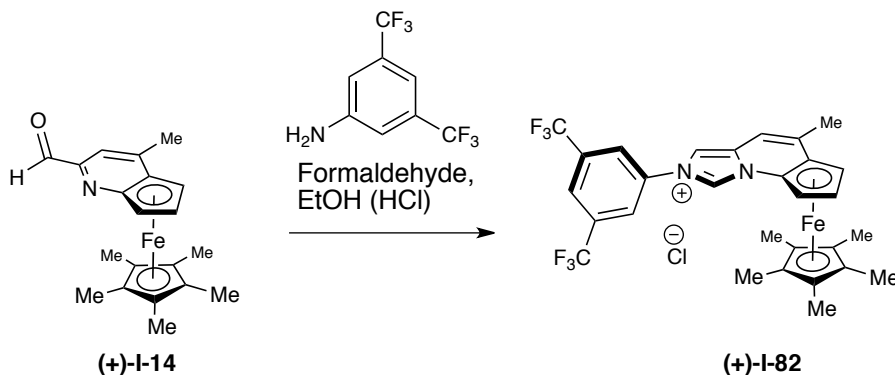
(+)-Ferrocenyl 2,6-dimethoxyphenyl imidazolium chloride ((+)-I-80)

A 2 dram vial equipped with a stir bar was charged with formaldehyde (37%, 69.7 mg, 0.859 mmol), THF (4.5 mL), and 2,6-dimethoxyaniline (79.0 mg, 0.515 mmol). The mixture was stirred at ambient temperature for 30 min. and then HCl (3.0 M in EtOH, 0.329 mL, 0.988 mmol) was added and the mixture was stirred for 30 min. (+)-Pentamethyl- η^5 -cyclopentadienyl (1-methyl- η^5 -cyclopenta[b]pyridinyl-3-carbaldehyde)iron ((+)-**I-14**) (150 mg, 0.429 mmol) was then added, and the reaction was allowed to stir at ambient temperature for ~3 h while monitoring by TLC analysis (90:10:1, CH_2Cl_2 :MeOH:AcOH, $R_f \sim 0.25$). The residue was purified by flash chromatography on neutral alumina (Acetone to 5:1, acetone:EtOH), and then washed with 5:1 Et_2O :EtOAc to afford the NHC as an orange solid (148 mg, 65%). Analytical data: ^1H NMR (500 MHz, Methanol- d_4) δ 11.85 (s, 1H), 7.42 (t, $J = 8.3$ Hz, 1H), 7.28 (s, 1H), 6.80 (s, 1H), 6.72 (d, $J = 8.4$ Hz, 2H), 6.32 (s, 1H), 4.11 (d, $J = 2.3$ Hz, 1H), 3.96 (d, $J = 2.5$ Hz, 1H), 3.89 (s, 6H), 2.34 (s, 3H), 1.68 (s, 19H). ; ^{13}C NMR (126 MHz, CDCl_3) δ 154.98, 139.56, 134.01, 132.11, 129.40, 115.50, 113.29, 105.53, 104.93, 89.72, 81.45, 76.65, 73.29, 65.61, 65.03, 56.84, 19.45, 9.83. IR (ATR, neat) 3022, 2898, 2362, 1624, 1603, 1541, 1258, 1115, 1029, 779 cm^{-1} . LCMS (ESI): Mass calcd for $\text{C}_{29}\text{H}_{33}\text{FeN}_2\text{O}_2$ $[\text{M}]^+$, 497.2; found 497.3.



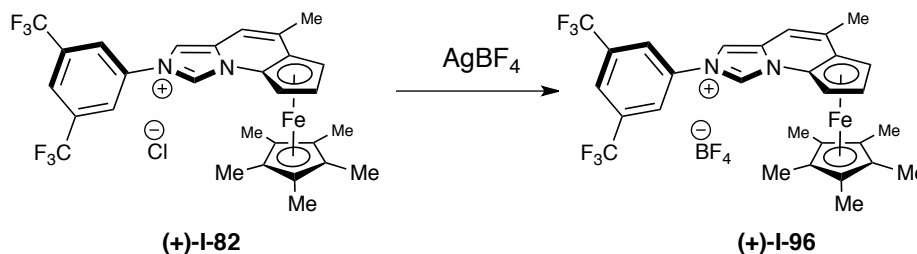
(+)-Ferrocenyl 2,6-dimethoxyphenyl imidazolium tetrafluoroborate ((+)-I-95)

A flame-dried 2 dram vial equipped with a stirbar was charged with the ferrocenyl imidazolium chloride (35 mg, 0.066 mmol). The solid was then dissolved in acetonitrile (1 mL) and then silver tetrafluoroborate (15.3 mg, 0.079 mmol) was added. The reaction mixture was allowed to stir at ambient temperature under nitrogen for 16 h. The reaction mixture was then concentrated in vacuo and the residue was purified by flash chromatography on neutral alumina (CH₂Cl₂:EtOH, 7:1) to afford the pure tetrafluoroborate salt of the NHC as an orange/red solid (33 mg, 86% yield). Analytical data: ¹H NMR (500 MHz, Methanol-*d*₄) δ 8.61 (s, 2H), 8.56 (s, 1H), 8.33 (s, 1H), 7.11 (s, 1H), 4.99 (d, *J* = 2.5 Hz, 1H), 4.51 (d, *J* = 2.6 Hz, 1H), 4.21 (t, *J* = 2.6 Hz, 1H), 2.44 (s, 3H), 1.64 (s, 15H); ¹³C NMR (126 MHz, CDCl₃) δ 142.59, 138.13, 135.16, 134.89, 133.08, 125.16, 124.93, 124.34, 122.99, 115.02, 107.10, 89.93, 82.75, 78.85, 74.74, 67.99, 63.05, 49.85, 49.46, 49.28, 29.53, 19.48, 9.67. IR (ATR, neat) 3128, 3060, 2946, 2909, 1632, 1603, 1486, 1266, 1114, 1031, 729 cm⁻¹. LCMS (ESI): Mass calcd for C₂₉H₃₃FeN₂O₂ [M]⁺, 497.2; found 497.3. [α]_D²⁰ = +47.8° (c = 0.01, MeOH).



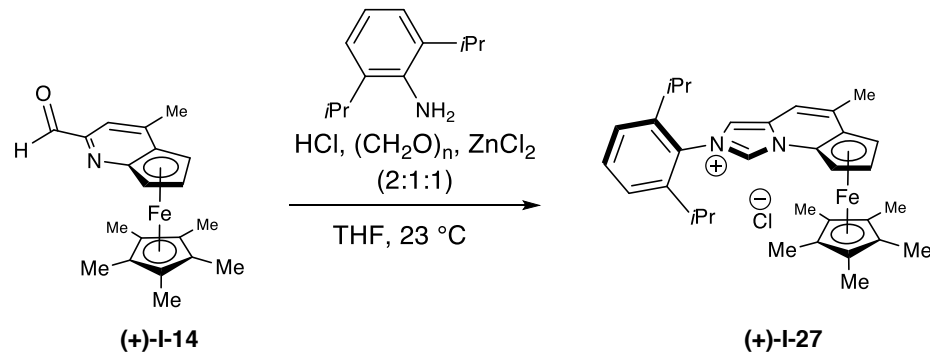
(+)-Ferrocenyl 3,5-bis(trifluoromethyl)phenyl imidazolium chloride ((+)-I-82)

A 2 dram vial equipped with a stir bar was charged with formaldehyde (37%, 69.7 mg, 0.859 mmol), THF (4.5 mL), and 3,5-bis(trifluoromethyl)aniline (118.0 mg, 0.515 mmol). The mixture was stirred at ambient temperature for 1 h and then HCl (3.0 M in EtOH, 0.329 mL, 0.988 mmol) was added and the mixture was stirred for 30 min. (+)-Pentamethyl- η^5 -cyclopentadienyl (1-methyl- η^5 -cyclopenta[b]pyridinyl-3-carbaldehyde)iron ((+)-**I-14**) (150 mg, 0.429 mmol) was then added, and the reaction was allowed to stir at ambient temperature for 24 h while monitoring by TLC analysis (90:10:1, CH₂Cl₂:MeOH:AcOH, R_f~0.25). After 24 h the reaction mixture was diluted with diethyl ether:pentane (1:1) and the resulting precipitate was filtered and washed with additional portions of ether:pentane to provide the NHC as a bright orange solid (133 mg, 51%). Analytical data: ¹H NMR (500 MHz, CDCl₃) δ 10.58 (s, 1H), 8.60 (s, 2H), 8.55 (s, 1H), 8.33 (s, 1H), 7.10 (s, 1H), 4.98 (d, J = 2.6 Hz, 1H), 4.51 (s, 1H), 4.27 - 4.16 (m, 1H), 2.43 (s, 3H), 1.67 - 1.61 (m, 15H); ¹³C NMR (126 MHz, CDCl₃) δ 142.59, 135.15, 134.87, 133.07, 124.32, 114.99, 107.07, 89.92, 82.74, 78.84, 74.72, 67.98, 63.01, 49.45, 19.46, 9.65. IR (ATR, neat) 3028, 2910, 2799, 1622, 1406, 1281, 1138, 1081, 1034, 698 cm⁻¹. LCMS (ESI): Mass calcd for C₂₉H₂₇F₆FeN₂ [M]⁺, 573.1; found 573.3.



(+)-Ferrocenyl phenyl 3,5-bis(trifluoromethyl)phenyl tetrafluoroborate ((+)-I-96)

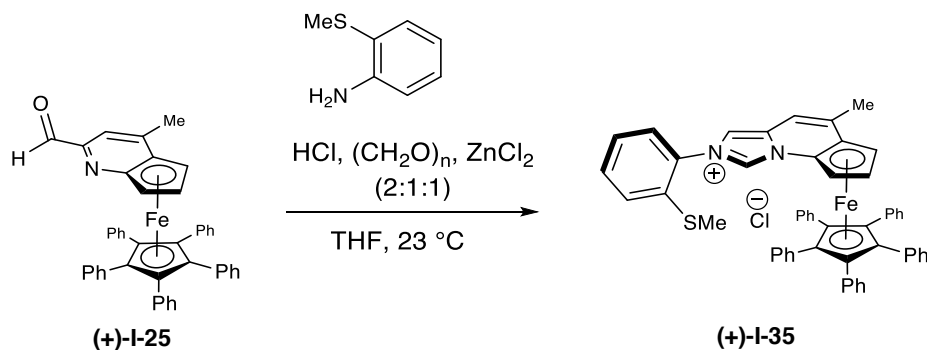
A flame-dried 2 dram vial equipped with a stirbar was charged with the ferrocenyl imidazolium chloride (25 mg, 0.041 mmol). The solid was then dissolved in acetonitrile (1 mL) and then silver tetrafluoroborate (9.6 mg, 0.049 mmol) was added. The reaction mixture was allowed to stir at ambient temperature under nitrogen for 16 h. The reaction mixture was then concentrated in vacuo and the residue was purified by flash chromatography on neutral alumina (CH_2Cl_2 :EtOH, 7:1) to afford the pure tetrafluoroborate salt of the NHC as an dark red solid (20.0 mg, 74% yield). Analytical data: ^1H NMR (500 MHz, CDCl_3) δ 10.10 (s, 1H), 7.24 (d, J = 1.48 Hz 1H), 7.05 (s, 1H), 7.02 (s, 1H), 6.86 (s, 1H), 5.60 (m, 1H), 4.20 (m, 1H), 4.04 (q, J = 2.55 Hz, 1H), 2.39 (s, 3H), 2.36 (s, 3H), 2.18 (s, 3H), 2.01 (s, 3H), 1.66 (s, 15H); ^{13}C NMR (126 MHz, CDCl_3) δ 141.46, 141.37, 134.68, 133.77, 131.33, 131.06, 130.14, 130.03, 129.92, 114.57, 105.25, 89.81, 81.56, 73.86, 66.04, 63.31, 21.31, 19.54, 17.78, 17.51, 9.84. IR (ATR, neat) 2917, 1708, 1622, 1572, 1474, 1384, 1280, 1180, 1081, 1035, 900, 534 cm^{-1} . LCMS (ESI): Mass calcd for $\text{C}_{29}\text{H}_{27}\text{F}_6\text{FeN}_2$ $[\text{M}]^+$, 573.1; found 573.3. $[\alpha]_D^{20} = +20.6^\circ$ ($c = 0.01$, MeOH).



(+)-Ferrocenyl 2,6-diisopropylphenyl imidazolium chloride ((+)-I-27)

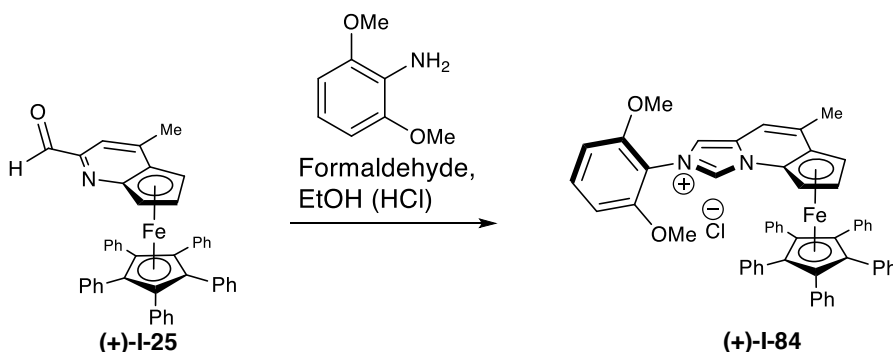
To a solution of 2,6-diisopropylaniline (13.7 μL , 0.072 mmol, 1.0 equiv.) and pentamethyl- η^5 -cyclopentadienyl (1-methyl- η^5 -cyclopenta[b]pyridinyl-3-carbaldehyde)iron (25.0 mg, 0.072 mmol, 1.0 equiv.) in THF (716 μL , 0.1 M) was added dropwise a solution of paraformaldehyde (2.6 mg, 0.086 mmol, 1.2 equiv.) and ZnCl_2 (11.7 mg, 0.072 mmol, 1.2 equiv.) in concentrated HCl (13.7 μL , 38% w/w, 2.4 equiv.). The dark-green solution was stirred at room temperature for 30 minutes, whereupon the reaction changed to a red-orange color and a small amount of precipitate was observed. The solvent was then removed *in vacuo* and the residue was redissolved in 1.0 mL dichloromethane. The resulting homogeneous solution was directly loaded on a column of neutral alumina and impurities were eluted using additional dichloromethane. The product was then eluted as a bright-orange band using CH_2Cl_2 :EtOH (5:1) to afford pure product (36 mg, 0.065 mmol, 90% yield). ^1H NMR (500 MHz, CDCl_3) δ 12.32 (s, 1H), 7.54 (t, $J = 7.8$ Hz, 1H), 7.33 (ddd, $J = 14.3, 7.9, 1.4$ Hz, 2H), 7.16 (s, 1H), 6.83 (s, 1H), 6.54 (s, 1H), 4.18 (d, $J = 2.6$ Hz, 1H), 4.02 (t, $J = 2.6$ Hz, 1H), 2.50 (p, $J = 6.8$ Hz, 1H), 2.39 (d, $J = 1.3$ Hz, 3H), 2.20 (p, $J = 6.8$ Hz, 1H), 1.71 (s, 15H), 1.41 (d, $J = 6.8$ Hz, 3H), 1.22 (d, $J = 6.9$ Hz, 3H), 1.10 (d, $J = 6.8$ Hz, 3H). ^{13}C NMR (126 MHz, CDCl_3) δ 145.85, 145.29, 141.69, 131.80, 131.03, 130.56, 124.82, 124.57, 115.00, 105.04, 90.39, 81.42, 77.16, 73.86, 65.81, 65.44, 29.02, 28.87,

25.09, 24.77, 24.66, 24.43, 19.59, 10.02. IR (ATR, neat): 3057, 2963, 2868, 1446, 1367, 808, 723 cm^{-1} . LCMS (ESI): Mass calcd for $\text{C}_{33}\text{H}_{41}\text{FeN}_2$ $[\text{M}]^+$, 521.6; found 521.4.



(+)-Pentaphenyl ferrocenyl 2-methylthiophenyl imidazolium chloride ((+)-I-35)

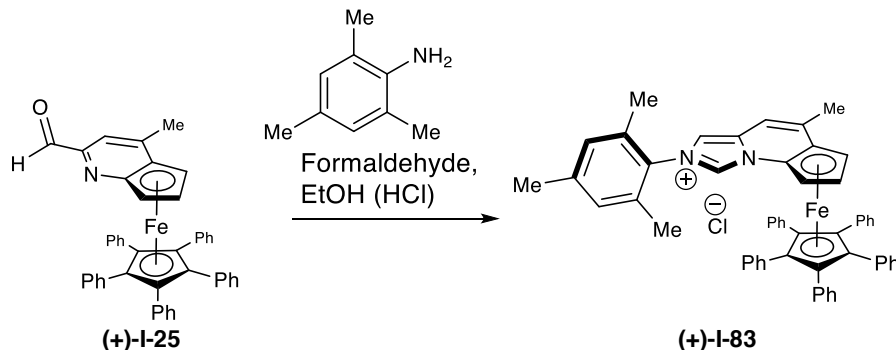
Prepared analogously to **I-27** using aldehyde **(+)-I-25** (30 mg, 0.045 mmol) and 2-(methylthio)aniline (7.6 mg, 0.055 mmol). The unpurified residue was purified by flash chromatography on neutral alumina using $\text{CH}_2\text{Cl}_2:\text{EtOH}(5:1)$ to afford **(+)-I-35** as a dark red solid (35 mg, 0.042 mmol, 93% yield). ^1H NMR (500 MHz, CDCl_3) δ 11.50 (d, $J = 1.5$ Hz, 1H), 7.74 (dd, $J = 8.2, 1.4$ Hz, 1H), 7.58 (d, $J = 1.4$ Hz, 1H), 7.52 (td, $J = 7.7, 1.3$ Hz, 1H), 7.38 (dt, $J = 8.0, 1.4$ Hz, 2H), 7.17 – 7.09 (m, 6H), 7.06 (dd, $J = 8.3, 6.8$ Hz, 11H), 6.98 – 6.83 (m, 12H), 6.31 (dd, $J = 2.9, 1.1$ Hz, 1H), 4.78 (dd, $J = 2.8, 1.1$ Hz, 1H), 4.55 (t, $J = 2.7$ Hz, 1H), 2.42 – 2.26 (m, 6H). ^{13}C NMR (126 MHz, CDCl_3) δ 138.71, 134.72, 133.89, 133.00, 132.30, 132.14, 131.48, 130.70, 128.07, 127.77, 127.59, 127.06, 127.03, 115.14, 110.27, 91.93, 87.87, 81.18, 77.16, 75.91, 67.84, 65.49, 20.41, 16.37) IR (ATR, neat): 3056, 2921, 1682, 1531, 731, 701 cm^{-1} . LCMS (ESI): Mass calcd for $\text{C}_{53}\text{H}_{41}\text{FeN}_2\text{S}$ $[\text{M}]^+$, 793.2, 794.2; found 793.4, 794.5.



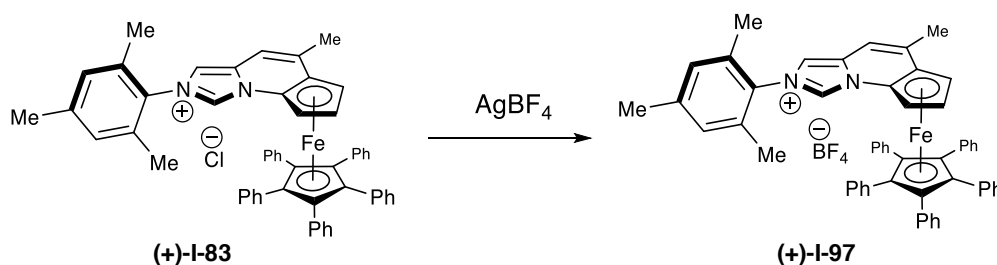
(+)-Ferrocenyl 2,6-dimethoxyphenyl pentaphenyl imidazolium chloride

Prepared analogously to **Cp* adduct** using aldehyde **I-25** (390 mg, 1.1 mmol) and 2,4,6-trimethyl aniline. The unpurified residue was purified by flash chromatography on neutral alumina using $\text{CH}_2\text{Cl}_2:\text{EtOH}(5:1)$ to afford the product as an orange solid (398 mg, 69%).

Analytical data: $^1\text{H NMR}$ (500 MHz, CDCl_3) δ 10.91 (s, 1H), 7.60 (s, 1H), 7.43 (t, $J = 8.6$ Hz, 1H), 7.17 - 7.10 (m, 5H), 7.10 - 7.00 (m, 10H), 6.94 - 6.85 (m, 10H), 6.68 (d, $J = 8.6$ Hz, 2H), 6.17 (dd, $J = 2.7, 1.2$ Hz, 1H), 4.73 (dd, $J = 2.8, 1.2$ Hz, 1H), 4.46 (t, $J = 2.7$ Hz, 1H), 3.64 (s, 6H), 2.32 (d, $J = 1.4$ Hz, 3H); $^{13}\text{C NMR}$ (126 MHz, CDCl_3) δ 154.25, 137.41, 133.84, 132.13, 132.00, 130.03, 127.43, 126.81, 116.73, 112.41, 110.64, 104.48, 91.77, 87.77, 87.73, 81.05, 75.63, 68.05, 64.52, 56.66, 20.34. IR (TR, neat): 3052, 2937, 2839, 1600, 1485, 1111, 741, 699 cm^{-1} . LCMS (ESI): Mass calcd for $\text{C}_{54}\text{H}_{43}\text{FeN}_2\text{O}_2$ $[\text{M}]^+$, 807.3; found 807.5.



(+)-Ferrocenyl mesityl pentaphenyl imidazolium chloride Prepared according to the general procedure using aldehyde **I-25** (390 mg, 1.1 mmol) and 2,4,6-trimethyl aniline. The unpurified residue was purified by flash chromatography on neutral alumina using $\text{CH}_2\text{Cl}_2:\text{EtOH}(8:1)$ to afford the product as an orange solid (398 mg, 69%). Analytical data for 22D: ^1H NMR (500 MHz, CDCl_3) 11.48 (s, 1H), 7.41 (d, $J = 1.5$ Hz, 1H), 7.17 - 7.10 (m, 4H), 7.06 (dd, $J = 8.4, 6.8$ Hz, 10H), 6.98 - 6.87 (m, 11H), 6.34 - 6.30 (m, 1H), 4.84 - 4.79 (m, 1H), 4.56 (t, $J = 2.7$ Hz, 1H), 2.38 (d, $J = 1.4$ Hz, 3H), 2.34 (s, 3H), 2.11 (s, 3H), 1.41 (s, 3H).

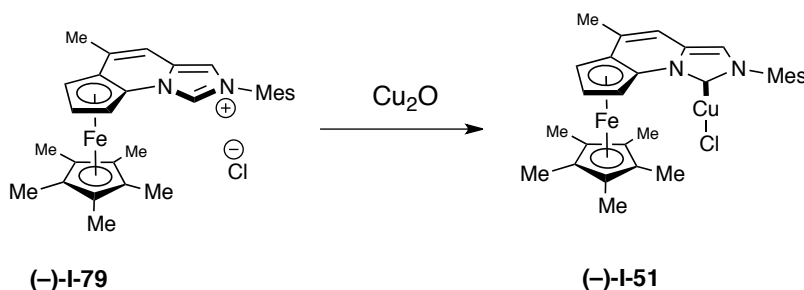


(+)-Ferrocenyl mesityl pentaphenyl imidazolium tetrafluoroborate

Prepared analogously to Cp* adduct using mesityl imidazolium chloride (60 mg, 0.073 mmol) and AgBF_4 (17 mg, 0.082 mmol, 1.2 equiv.). The unpurified residue was purified by flash chromatography on neutral alumina using $\text{CH}_2\text{Cl}_2:\text{EtOH}(8:1)$ to afford 22D as an orange solid (57 mg, 0.065 mmol, 89% yield). ^1H NMR (500 MHz, CDCl_3) δ 11.72 (d, $J = 1.5$ Hz, 1H), 7.24 (d, $J = 1.4$ Hz, 1H), 7.19 - 7.10 (m, 5H), 7.11 - 7.02 (m, 11H), 7.03 - 6.95 (m, 2H), 6.95 - 6.86

(m, 11H), 6.39 (dd, $J = 2.9, 1.1$ Hz, 1H), 4.80 (dd, $J = 2.7, 1.1$ Hz, 1H), 4.58 (t, $J = 2.7$ Hz, 1H), 2.38 (d, $J = 1.3$ Hz, 3H), 2.34 (s, 3H), 2.16 (s, 3H), 1.41 (s, 3H). ^{13}C NMR (126 MHz, CDCl_3) δ 141.04, 139.12, 135.11, 133.82, 133.59, 131.96, 131.36, 131.13, 130.09, 129.20, 127.50, 126.98, 114.41, 110.03, 92.51, 87.85, 81.04, 75.54, 67.47, 65.23, 21.15, 20.44, 18.15, 17.22. IR (TR, neat): 3053, 2919, 1600, 1501, 739, 698 cm^{-1} .

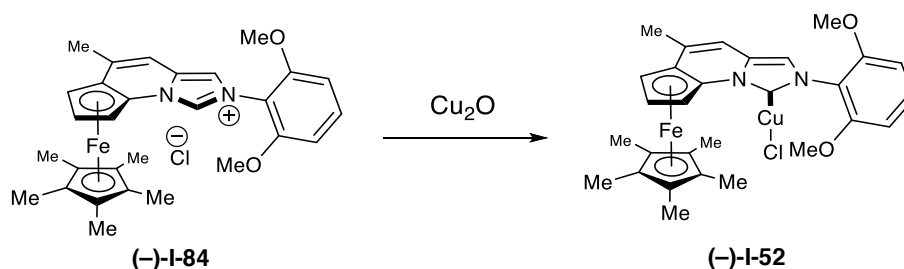
1.7.2 Synthesis of copper(I) chloride complexes



(-)-Ferrocenyl mesityl imidazolium Copper Chloride Complex ((-)-I-51)

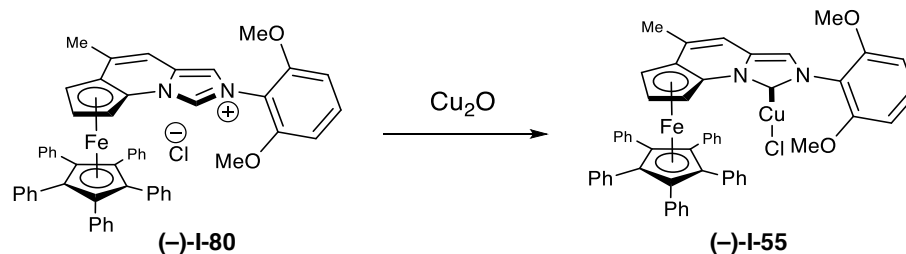
A flame-dried 2 dram vial equipped with a stirbar was brought into the glovebox and charged with the (-)-ferrocenyl imidazolium chloride (20 mg, 0.039 mmol) and copper(I) oxide (5.3 mg, 0.037 mmol). The vial was then sealed with a screw-cap with a teflon coated septa and then brought out of the glovebox. THF (0.37 mL) was then added and the mixture was heated to 60 °C. After 24 h the solution was concentrated and the residue was purified by column chromatography on silica gel (CH_2Cl_2 , Rf~0.4) to provide the complex as an orange solid (18 mg, 0.031 mmol). X-ray quality crystals were obtained by vapor diffusion (DCM /pentane, -30 °C). Analytical data: ^1H NMR (500 MHz, CDCl_3) δ 7.08 (s, 1H), 7.07 (s, 1H), 7.05 (s, 1H), 6.78

(s, 1H), 5.43 (m, 1H), 4.09 (s, 1H) 3.89 (d, $J = 2.89$ Hz, 1H), 2.39 (s, 3H), 2.29 (s, 3H), 2.29 (s, 3H), 2.16 (s, 3H), 1.97 (s, 3H), 1.67 (s, 15H); ^{13}C NMR (126 MHz, CDCl_3) δ 139.85, 136.62, 136.55, 135.53, 134.80, 131.51, 129.70, 129.66, 114.72, 107.96, 93.73, 81.21, 77.37, 71.73, 65.53, 62.79, 30.10, 21.27, 19.28, 18.35, 17.96, 10.22.



(-)-Ferrocenyl 2,6-dimethoxyphenyl imidazolium Copper Chloride Complex ((-)-I-52)

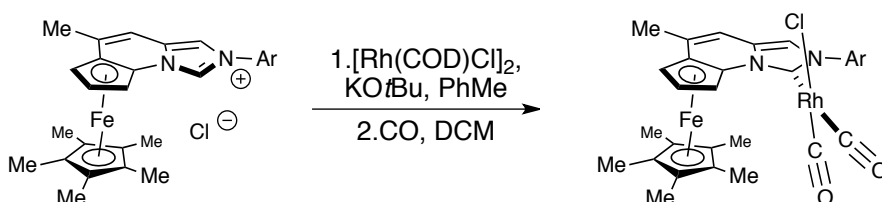
Prepared analogously to **I-51** using 2,6-dimethoxyphenyl imidazolium chloride (123 mg, 0.231 mmol) and copper(I) oxide (36 mg, 0.254 mmol). Obtained as a bright orange solid (130 mg, 0.218 mmol, 95% yield). X-ray quality crystals were obtained by vapor diffusion ($\text{CH}_2\text{Cl}_2/\text{pentane}$, -30 °C). ^1H NMR (500 MHz, CDCl_3) δ 7.39 (t, $J = 8.5$ Hz, 1H), 7.03 (s, 1H), 6.75 – 6.62 (m, 3H), 5.53 (dd, $J = 2.6, 1.2$ Hz, 1H), 3.99 (dd, $J = 2.6, 1.2$ Hz, 1H), 3.88 – 3.71 (m, 7H), 2.25 (d, $J = 1.4$ Hz, 3H), 1.67 (s, 15H). ^{13}C NMR (126 MHz, CDCl_3) δ 171.05, 156.00, 155.87, 135.08, 130.67, 130.05, 118.17, 115.88, 107.81, 104.72, 104.70, 93.18, 81.01, 71.25, 65.03, 62.85, 56.31, 56.10, 19.21, 9.99. IR (ATR, neat): 3107, 2921, 2852, 1596, 1481, 1100, 723 cm^{-1} . LCMS (ESI $^+$) mass calcd. for $\text{C}_{29}\text{H}_{32}\text{CuFeN}_2\text{O}_2$ [M-Cl] $^+$, 559.1; found 559.3.



(-)-Ferrocenyl 2,6-dimethoxyphenyl imidazolium Copper Chloride Complex ((-)-I-55)

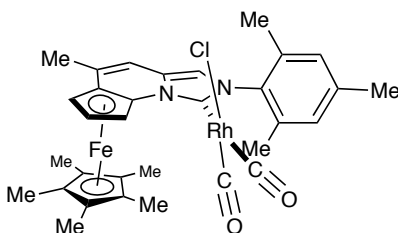
Prepared analogously to **I-52** using pentaphenyl imidazolium chloride (40 mg, 0.047 mmol) and copper(I) oxide (7.5 mg 0.052 mmol). Obtained as a bright orange solid (37 mg, 0.041 mmol, 86% yield) ^1H NMR (500 MHz, CDCl_3 -*d*) δ 7.37 (t, $J = 8.5$ Hz, 1H), 7.18 – 7.08 (m, 5H), 7.05 (dd, $J = 8.4, 6.8$ Hz, 10H), 7.01 – 6.92 (m, 11H), 6.77 (d, $J = 1.5$ Hz, 1H), 6.65 (d, $J = 8.5$ Hz, 2H), 6.04 (dd, $J = 2.7, 1.2$ Hz, 1H), 4.64 (dd, $J = 2.7, 1.2$ Hz, 1H), 4.38 (t, $J = 2.7$ Hz, 1H), 3.74 (s, 3H), 3.44 (s, 3H), 2.20 (d, $J = 1.3$ Hz, 3H). ^{13}C NMR (126 MHz, CDCl_3) δ 172.81, 155.74, 155.49, 147.70, 134.79, 133.86, 132.41, 132.07, 130.73, 130.62, 127.63, 127.42, 126.52, 117.90, 117.07, 116.29, 111.98, 104.66, 104.59, 104.23, 97.13, 87.61, 80.34, 73.90, 67.02, 63.38, 56.25, 55.98, 20.31. IR (ATR, neat): 3084, 3056, 2935, 2836, 1599, 1481, 1259, 1109, 740, 698. cm^{-1} . LCMS (ESI⁺) mass calcd. for $\text{C}_{54}\text{H}_{42}\text{CuFeN}_2\text{O}_2$ [M-Cl]⁺, 869.2; found 869.1.

1.7.3 Synthesis of Rhodium Carbonyl Complexes

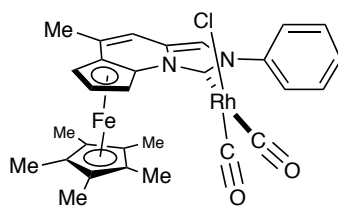


General procedure for the synthesis of rhodium dicarbonyl chloride complexes I-57–64.

CAUTION: Carbon Monoxide is toxic! All reactions using carbon monoxide should be performed in a well-ventilated fume hood, and the use of a CO detector is highly recommended for additional safety. A flame-dried 2 dram vial equipped with a stirbar was brought into a glovebox and charged with ferrocenyl imidazolium chloride (0.125 mmol, 2.2 eq.), $[\text{RhCODCl}]_2$ (0.056 mmol, 1 eq.), and potassium *tert*-butoxide (0.125 mmol, 2.2 eq). The vial was then charged with 1 mL of dry toluene (0.06 M) and stirred at 23 °C for 12 hours. The solution was eluted through a short plug of silica with 1:1 ethyl acetate:hexanes and concentrated in vacuo. The resulting concentrate was redissolved in 1 mL dry dichloromethane, and CO gas was bubbled through the solution while stirring for 2 hours at 23 °C. The solution was then concentrated in vacuo and washed with ice-cold *n*-pentane to remove residual 1,5-cyclooctadiene.

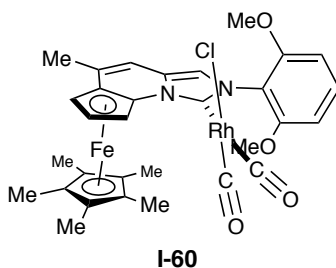
**I-58**

[RhCl(CO)₂(NHC-Mes)] (I-58): Obtained as dark red crystals (65 mg, 77% yield). Analytical data: ¹H NMR (500 MHz, CDCl₃) δ 7.08 (s, 1H), 7.03 (s, 2H), 6.71 (s, 1H), 5.91 – 5.85 (m, 1H), 3.98 – 3.95 (m, 1H), 3.86 (t, *J* = 2.6 Hz, 1H), 2.40 (s, 3H), 2.25 (s, 3H), 2.14 (s, 3H), 2.09 (s, 3H), 1.70 (s, 15H). ¹³C NMR (126 MHz, CDCl₃) δ 185.49 (d, *J*_{Rh,C} = 54.4 Hz), 183.12 (d, *J*_{Rh,C} = 74.9 Hz), 168.61 (d, *J*_{Rh,C} = 44.5 Hz), 139.48, 136.89, 136.49, 136.38, 133.58, 133.00, 129.73, 128.82, 115.08, 107.21, 93.48, 80.38, 76.40, 71.39, 67.31, 64.90, 21.23, 19.04, 18.98, 17.76, 10.04. IR (ν_{CO}) in CH₂Cl₂: 2078.49, 1997.38 cm⁻¹. TEP = 2049.21 cm⁻¹. X-ray quality crystals were obtained after slow evaporation of the reaction mixture (dichloromethane).

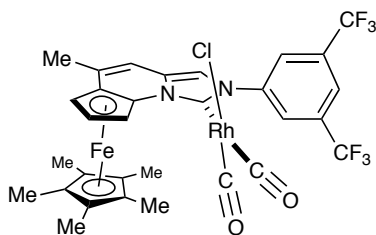
**I-62**

[RhCl(CO)₂(NHC-Ph)] (I-62): Obtained as dark red crystals (61 mg, 85% yield). Analytical data: ¹H NMR (500 MHz, CDCl₃) δ 7.87 – 7.81 (m, 2H), 7.59 – 7.50 (m, 3H), 7.37 (s, 1H), 6.71 (d, *J* = 1.5 Hz, 1H), 5.90 (dd, *J* = 2.7, 1.2 Hz, 1H), 3.96 (dd, *J* = 2.7, 1.2 Hz, 1H), 3.88 (t, *J* = 2.7 Hz, 1H), 2.25 (s, 3H), 1.65 (s, 15H). ¹³C NMR (126 MHz, CDCl₃) δ 185.87 (d, *J*_{Rh,C} = 54.4 Hz), 183.06 (d, *J*_{Rh,C} = 74.7 Hz), 167.73 (d, *J*_{Rh,C} = 44.7 Hz), 140.77, 136.91, 133.27, 129.27, 126.44,

114.70, 107.11, 93.26, 81.34, 80.61, 76.91, 71.78, 67.29, 65.21, 19.18, 9.91. IR (ν_{CO}) in CH_2Cl_2 : 2078.95, 1999.84 cm^{-1} . TEP = 2050.29 cm^{-1} . X-ray quality crystals were obtained by precipitation with n-pentane from a saturated dichloromethane solution at 23 °C.



[RhCl(CO)₂(NHC-2,6-OMe)] (I-60): Obtained as dark red crystals (45 mg, 71% yield). Analytical data: ¹H NMR (500 MHz, CDCl₃) δ 7.46 (t, J = 8.5 Hz, 1H), 7.11 (s, 1H), 6.72 (d, J = 8.2 Hz, 1H), 6.67 (m, 2H), 5.82 (s, 1H), 3.90 (s, 1H), 3.81 – 3.76 (m, 4H), 3.73 (s, 3H), 2.21 (s, 3H), 1.67 (s, 15H). ¹³C NMR (126 MHz, CDCl₃) δ 185.98 (d, $J_{\text{Rh,C}}$ = 54.1 Hz), 183.24 (d, $J_{\text{Rh,C}}$ = 74.8 Hz), 169.96 (d, $J_{\text{Rh,C}}$ = 44.6 Hz), 157.39, 155.66, 135.04, 132.03, 130.92, 118.29, 116.63, 107.56, 104.74, 103.09, 93.21, 80.39, 76.34, 71.29, 66.77, 64.72, 56.50, 55.41, 18.95, 9.74. IR (ν_{CO}) in CH_2Cl_2 : 2075.31, 1996.30 cm^{-1} . TEP = 2047.65 cm^{-1} . X-ray quality crystals were obtained by precipitation with n-pentane from a saturated dichloromethane solution at 23 °C.

**I-64**

[RhCl(CO)₂(NHC-3,5-CF₃)] (I-64): Obtained as dark red crystals (51 mg, 53% yield). Analytical data: ¹H NMR (500 MHz, CDCl₃) δ 8.47 (s, 2H), 8.04 (s, 1H), 7.47 (s, 1H), 6.72 (s, 1H), 5.87 (d, *J* = 2.7 Hz, 1H), 4.01 (s, 1H), 3.93 (m, 1H), 2.27 (s, 3H), 1.65 (s, 15H). ¹³C NMR (126 MHz, CDCl₃) δ 184.85 (d, *J*_{Rh,C} = 54.5 Hz), 182.65 (d, *J*_{Rh,C} = 74.2 Hz), 168.93 (d, *J*_{Rh,C} = 44.4 Hz), 141.83, 138.35, 134.12, 132.66 (q, *J*_{C,F} = 34.5 Hz), 126.45 (m), 123.74, 122.80 (m), 121.57, 113.70, 106.41, 92.79, 80.70, 76.32, 72.09, 67.22, 65.51, 19.14, 9.84. IR (ν_{CO}) in CH₂Cl₂: 2084.41, 2004.32 cm⁻¹. TEP = 2053.95 cm⁻¹. X-ray quality crystals were obtained by precipitation with n-pentane from a saturated dichloromethane solution at 23 °C.

1.7.4 Calculation of Tolman Electronic Parameter

Tolman electronic parameters (TEP) for complexes **I-57–64** were calculated using eqns. (1) and (2).¹⁰²

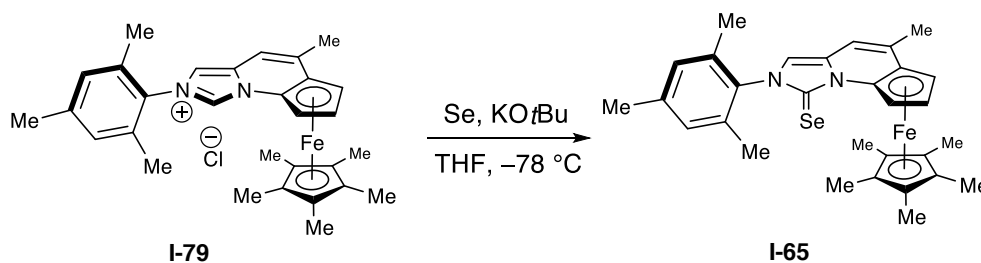
$$\nu_{Ir} = 0.8695\nu_{av}(\text{CO})[\text{Rh}] + 250.7 \text{ cm}^{-1}$$

$$\text{TEP} = 0.847\nu_{Ir} + 336 \text{ cm}^{-1}$$

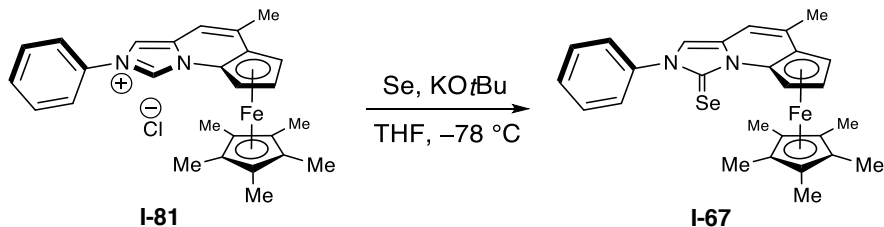
where $\nu_{av}(\text{CO})[\text{Rh}]$ is the average of the *cis* and *trans* carbonyl A_1 vibrational frequencies obtained by solution-phase IR spectroscopy.

1.7.5 General Synthesis of Selenourea Compounds.

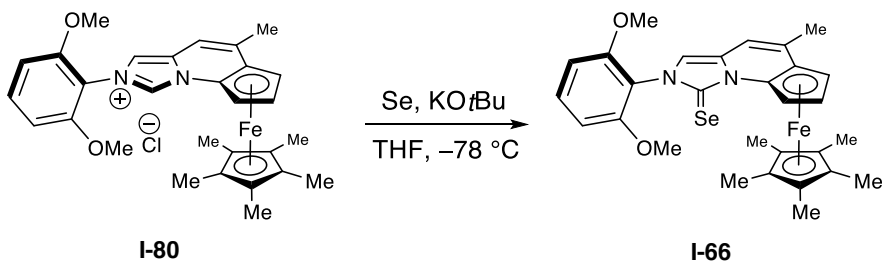
A modified synthesis of a reported procedure was used.¹ The NHC salt (0.04 mmol) and KO^tBu (1.2 – 1.8 equiv.) were weighed into a vial. Excess Se (10 mg) was added at -76 °C, followed by a stirrer bar, and the vial was purged with N₂. Dry THF (1 mL) was added and the resulting suspension was stirred at room temperature overnight. The solvent was then removed under vacuum, diluted with CH₂Cl₂ (5 mL), and passed through a pad of celite. The celite was washed with more CH₂Cl₂ (3 x 5 mL) and dried under vacuum. The crude product was loaded on a short alumina column and eluted with CH₂Cl₂ to afford the pure product.



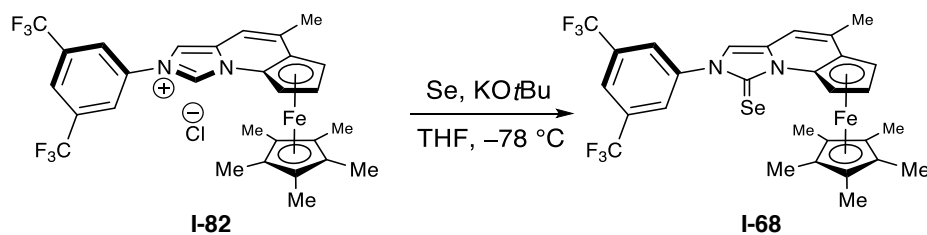
I-65 Obtained as an orange solid in 65% yield (15.3 mg). ¹H NMR (400 MHz, Acetone-*d*₆) δ 7.32 (s, 1H), 7.01 (d, J = 10.9 Hz, 2H), 6.76 (s, 1H), 6.63 (dd, J = 1.1, 1.0 Hz, 1H), 4.06 (dd, J = 1.1, 1.0 Hz, 1H), 3.85 (t, J = 2.1 Hz, 1H), 2.33 (s, 3H), 2.23 (s, 3H), 2.10 (s, 3H), 1.92 (s, 3H), 1.74 (s, 15H); ¹³C NMR (125 MHz, Acetone-*d*₆) δ 150.95, 139.51, 136.73, 136.16, 135.85, 135.22, 130.94, 129.69, 129.65, 113.79, 108.95, 94.62, 81.21, 77.55, 71.35, 65.29, 64.94, 21.10, 18.96, 18.68, 18.32, 10.42; ⁷⁷Se NMR (76 MHz, Acetone-*d*₆) δ 94.47.



I-67 Obtained as an orange solid in 95% yield (20.7 mg). ^1H NMR (500 MHz, Acetone- d_6) δ 7.65-7.62 (m, 2H), 7.57-7.48 (m, 4H), 6.76 (d, $J = 1.8$ Hz, 1H), 6.67 (dd, $J = 1.8, 1.7$ Hz, 1H), 4.05 (dd, $J = 1.8, 1.7$ Hz, 1H), 3.85 (t, $J = 3.4$ Hz, 1H), 2.23 (d, $J = 1.7$ Hz, 3H), 1.71 (s, 15H); ^{13}C NMR (125 MHz, Acetone- d_6) δ 151.61, 140.40, 135.44, 130.65, 129.67, 129.23, 128.05, 114.92, 108.64, 94.08, 81.32, 77.67, 71.47, 65.64, 65.47, 18.93, 10.15; ^{77}Se NMR (76 MHz, Acetone- d_6) δ 111.89.

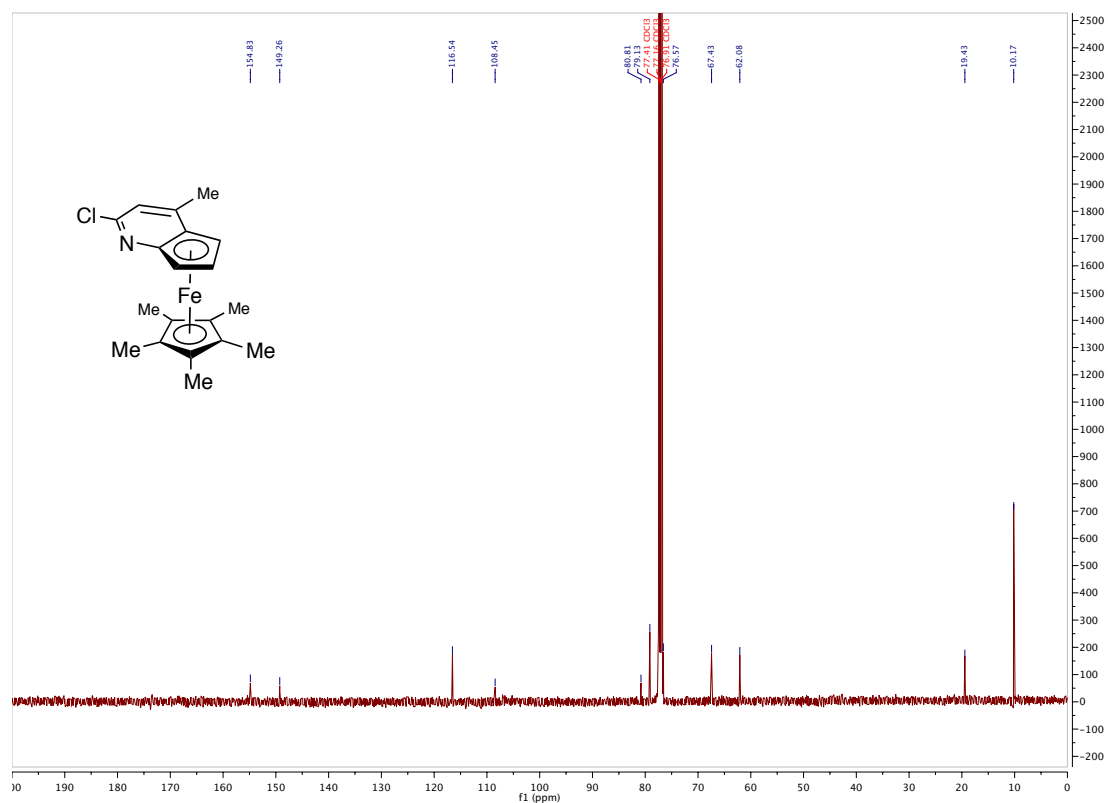
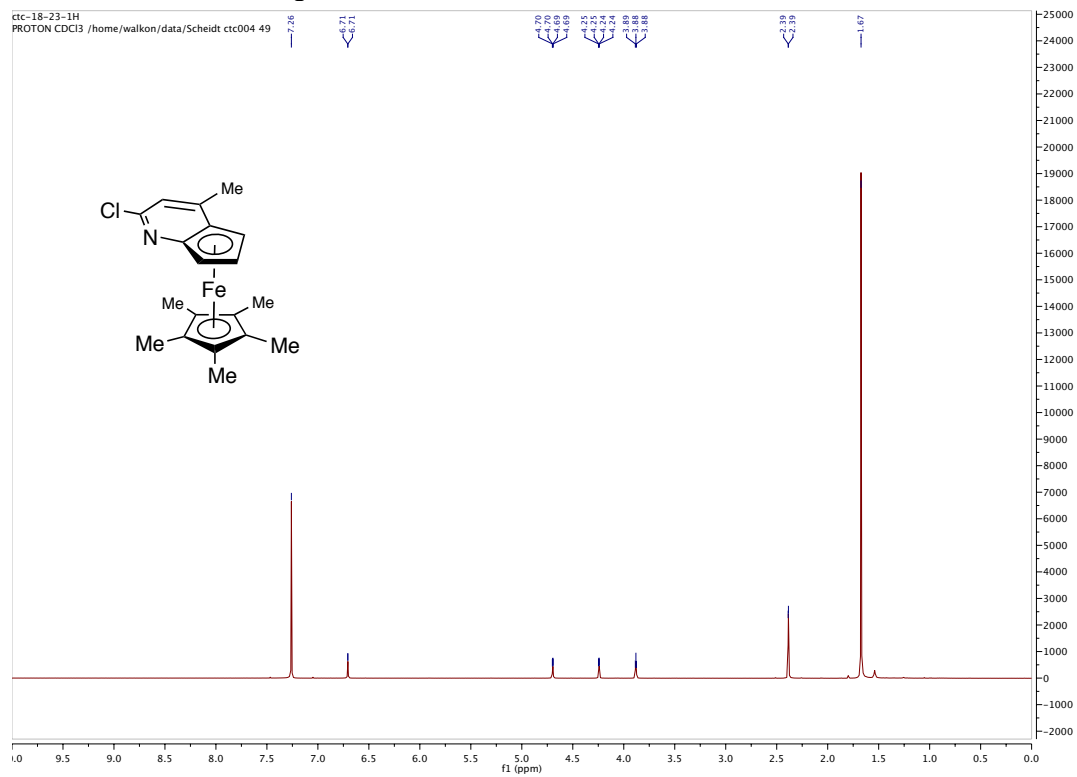


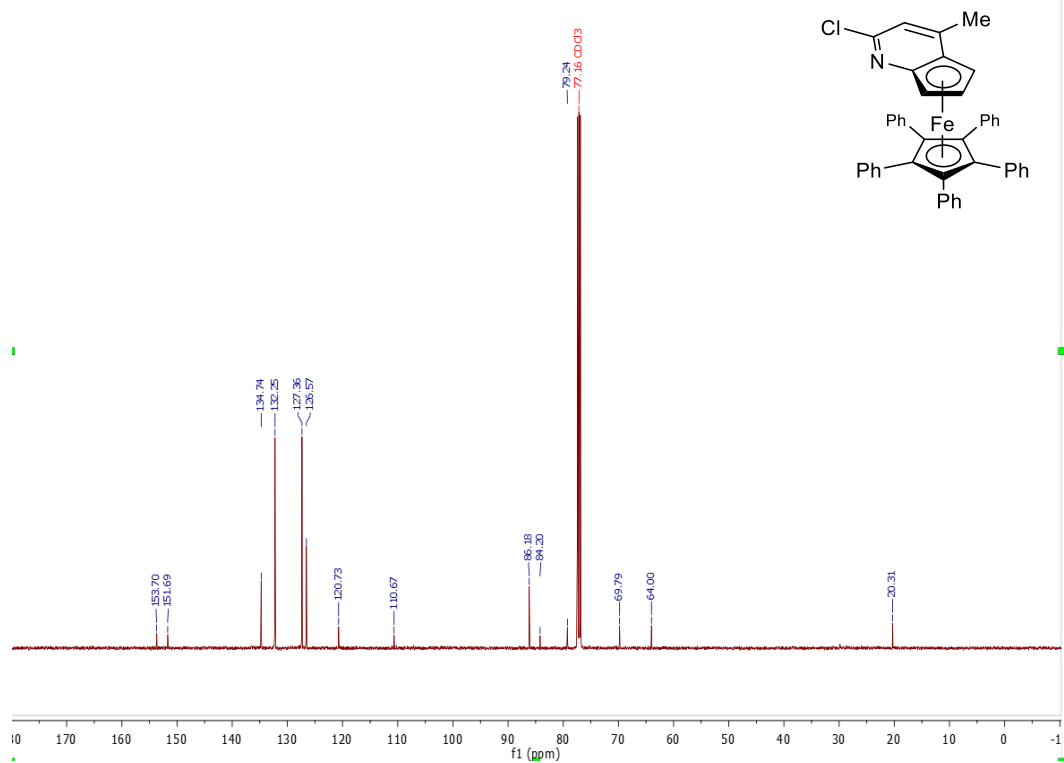
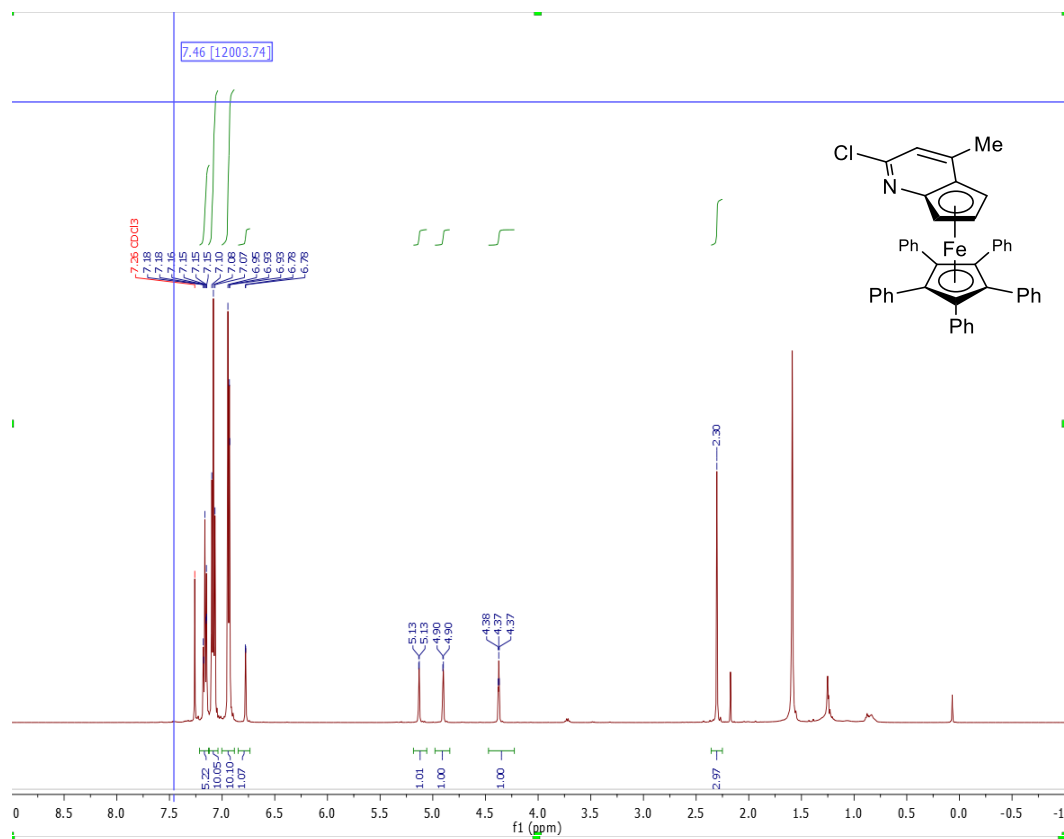
I-66 Obtained as an orange solid in 87% yield (21.0 mg). ^1H NMR (500 MHz, Acetone- d_6) δ 7.43 (t, $J = 8.5$ Hz, 1H), 7.22 (s, 1H), 6.80, (t, $J = 7.5$ Hz, 2H), 6.71 (d, $J = 1.6$ Hz, 1H), 6.64 (dd, $J = 1.3, 1.3$ Hz, 1H), 4.00 (dd, $J = 1.4, 1.3$ Hz, 1H), 3.80 (t, $J = 2.6$ Hz, 1H), 3.79 (s, 3H), 3.75 (s, 3H), 2.21 (d, $J = 1.0$ Hz, 3H), 1.73 (s, 15H); ^{13}C NMR (125 MHz, Acetone- d_6) δ 157.64, 157.48, 153.06, 134.09, 131.30, 130.04, 117.86, 115.63, 108.96, 105.65, 94.41, 81.28, 77.47, 71.08, 65.14, 56.49, 56.38, 18.92, 10.25; ^{77}Se NMR (76 MHz, Acetone- d_6) δ 99.96.

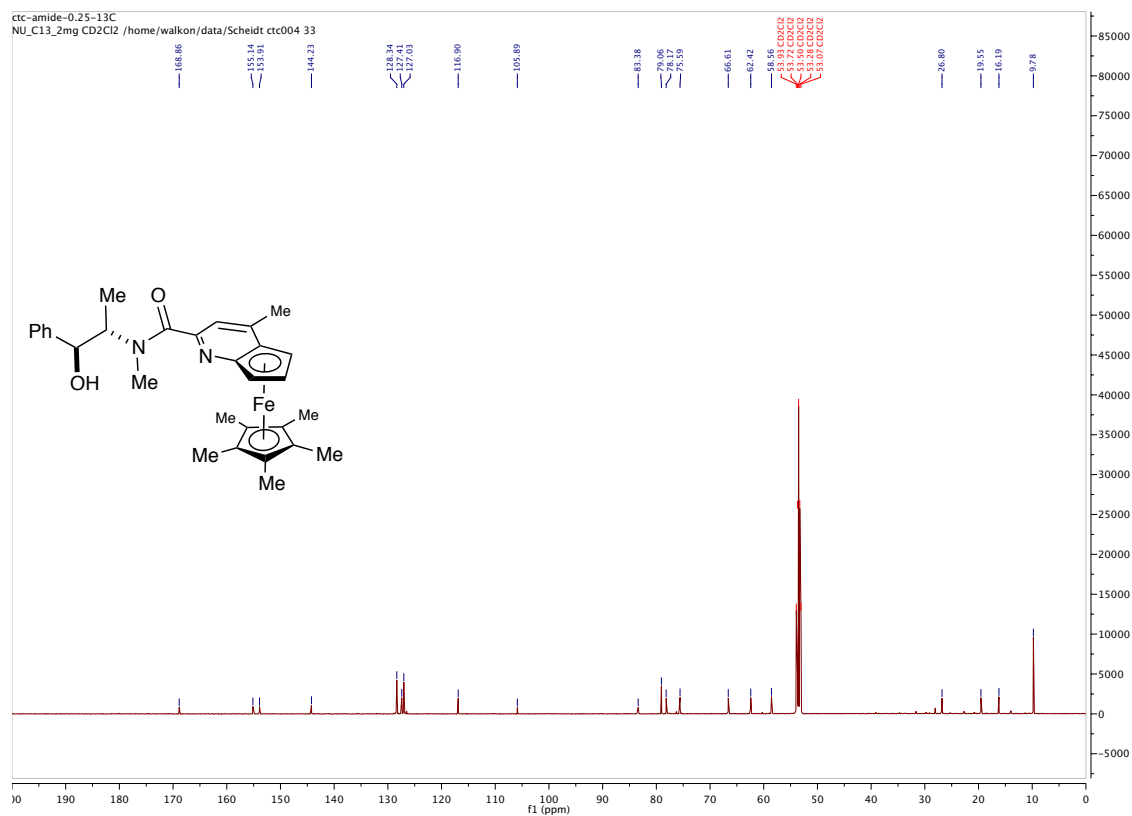
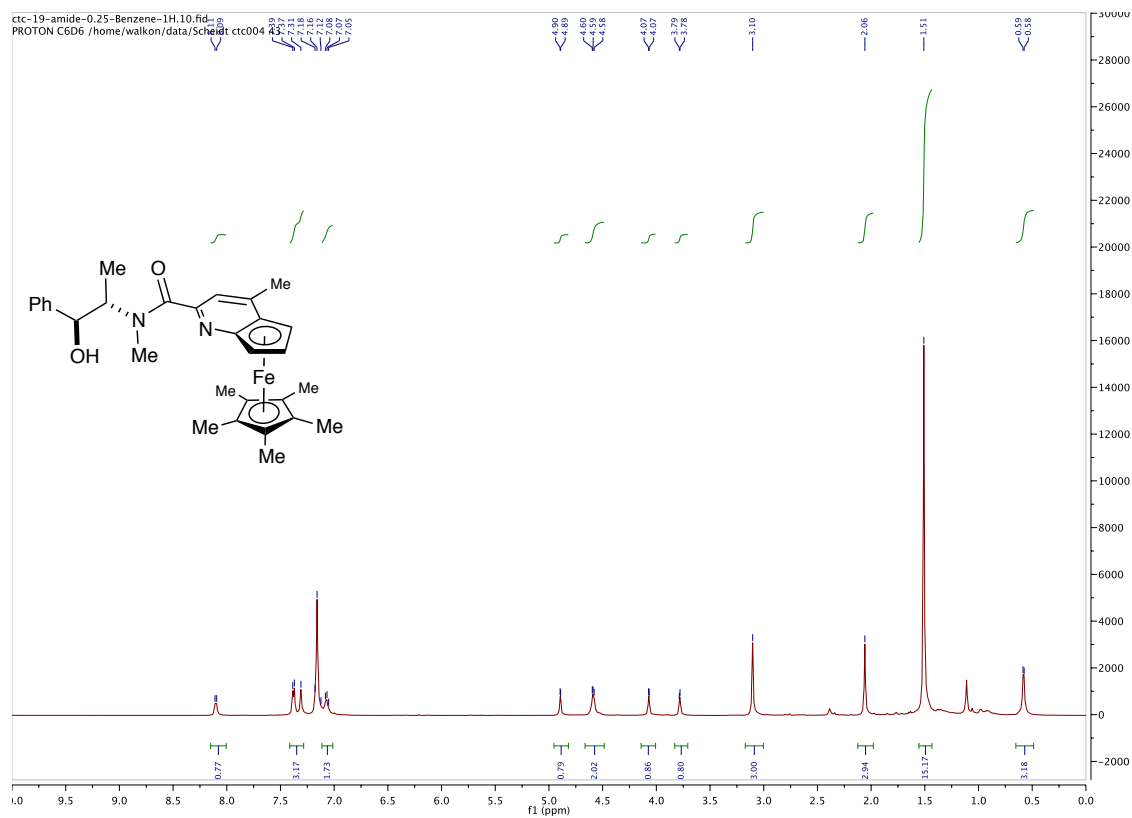


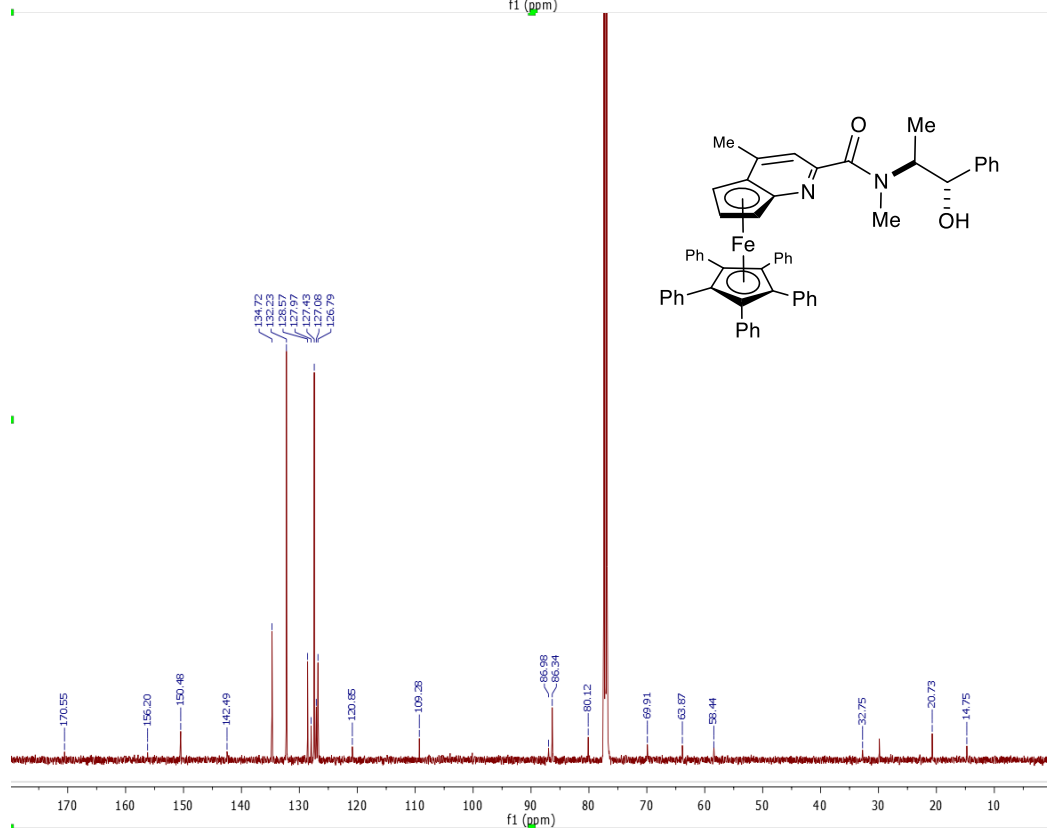
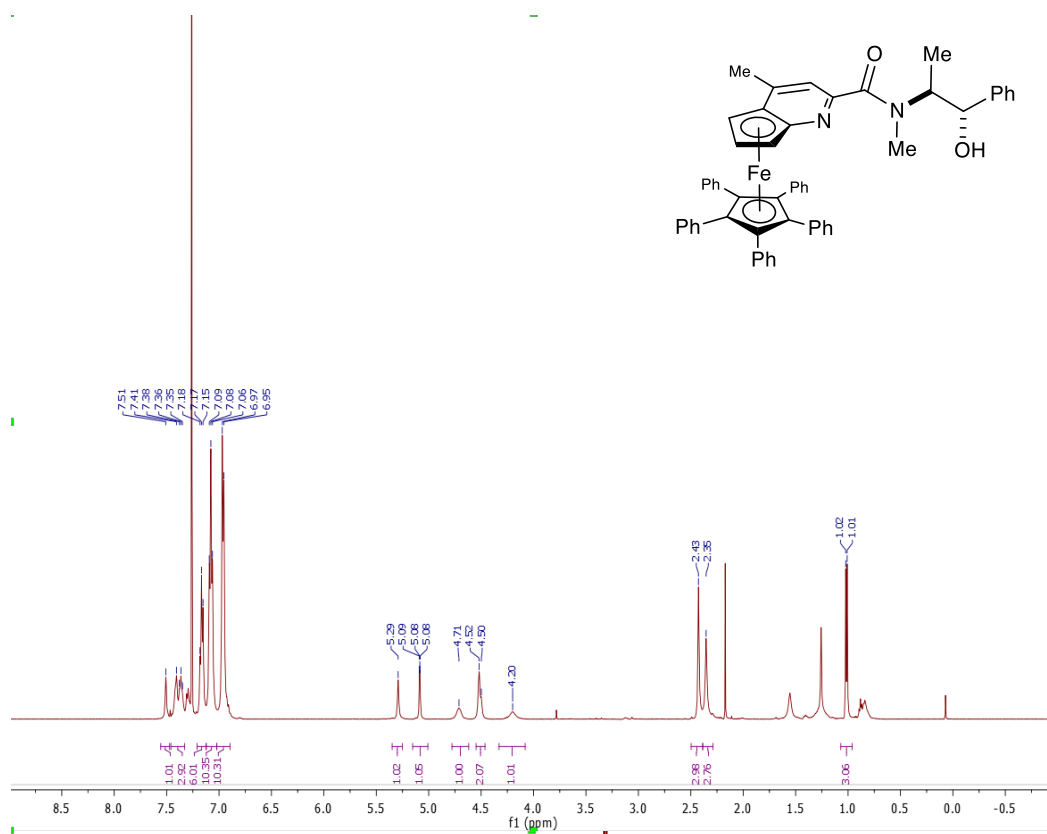
I-68 Obtained as an orange solid in 91% yield (24.8 mg). ^1H NMR (500 MHz, Acetone-*d*₆) δ 8.50 (s, 2H), 8.18 (s, 1H), 7.86 (s, 1H), 6.79 (d, $J = 1.4$ Hz, 1H), 6.57 (dd, $J = 1.4, 1.2$ Hz, 1H), 2.24 (d, $J = 1.4$ Hz, 3H), 1.70 (s, 15H); ^{13}C NMR (125 MHz, Acetone-*d*₆) δ 151.93, 141.65, 136.48, 132.80, 132.53, 132.26, 131.99, 131.24, 129.01, 127.33, 125.16, 123.00, 122.81, 120.84, 114.50, 108.38, 93.74, 81.48, 77.60, 71.80, 65.80, 65.66, 18.95, 10.16; ^{77}Se NMR (76 MHz, Acetone-*d*₆) δ 117.36.

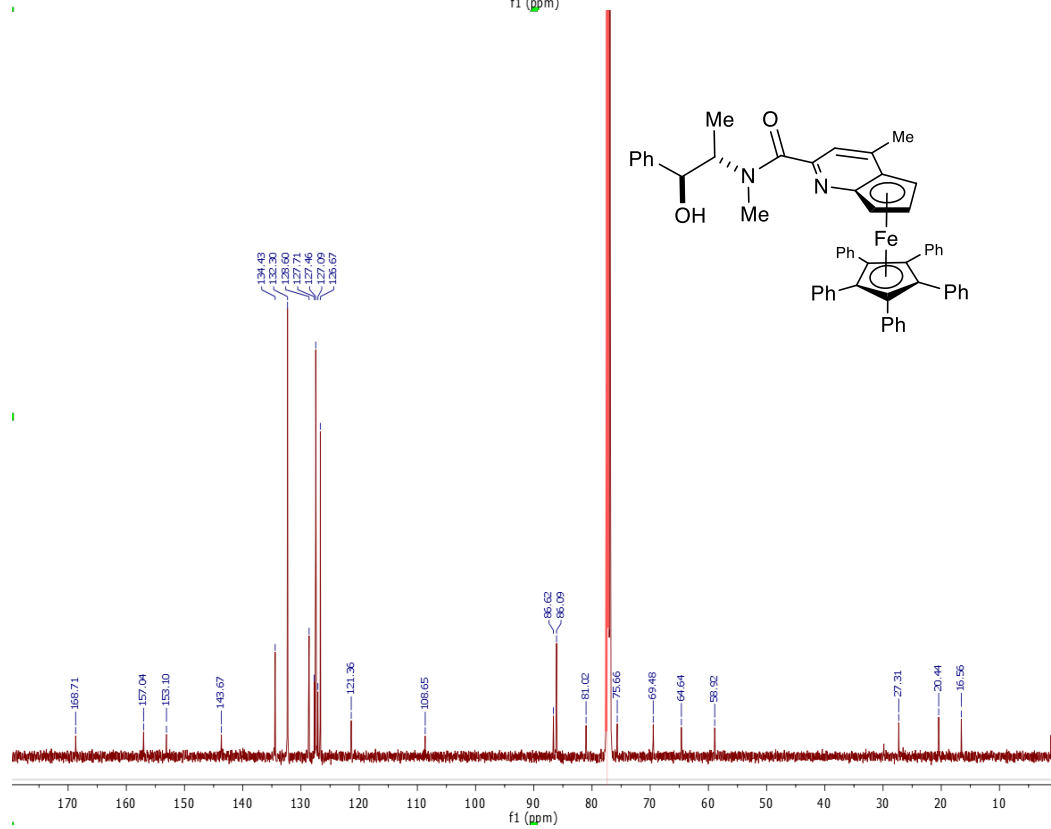
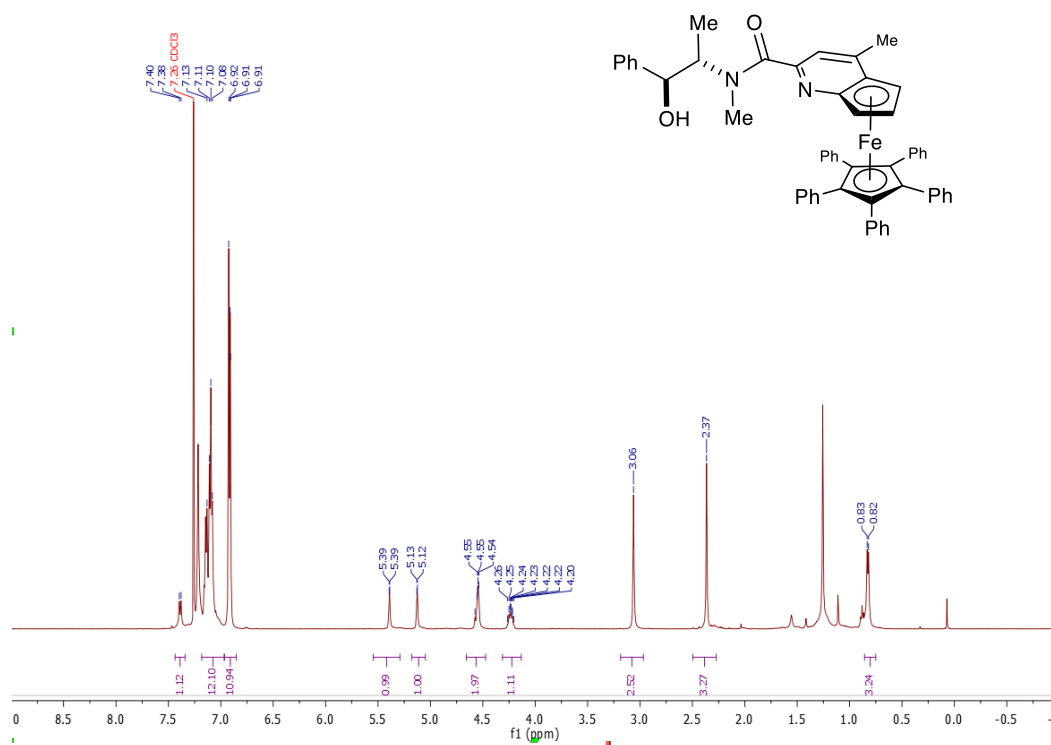
1.7.6 Selected NMR Spectra

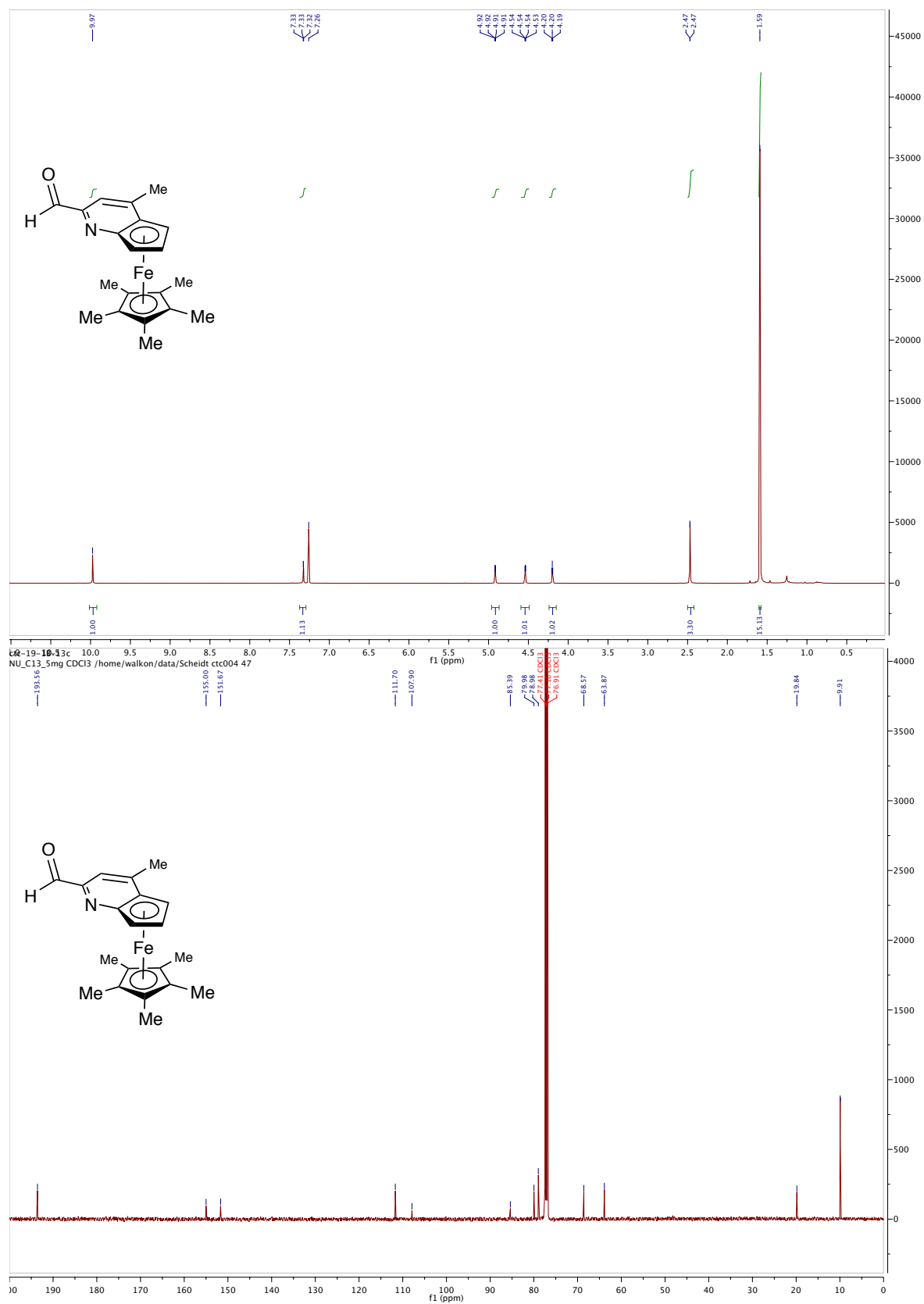


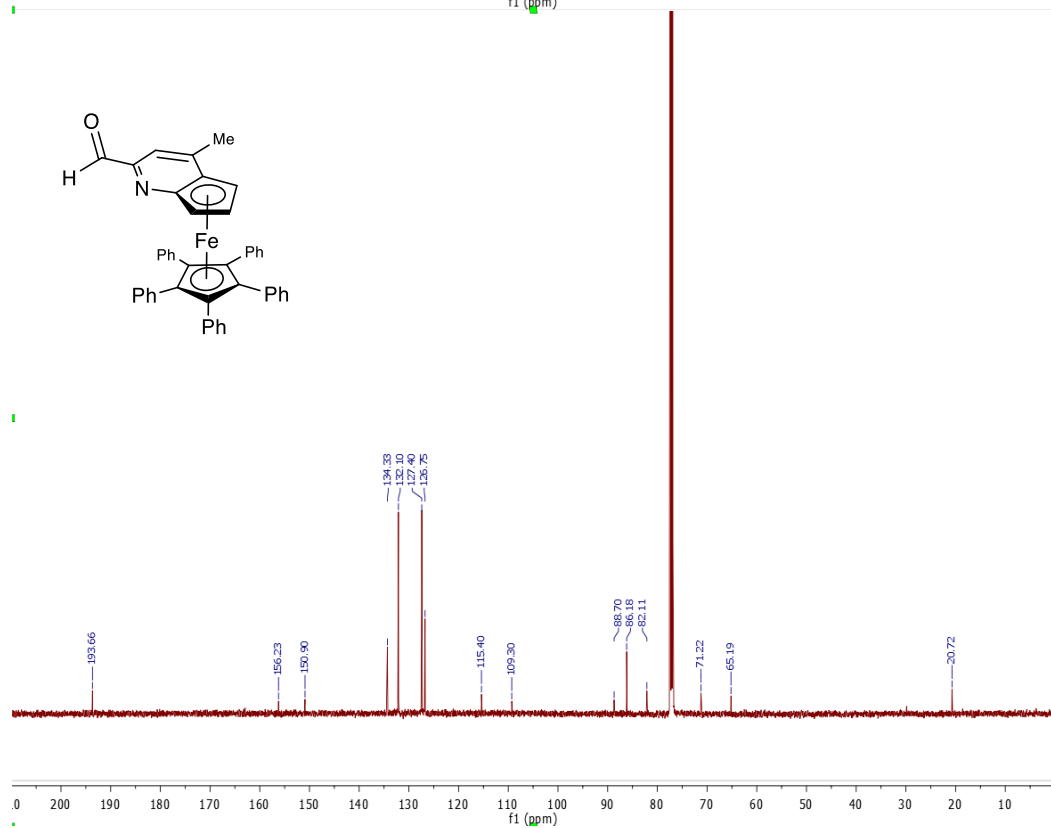
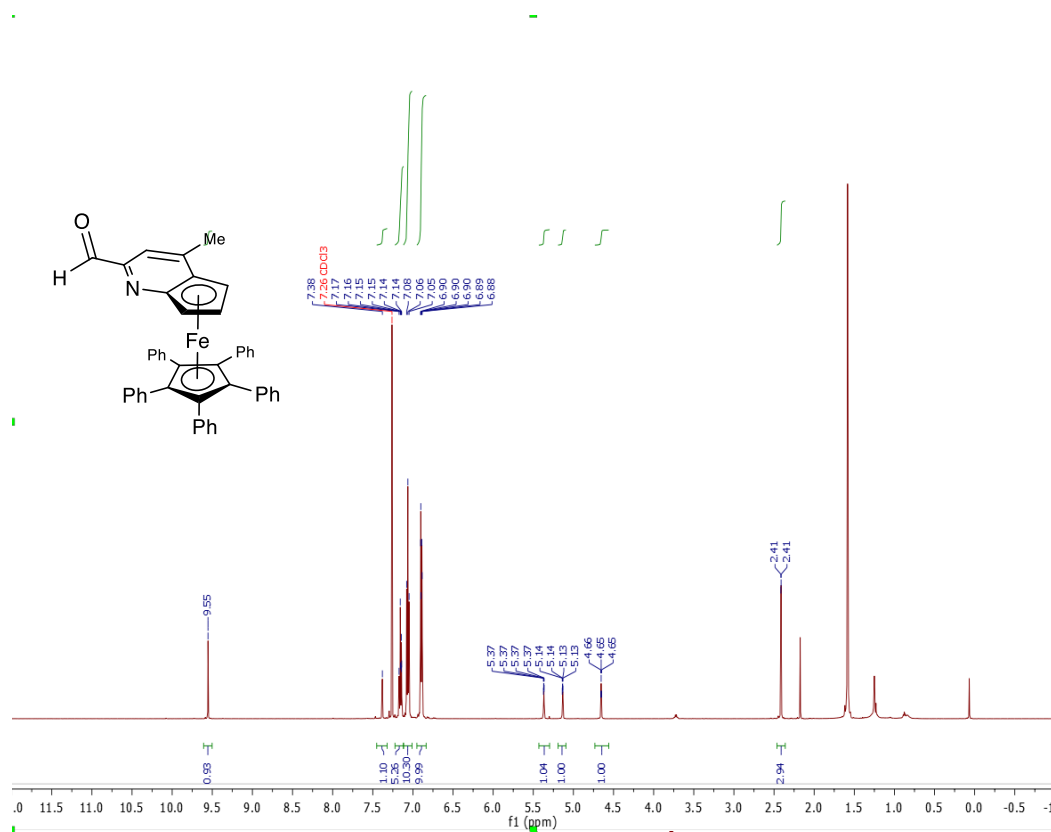


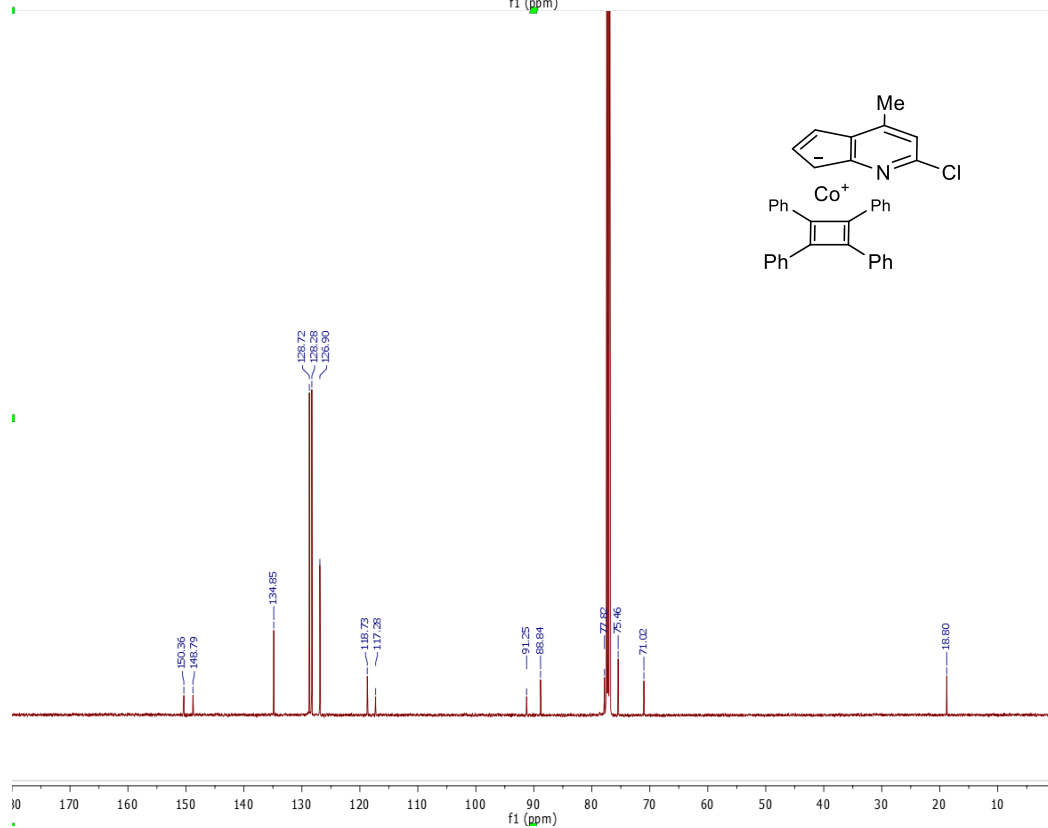
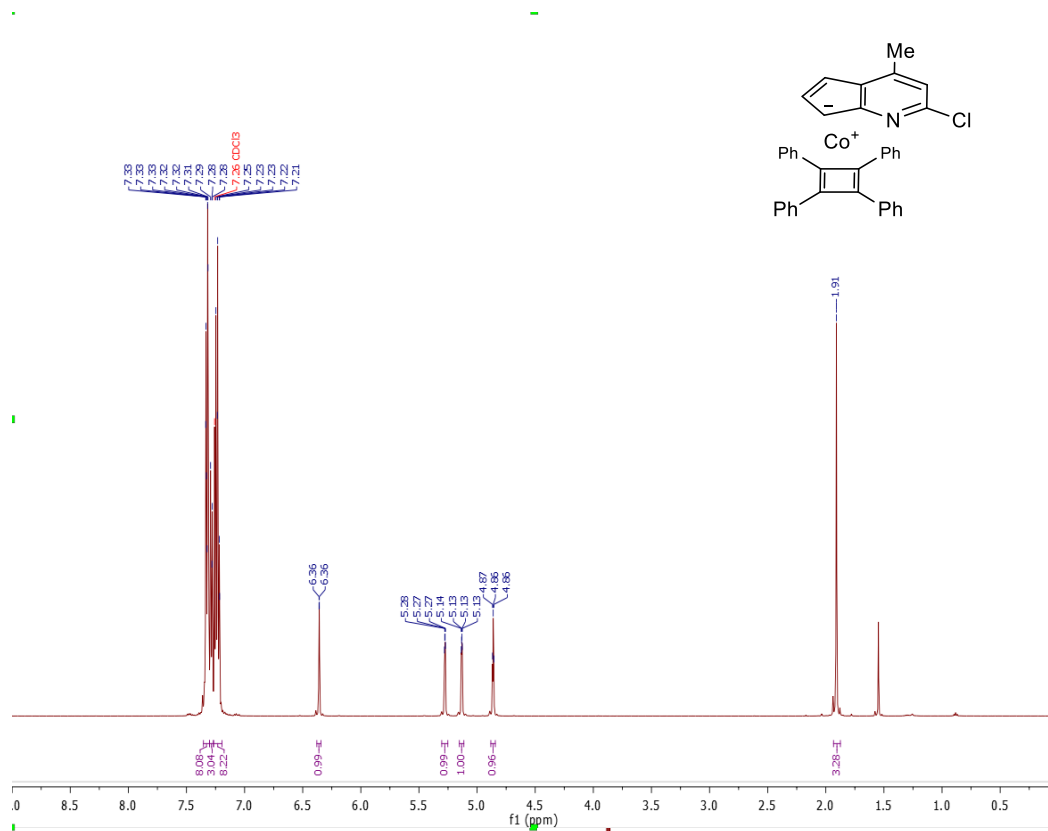


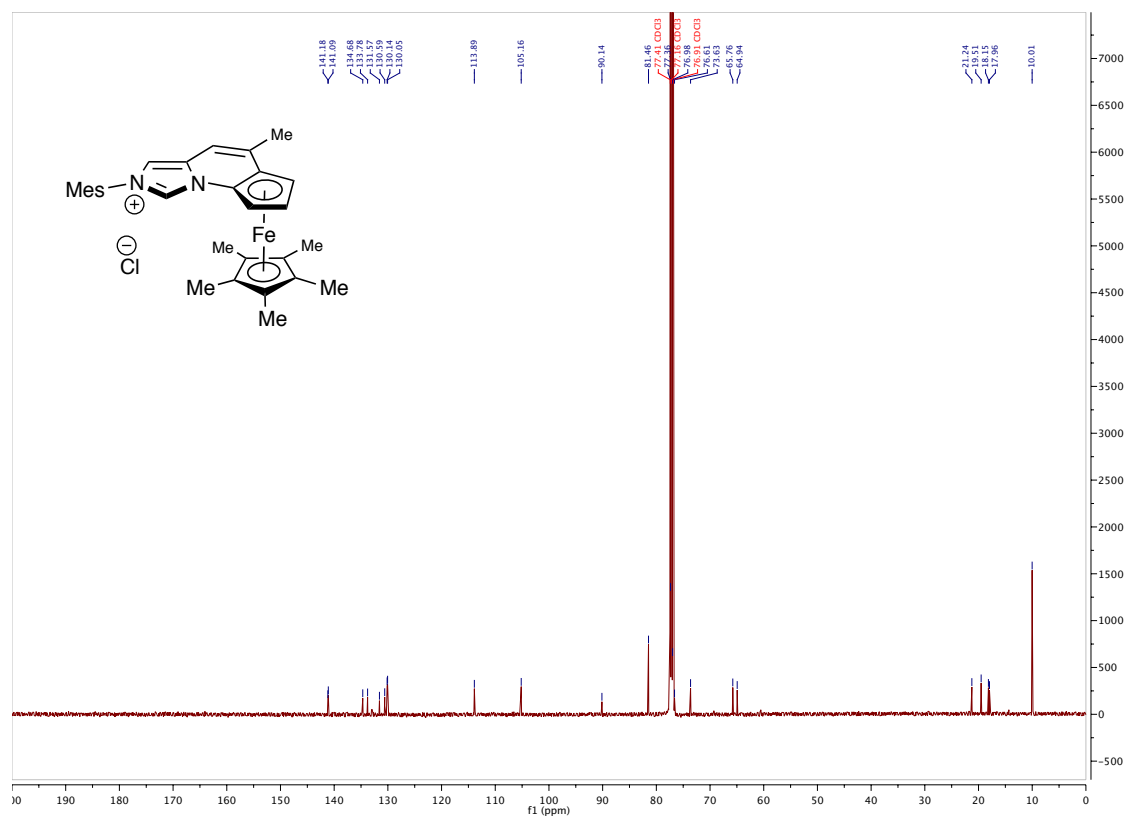
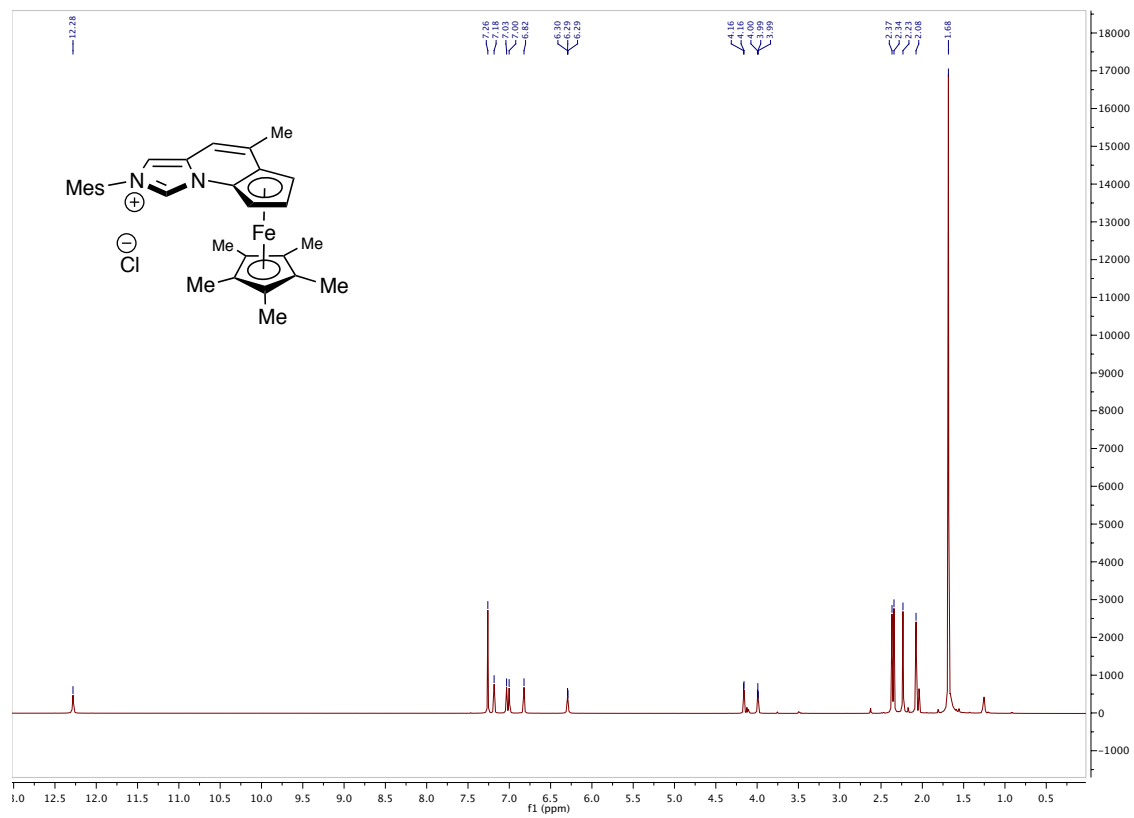


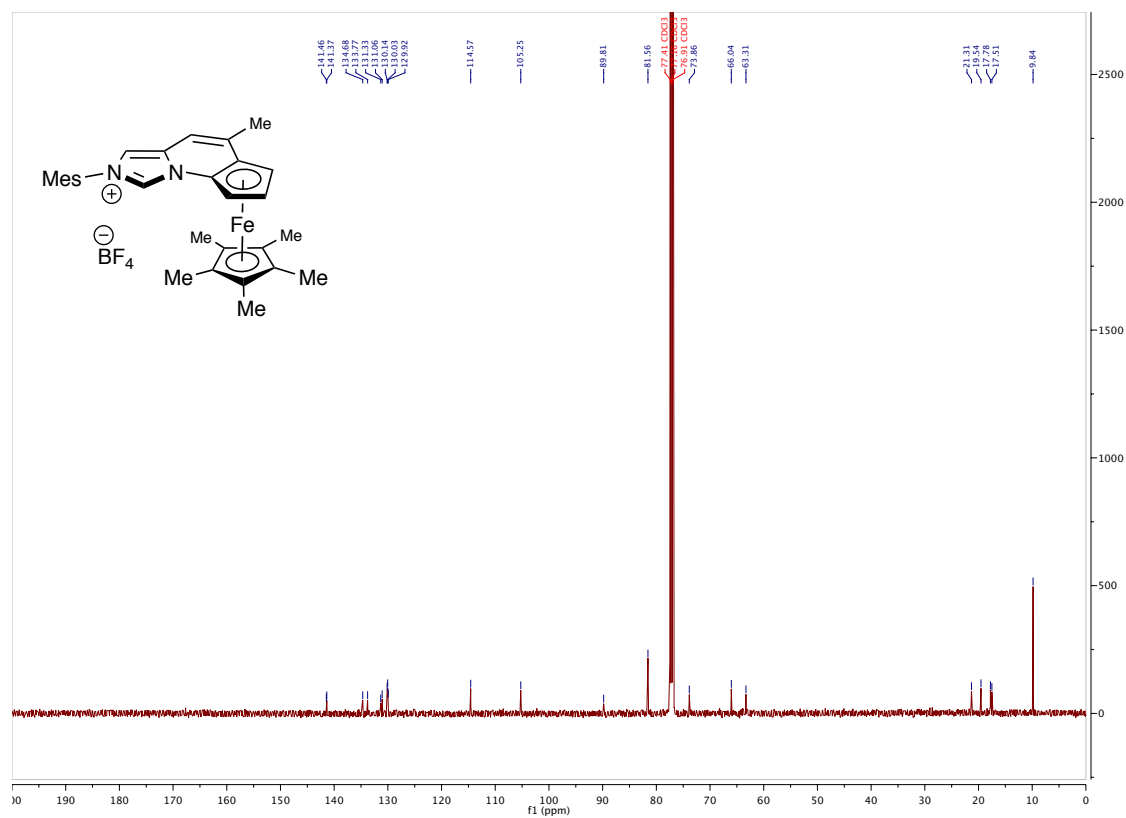
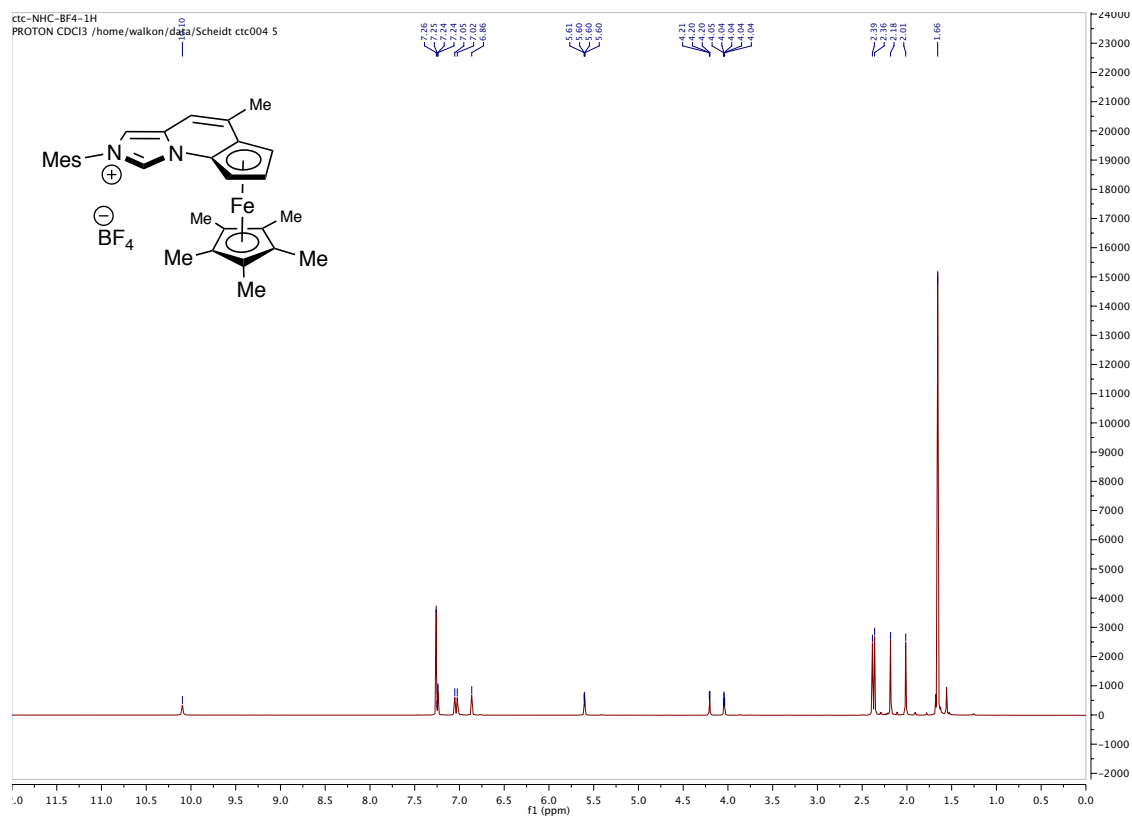


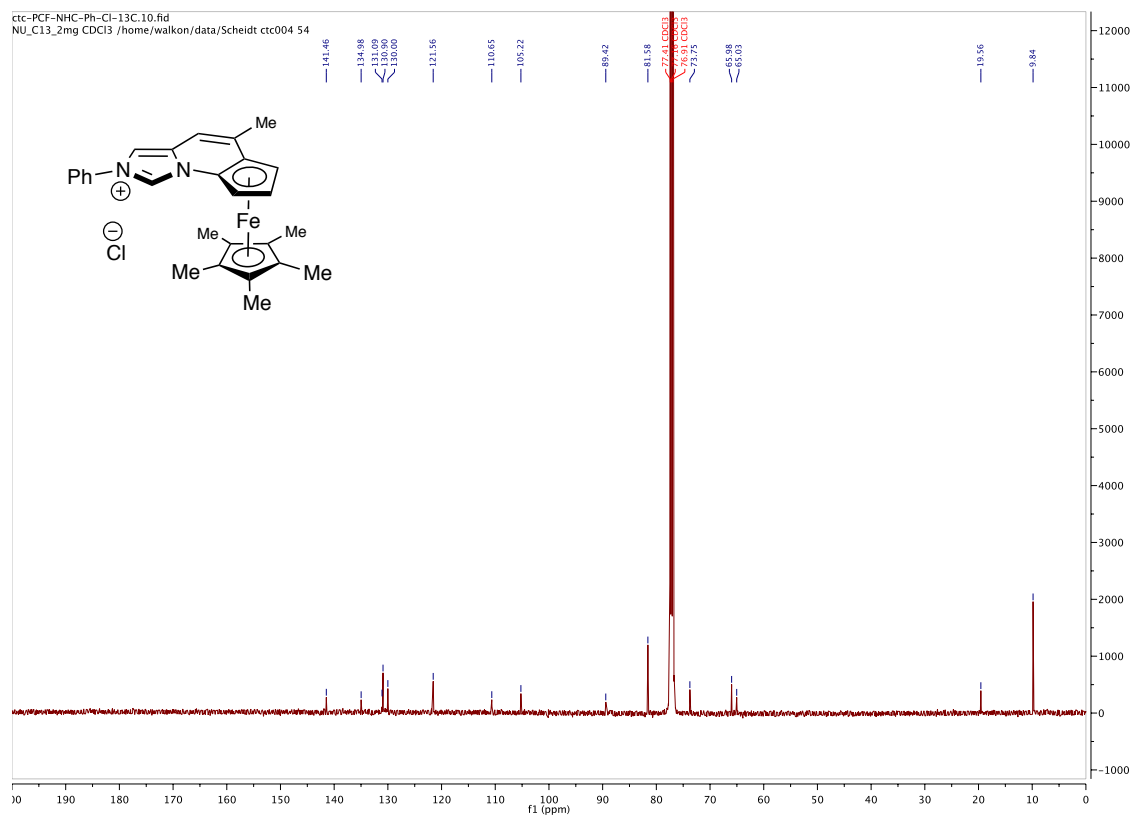
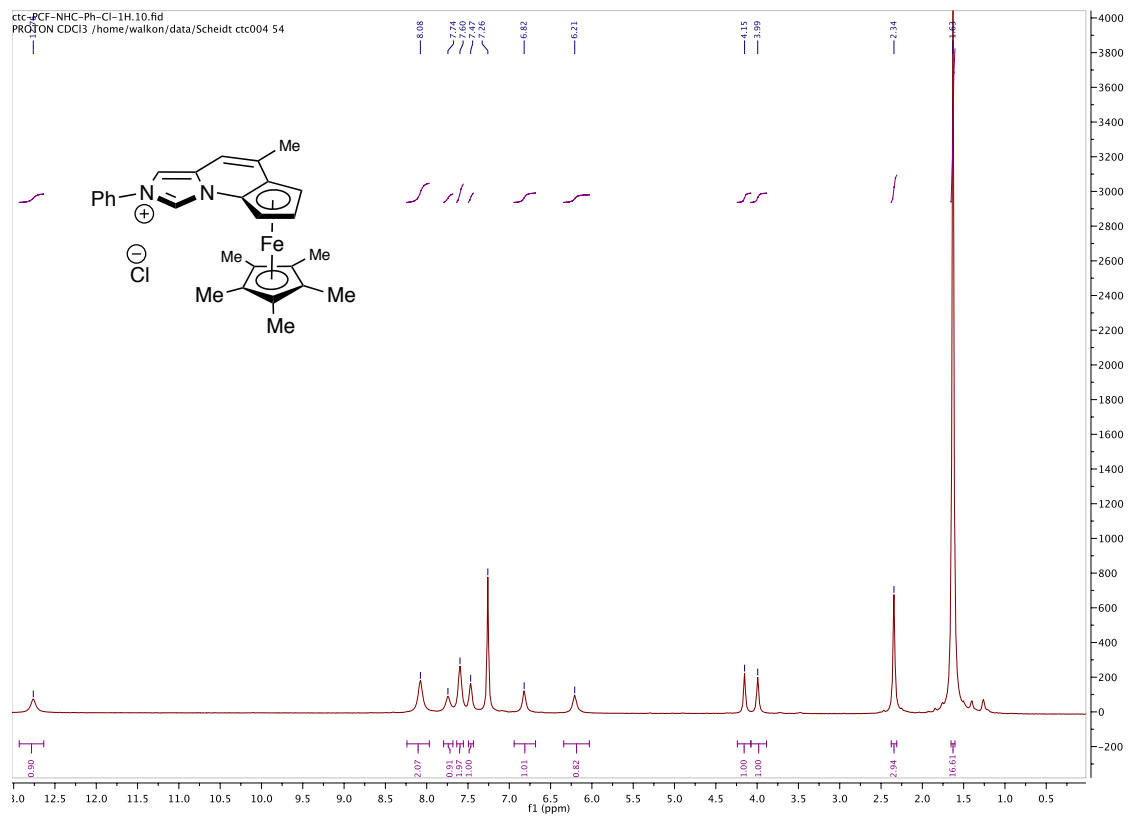


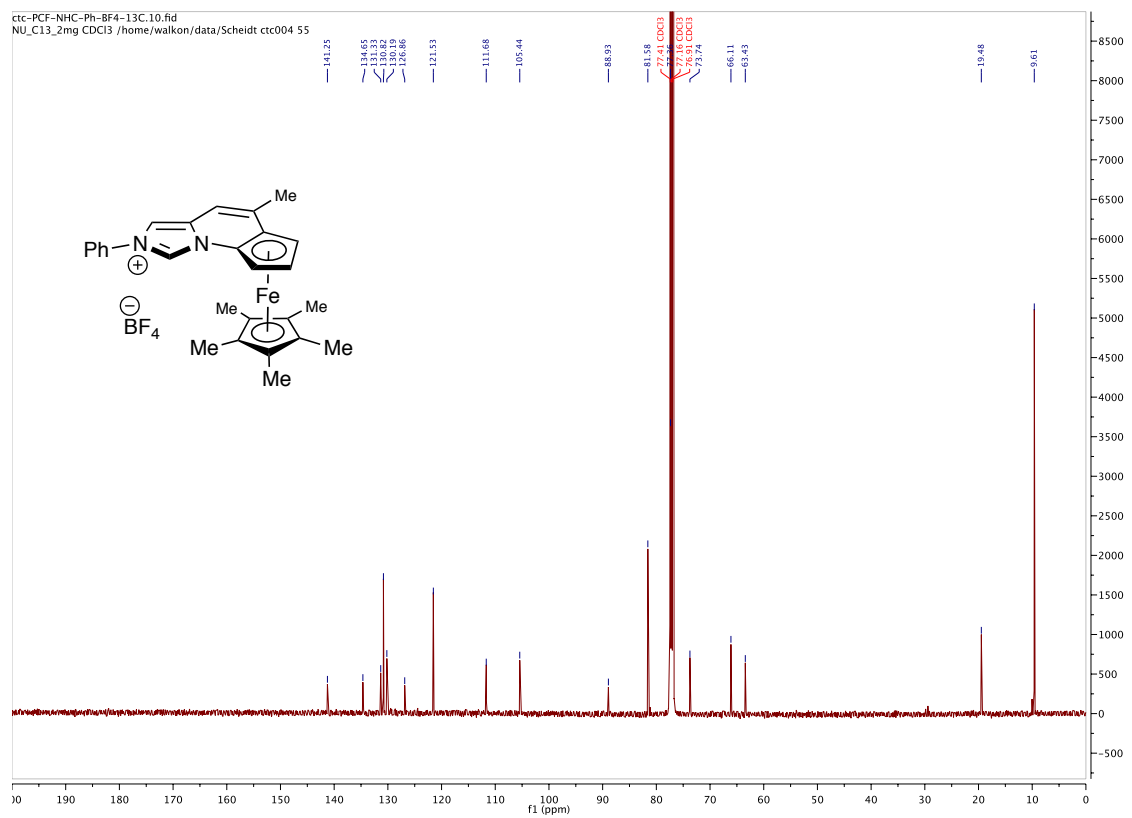
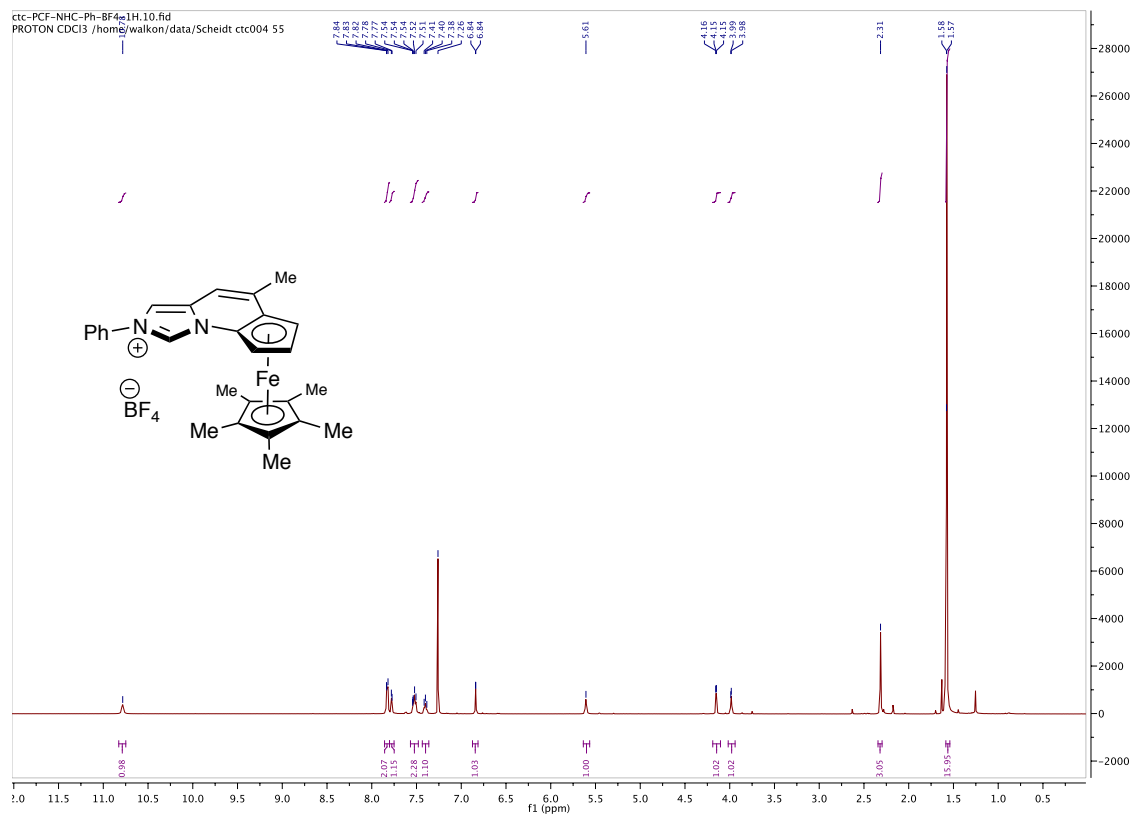


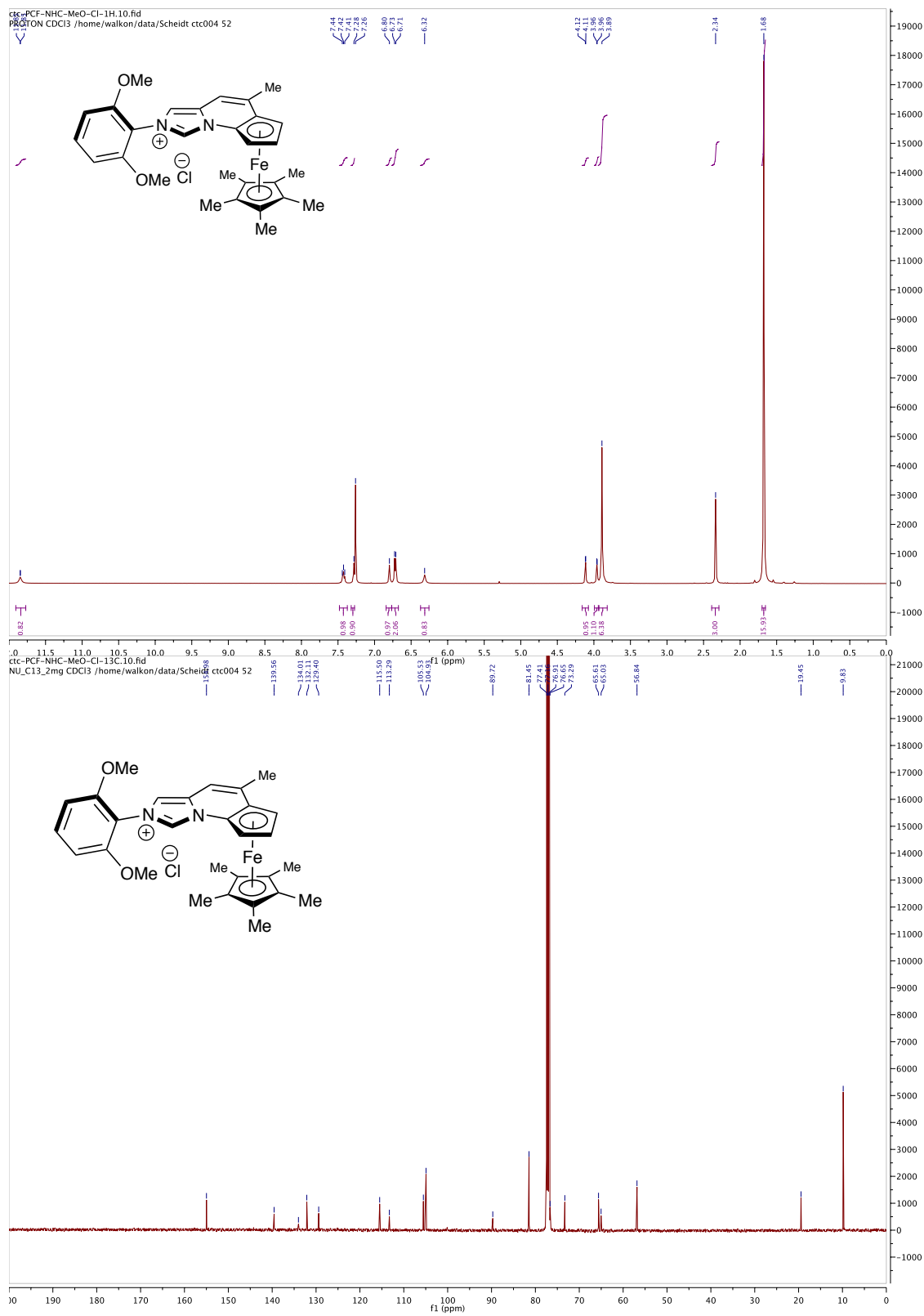


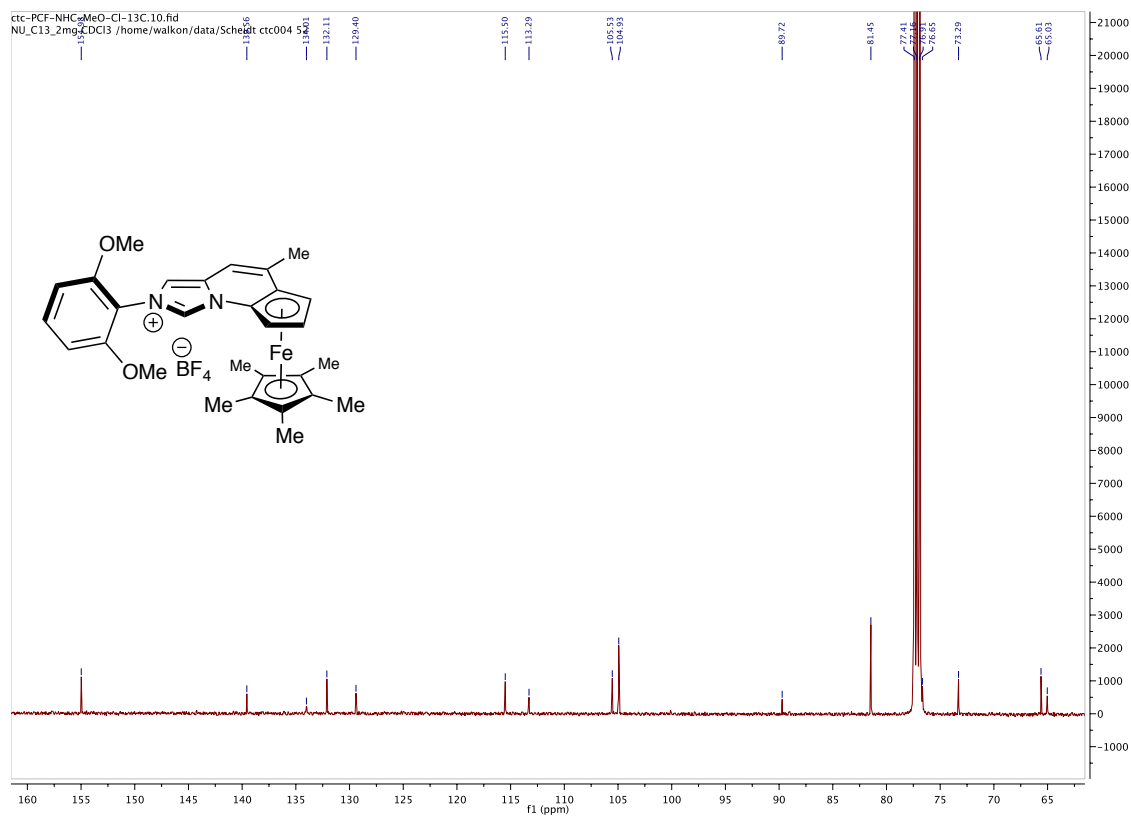
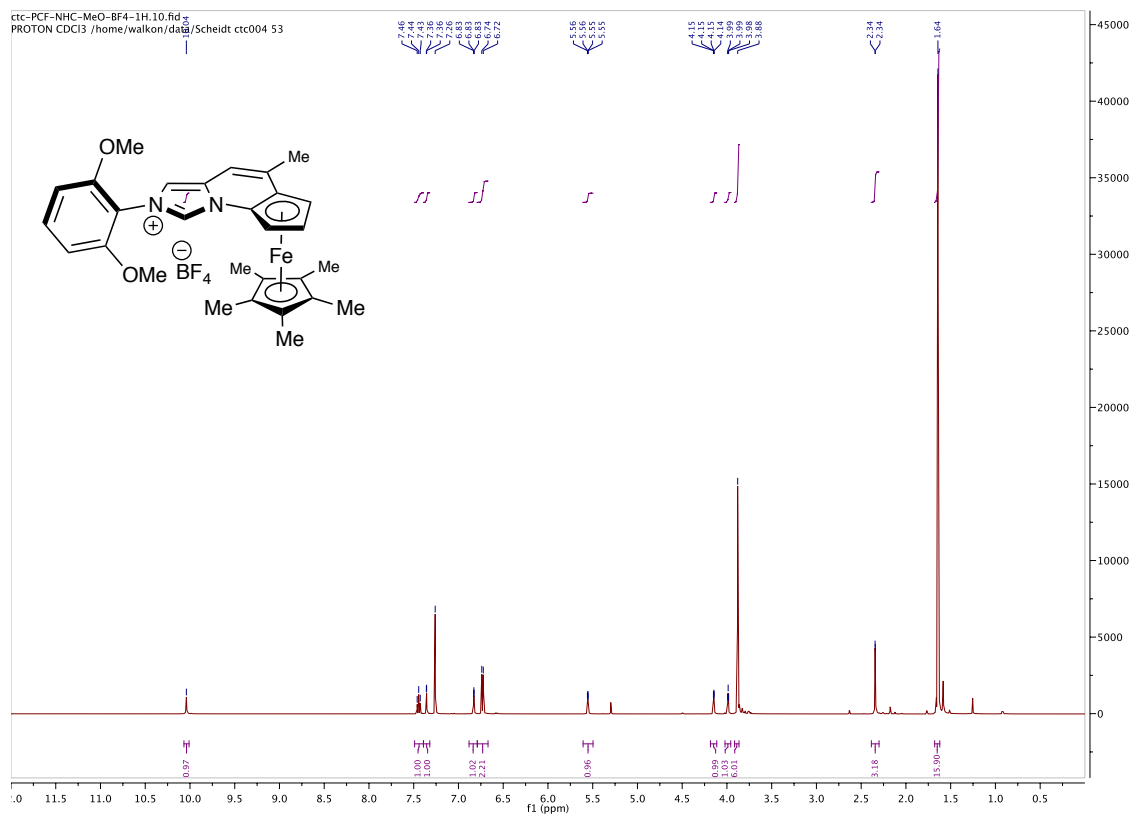


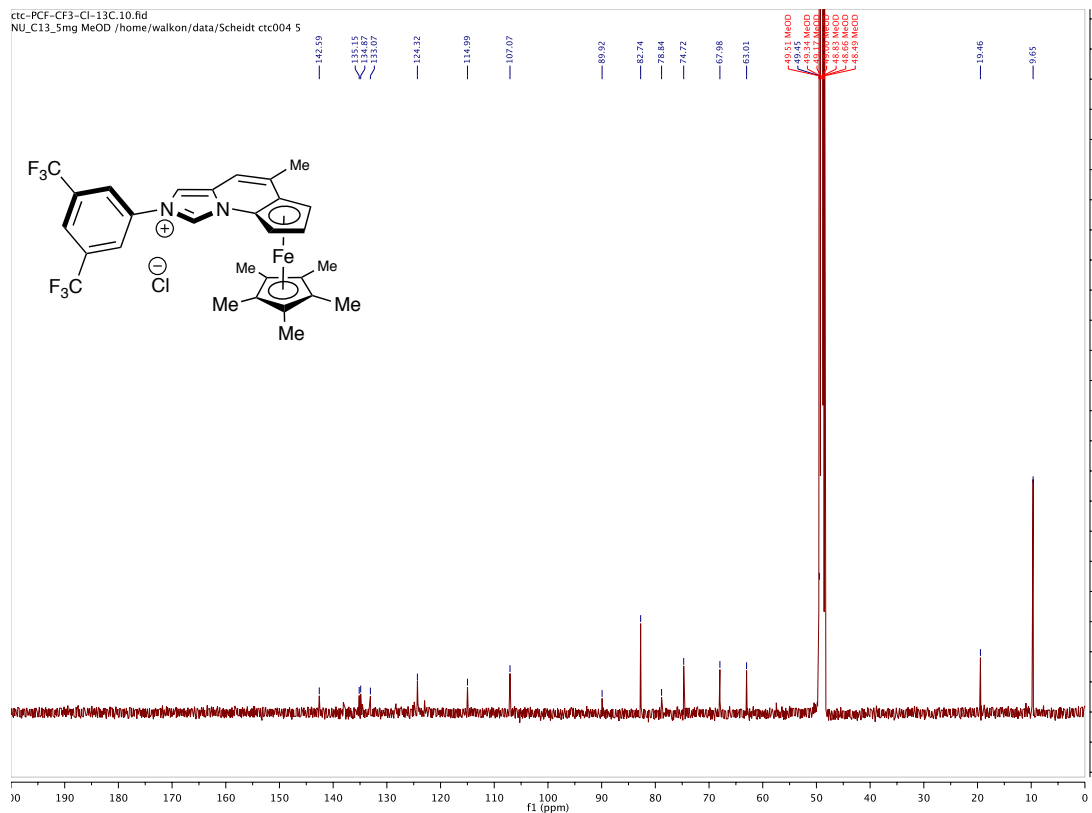
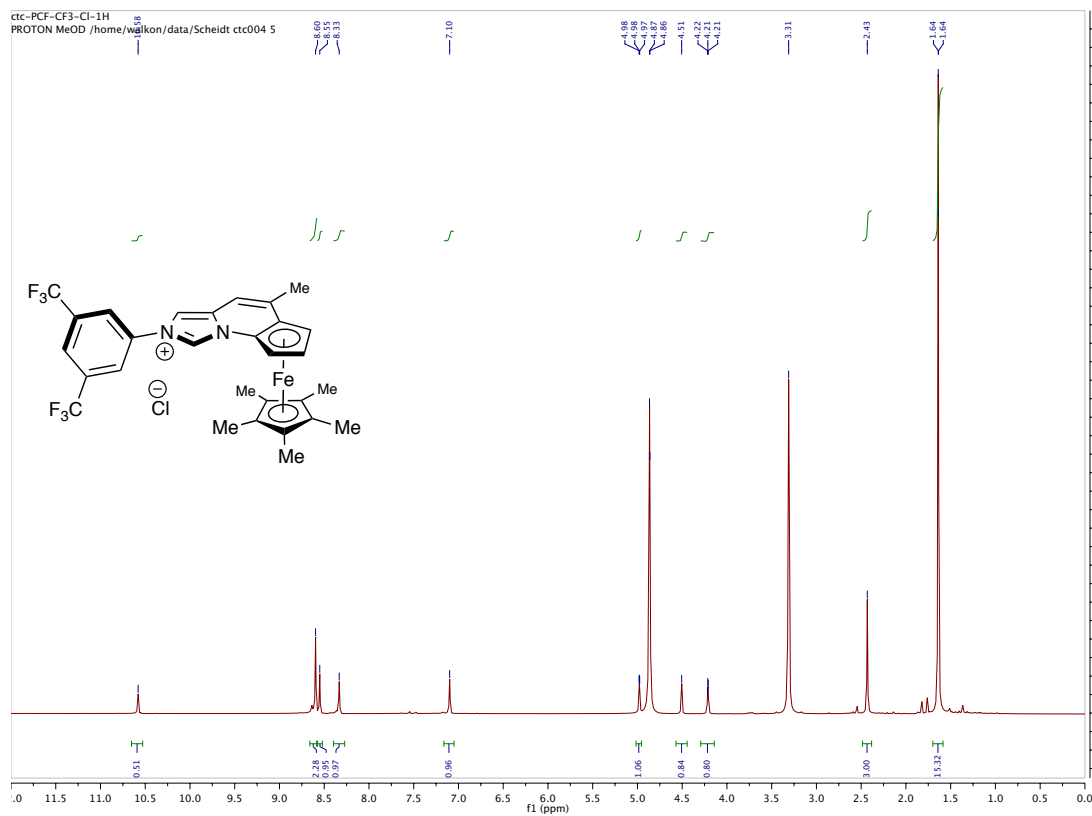


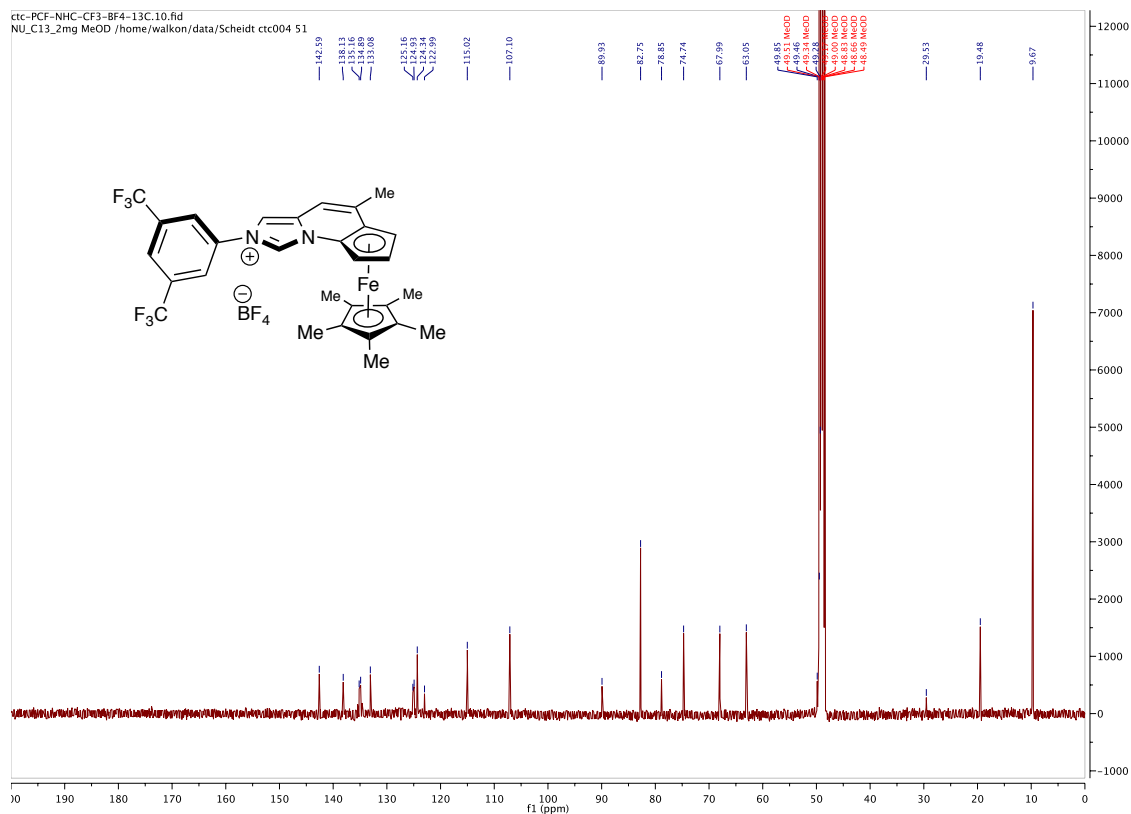
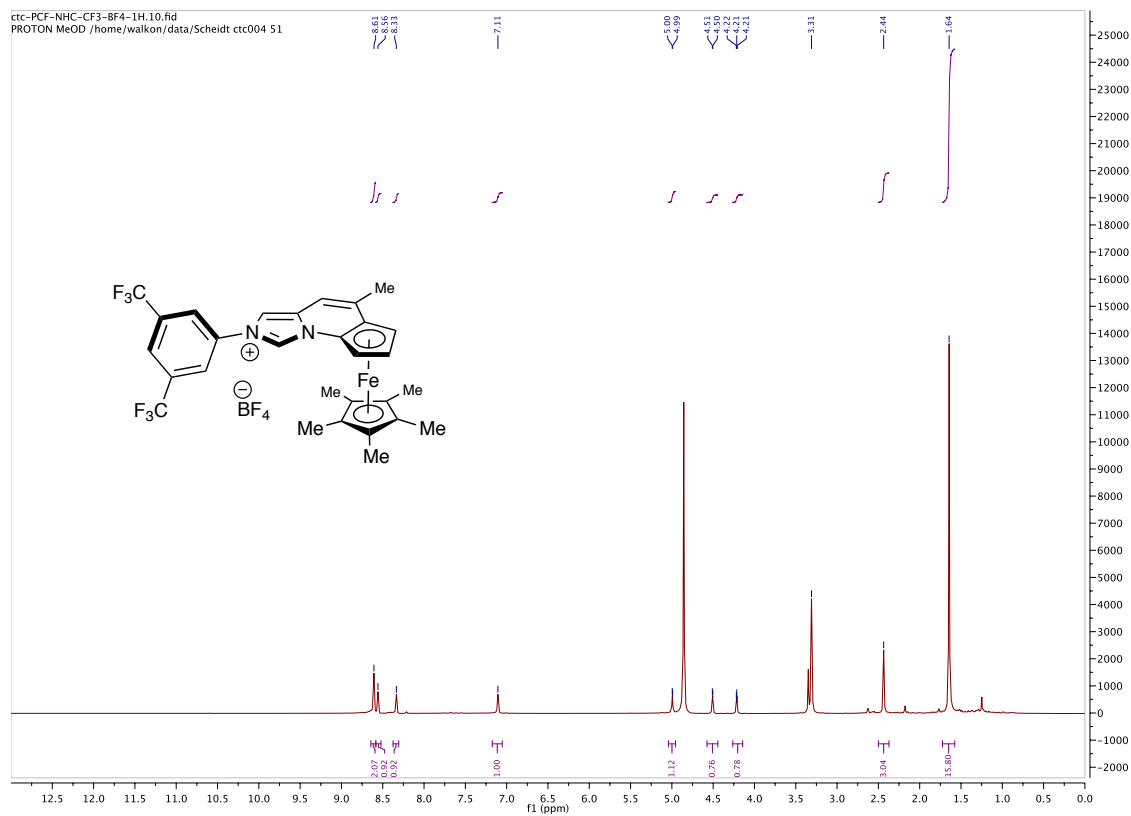


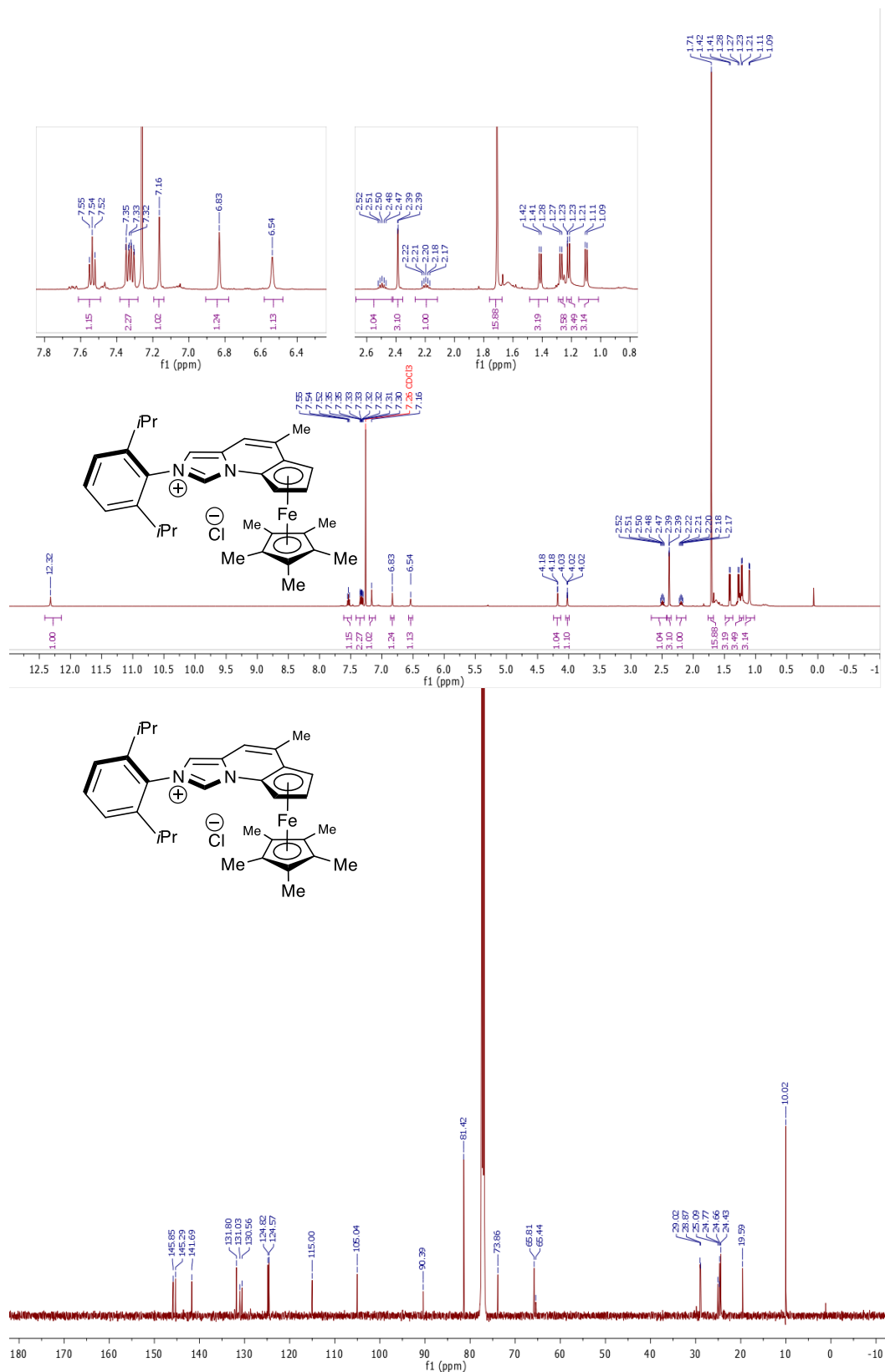


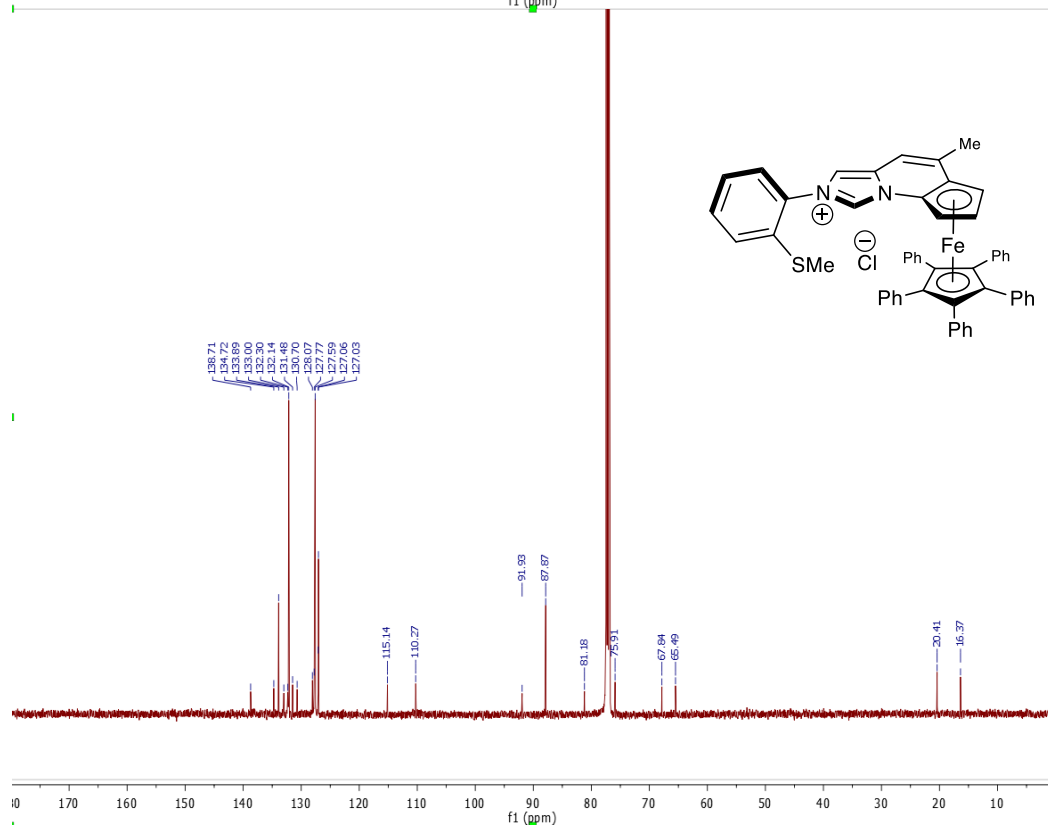
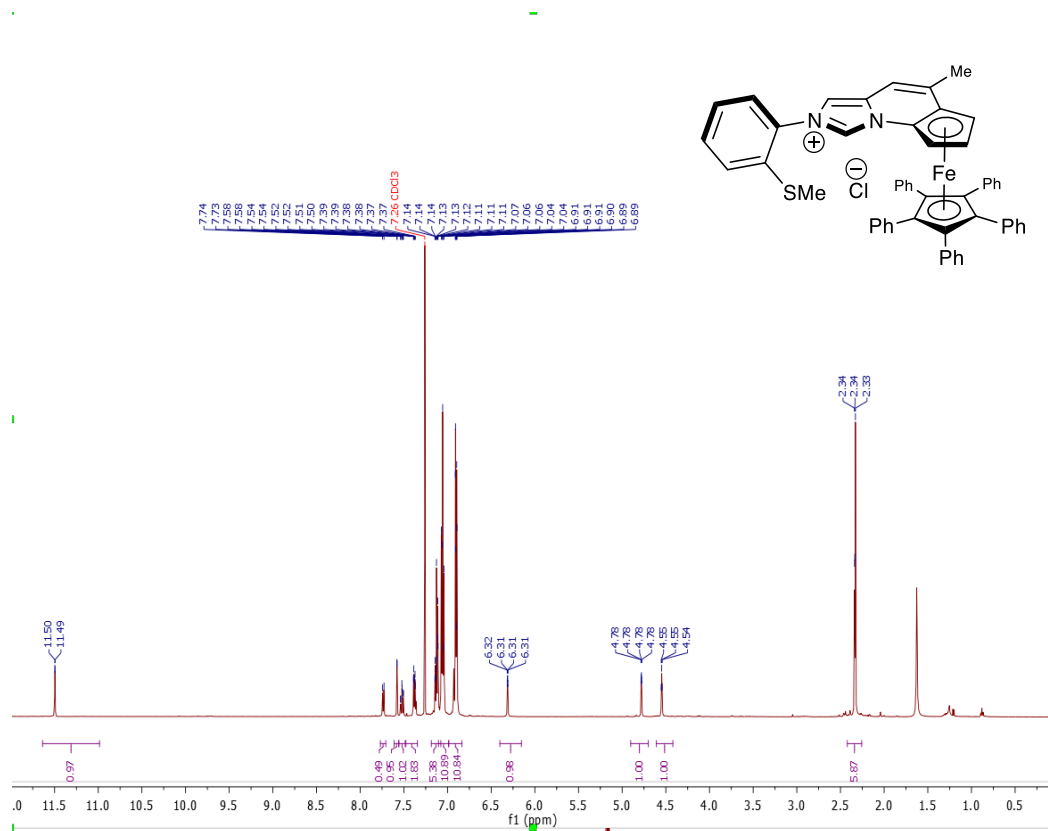


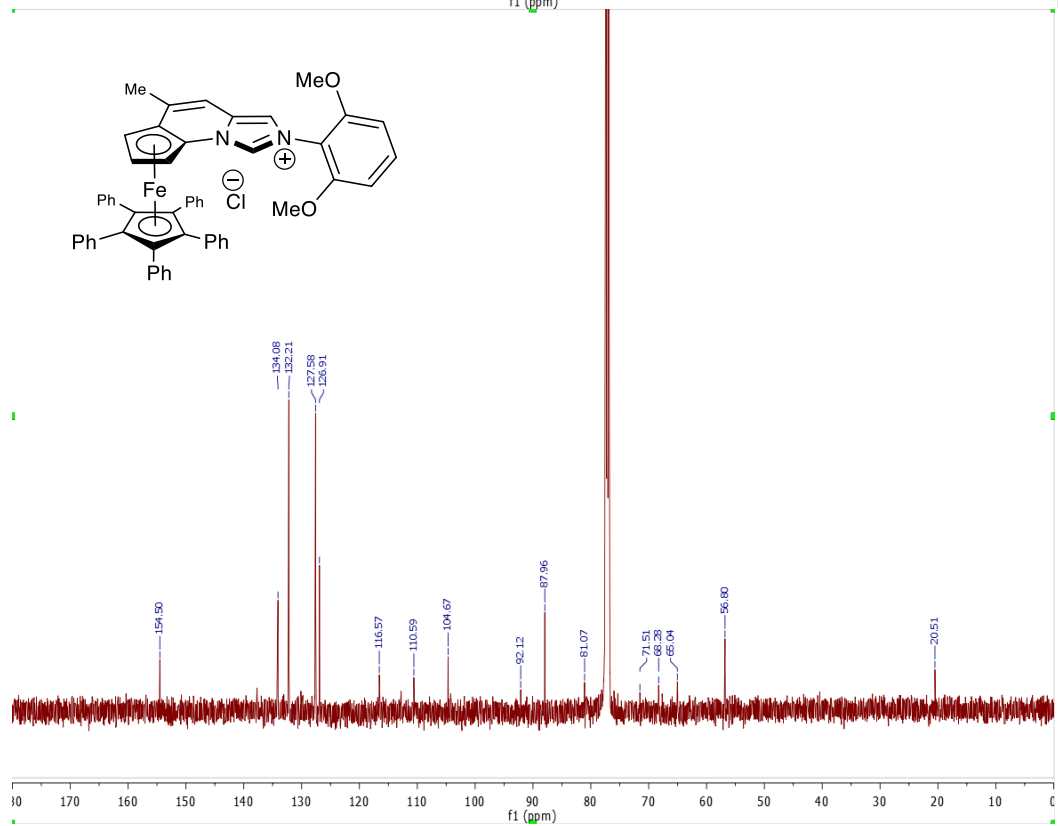
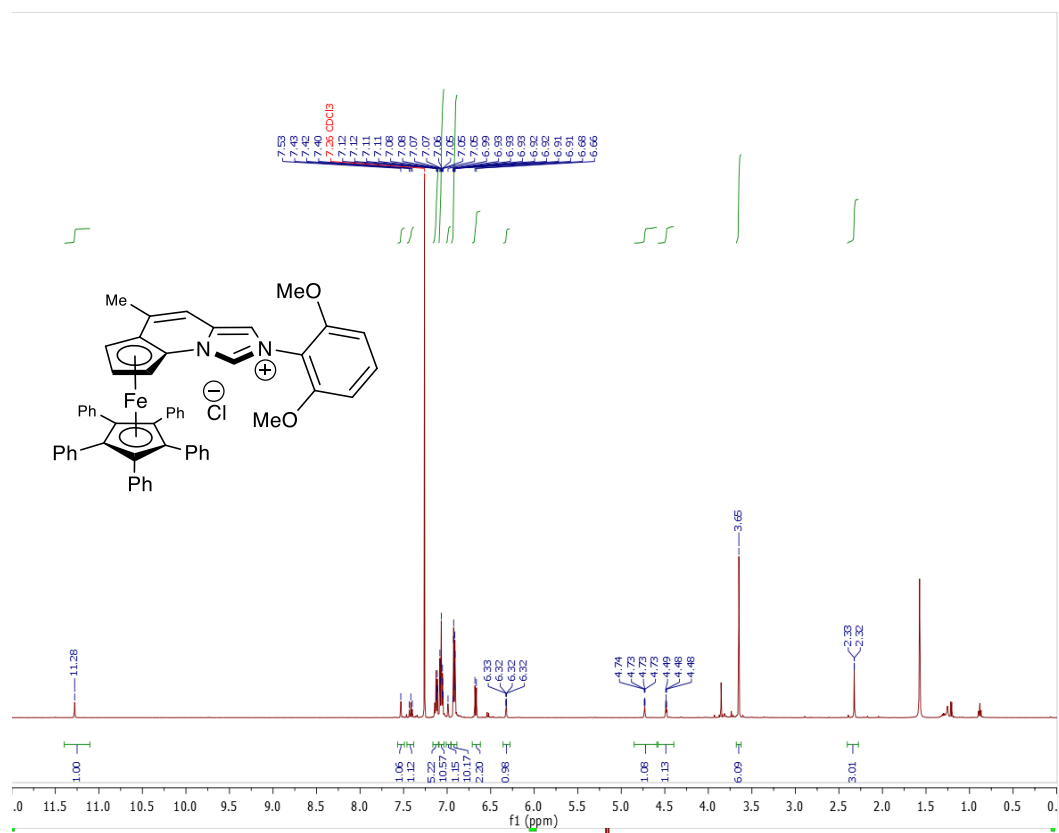


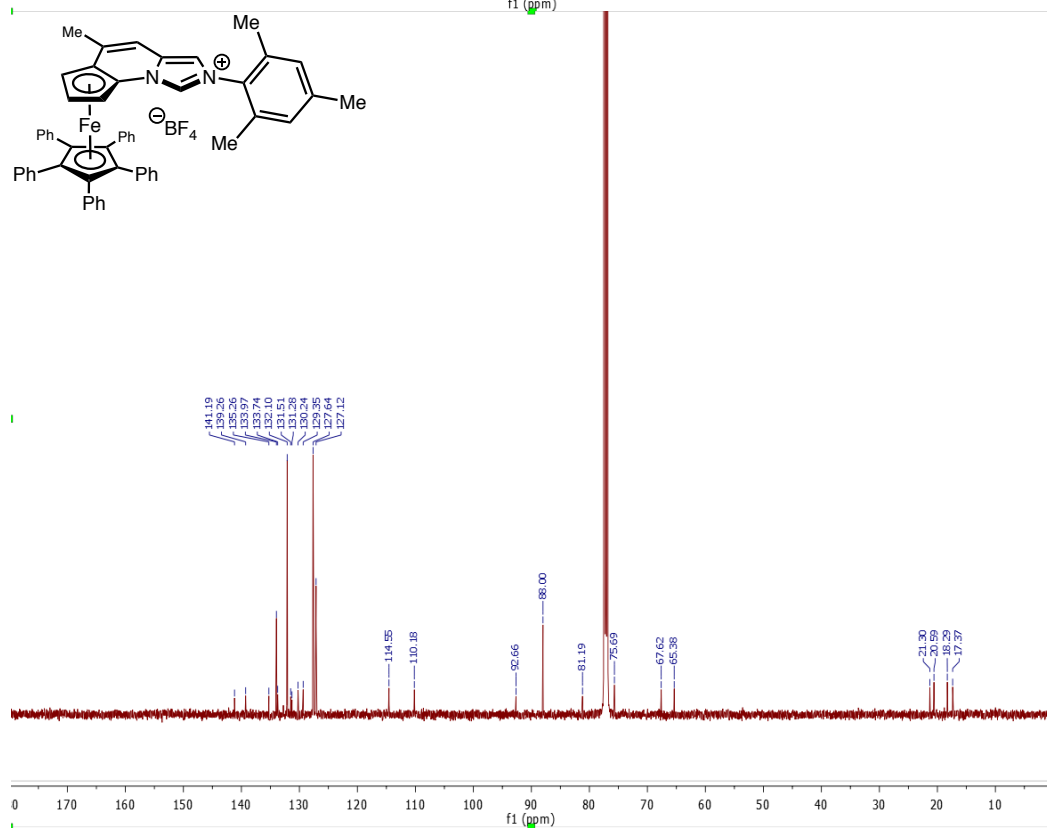
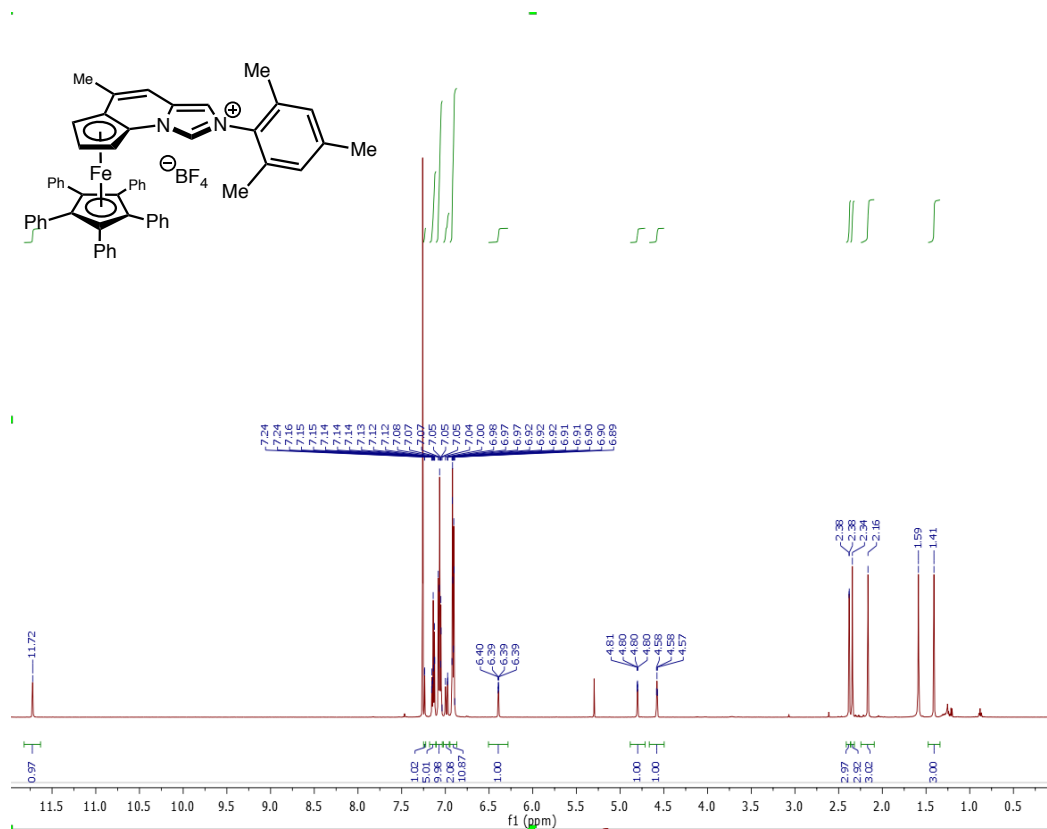


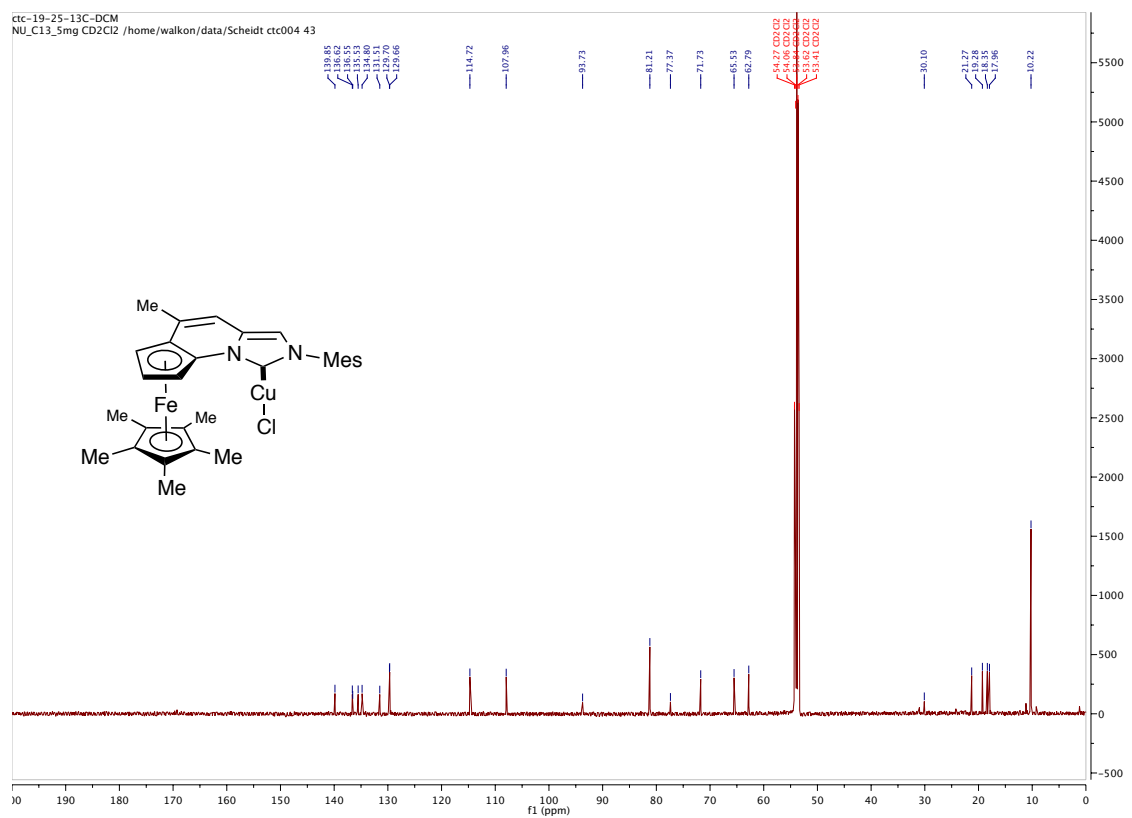
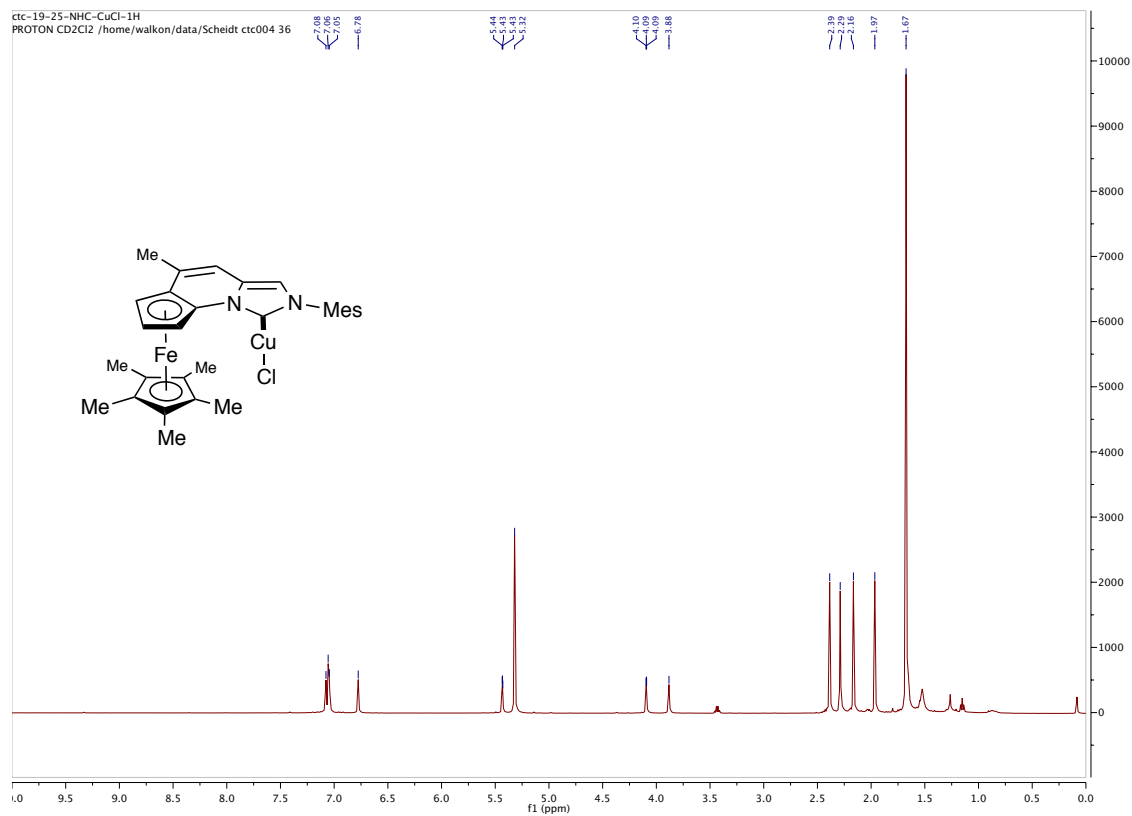


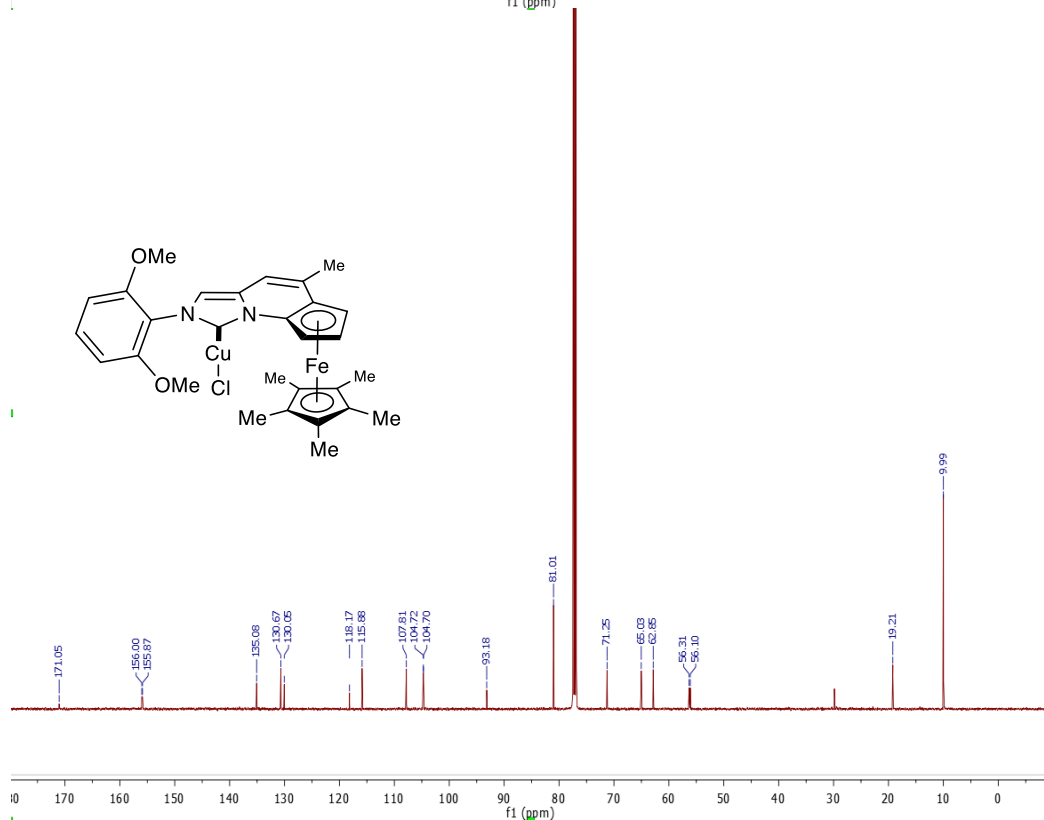
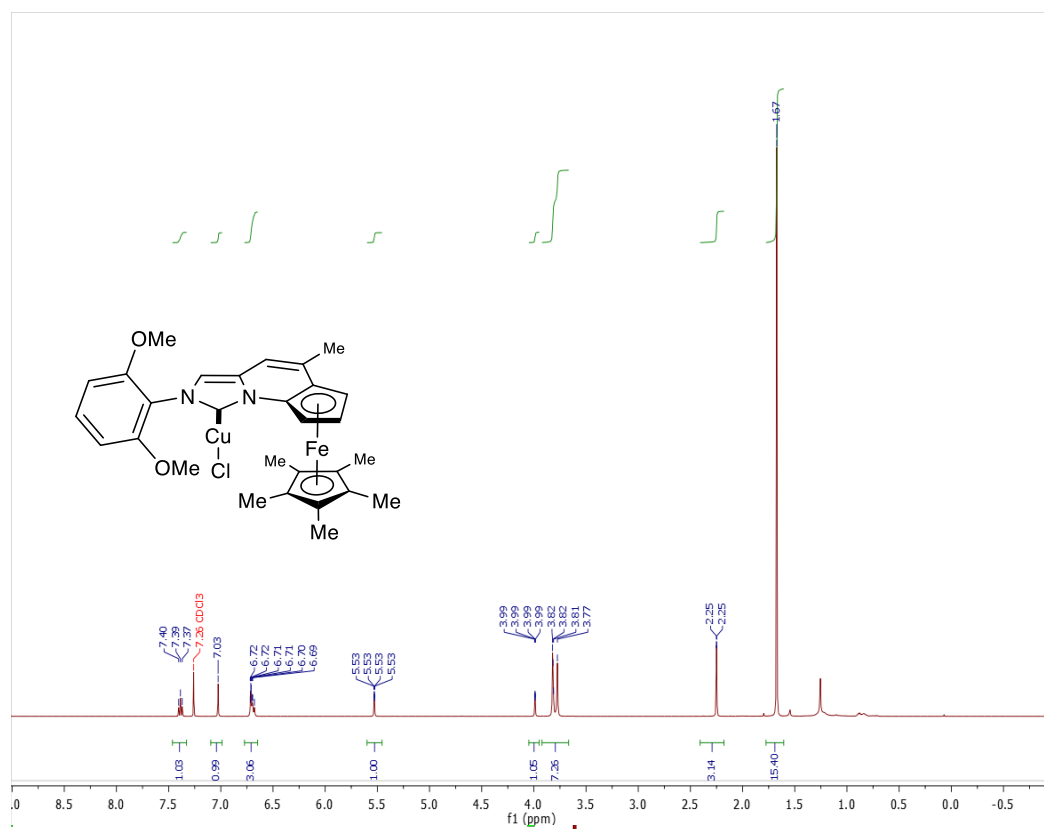


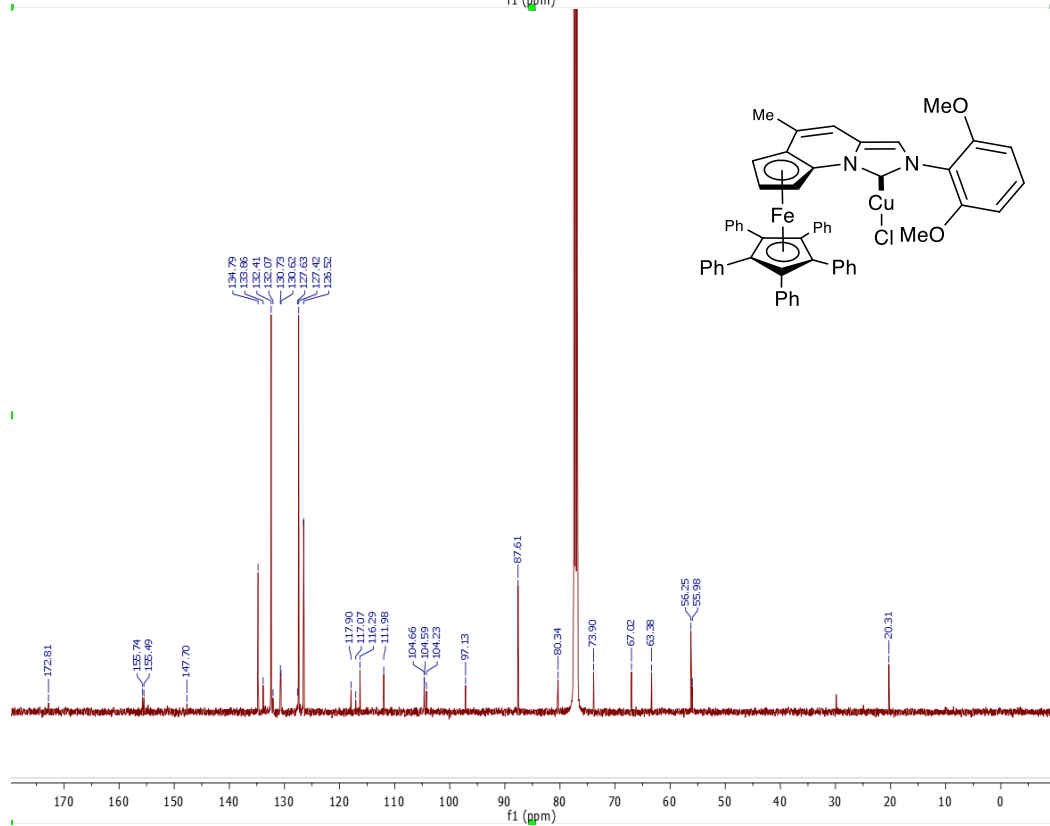
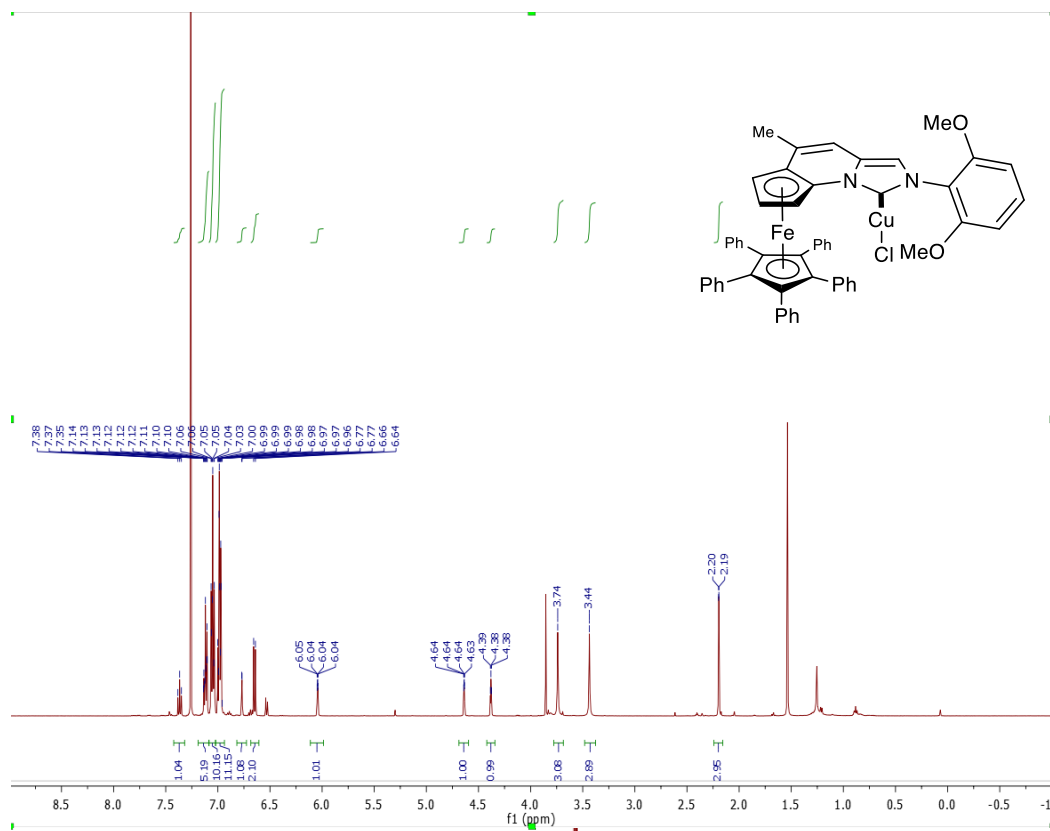


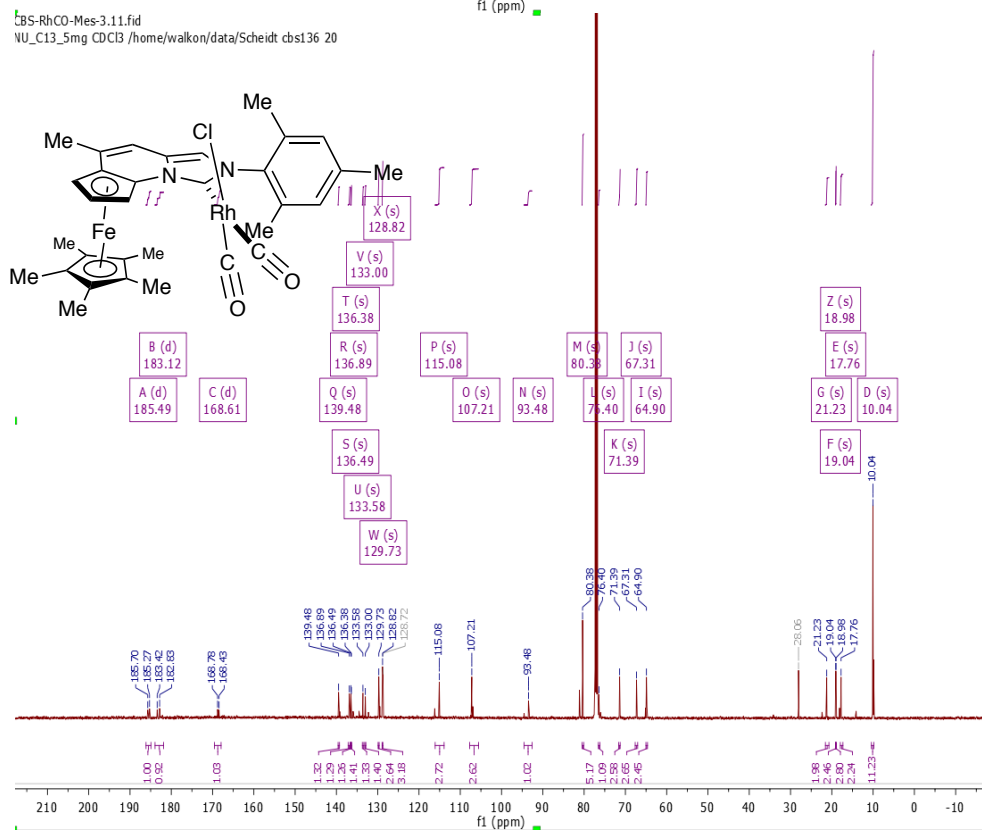
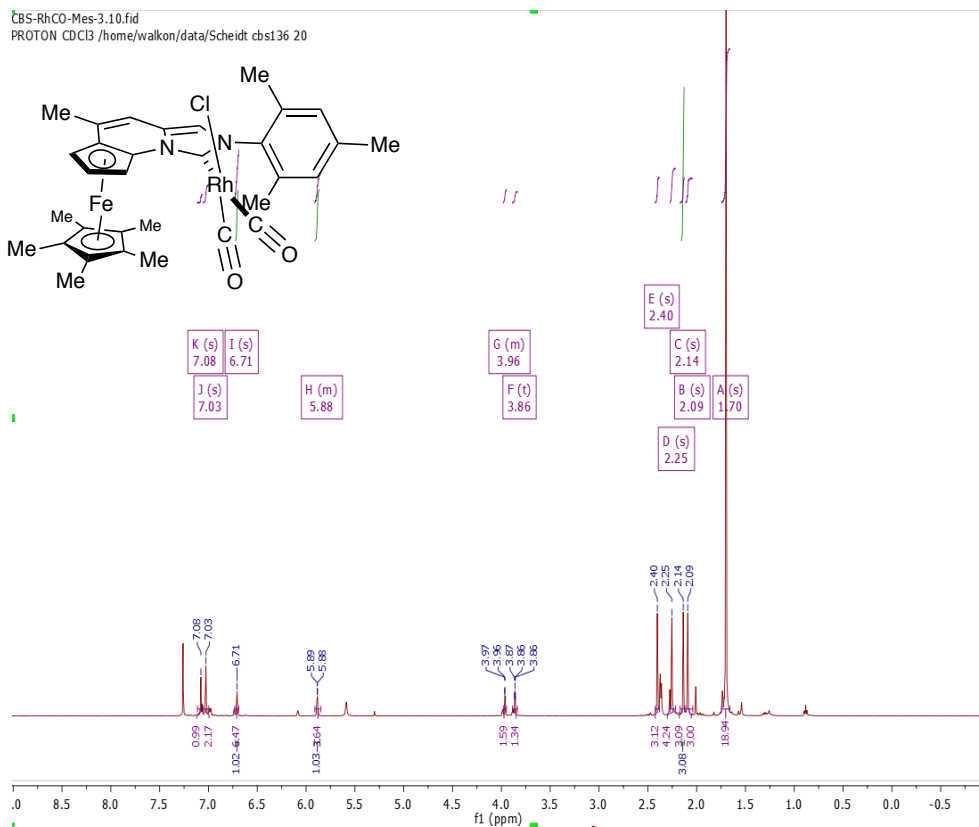




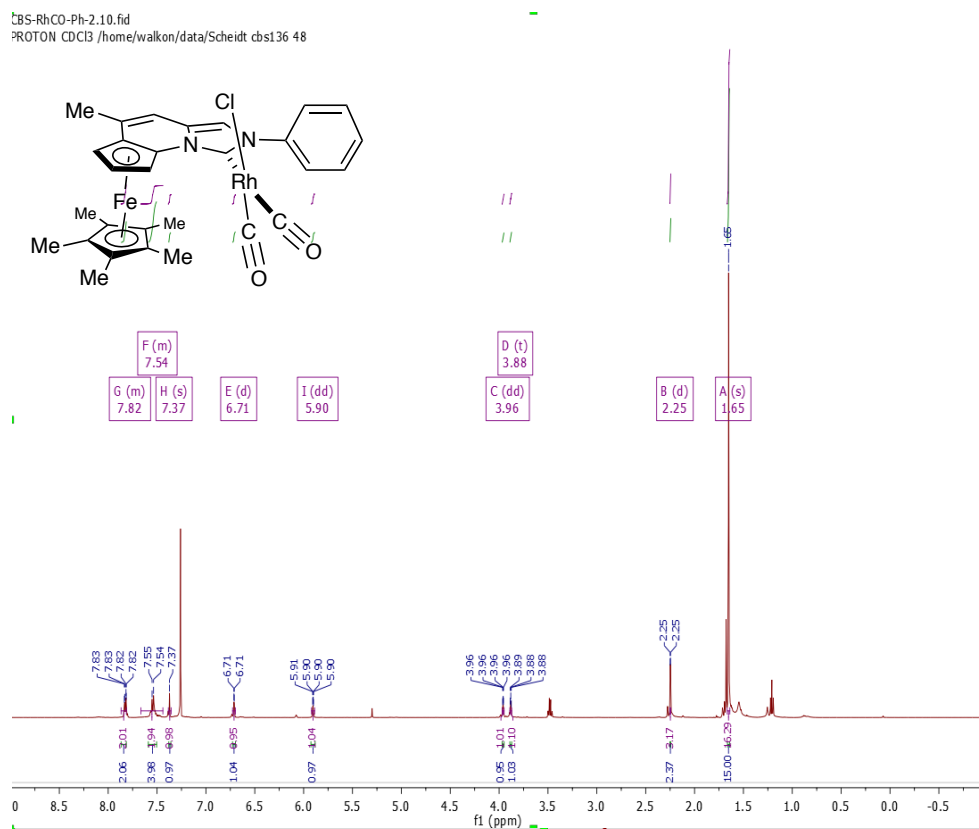




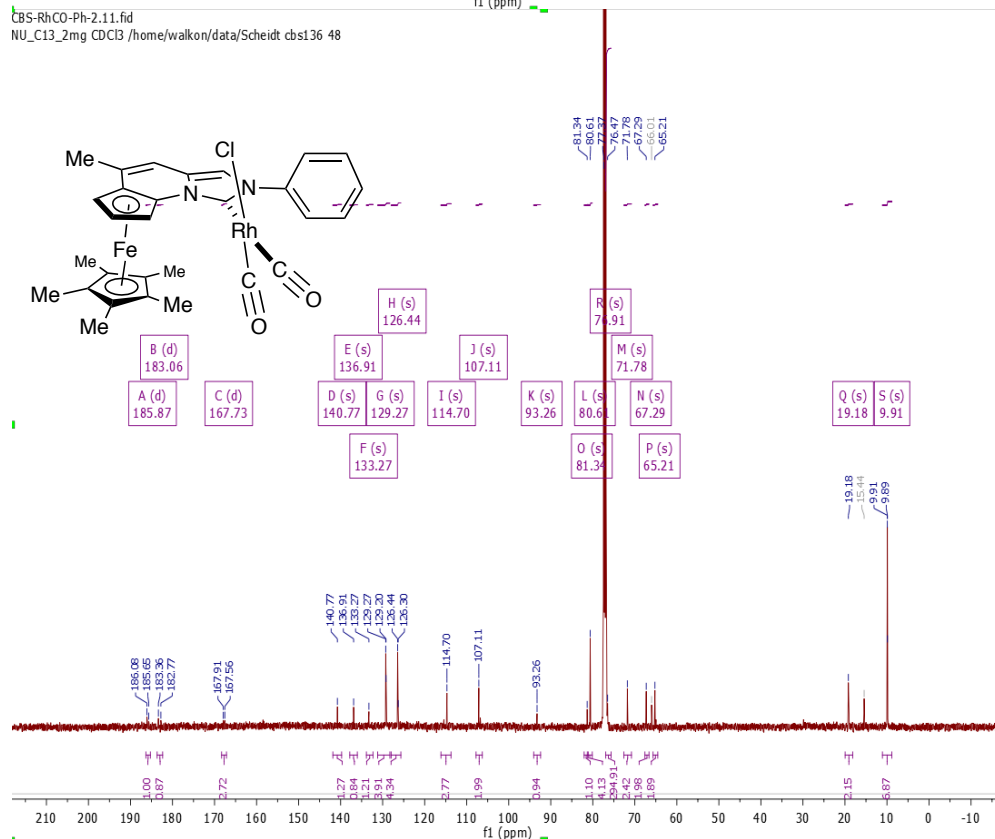


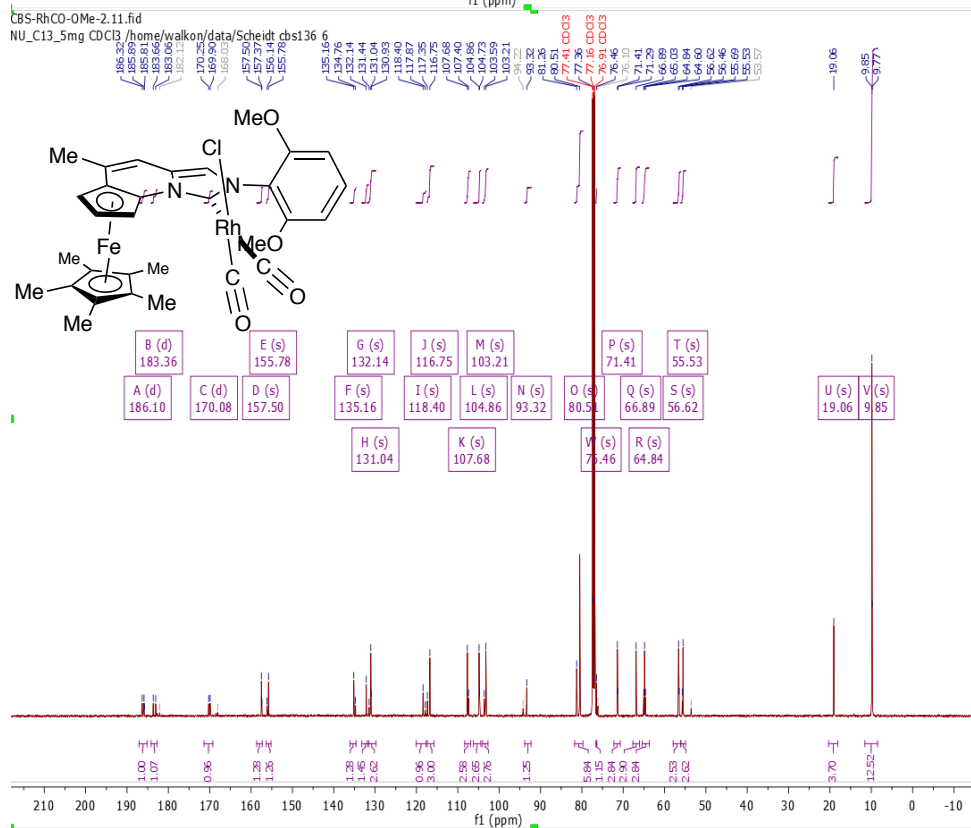
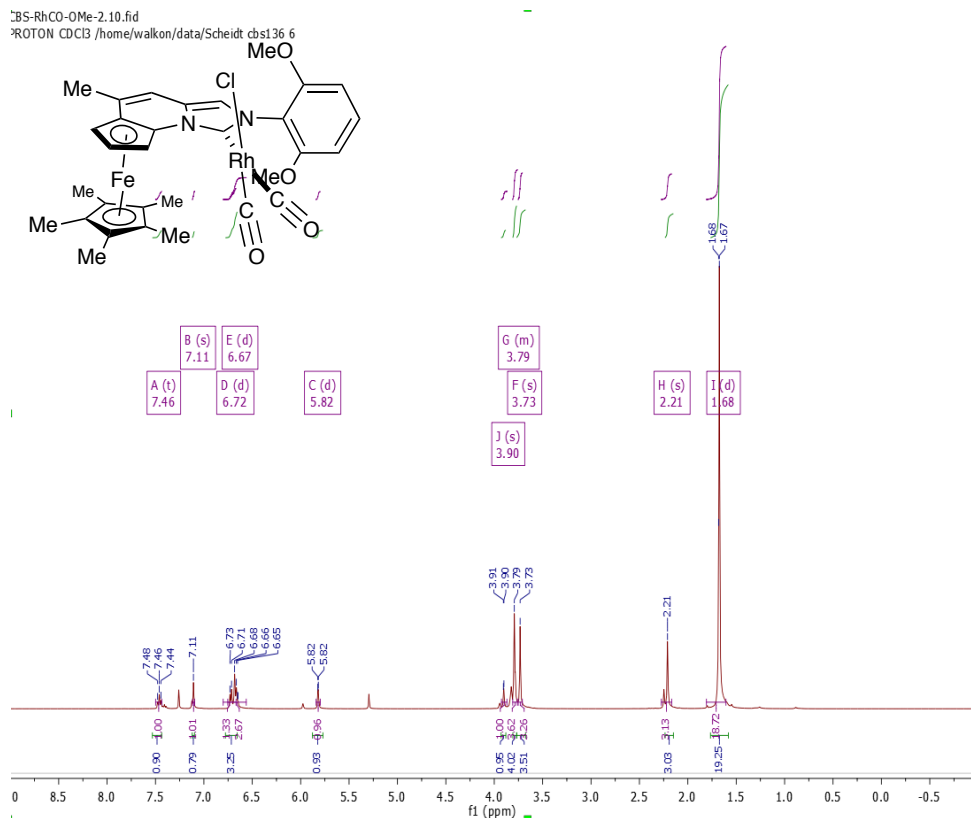


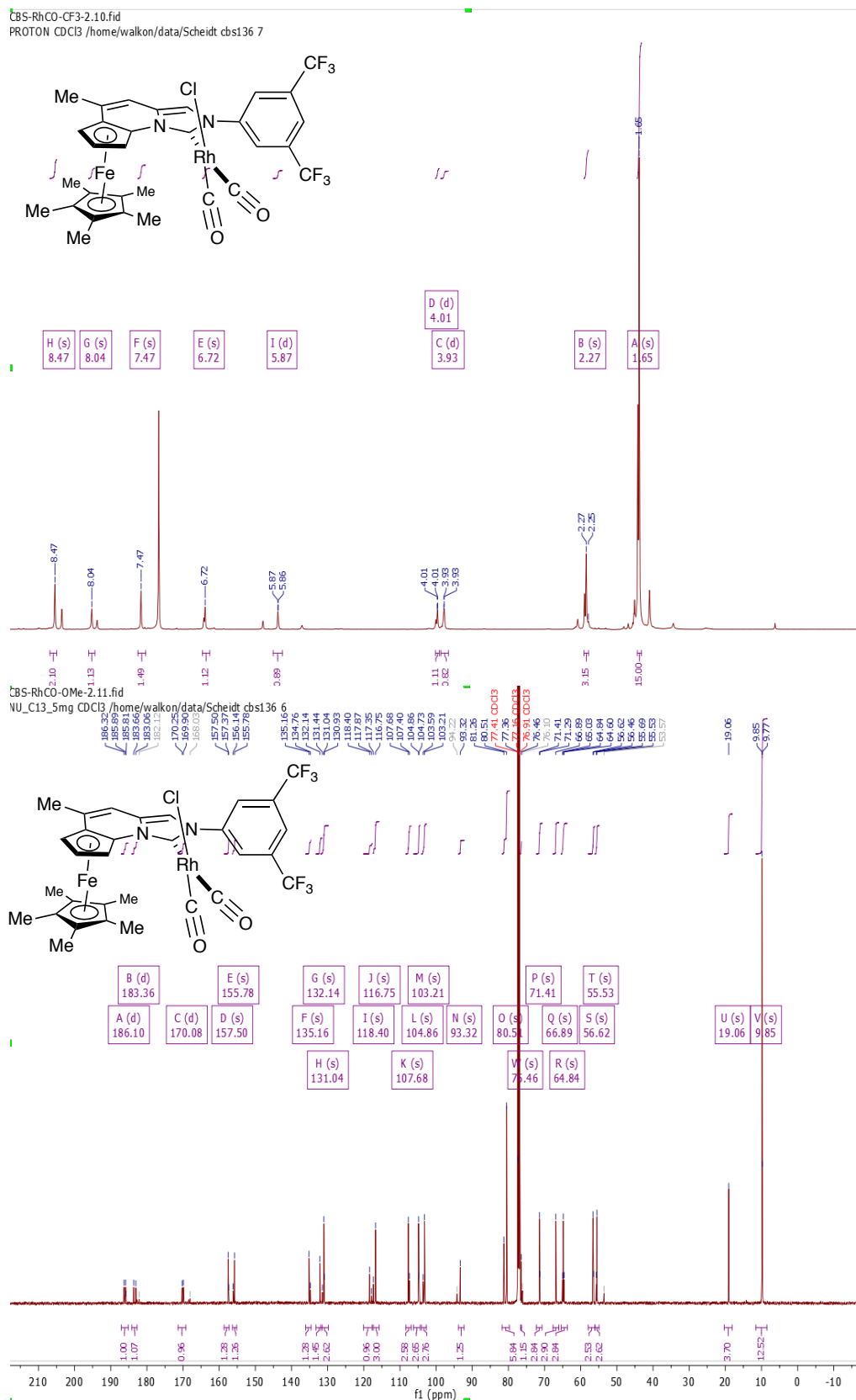
CBS-RhCO-Ph-2.10.fid
 PROTON CDCl3 /home/walkon/data/Scheidt cbs136 48



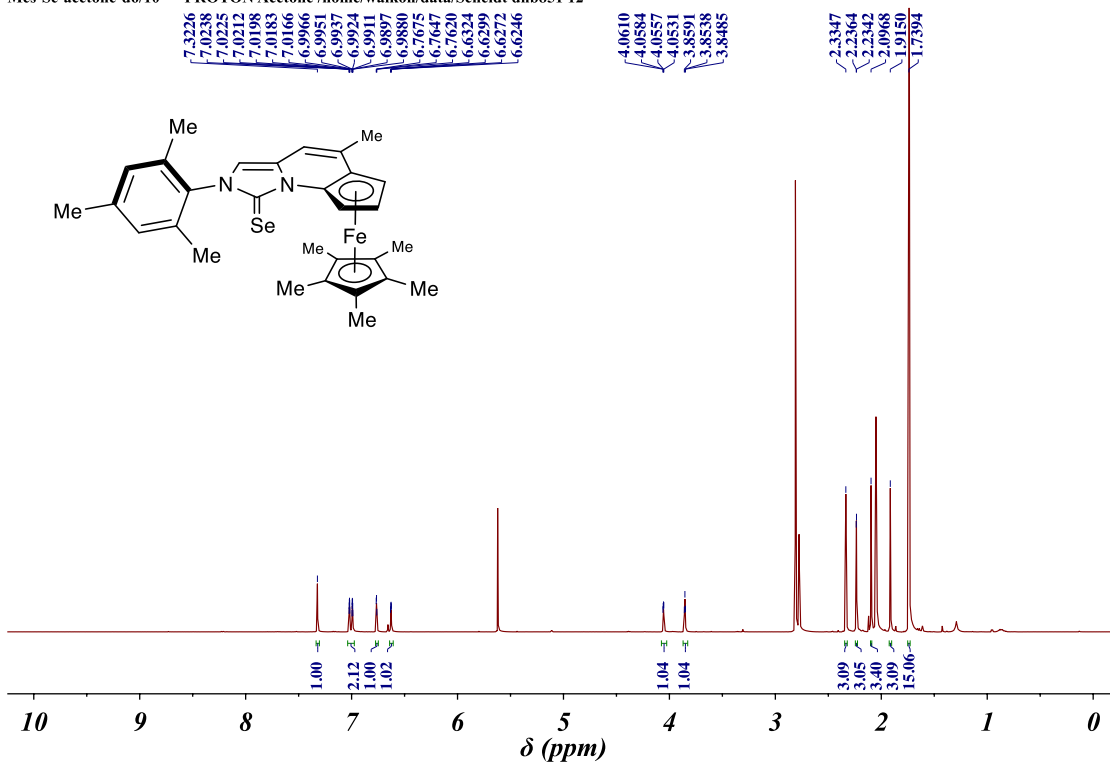
CBS-RhCO-Ph-2.11.fid
 NU_C13_2mg CDCl3 /home/walkon/data/Scheidt cbs136 48



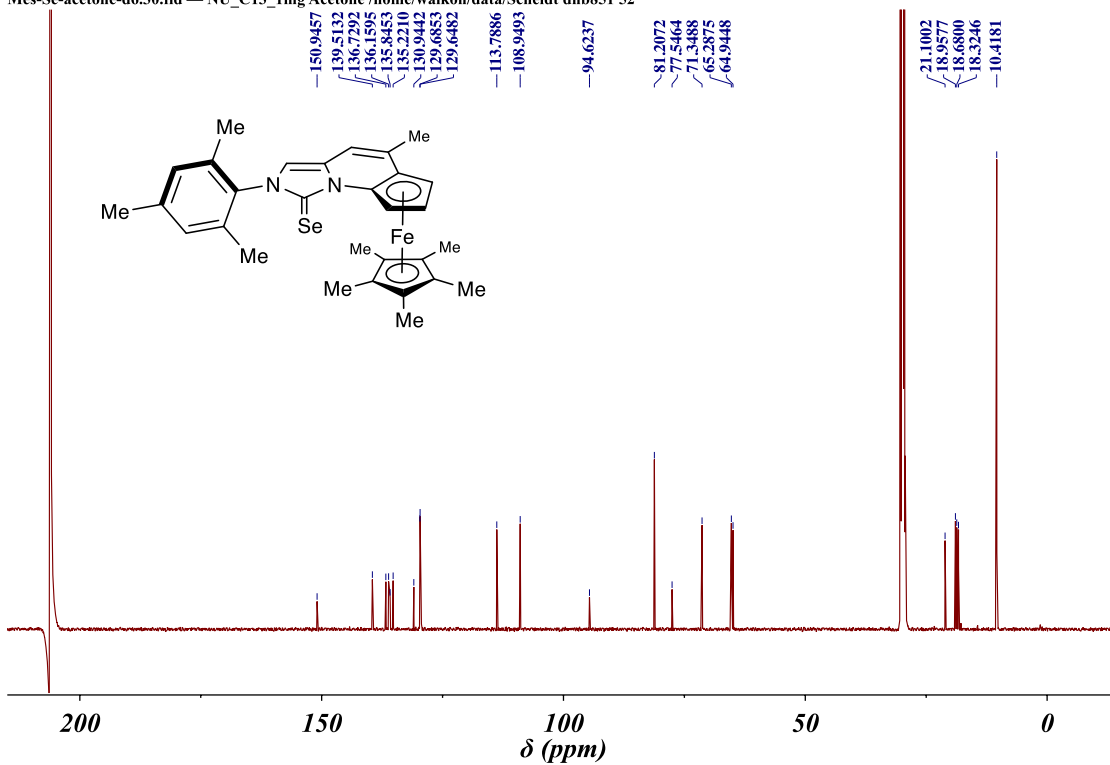




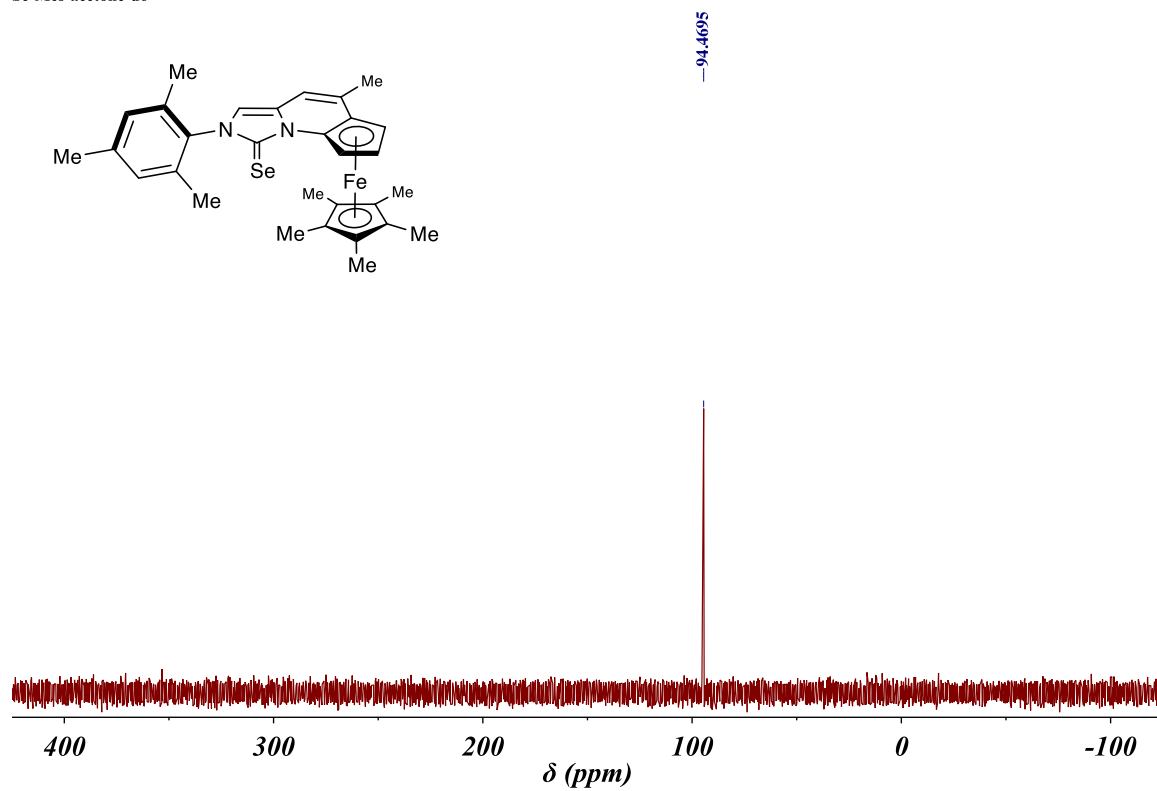
Mes-Se-acetone-d6/10 — PROTON Acetone /home/walkon/data/Scheidt dnb851 12



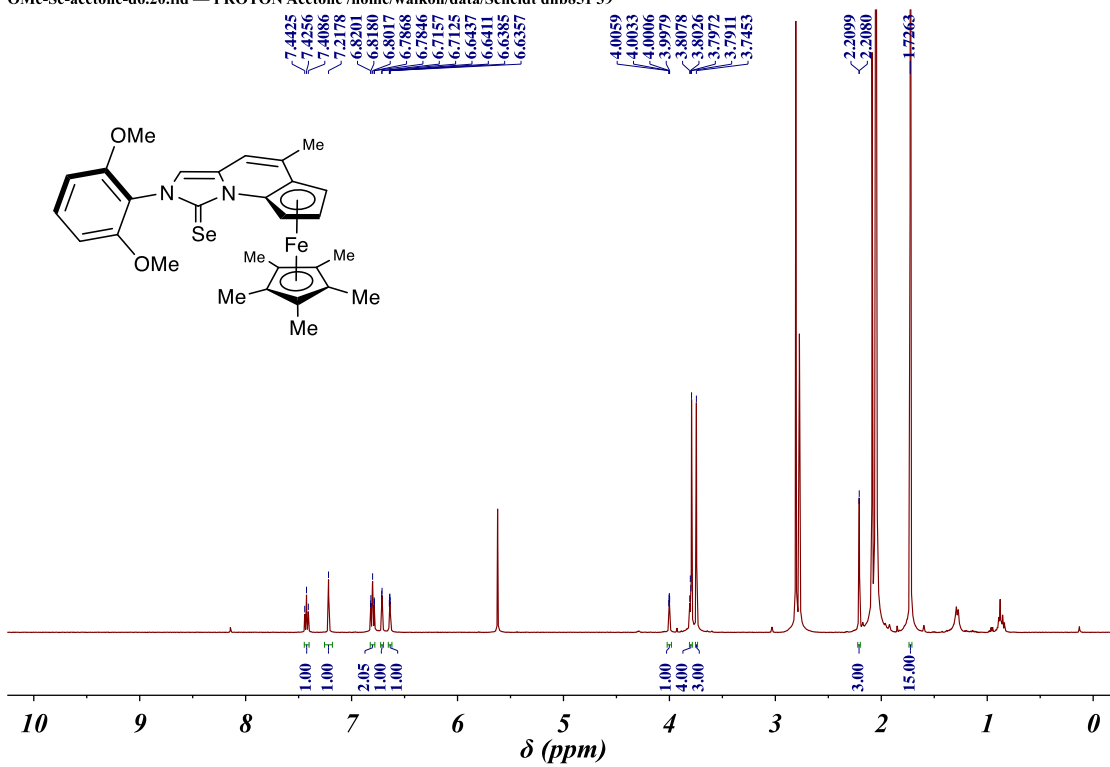
Mes-Se-acetone-d6.30.fid — NU_C13_1mg Acetone /home/walkon/data/Scheidt dnb851 52



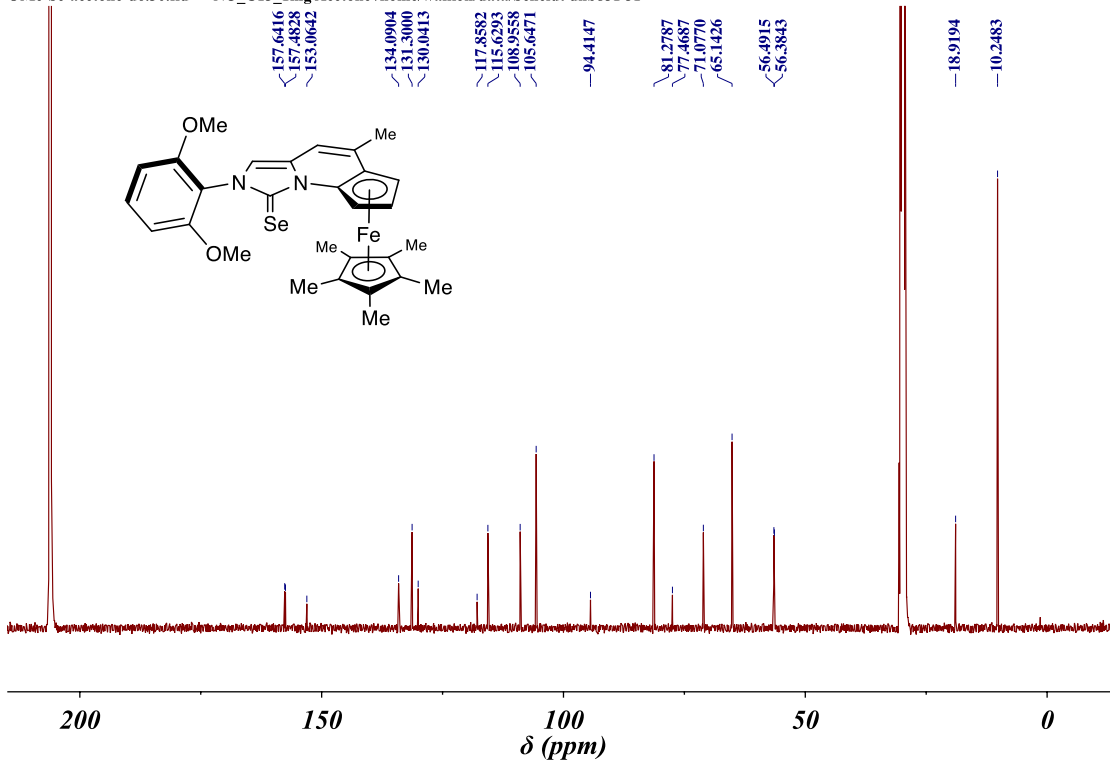
Se-Mes-acetone-d6 —



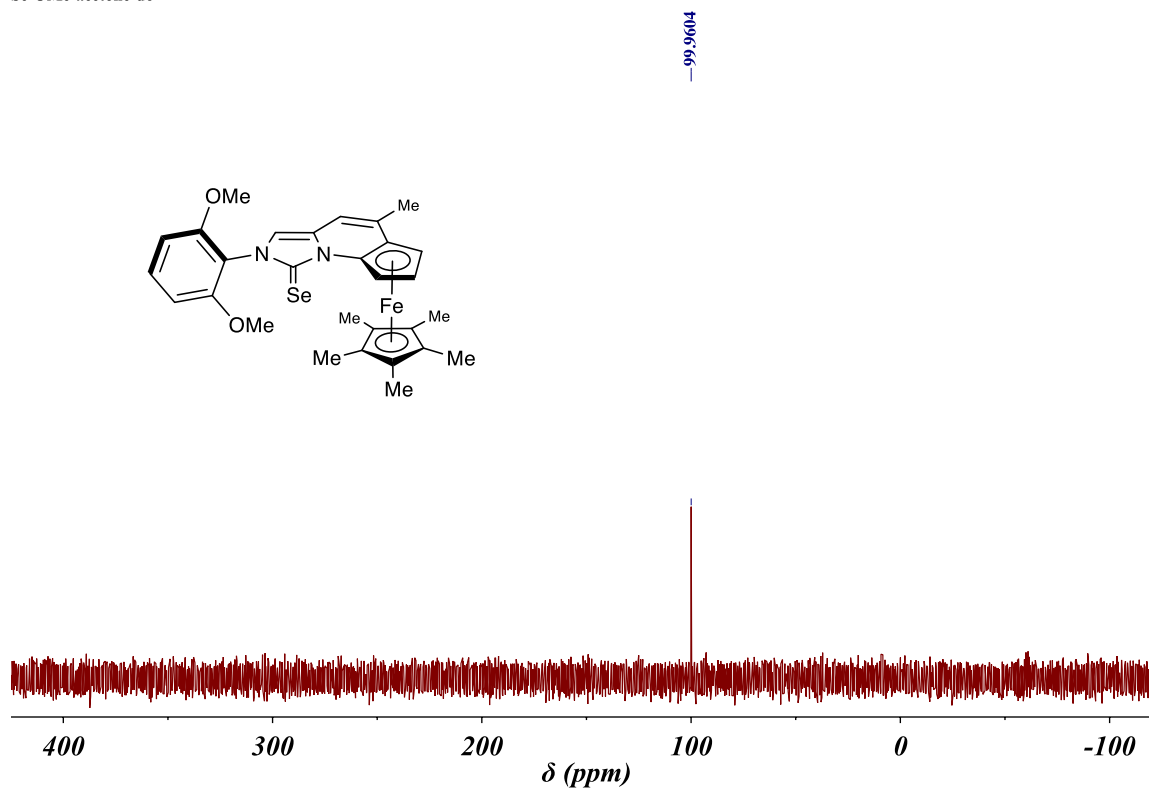
OMe-Se-acetone-d6.20.fid — PROTON Acetone /home/walkon/data/Scheidt dnb851 39



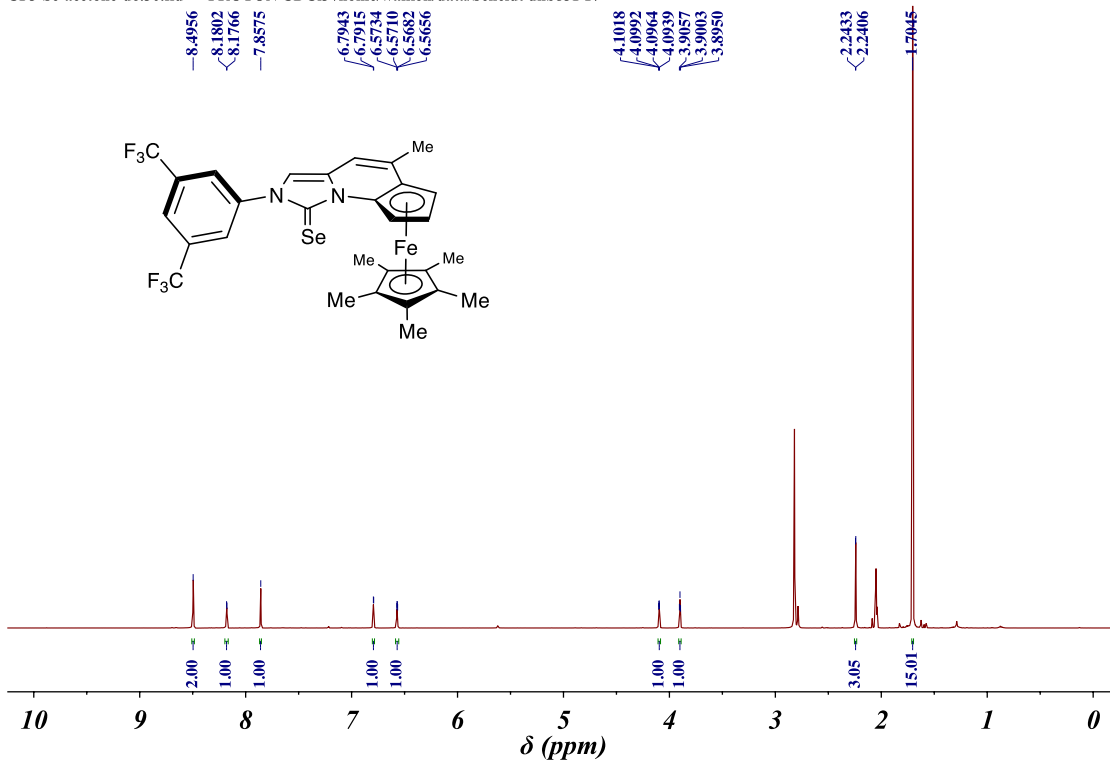
OMe-Se-acetone-d6.30.fid — NU_C13_1mg Acetone /home/walkon/data/Scheidt dnb851 51



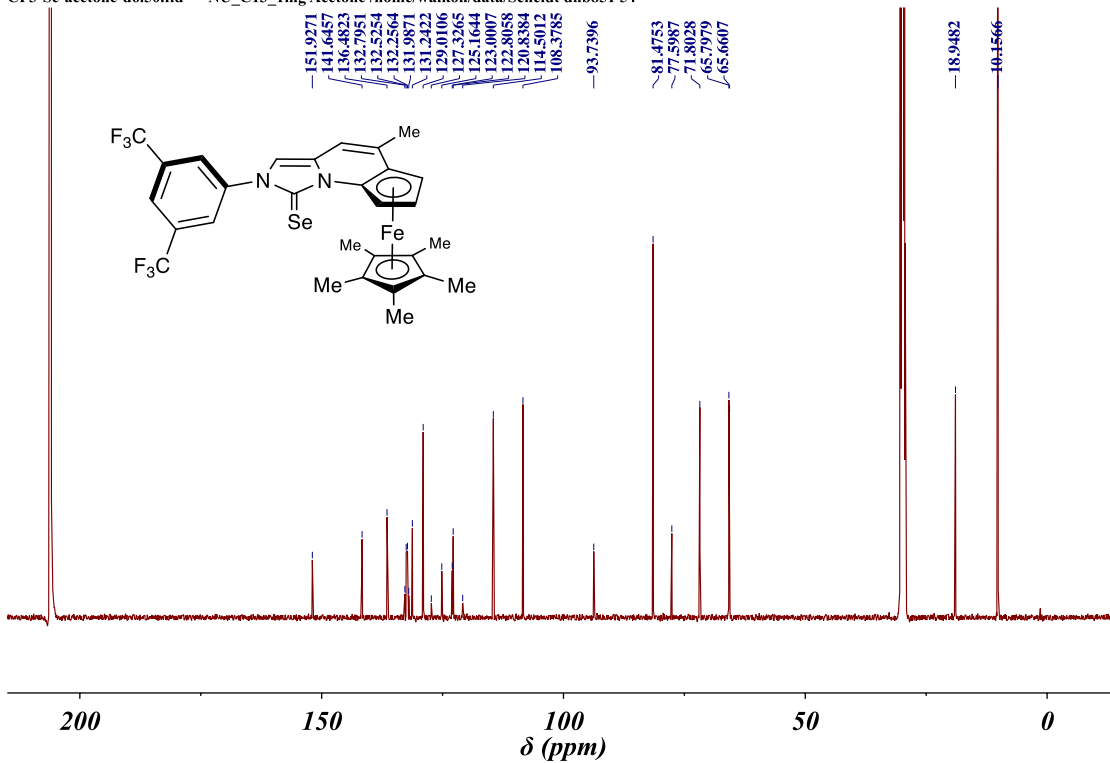
Se-OMe-acetone-d6 — —



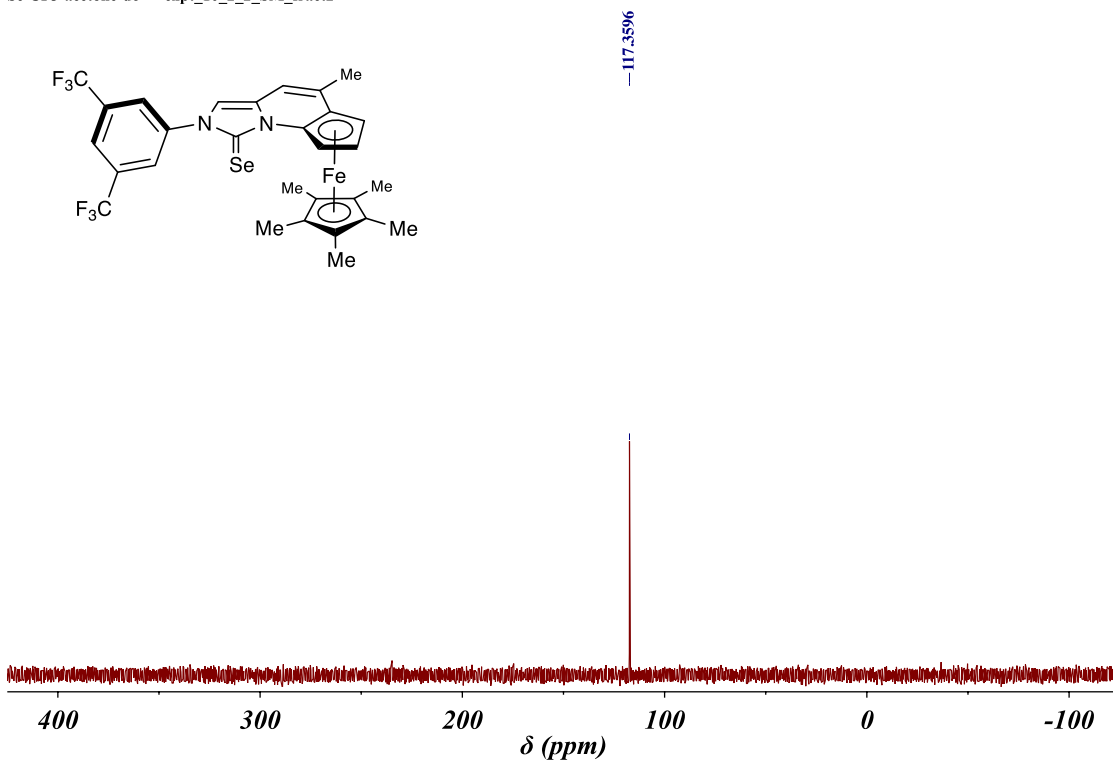
CF3-Se-acetone-d6.30.fid — PROTON CDCI3 /home/walkon/data/Scheidt dnb851 17



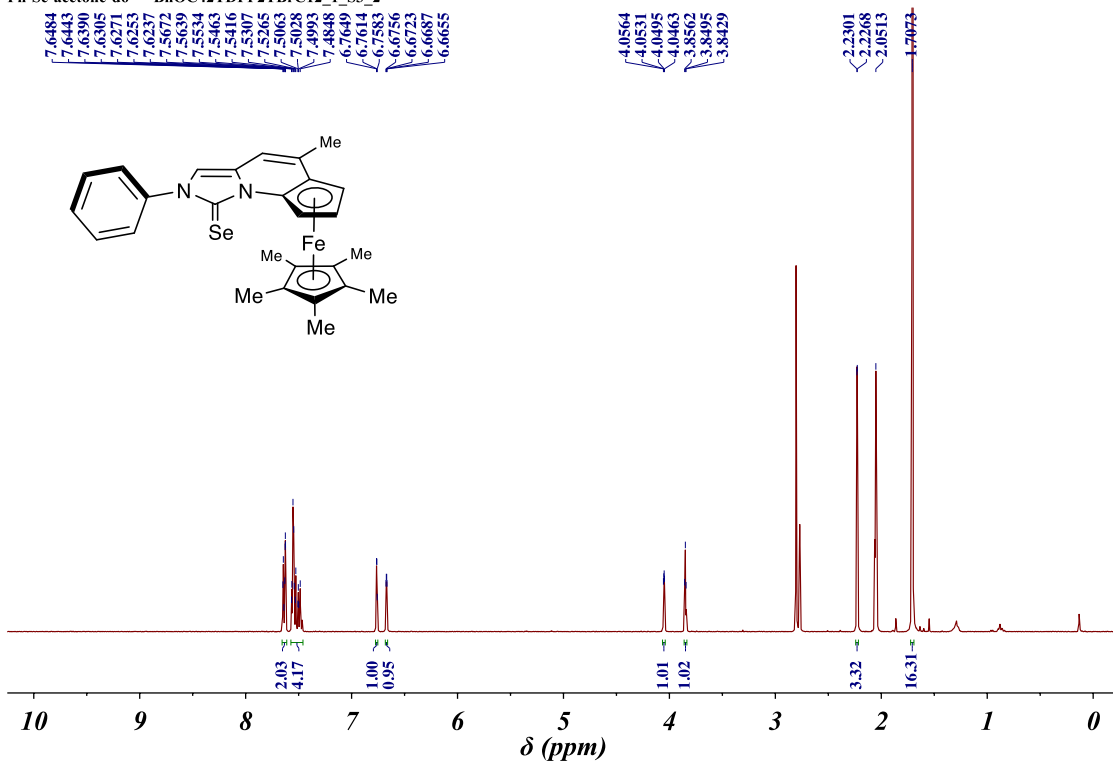
CF3-Se-acetone-d6.50.fid — NU_C13_1mg Acetone /home/walkon/data/Scheidt dnb851 54



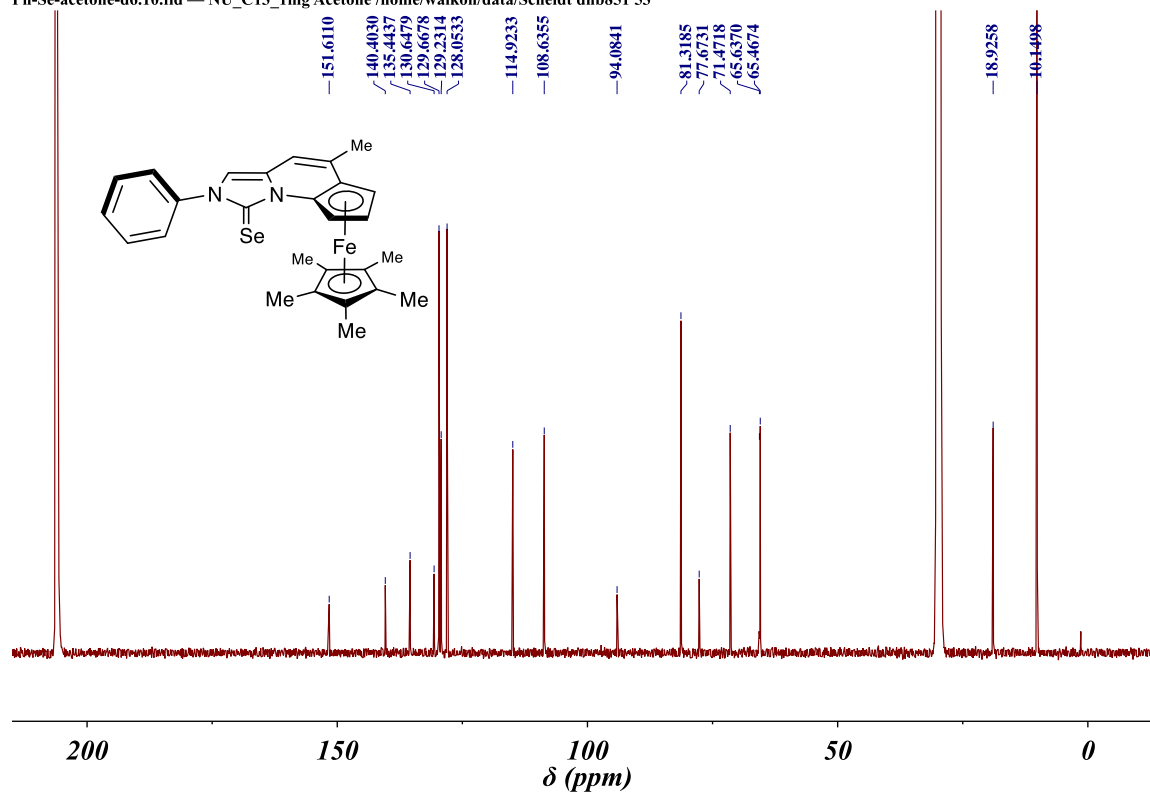
Se-CF3-acetone-d6 — expt_10_2_2_SM_fract2 —



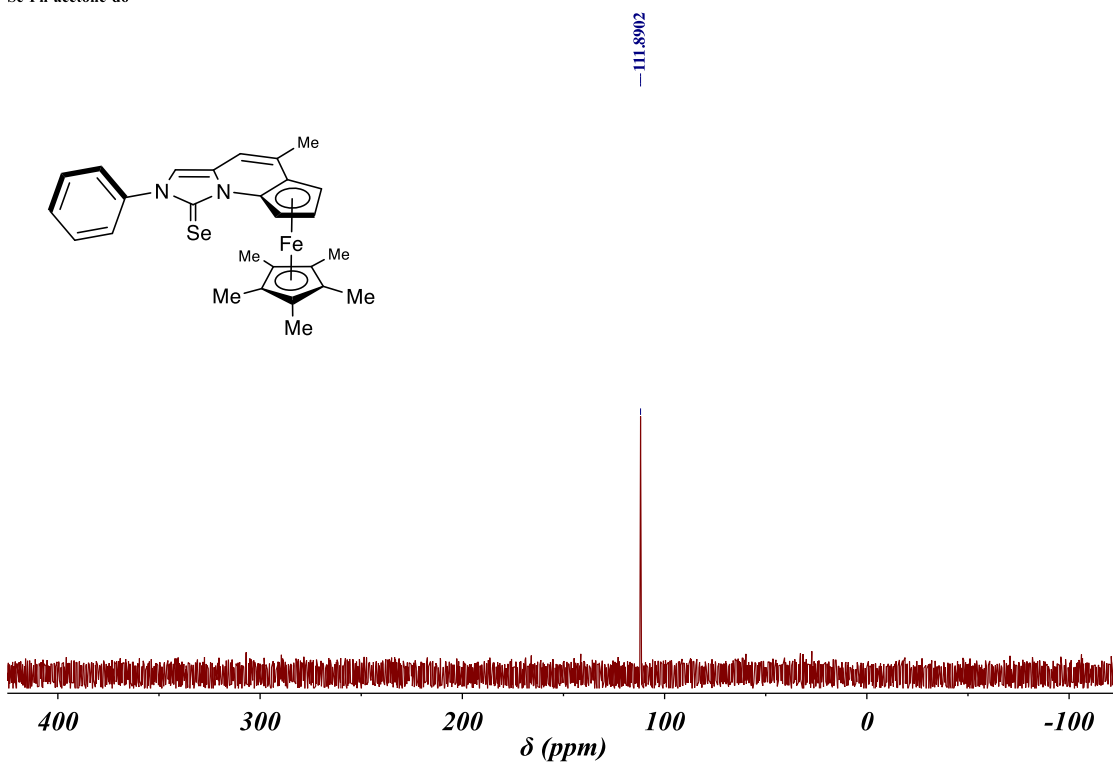
Ph-Se-acetone-d6 — BnOC42DPP2TBrC12_1_S3_2 —



Ph-Se-acetone-d6.10.fid — NU_C13_1mg Acetone /home/walkon/data/Scheidt dnb851 53



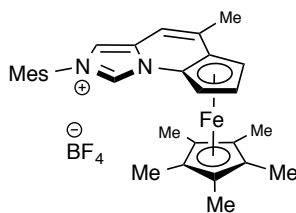
Se-Ph-acetone-d6 — —



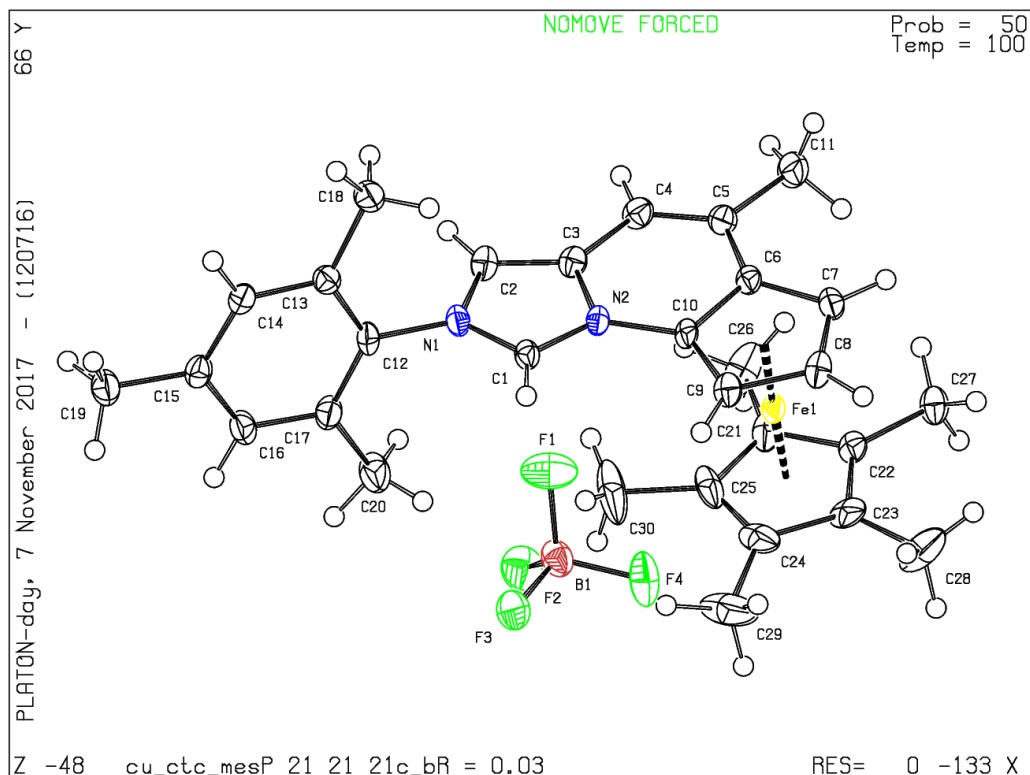
1.7.7 X-Ray Crystal Structure Data

Determination of Absolute Stereochemistry of (+)-Ferrocenyl Mesityl Imidazo[1,5-a]pyridinium Tetrafluoroborate ((+)-**I-93**)

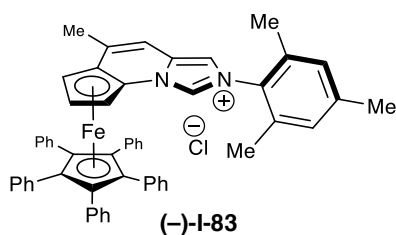
The absolute stereochemistry of (+)-ferrocenyl mesityl imidazo[1,5-a]pyridinium tetrafluoroborate (**(+)-I-93**) was determined by the X-ray diffraction. Recrystallized from solvent diffusion of Et₂O into CH₂Cl₂.



X-ray diffraction was performed at 100.03 K and raw frame data were processed using SAINT. Molecular structures was solved using direct methods and refined on F2 by full-matrix least-square techniques. The GOF = 1.039 for 352 variables refined to R1 = 0.0298 for 4427 reflections with $I > 2\sigma(I)$. A multi-scan absorption correction was performed and the Flack parameter was -0.0090(19). Further information can be found in the CIF file. This crystal was deposited in the Cambridge Crystallographic Data Centre and assigned as CCDC 1007913.



Determination of Structure of pentaphenyl ferrocenyl mesityl imidazo[1,5-a]pyridine rhodium biscarbonyl chloride



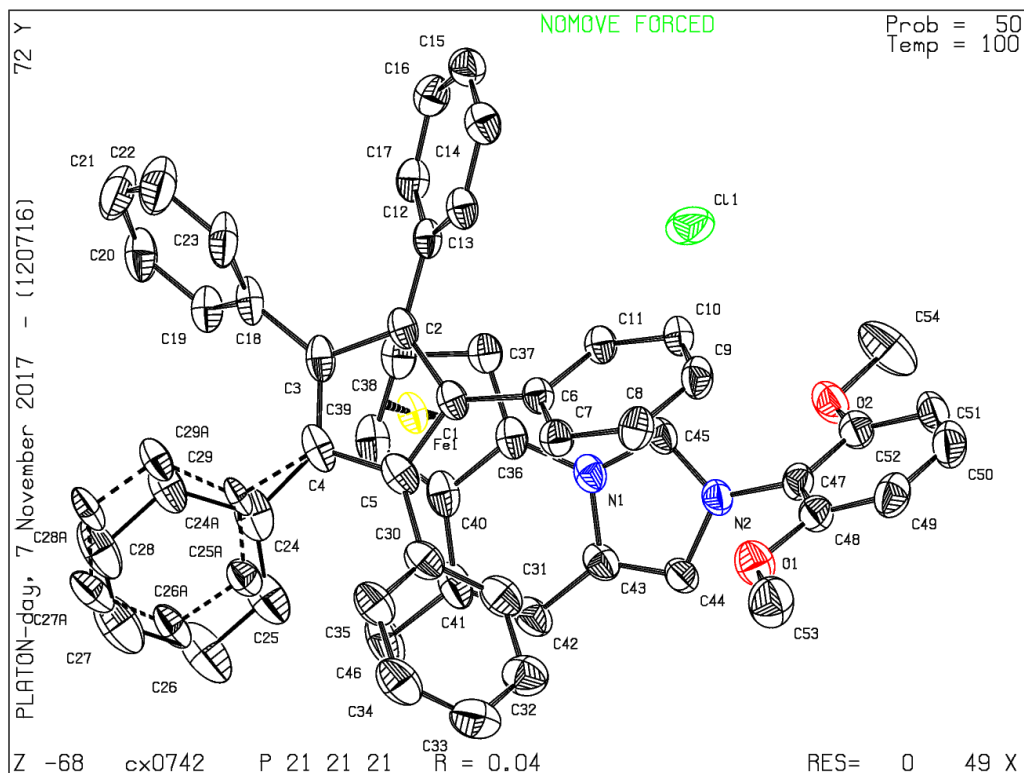
Single crystals of $C_{54}H_{43}ClFeN_2O_2$ (-)-I-83 were supplied. A suitable crystal was selected and the crystal was mounted on a glass fibre in Paratone oil on a Kappa Apex 2 diffractometer. The crystal was kept at 99.92 K during data collection. Using Olex2 [1], the structure was solved

with the ShelXT [2] structure solution program using Direct Methods and refined with the ShelXL [3] refinement package using Least Squares minimisation.

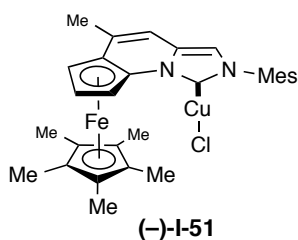
Crystal Data for $C_{54}H_{43}ClFeN_2O_2$ ($M = 843.20$): orthorhombic, space group $P2_12_12_1$ (no. 19), $a = 15.2023(6) \text{ \AA}$, $b = 16.6473(6) \text{ \AA}$, $c = 19.3683(8) \text{ \AA}$, $V = 4901.7(3) \text{ \AA}^3$, $Z = 4$, $T = 99.92 \text{ K}$, $\mu(\text{MoK}\alpha) = 0.401 \text{ mm}^{-1}$, $D_{\text{calc}} = 1.143 \text{ g/mm}^3$, 120232 reflections measured ($3.226 \leq 2\theta \leq 61.114$), 14917 unique ($R_{\text{int}} = 0.0749$, $R_{\text{sigma}} = 0.0574$) which were used in all calculations. The final R_1 was 0.0441 ($I > 2\sigma(I)$) and wR_2 was 0.1037 (all data).

Refinement Details. The enhanced rigid-bond restraint (SHELX keyword RIGU) was applied on the disordered phenyl ring. (Acta Cryst. A68 (2012) 448-451)

Solvent Treatment Details. The solvent masking procedure as implemented in Olex2 was used to remove the electronic contribution of solvent molecules from the refinement. As the exact solvent content is not known, only the atoms used in the refinement model are reported in the formula here. Total solvent accessible volume / cell = 1188.0 \AA^3 [24.2%] Total electron count / cell = 289.4



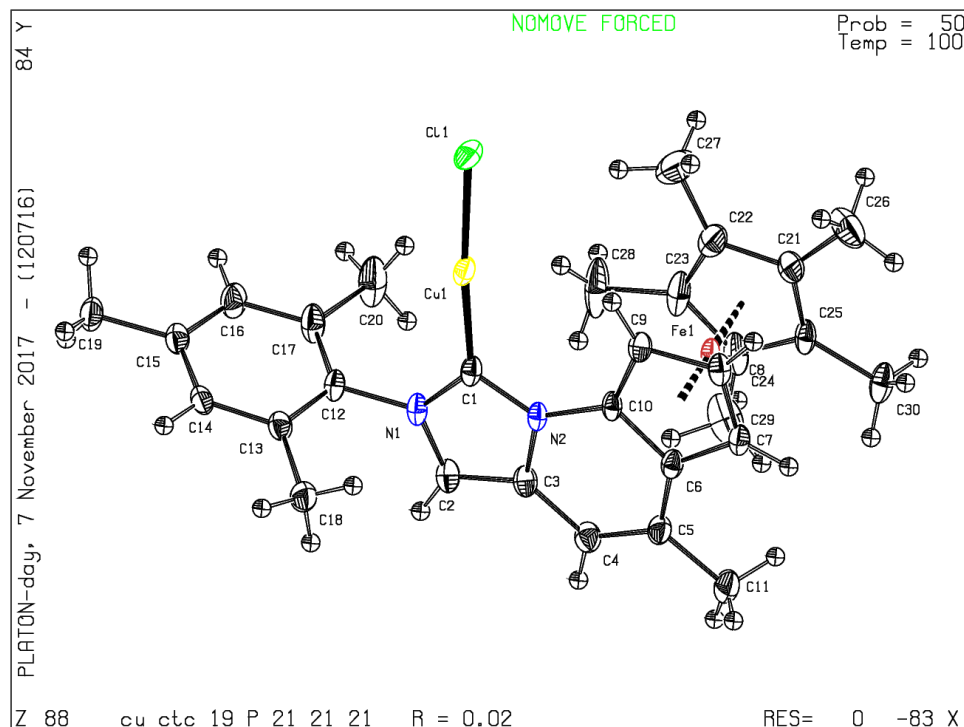
Determination of Structure of (-)-Ferrocenyl Mesityl Imidazo[1,5-a]pyridine Copper Chloride Complex (-)-I-51



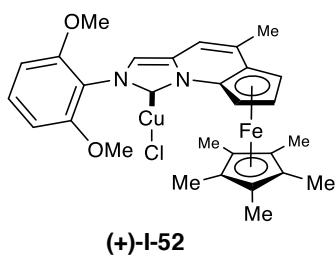
The absolute stereochemistry/structure of (-)-ferrocenyl mesityl imidazo[1,5-a]pyridine copper chloride complex was determined by the X-ray diffraction. Recrystallized from slow evaporation of CH_2Cl_2 /pentane at $-30\text{ }^\circ\text{C}$.

X-ray diffraction was performed at 100.04 K and raw frame data were processed using SAINT. Molecular structures was solved using direct methods and refined on F2 by full-matrix

least-square techniques. The GOF = 1.047 for 325 variables refined to $R1 = 0.0201$ for 4072 reflections with $I > 2\sigma(I)$. A multi-scan absorption correction was performed and the Flack parameter was 0.033(2). Further information can be found in the CIF file. This crystal was deposited in the Cambridge Crystallographic Data Centre and assigned as CCDC 1007914.



Determination of Structure of (+)-Ferrocenyl 2,6-dimethoxyphenyl Imidazo[1,5-a]pyridine Copper Chloride Complex (+)-I-52

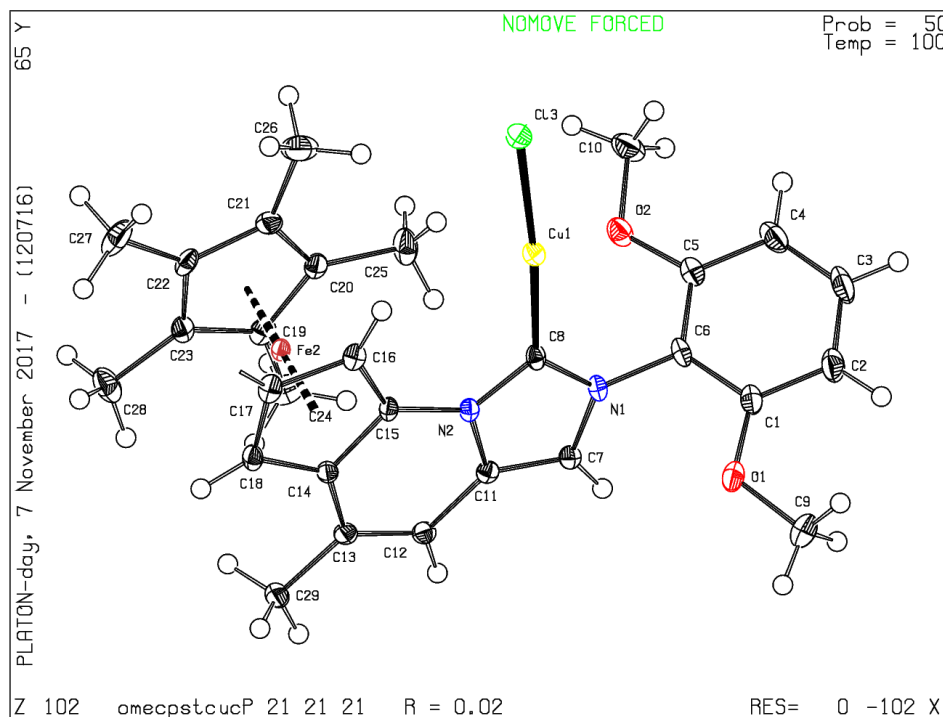


Single crystals of $C_{29}H_{32}ClCuFeN_2O_2$ ((+)-I-52) were recrystallized from slow evaporation of CH_2Cl_2 /pentane at $-30\text{ }^\circ\text{C}$.

A suitable crystal was selected and mounted in inert oil and transferred to the cold gas stream of a 'Bruker APEX-II CCD' diffractometer. The crystal was kept at 99.98 K during data collection. Using Olex2 [1], the structure was solved with the ShelXS [4] structure solution program using Direct Methods and refined with the ShelXL [3] refinement package using Least Squares minimisation. A multi-scan absorption correction was performed and the Flack parameter was -0.005(1)

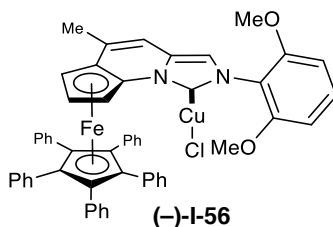
Crystal Data for $C_{29}H_{32}ClCuFeN_2O_2$ ($M = 595.40$): orthorhombic, space group $P2_12_12_1$ (no. 19), $a = 11.4799(10)$ Å, $b = 15.0428(13)$ Å, $c = 15.3127(13)$ Å, $V = 2644.3(4)$ Å³, $Z = 4$, $T = 99.98$ K, $\mu(\text{CuK}\alpha) = 6.549$ mm⁻¹, $D_{\text{calc}} = 1.496$ g/mm³, 45535 reflections measured ($8.24 \leq 2\theta \leq 136.396$), 4798 unique ($R_{\text{int}} = 0.0305$, $R_{\text{sigma}} = 0.0179$) which were used in all calculations. The final R_1 was 0.0211 ($I > 2\sigma(I)$) and wR_2 was 0.0558 (all data).

Refinement Details. No special refinement necessary.



Determination of Structure of (-)-pentaphenyl ferrocenyl 2,6-dimethoxyphenyl

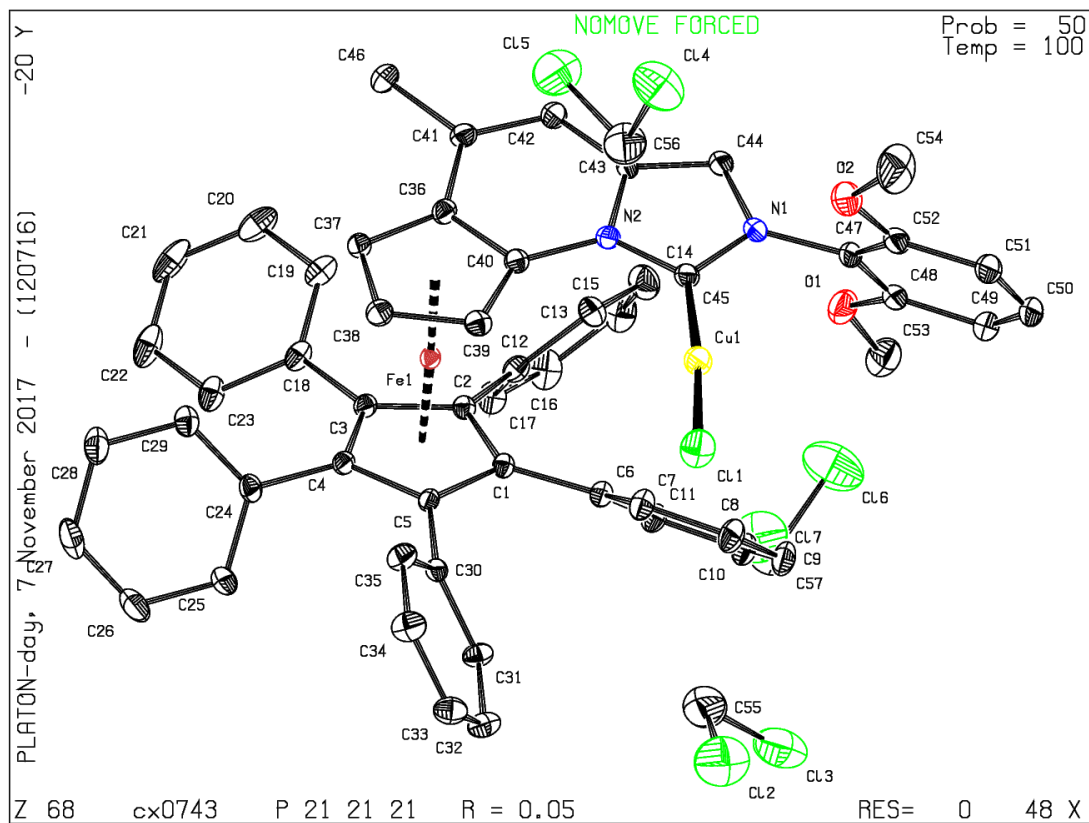
Imidazo[1,5-a]pyridine Copper Chloride Complex (-)-I-56



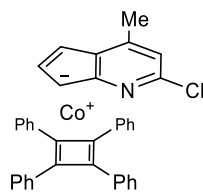
Single crystals of $C_{57}H_{48}Cl_7CuFeN_2O_2$ (-)-I-56 were submitted. A suitable crystal was selected and The crystal was mounted on a glass fibre in Paratone oil on a Kappa Apex 2 diffractometer. The crystal was kept at 100.04 K during data collection. Using Olex2 [1], the structure was solved with the ShelXT [2] structure solution program using Direct Methods and refined with the ShelXL [3] refinement package using Least Squares minimisation. The absolute structure parameter y (Hooft, Straver & Spek, 2008) was calculated using PLATON (Spek, 2010). The resulting value was $y=0.001(3)$ indicating that the absolute structure has probably been determined correctly.

Crystal Data for $C_{57}H_{48}Cl_7CuFeN_2O_2$ ($M=1160.51$): orthorhombic, space group $P2_12_12_1$ (no. 19), $a = 15.6465(4)$ Å, $b = 16.9240(4)$ Å, $c = 19.6011(5)$ Å, $V = 5190.4(2)$ Å³, $Z = 4$, $T = 100.04$ K, $\mu(\text{MoK}\alpha) = 1.095$ mm⁻¹, $D_{\text{calc}} = 1.485$ g/mm³, 198690 reflections measured ($3.18 \leq 2\Theta \leq 66.432$), 19753 unique ($R_{\text{int}} = 0.0438$, $R_{\text{sigma}} = 0.0358$) which were used in all calculations. The final R_1 was 0.0479 ($I > 2\sigma(I)$) and wR_2 was 0.1371 (all data).

Refinement Details. No special refinement necessary.



Determination of Structure of (η -tetraphenylcyclobutadiene)-[η -(2-chloro-4-methylcyclopenta[b]pyridin-7-yl)]cobalt I-49



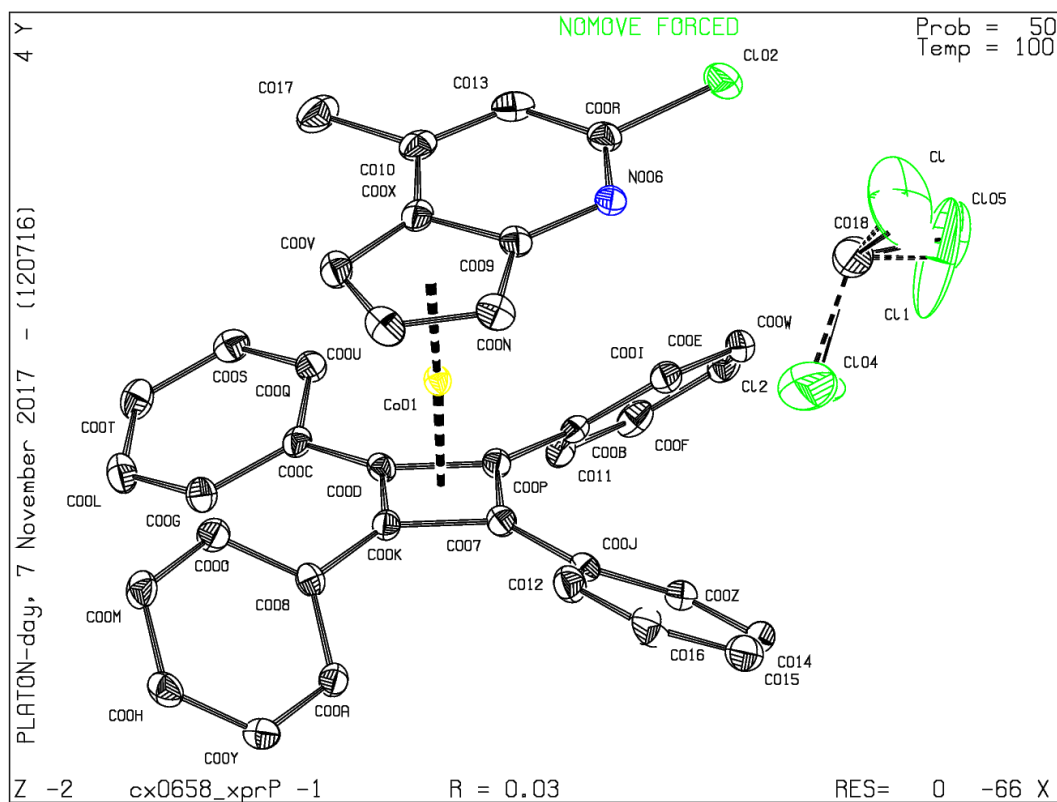
I-49

Single crystals of $C_{38}DCl_4CoH_{27}N$ **I-49** were crystallized from liquid-liquid diffusion of $CDCl_3$ /pentane in an NMR tube. A suitable crystal was selected and mounted in inert oil and transferred to the cold gas stream of a Bruker APEX-II CCD diffractometer. The crystal was kept at 100.01 K during data collection. Using Olex2 [1], the structure was solved with the ShelXT

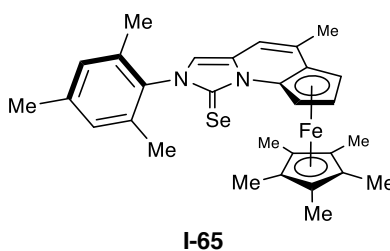
[2] structure solution program using Direct Methods and refined with the ShelXL [3] refinement package using Least Squares minimisation.

Crystal Data for $C_{38}DCl_4CoH_{27}N$ ($M=700.35$): triclinic, space group P-1 (no. 2), $a = 11.4645(6)$ Å, $b = 11.7797(6)$ Å, $c = 13.1312(7)$ Å, $\alpha = 79.119(2)^\circ$, $\beta = 68.4940(10)^\circ$, $\gamma = 75.0180(10)^\circ$, $V = 1585.06(14)$ Å³, $Z = 2$, $T = 100.01$ K, $\mu(\text{CuK}\alpha) = 7.567$ mm⁻¹, $D_{\text{calc}} = 1.467$ g/mm³, 21904 reflections measured ($10.108 \leq 2\theta \leq 130.26$), 5399 unique ($R_{\text{int}} = 0.0415$, $R_{\text{sigma}} = 0.0348$) which were used in all calculations. The final R_1 was 0.0275 ($I > 2\sigma(I)$) and wR_2 was 0.0728 (all data). This crystal was deposited in the Cambridge Crystallographic Data Centre and assigned as CCDC 1495134.

Refinement Details. No special refinement necessary.



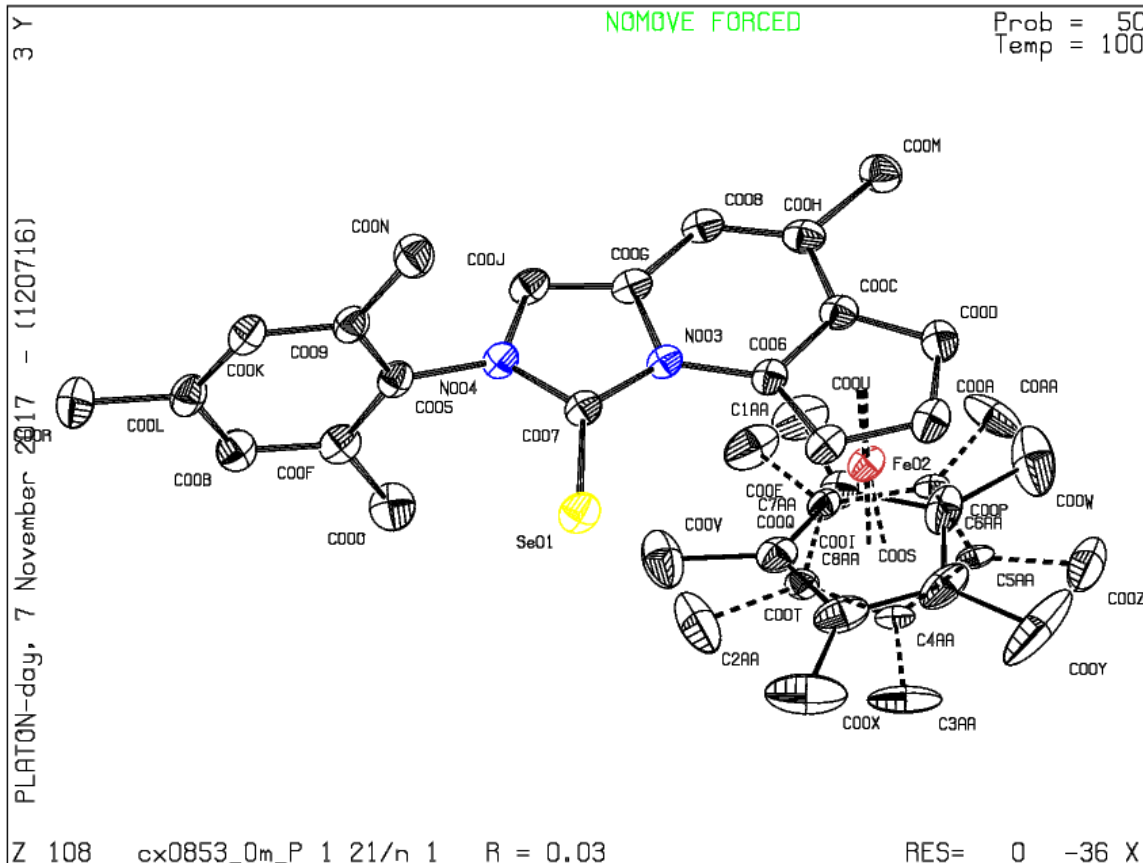
Determination of Structure of Ferrocenyl Mesityl Imidazo[1,5-a]pyridine Selenium Complex I-65



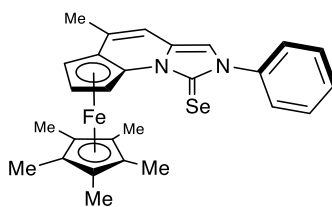
Single crystals of $C_{30}H_{34}FeN_2Se$ **I-65** were recrystallized via the slow evaporation of acetone at 23 °C. A suitable crystal was selected and mounted in inert oil and transferred to the cold gas stream of a 'Bruker APEX-II CCD' diffractometer. The crystal was kept at 100.02 K during data collection. Using Olex2 [1], the structure was solved with the ShelXT [2] structure solution program using Intrinsic Phasing and refined with the ShelXL [3] refinement package using Least Squares minimisation. SADABS-2014/5 (Bruker,2014/5) was used for absorption correction. $wR_2(\text{int})$ was 0.0979 before and 0.0628 after correction. The Ratio of minimum to maximum transmission is 0.7694.

Crystal Data for $C_{30}H_{34}FeN_2Se$ ($M = 557.40$): monoclinic, space group $P2_1/n$ (no. 14), $a = 16.5941(8) \text{ \AA}$, $b = 8.5541(4) \text{ \AA}$, $c = 18.8413(9) \text{ \AA}$, $\beta = 106.008(3)^\circ$, $V = 2570.8(2) \text{ \AA}^3$, $Z = 4$, $T = 100.02 \text{ K}$, $\mu(\text{CuK}\alpha) = 6.467 \text{ mm}^{-1}$, $D_{\text{calc}} = 1.440 \text{ g/mm}^3$, 29416 reflections measured ($6.294 \leq 2\theta \leq 133.244$), 4533 unique ($R_{\text{int}} = 0.0565$, $R_{\text{sigma}} = 0.0384$) which were used in all calculations. The final R_1 was 0.0295 ($I > 2\sigma(I)$) and wR_2 was 0.0752 (all data).

Refinement Details. The enhanced rigid-bond restraint (SHELX keyword RIGU) was applied on the disordered Cp* ring. (Acta Cryst. A68 (2012) 448-451)



Determination of Structure of Ferrocenyl Phenyl Imidazo[1,5-a]pyridine Selenium Complex I-67



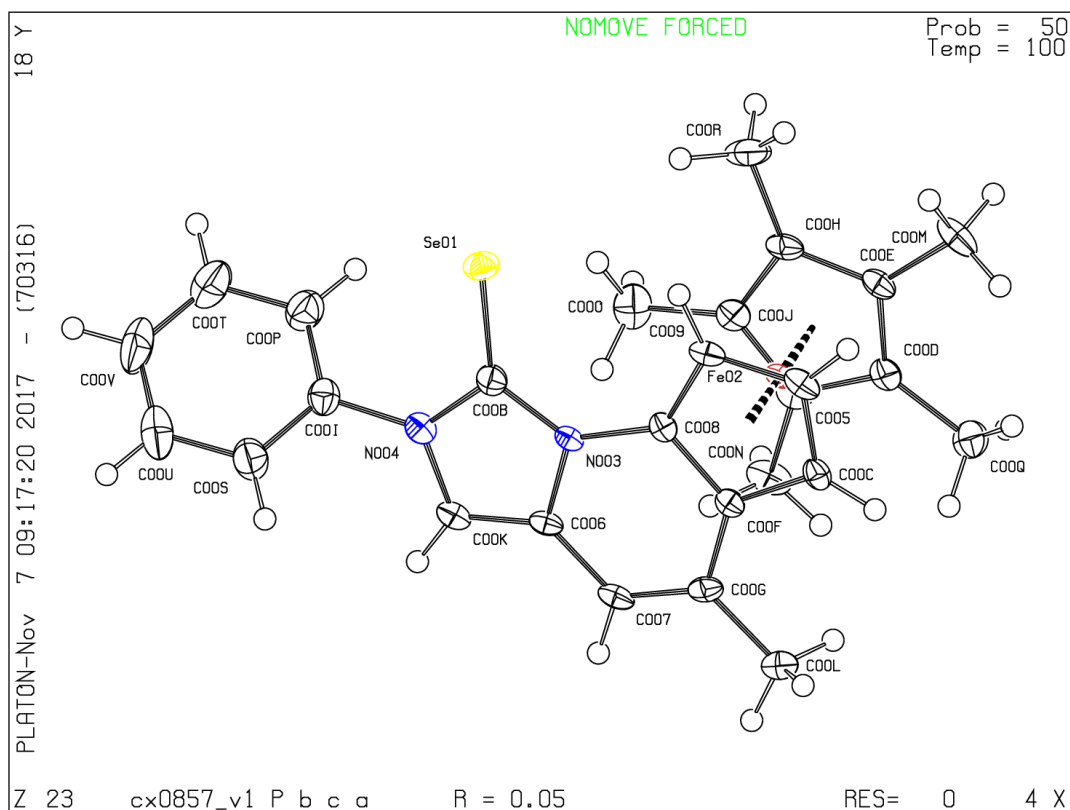
I-67

Single crystals of $C_{27}H_{28}FeN_2Se$ **I-67** were via the slow evaporation of acetone at 23 °C. A suitable crystal was selected and mounted in inert oil and transferred to the cold gas stream of a 'Bruker APEX-II CCD' diffractometer. The crystal was kept at 100.0 K during data collection. Using Olex2 [1], the structure was solved with the ShelXT [2] structure solution program using

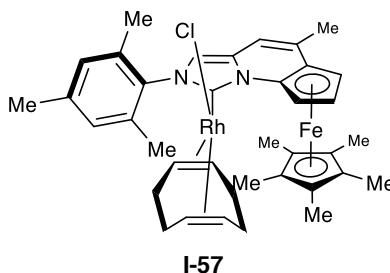
Intrinsic Phasing and refined with the ShelXL [3] refinement package using Least Squares minimisation.

Crystal Data for $C_{27}H_{28}FeN_2Se$ ($M=515.32$): orthorhombic, space group $Pbca$ (no. 61), $a = 40.6140(19)$ Å, $b = 13.5714(6)$ Å, $c = 8.4756(4)$ Å, $V = 4671.7(4)$ Å³, $Z = 8$, $T = 100.0$ K, $\mu(CuK\alpha) = 7.071$ mm⁻¹, $D_{calc} = 1.465$ g/mm³, 19682 reflections measured ($7.834 \leq 2\Theta \leq 133.386$), 4095 unique ($R_{int} = 0.0681$, $R_{sigma} = 0.0540$) which were used in all calculations. The final R_1 was 0.0513 ($I > 2\sigma(I)$) and wR_2 was 0.1175 (all data).

Refinement Details. Reflections (2 5 4), (0 4 4), and (4 2 8), with error/esd -13.28 , -11.67 , and -8.63 respectively, were omitted from refinement.



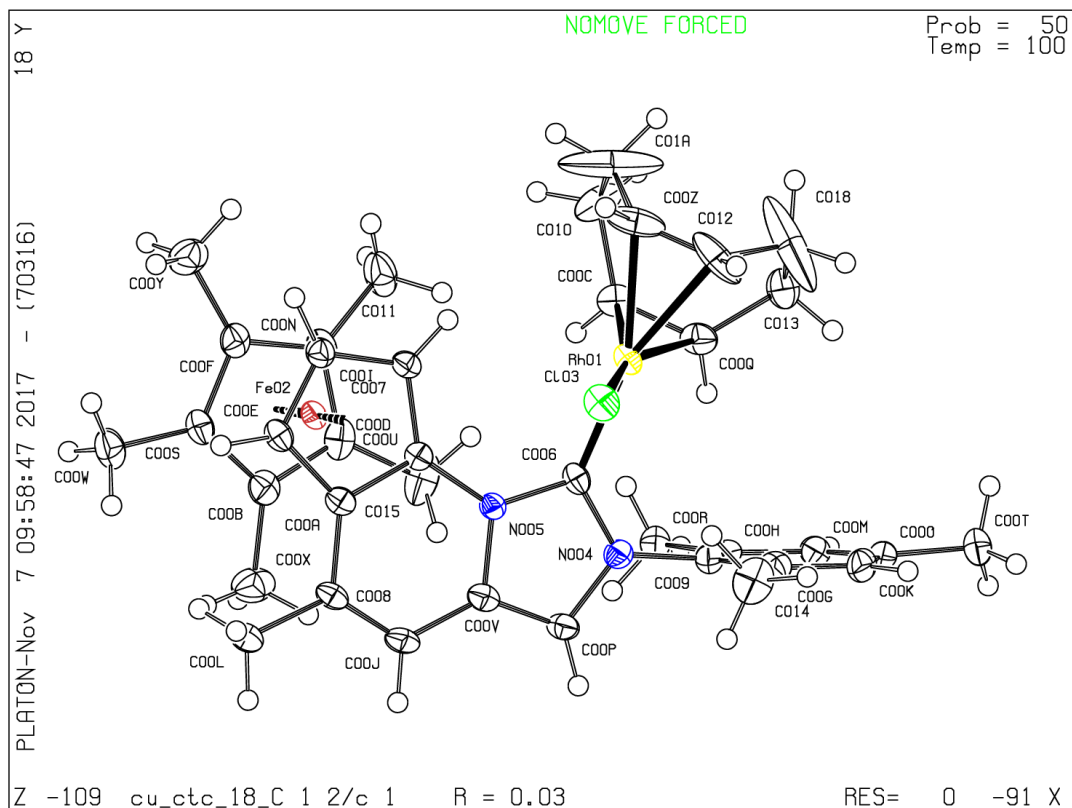
**Determination of Structure of Ferrocenyl Mesityl Imidazo[1,5-a]pyridine Rh(cod)Cl
complex I-57**



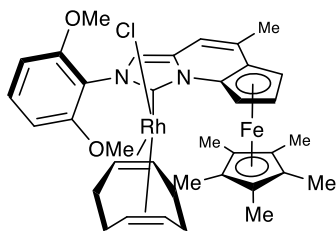
Single crystals of $C_{38}H_{46}ClFeN_2Rh$ **I-57** were recrystallized from slow evaporation of CH_2Cl_2 /pentane at $-30\text{ }^\circ\text{C}$. A suitable crystal was selected and mounted in inert oil and transferred to the cold gas stream of a 'Bruker APEX-II CCD' diffractometer. The crystal was kept at 100.02 K during data collection. Using Olex2 [1], the structure was solved with the ShelXT [2] structure solution program using Intrinsic Phasing and refined with the ShelXL [3] refinement package using Least Squares minimisation.

Crystal Data for $C_{38}H_{46}ClFeN_2Rh$ ($M=724.98$): monoclinic, space group $C2/c$ (no. 15), $a = 18.2077(8)\text{ \AA}$, $b = 25.3690(12)\text{ \AA}$, $c = 16.6634(7)\text{ \AA}$, $\beta = 113.796(3)^\circ$, $V = 7042.7(6)\text{ \AA}^3$, $Z = 8$, $T = 100.02\text{ K}$, $\mu(\text{CuK}\alpha) = 7.989\text{ mm}^{-1}$, $D_{\text{calc}} = 1.367\text{ g/mm}^3$, 34013 reflections measured ($6.346 \leq 2\theta \leq 130.406$), 5994 unique ($R_{\text{int}} = 0.0611$, $R_{\text{sigma}} = 0.0402$) which were used in all calculations. The final R_1 was 0.0346 ($I > 2\sigma(I)$) and wR_2 was 0.0853 (all data).

Refinement Details. The solvent masking procedure as implemented in Olex2 was used to remove the electronic contribution of solvent molecules from the refinement. As the exact solvent content is not known, only the atoms used in the refinement model are reported in the formula here. Total solvent accessible volume / cell = 7042.7 \AA^3 [11.6%] Total electron count / cell = 376



Determination of Structure of Ferrocenyl 2,6-dimethoxyphenyl Imidazo[1,5-a]pyridine Rh(cod)Cl complex I-59



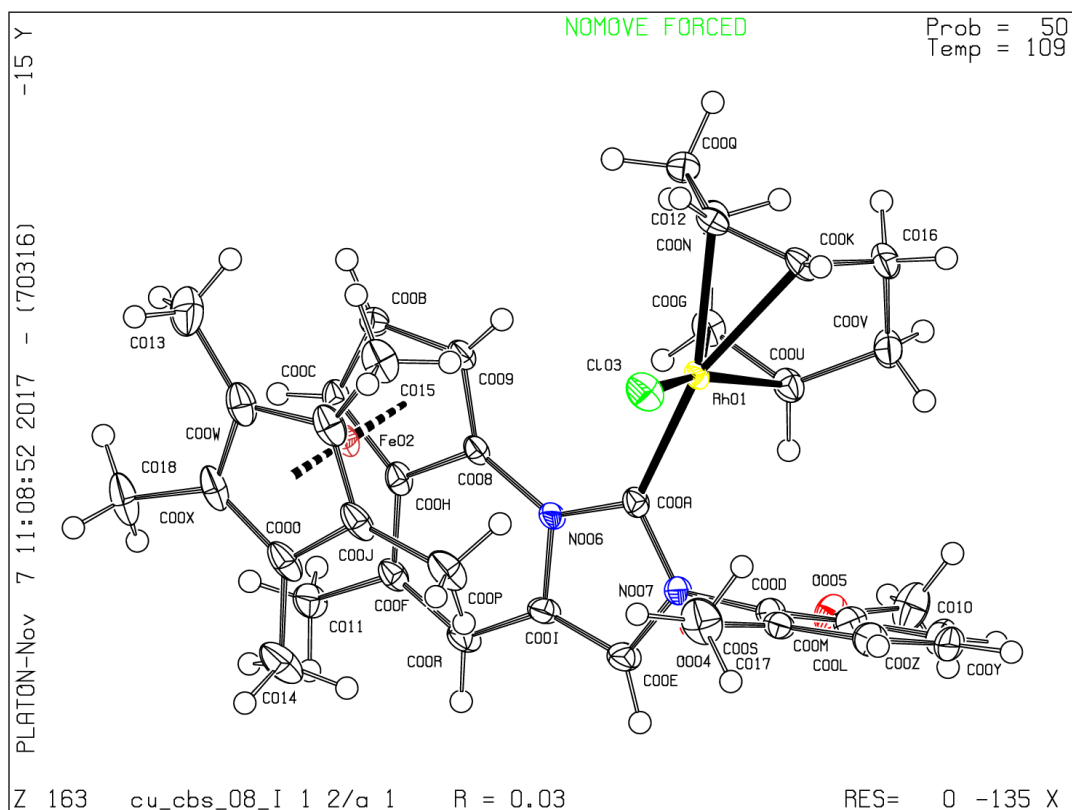
I-59

Single crystals of $C_{37}H_{44}ClFeN_2O_2Rh$ **I-59** were recrystallized from slow liquid-liquid diffusion of CH_2Cl_2 /pentane at -30 °C. A suitable crystal was selected and mounted in inert oil and transferred to the cold gas stream of a 'Bruker APEX-II CCD' diffractometer. The crystal was kept at 109.15 K during data collection. Using Olex2 [1], the structure was solved with the

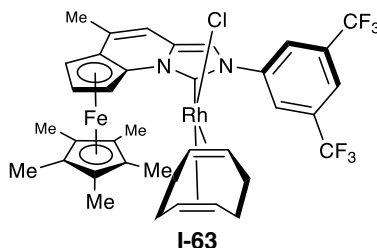
ShelXT [2] structure solution program using Intrinsic Phasing and refined with the ShelXL [3] refinement package using Least Squares minimisation.

Crystal Data for $C_{37}H_{44}ClFeN_2O_2Rh$ ($M=742.95$): monoclinic, space group $I2/a$ (no. 15), $a = 25.2931(8) \text{ \AA}$, $b = 10.2703(3) \text{ \AA}$, $c = 27.5238(8) \text{ \AA}$, $\beta = 116.096(2)^\circ$, $V = 6420.9(3) \text{ \AA}^3$, $Z = 8$, $T = 109.15 \text{ K}$, $\mu(\text{CuK}\alpha) = 8.827 \text{ mm}^{-1}$, $D_{\text{calc}} = 1.537 \text{ g/mm}^3$, 40027 reflections measured ($7.152 \leq 2\theta \leq 130.366$), 5473 unique ($R_{\text{int}} = 0.0462$, $R_{\text{sigma}} = 0.0225$) which were used in all calculations. The final R_1 was 0.0277 ($I > 2\sigma(I)$) and wR_2 was 0.0640 (all data).

Refinement Details. No special refinement necessary.



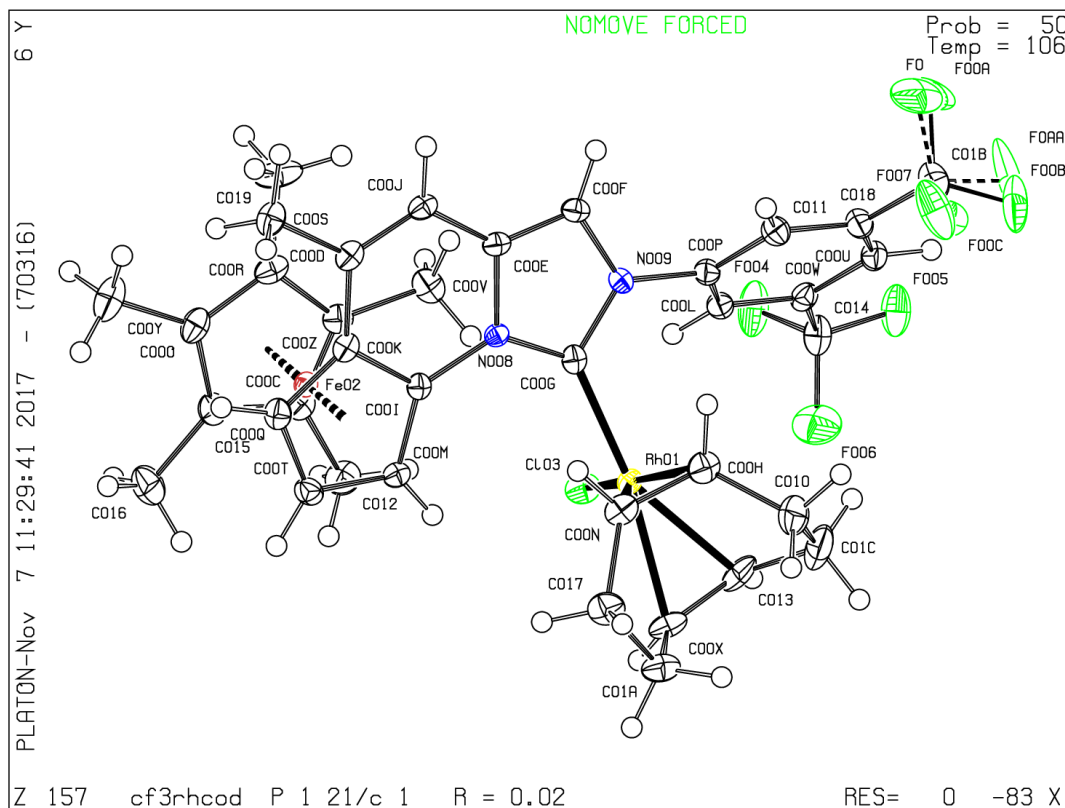
Determination of Structure of Ferrocenyl 3,5-bis(trifluoromethyl)phenyl Imidazo[1,5-a]pyridine Rh(cod)Cl complex I-63



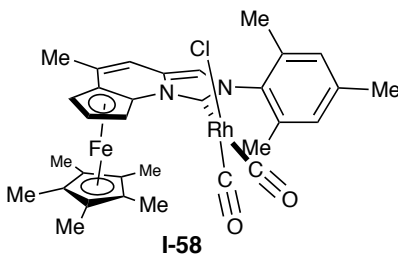
Single crystals of $C_{37}H_{38}ClF_6FeN_2Rh$ **I-63** were recrystallized from slow liquid-liquid diffusion of CH_2Cl_2 /pentane at $-30\text{ }^\circ\text{C}$. A suitable crystal was selected and mounted in inert oil and transferred to the cold gas stream of a diffractometer. The crystal was kept at 105.89 K during data collection. Using Olex2 [1], the structure was solved with the ShelXT [2] structure solution program using Intrinsic Phasing and refined with the ShelXL [3] refinement package using Least Squares minimisation.

Crystal Data for $C_{37}H_{38}ClF_6FeN_2Rh$ ($M = 818.90$): monoclinic, space group $P2_1/c$ (no. 14), $a = 14.8184(4)\text{ \AA}$, $b = 15.4755(4)\text{ \AA}$, $c = 15.8671(4)\text{ \AA}$, $\beta = 112.4720(10)^\circ$, $V = 3362.38(15)\text{ \AA}^3$, $Z = 4$, $T = 105.89\text{ K}$, $\mu(\text{CuK}\alpha) = 8.711\text{ mm}^{-1}$, $D_{\text{calc}} = 1.618\text{ g/mm}^3$, 55596 reflections measured ($6.454 \leq 2\Theta \leq 130.262$), 5705 unique ($R_{\text{int}} = 0.0518$, $R_{\text{sigma}} = 0.0199$) which were used in all calculations. The final R_1 was 0.0195 ($I > 2\sigma(I)$) and wR_2 was 0.0540 (all data).

Refinement Details. No special refinement necessary.

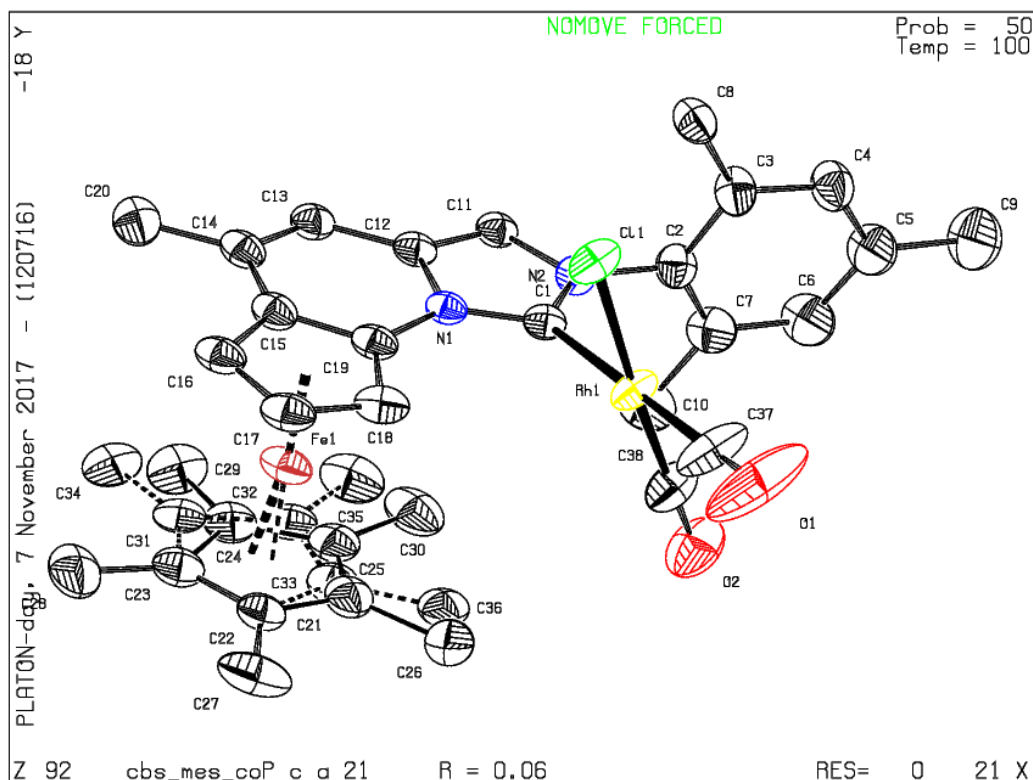


Determination of Structure of Ferrocenyl mesityl imidazo[1,5-a]pyridine rhodium biscarbonyl chloride I-58

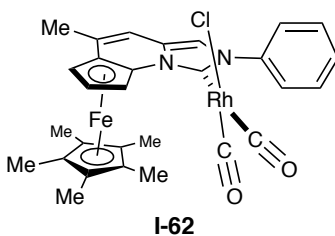


Recrystallized from slow evaporation of dichloromethane. X-ray diffraction was performed at 99.97 K and raw frame data were processed using SAINT. Molecular structures was solved using direct methods and refined on F2 by full-matrix least-square techniques. The GOF = 1.085 for 419 variables refined to R1 = 0.0611 for 5603 reflections with $I > 2\sigma(I)$. Further

information can be found in the CIF file. This crystal structure was deposited in the Cambridge Crystallographic Data Centre and assigned as CCDC 1016510.

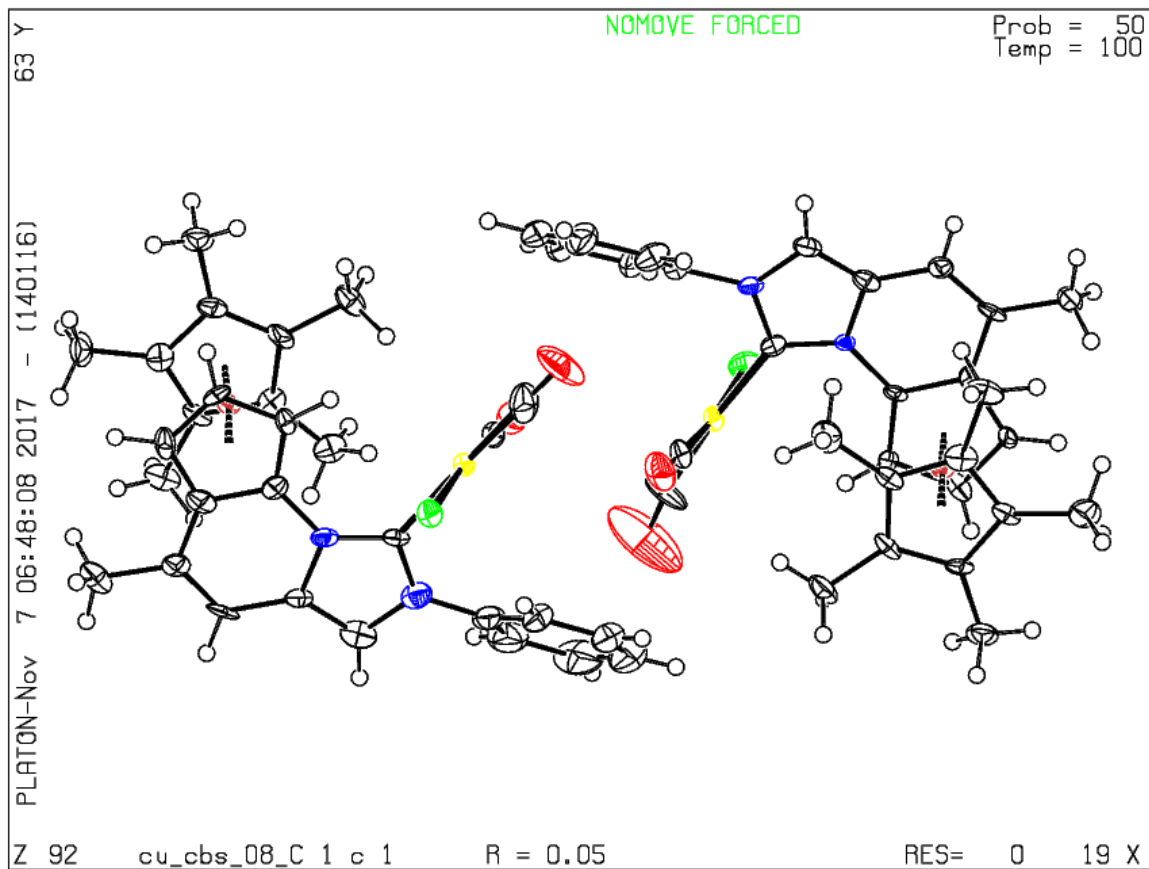


Determination of Structure of Ferrocenyl phenyl imidazo[1,5-a]pyridine rhodium biscarbonyl chloride I-62

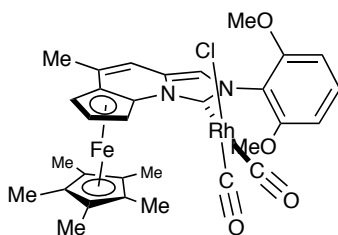


Recrystallized from slow evaporation of CH_2Cl_2 /pentane. X-ray diffraction was performed at 99.95 K and raw frame data were processed using SAINT. Molecular structures was solved using direct methods and refined on F2 by full-matrix least-square techniques. The GOF = 1.017

for 680 variables refined to $R1 = [_refine_ls_R_factor_gt]$ for 0.0537 reflections with $I > 2\sigma(I)$. A multi-scan absorption correction was performed. Further information can be found in the CIF file. This crystal structure was deposited in the Cambridge Crystallographic Data Centre and assigned as CCDC 1016508.

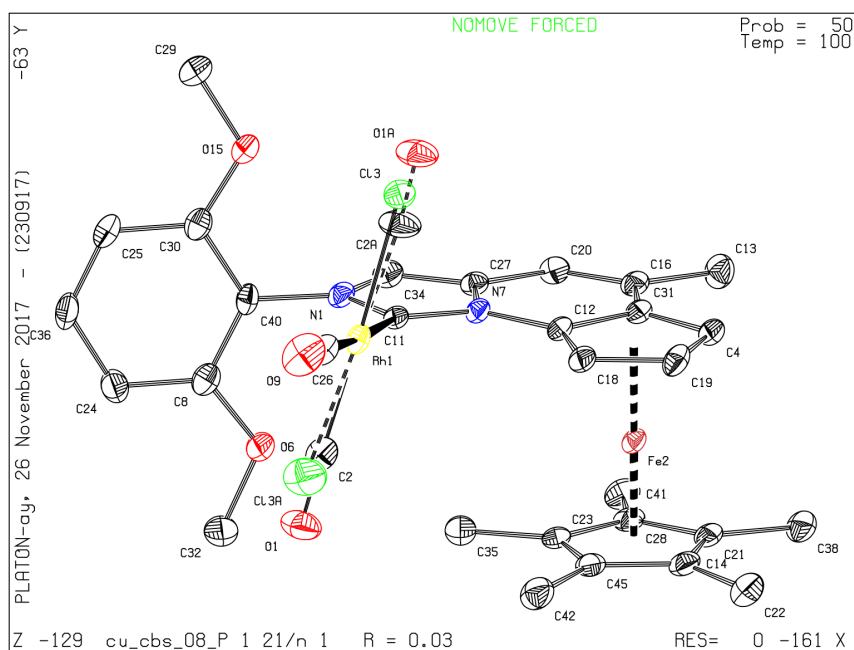


Determination of Structure of Ferrocenyl 2,6-dimethoxyphenyl imidazo[1,5-a]pyridine rhodium biscarbonyl chloride I-60

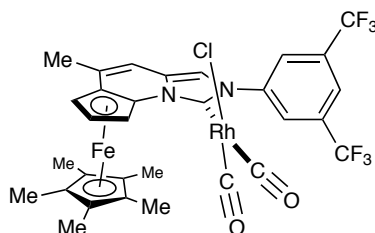


I-60

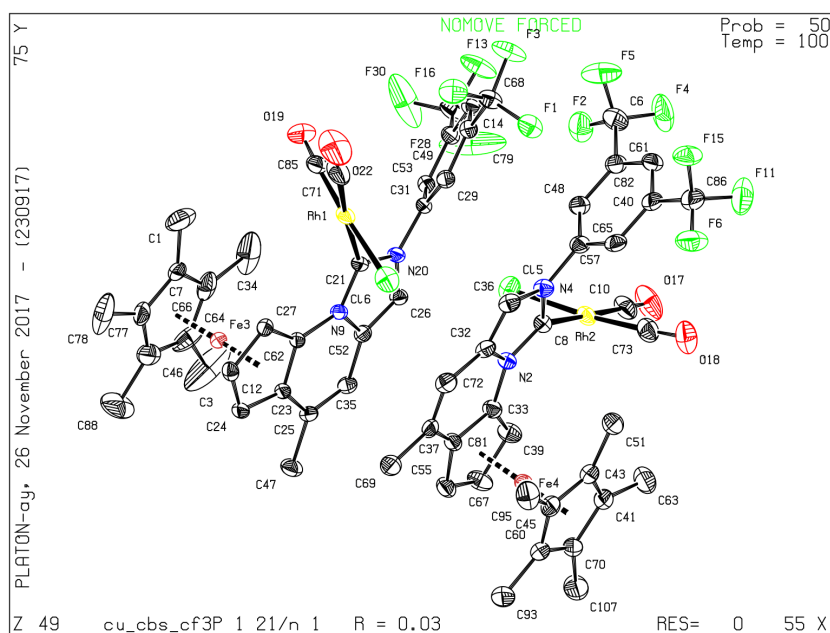
Recrystallized from slow evaporation of CH_2Cl_2 /pentane. X-ray diffraction was performed at 100.01 K and raw frame data were processed using SAINT. Molecular structures was solved using direct methods and refined on F2 by full-matrix least-square techniques. The GOF = 1.052 for 391 variables refined to $R1 = 0.0314$ for 4262 reflections with $I > 2\sigma(I)$. A multi-scan absorption correction was performed. Further information can be found in the CIF file. This crystal structure was deposited in the Cambridge Crystallographic Data Centre and assigned as CCDC 1016507.



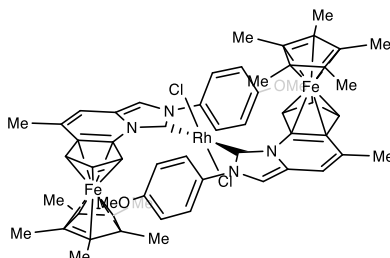
Determination of Structure of Ferrocenyl 3,5-bis(trifluoromethyl)phenyl imidazo[1,5-a]pyridine rhodium biscarbonyl chloride I-64



Recrystallized from slow evaporation of CH_2Cl_2 /pentane. X-ray diffraction was performed at 99.98 K and raw frame data were processed using SAINT. Molecular structures was solved using direct methods and refined on F2 by full-matrix least-square techniques. The GOF = 1.040 for 805 variables refined to $R1 = 0.0346$ for 9629 reflections with $I > 2\sigma(I)$. A multi-scan absorption correction was performed. Further information can be found in the CIF file. This crystal structure was deposited in the Cambridge Crystallographic Data Centre and assigned as CCDC 1016509.



Determination of Structure of Ferrocenyl p-methoxyphenyl imidazo[1,5-a]pyridine rhodium dimer I-69



Single crystals of $C_{56}H_{60}Cl_2Fe_2N_4O_2Rh$ **I-69** were grown from slow evaporation of THF. A suitable crystal was selected and mounted in inert oil and transferred to the cold gas stream of a 'Bruker APEX-II CCD' diffractometer. The crystal was kept at 109.83 K during data collection. Using Olex2 [1], the structure was solved with the ShelXT [2] structure solution program using Intrinsic Phasing and refined with the ShelXL [3] refinement package using Least Squares minimisation.

Crystal Data for $C_{56}H_{60}Cl_2Fe_2N_4O_2Rh$ ($M=1106.59$): monoclinic, space group $P2_1/c$ (no. 14), $a = 13.7036(4) \text{ \AA}$, $b = 13.3214(4) \text{ \AA}$, $c = 13.6971(4) \text{ \AA}$, $\beta = 98.169(2)^\circ$, $V = 2475.05(13) \text{ \AA}^3$, $Z = 2$, $T = 109.83 \text{ K}$, $\mu(\text{CuK}\alpha) = 8.659 \text{ mm}^{-1}$, $D_{\text{calc}} = 1.485 \text{ g/mm}^3$, 28622 reflections measured ($6.516 \leq 2\theta \leq 130.066$), 4195 unique ($R_{\text{int}} = 0.0795$, $R_{\text{sigma}} = 0.0423$) which were used in all calculations. The final R_1 was 0.0474 ($I > 2\sigma(I)$) and wR_2 was 0.1204 (all data).

Refinement Details. No special refinement necessary.

1.7.8 Extended Details for Buried Volume Calculations

Buried volume calculations were performed using the SambVca 2 web application¹²³ available online at <https://www.molnac.unisa.it/OMtools/sambvca2.0/index.html>. The crystal structures of CuCl complexes **I-51**, **I-52**, **I-55**, and **I-70** were uploaded in .xyz format. The xz plane was defined by the imidazopyridine ring system, the z-axis was oriented along the xz projection of NHC-metal bond, and the center of the sphere was set at a 2.0 Å distance from the carbene carbon along the z-axis. All Cu, Cl, hydrogen atoms were excluded from the analysis. All calculations used atomic radii as described by Bondi¹²⁴ scaled by a factor of 1.17.

Calculation Parameters

Mesh spacing: 0.10 Å

M-L: 2.0 Å

Extended parameters for %V_{Bur} using a 3.5 Å radius sphere:

| | V Free | V Buried | V Total | V Exact | | |
|-------------|----------|-------------|----------|---------|------|-------------|
| | 110 | 69.6 | 179.5 | 179.6 | | |
| | %V_Free | %V_Bur | % Tot/Ex | | | |
| | 61.3 | 38.7 | 100 | | | |
| I-51 | Quadrant | V_f | V_b | V_t | %V_f | %V_b |
| | SW | 27.1 | 17.7 | 44.9 | 60.5 | 39.5 |
| | NW | 31.1 | 13.8 | 44.9 | 69.3 | 30.7 |
| | NE | 29.9 | 14.9 | 44.9 | 66.7 | 33.3 |
| | SE | 21.8 | 23.1 | 44.8 | 48.5 | 51.5 |

| | | | | | | |
|-------------|----------|----------|----------|---------|------|------|
| | V Free | V Buried | V Total | V Exact | | |
| | 87.4 | 92.1 | 179.5 | 179.6 | | |
| | %V_Free | %V_Bur | % Tot/Ex | | | |
| | 48.7 | 51.3 | 100 | | | |
| I-55 | Quadrant | V_f | V_b | V_t | %V_f | %V_b |
| | SW | 18.8 | 26.1 | 44.9 | 41.8 | 58.2 |
| | NW | 24.1 | 20.8 | 44.8 | 53.7 | 46.3 |
| | NE | 30.6 | 14.3 | 44.9 | 68.1 | 31.9 |
| | SE | 14 | 30.9 | 44.9 | 31.2 | 68.8 |
| | V Free | V Buried | V Total | V Exact | | |
| | 108.6 | 70.9 | 179.5 | 179.6 | | |
| | %V_Free | %V_Bur | % Tot/Ex | | | |
| | 60.5 | 39.5 | 100 | | | |
| I-52 | Quadrant | V_f | V_b | V_t | %V_f | %V_b |
| | SW | 24.6 | 20.3 | 44.9 | 54.7 | 45.3 |
| | NW | 32.3 | 12.6 | 44.9 | 72 | 28 |
| | NE | 30 | 14.9 | 44.8 | 66.8 | 33.2 |
| | SE | 21.8 | 23.1 | 44.9 | 48.5 | 51.5 |
| | V Free | V Buried | V Total | V Exact | | |
| | 110.3 | 69.2 | 179.5 | 179.6 | | |
| | %V_Free | %V_Bur | % Tot/Ex | | | |
| | 61.5 | 38.5 | 100 | | | |
| I-70 | Quadrant | V_f | V_b | V_t | %V_f | %V_b |
| | SW | 27.7 | 17.1 | 44.9 | 61.8 | 38.2 |
| | NW | 31.9 | 13 | 44.9 | 71.1 | 28.9 |
| | NE | 30.3 | 14.6 | 44.9 | 67.5 | 32.5 |
| | SE | 20.4 | 24.5 | 44.8 | 45.4 | 54.6 |

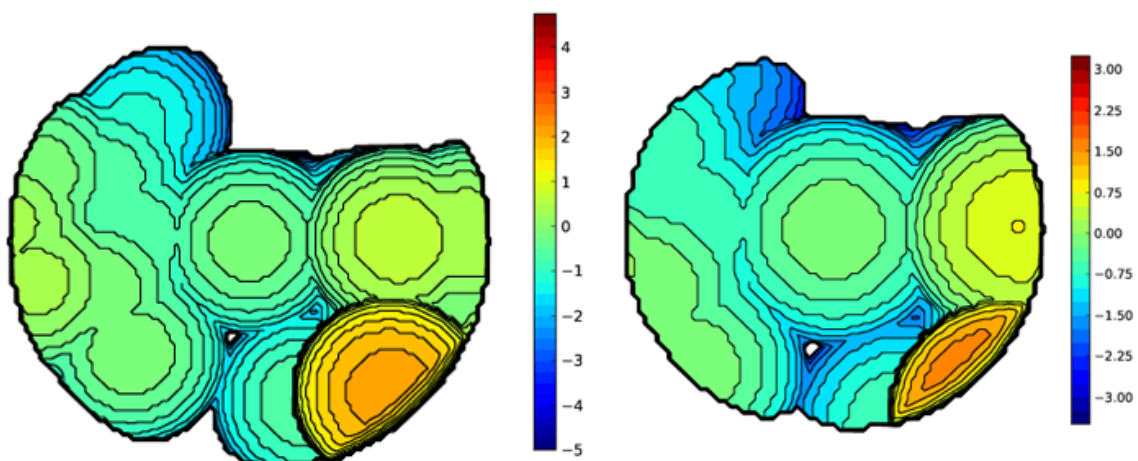
Extended parameters for %V_{Bur} using a 5.0 Å radius sphere:

| | | | | | | |
|-------------|----------|----------|----------|---------|------|------|
| | V Free | V Buried | V Total | V Exact | | |
| | 315.7 | 207.6 | 523.3 | 523.6 | | |
| | %V_Free | %V_Bur | % Tot/Ex | | | |
| | 60.3 | 39.7 | 99.9 | | | |
| I-51 | Quadrant | V_f | V_b | V_t | %V_f | %V_b |
| | SW | 77.8 | 53 | 130.8 | 59.5 | 40.5 |
| | NW | 85.7 | 45.1 | 130.8 | 65.5 | 34.5 |
| | NE | 96.4 | 34.4 | 130.8 | 73.7 | 26.3 |
| | SE | 55.6 | 75.2 | 130.8 | 42.5 | 57.5 |

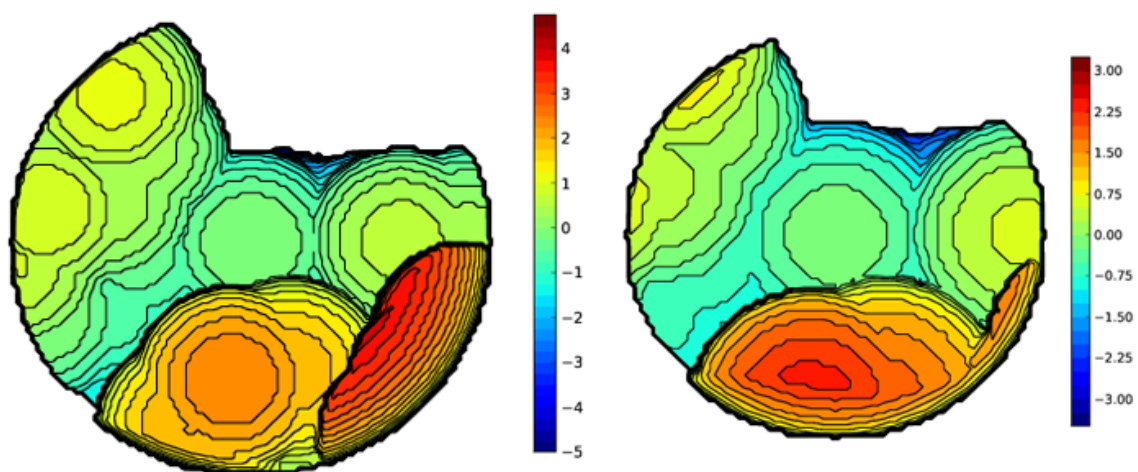
| | | | | | | |
|-------------|----------|----------|----------|---------|------|------|
| | V Free | V Buried | V Total | V Exact | | |
| | 253.3 | 270 | 523.3 | 523.6 | | |
| | %V_Free | %V_Bur | % Tot/Ex | | | |
| | 48.4 | 51.6 | 99.9 | | | |
| I-55 | Quadrant | V_f | V_b | V_t | %V_f | %V_b |
| | SW | 53.4 | 77.4 | 130.8 | 40.8 | 59.2 |
| | NW | 70.6 | 60.2 | 130.8 | 54 | 46 |
| | NE | 97.2 | 33.6 | 130.8 | 74.3 | 25.7 |
| | SE | 32.1 | 98.7 | 130.8 | 24.6 | 75.4 |
| | V Free | V Buried | V Total | V Exact | | |
| | 321.3 | 202 | 523.3 | 523.6 | | |
| | %V_Free | %V_Bur | % Tot/Ex | | | |
| | 61.4 | 38.6 | 99.9 | | | |
| I-52 | Quadrant | V_f | V_b | V_t | %V_f | %V_b |
| | SW | 84.5 | 46.3 | 130.8 | 64.6 | 35.4 |
| | NW | 89.2 | 41.6 | 130.8 | 68.2 | 31.8 |
| | NE | 96.2 | 34.6 | 130.8 | 73.6 | 26.4 |
| | SE | 51.3 | 79.5 | 130.8 | 39.2 | 60.8 |
| | V Free | V Buried | V Total | V Exact | | |
| | 307.3 | 216 | 523.3 | 523.6 | | |
| | %V_Free | %V_Bur | % Tot/Ex | | | |
| | 58.7 | 41.3 | 99.9 | | | |
| I-70 | Quadrant | V_f | V_b | V_t | %V_f | %V_b |
| | SW | 67.8 | 63 | 130.8 | 51.8 | 48.2 |
| | NW | 89.7 | 41.1 | 130.8 | 68.6 | 31.4 |
| | NE | 95.6 | 35.2 | 130.8 | 73.1 | 26.9 |
| | SE | 54.1 | 76.7 | 130.8 | 41.4 | 58.6 |

Steric contour maps generated using 5.0 Å (left col.) and 3.5 Å (right col.) radius spheres

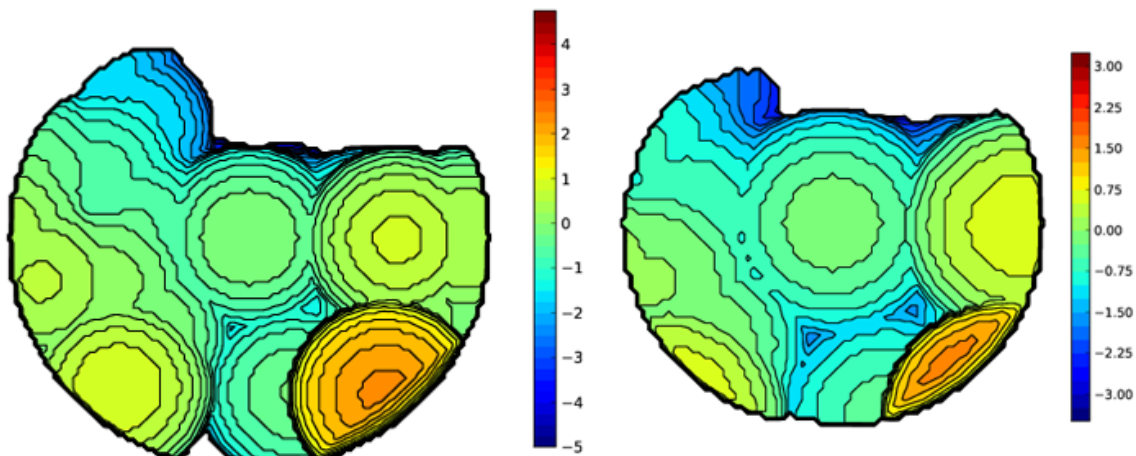
I-51



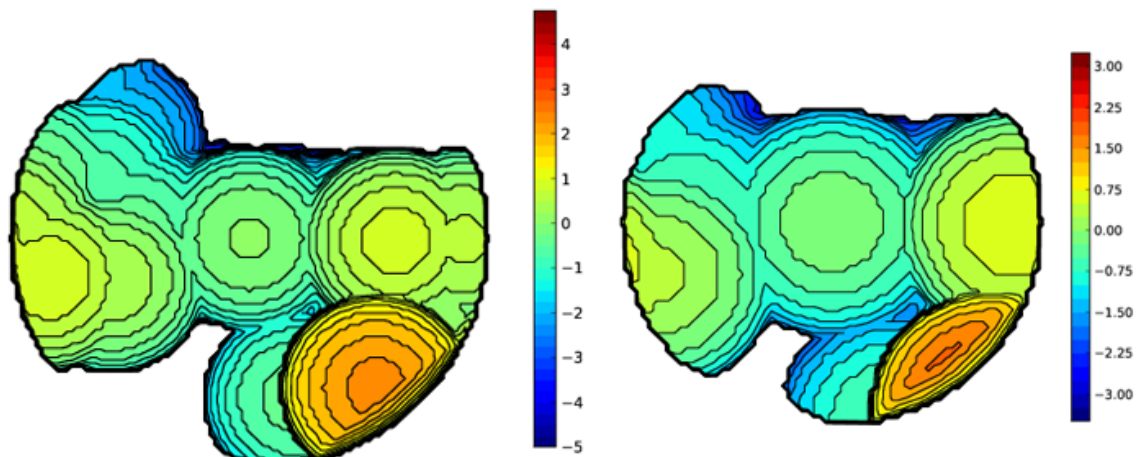
I-55



I-52



I-70



Chapter 2: Enantioselective Synthesis of α -amidoboronates Mediated by Planar-Chiral NHC-Cu(I) Complexes

2.1 Introduction

The abundance of peptides and their constituent α -amino acids in biological processes imparts an obvious importance to the study of their function and application in medicine. While only 21 eukaryotic proteinogenic amino acids (along with their post-translational derivatives) are known, the development of therapeutics which target peptide-binding sites in receptors or enzymes has necessitated the supplementation of this biological “alphabet” through the introduction of analogous unnatural motifs.¹²⁵⁻¹²⁷ These “peptidomimetics” can be incorporated in bioactive compounds to selectively emulate the topological features of natural peptides while altering other properties such as conformational stability, bioavailability, or electrophilicity. For example, this approach is evident in the development of thrombin inhibitor argatroban, where researchers sought to mimic the Phe-Pro-Arg fragment of the natural substrate fibrinogen, where replacement of a sensitive amide bond with a sulfonamide moiety significantly improved bioavailability (**Figure 2-1**).¹²⁸⁻¹²⁹

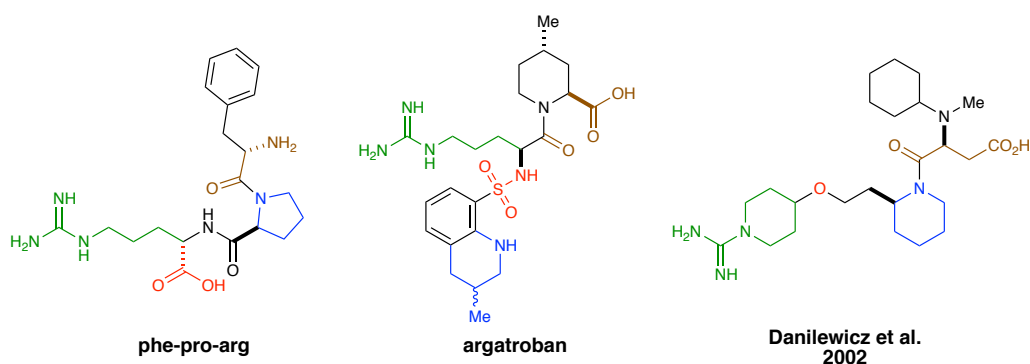


Figure 2-1. PheProArg and associated peptidomimetics.

2.1.1 α -aminoboronic acids in medicinal chemistry

Boronic acids and their corresponding esters have emerged as particularly useful tools in diverse areas of medicinal chemistry, including serving as peptidomimetic amino acid analogs¹³⁰⁻¹³⁴ Although organoboron chemistry is popularly associated with use in synthetic methodology (i.e., oxidations, reductions, C-C bond-forming reactions), as early as the 1960s simple arylboronic acids were known to be effective protease inhibitors and useful compounds for targeted boron neutron capture therapy.¹³⁵ While recent advances have included purposing the facile process of boron-diol exchange towards the design of synthetic carbohydrate receptors and transmembrane carriers of ribonucleosides, the most prominent developments of the last 20 years have involved boron-containing peptidomimetic drugs.¹³⁶⁻¹⁴⁰ This has been exemplified by the FDA approval of 20S proteasome inhibitors bortezomib (Velcade[®], 2003)¹⁴¹ and ixazomib (Ninlaro[®], 2015)¹⁴² for treatment of multiple myeloma, and carbapenemase inhibitor vaborbactam in 2017 as a combination therapy with β -lactam antibiotic meropenem (Vabomere[®])¹⁴³ for complicated urinary tract infections (cUTIs) (**Figure 2-2**).

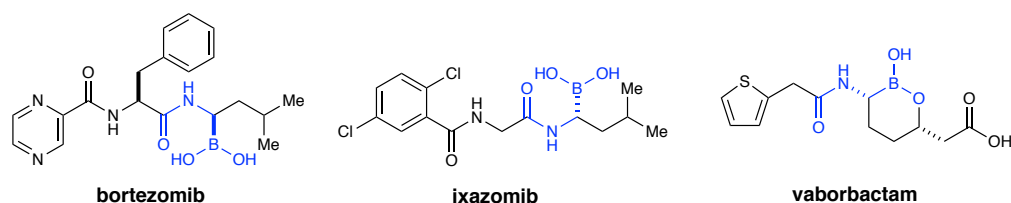


Figure 2-2. Approved drugs containing the α -aminoboronate motif.

The key element found of all boron-containing protease inhibitors is the α -aminoboronic acid motif, which can be considered a non-natural amino acid derivative. The bioactivity of this residue can be ascribed to both its ability to function as a bioisostere of a peptide carboxyl-terminus and propensity to form a stable tetrahedral borate upon nucleophilic attack by the

active residues of a target enzyme (**Figure 2-3**). Consequently, the α -amidoboronate moiety can be used as an electrophilic “warhead” for reversible covalent protease inhibition, guided by the peptide to which it is attached.^{138,140,144}

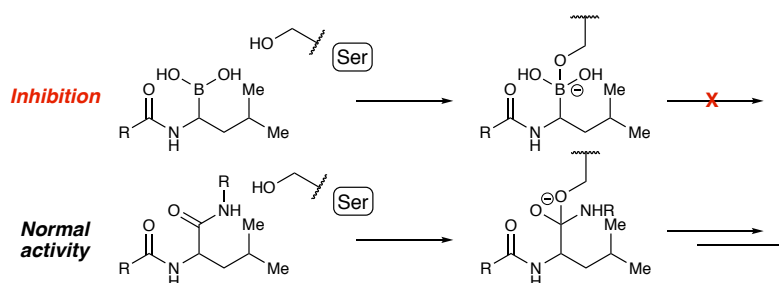


Figure 2-3. Inhibitory mechanism of the α -aminoboronate motif against serine proteases.

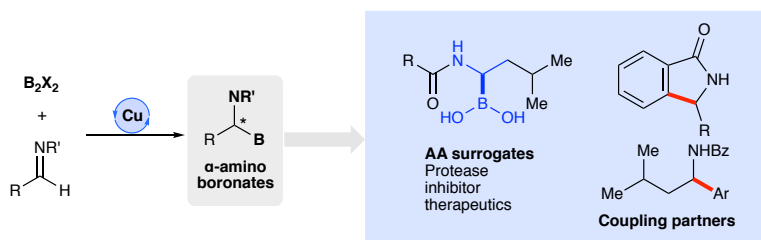


Figure 2-4. Synthesis and application of α -aminoboronates.

2.1.2 Synthetic challenges

Despite the importance of boronic-acid peptidomimetics, the synthesis of α -amidoboronates is complicated by the inherent difficulties associated with the installation of a Lewis basic functionality adjacent to one which is highly Lewis acidic (**Figure 2-5**).¹⁴⁵ In protic solvents, for example, the conversion of α -aminoboronates to their corresponding deboronated amines is commonly observed. Given that aminoboronates containing tertiary amines do not undergo this mode of decomposition, it is likely that deborylation occurs via intramolecular attack of boron by the germinal amine via a three-membered transition state (**II-2**), followed by

ring-opening with concerted proton migration or formation of the zwitterion (**II-3**) before protonation.¹⁴⁵

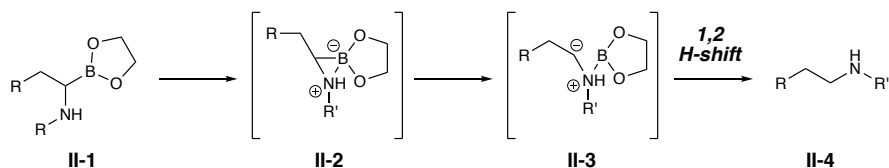
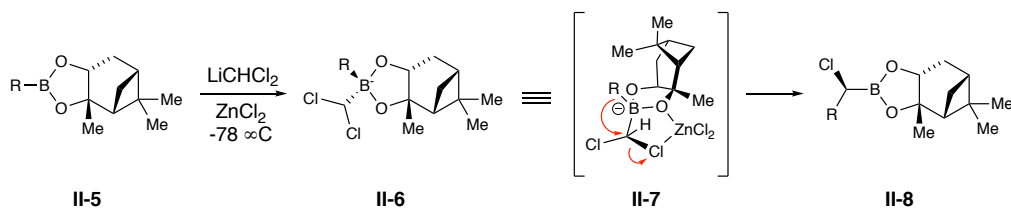


Figure 2-5. Postulated mode of α -aminoboronate decomposition.

2.1.3 Matteson homologation

Most synthetic methods for the construction of aminoboronates involve the catalytic addition of boron to unsaturated carbon (i.e. aldimines, ketimines, and enamines). However, the strategies used in industrial settings almost exclusively employ a homologation-substitution sequence first disclosed by Matteson in 1980, where the nitrogen atom is installed as in the final step (**Scheme 2-1**).¹³⁷ Here, a chiral pinene-derived boronate (**II-5**) is alkylated by (lithium)dichloromethane which arranges via **II-7** to the α -chloroboronic ester (**II-8**) upon warming to room temperature. This adduct can then undergo S_N2 substitution with LiHMDS to yield enantiopure α -aminoboronates. This strategy, while elegant, requires expensive chiral starting material as well as cryogenic conditions due to the use of organolithium reagents. Thus, the development of alternative methodology for the synthesis of α -aminoboronates is an area of ongoing interest.

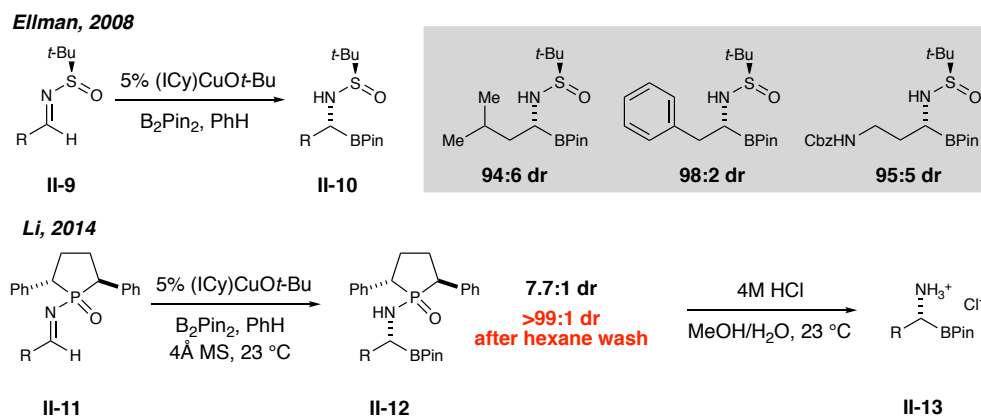
Scheme 2-1. Matteson method of enantiopure α -aminoboronate synthesis



2.1.4 Substrate-directed stereoselective synthesis

Recently disclosed methods for the synthesis of α -aminoboronates have relied on both enantioselective catalysis and chiral auxiliaries, with the far majority relying on transition metal catalysis to construct the C-B bond.¹⁴⁶ Of those which rely on substrate control for stereoselectivity, the strategy disclosed by Beenan et al. in 2008 remains the most general and selective (**Scheme 2-2**). Here, the NHC-Cu(I) catalyzed borylation of chiral *tert*-butylsulfinyl aldimines was found to deliver a range of alkyl and aryl products in uniformly excellent diastereoselectivity.¹⁴⁷ Li et al. later disclosed a related method which instead used a chiral N-phosphinyl directing group for both stereocontrol and group-assisted purification (GAP). While the selectivity observed with the use of this directing group was moderate, it was demonstrated that a small selection of products could be isolated in high enantiopurity (up to 98:2 er) by simply washing away the minor diastereomer and reaction side-products, albeit at considerable cost to yield.¹⁴⁸

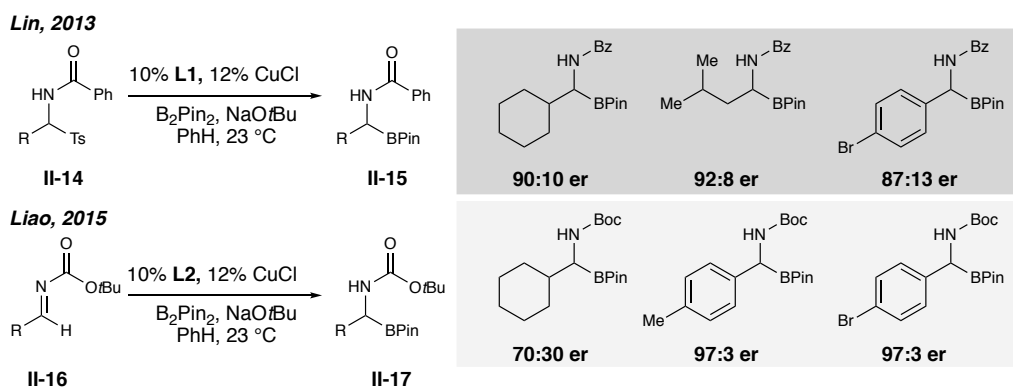
Scheme 2-2. Diastereoselective methods of α -aminoboronate synthesis.



2.1.5 Catalytic enantioselective methods

Given the considerable cost of stoichiometric quantities of chiral auxiliary, there has been a corresponding interest in the development of catalytic enantioselective methods which can replicate the high levels of stereoselectivity observed in the borylation of chiral substrates such as Ellman's *tert*-butylsulfinyl aldimines. The use of a chiral ligand in the enantioselective borylation of aldimines was first disclosed by Fernandez *et al.* who were able to obtain *N*-tosyl aminoboronates in largely excellent yields at elevated temperatures, however, with few exceptions, enantioselectivity was poor.¹⁴⁹ This was followed by reports of the Cu(I)-catalyzed borylations of *N*-benzoyl and *N*-Boc aldimines by Lin *et al.*¹⁵⁰ and Liao *et al.*¹⁵¹ respectively (**Scheme 2-3**). Interestingly, Liao's report additionally demonstrated that enantioselectivity of their reaction could be completely reversed through the addition of a large anionic additive (NaBARF). A wide selection of α -aryl aminoboronates could be obtained in excellent selectivity; however, alkyl aldimines could not be obtained in satisfactory yield or selectivity. Similarly, Morken and Hong's report of a Pt-catalyzed diborylation of *N*-trimethylsilyl aldimines observed a complete failure of alkyl aldyldimines to react under their conditions (**Scheme 2-4**).¹⁵²

Scheme 2-3. Catalytic enantioselective strategies for α -aminoboronate synthesis.



Complementary to these methods, the Miura and Tang groups have introduced strategies which use alternative substrates that do not contain a C-N double bond (**Scheme 2-4**). Tang *et al.* were able to obtain a selection of tertiary α -aminoboronates through the hydroboration of enamines with a chiral Rh(I)-phosphine catalyst (**Figure 2-6**).¹⁵³ Substrate scope, however, was limited to aryl-substituted enamines. Miura *et al.* demonstrated a highly divergent approach towards construction of aminoboronates through the hydroamination of alkenyl dan boronates (dan = 1,8-diaminonaphthyl). Although somewhat more laborious to construct than adimines, a selection of both aryl and aliphatic vinyl boronates underwent hydroamination in excellent enantioselectivity.¹⁵⁴ Nevertheless, as in the case of Tang *et al.*, substrate scope was highly constrained due to the necessity that secondary amines must be used, thus rendering subsequent *N*-deprotection of the corresponding aminoboronates highly difficult. Most recently, Tartosa¹⁵⁵ and Xu¹⁵⁶ have independently disclosed Cu(I) mediated hydroborations of α,β -unsaturated amidoacrylonitriles and amidoacrylate esters. While both techniques are highly enantioselective, the requirement of activating (and likely directing) substitution in the β -position severely limits their scope and applicability to therapeutically relevant motifs.

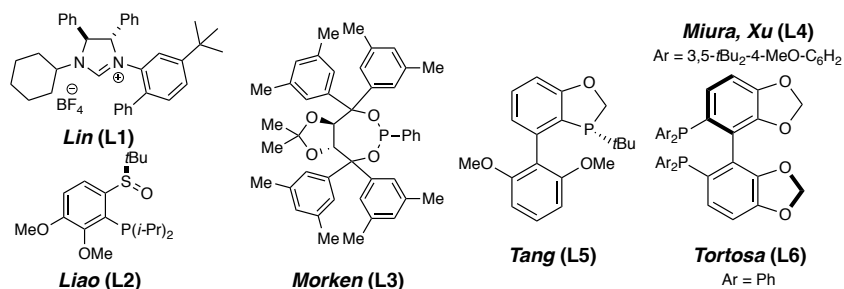
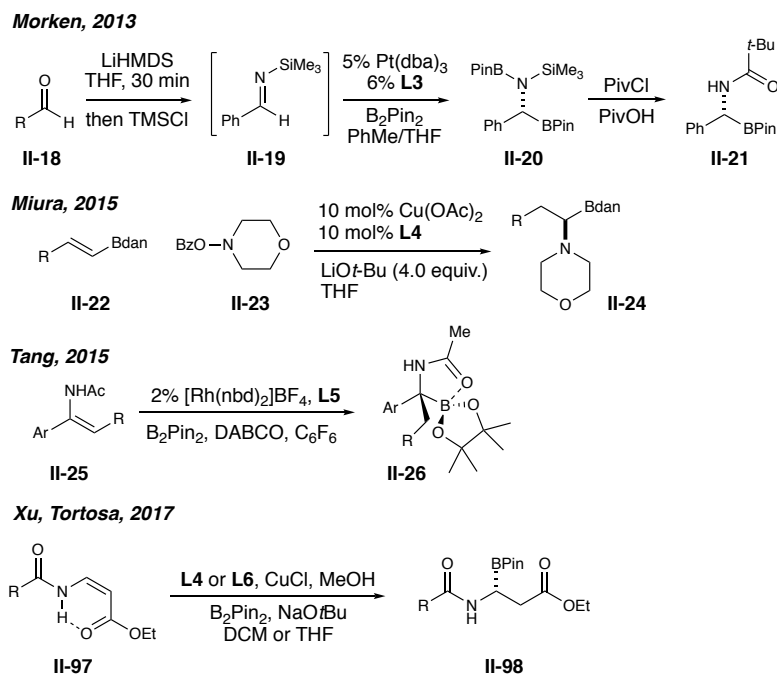


Figure 2-6. Chiral ligands employed in α -aminoboronate synthesis.

Scheme 2-4. Approaches not utilizing Cu(I) or hydroboration of a C=N bond.

2.1.6 Aliphatic α -aminoboronates

Although the synthesis of α -aminoboronates remains a heavily studied area, the methodology disclosed to date contains a peculiar deficiency given the nature of α -aminoboronates which are used in therapeutic substances (**Figure 2-7**). Boronic acid-containing peptidomimetics almost exclusively contain the α -alkyl aminoboronate motif, yet there exist no highly stereoselective methods for their construction which (i) do not rely upon the use of chiral auxiliaries, or (ii) do not require activating functionality in the β -position relative to nitrogen. Efforts are further complicated by the instability of certain alkyl aldimine starting materials and products to silica gel chromatography, thus necessitating the use of silica deactivation techniques and multiple columns to yield pure materials. To address these shortcomings, we sought to develop a system which could (1) deliver both α -alkyl and α -aryl α -amidoboronates in high enantioselectivities and yields; (2) rely on starting materials readily prepared from commercially

available reagents; and (3) eliminate the need for the tedious and problematic chromatographic isolation of products.

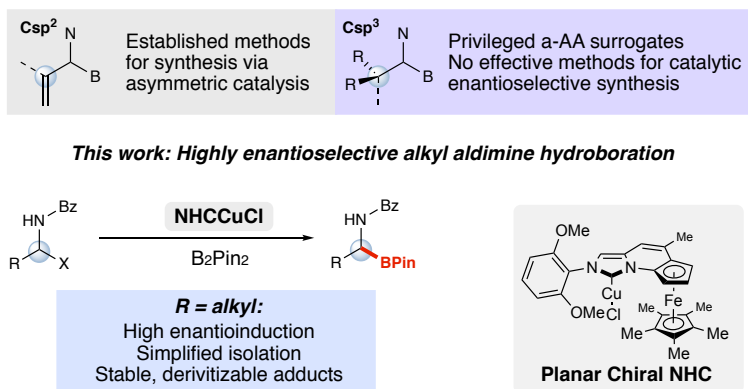
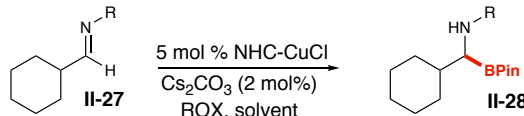


Figure 2-7. Our approach towards alkyl α -aminoboronate synthesis.

2.2 Catalytic borylation of aldimines with planar chiral NHC-Cu(I) complexes

Recently, we disclosed the highly successful application of a new family of planar chiral Cu(I)-NHC complexes towards conjugate borylations of enones and enoates⁶⁶ and reasoned that this system could potentially be adapted to the hydroboration of alkyl aldimines. Upon exposing a selection of *N*-tosyl, Boc, and benzoyl imines to conditions similar to those employed in our conjugate borylation protocol (**Table 2-1, entry 1**), we detected no borylated adduct, but rather varying proportions of starting material and amide presumably formed through a protodeborylation process as detailed in **Figure 2-5**. Switching the alcohol to ethanol or isopropanol not alleviate this problem, nor did a reduction in temperature. However, completely omitting the alcohol from the reaction allowed for complete consumption of benzoyl imine **II-27**, although enantioselectivity remained poor across a variety of solvents when using catalyst **A** (**Table 2-2, bottom**). Yields as observed by ¹H NMR were only greatly improved when an alkoxide base was used in place of a protic additive and *N*-benzoyl imines were used as substrates.

Table 2–1. Initial optimization of yield.


| Entry | R | ROH/Alkoxide (mol %) | Solvent | yield (%) ^a |
|-----------------|-----|----------------------|---------|------------------------|
| 1 | Boc | MeOH | PhMe | 0 |
| 2 | Boc | EtOH | PhMe | 0 |
| 3 | Boc | <i>i</i> PrOH | PhMe | 0 |
| 4 | Boc | - | PhMe | 23 |
| 5 | Boc | NaOMe | PhMe | 48 |
| 6 | Ts | NaOMe | PhMe | 0 |
| 7 | Bz | NaOMe | PhMe | 40 |
| 8 | Bz | NaOMe | THF | 56 |
| 9 | Boc | NaOMe | THF | 51 |
| 10 ^b | Bz | NaOMe | THF | 42 |
| 11 ^c | Bz | NaOMe | THF | 54 |

^aYields determined by ¹H NMR of the unpurified product integrated against an internal standard. ^bRun at 4 °C.

^cK₂CO₃ instead of Cs₂CO₃.

2.2.1 *In-situ generation of aldimines from inert α-tosyl precursors*

¹H NMR spectroscopic analysis of the reaction mixture revealed that product could not be observed in yields over 54% under these conditions. As small amounts of the aldehyde decomposition product and its borylated adduct were observed via GCMS, it was thought that the aliphatic imines were undergoing significant hydrolysis despite their immediate use following their crude purification via filtration through celite. As the typical process for preparation of the acyl aldimines used in this study involves the base-catalyzed elimination of sulfinate from an α-tosyl alkyl benzamides (**II-29**), preparation of the highly sensitive imines *in-situ* from **II-29** could occur through the inclusion of several equivalents of carbonate base in the reaction.¹⁵⁰ Indeed, yields of **II-30** as measured by ¹H NMR exceeded 70% when using this strategy, and enantioselectivity remained unchanged.

The necessary exclusion of protic additives in this transformation sharply diverges from the analogous borylation of aldehydes and ketones.¹⁵⁷⁻¹⁶⁰ These reactions can similarly be

catalyzed by Cu(I)-NHC systems, although yield is poor without inclusion of a proton source. DFT-based mechanistic studies by Ito¹⁶¹ and Lin¹⁶² have suggested this dependency is due to the accelerated cleavage of the Cu-O bond through the protonation of oxygen, which hastens catalyst turnover. Additionally, this suppresses a 1,2 shift from **II-28** to its protodeborylated adduct (**Figure 2-5**), preventing formation of the minor enantiomer. We speculate that in the case of C=N systems bound through nitrogen to a carbonyl-containing group such as benzoyl or boc, the intramolecular dative coordination of the carbonyl oxygen to the Lewis acidic boronate is a stabilizing factor which works in hand with steric encumbrance to slow this isomerization from **II-28**. Why proton sources depress yield less clear, although it is likely that protic additives catalyze the isomerization as detailed in **Figure 2-5**.

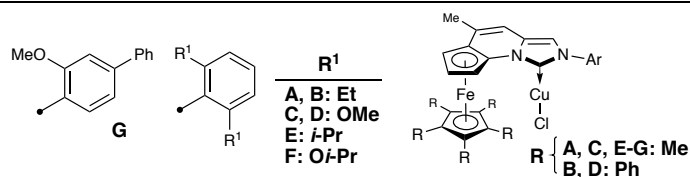
2.2.2 Optimization of enantioselectivity

Having identified conditions which could provide complete conversion, our focus was shifted to optimizing enantioselectivity. It was found that a pairing of NaOtBu in THF offered a slight improvement in selectivity, although catalyst **A** (**Table 2-2**) still only offered poor selectivity. Surprisingly, the screening of catalyst derivatives with bulkier substitution on the wingtip N-aryl ring or the Cp-ring (entries 6-10) of the ferrocene depressed yield and provided only meager improvements in selectivity. A large increase in enantioselectivity was only observed upon switching to catalyst **C**, which bears 2,6-methoxy substitution on the pendant *N*-aryl ring, rather than 2,6-ethyl as found in **A**. A reexamination of solvents and alkoxide bases confirmed THF and NaOtBu as ideal for selectivity and revealed a minor sensitivity to the alkoxide cation (entries 13-16). Smaller or larger alkoxides such as NaOMe and sodium *tert*-

pentoxide significantly diminished enantioselectivity, while use of lower temperatures provided no change in this property.

Table 2–2. Optimization of enantioselectivity.

| Entry | Catalyst | Z | ROH/Alkoxide (mol %) | Solvent | yield (%) ^a | er |
|-----------------|----------|-----|----------------------|---------|------------------------|-------|
| 1 | A | Bz | NaOMe (10) | THF | 84 | 60:40 |
| 2 | A | Bz | NaOMe (10) | PhMe | 68 | 53:47 |
| 3 | A | Bz | NaOt-Bu (10) | THF | 78 | 69:31 |
| 4 | B | Bz | NaOt-Bu(10) | THF | 42 | 71:29 |
| 5 | C | Bz | NaOt-Bu (10) | THF | 91 | 97:3 |
| 6 | D | Bz | NaOt-Bu (10) | THF | 36 | 68:32 |
| 7 | E | Bz | NaOt-Bu (10) | THF | 54 | 57:43 |
| 8 | F | Bz | NaOt-Bu (10) | THF | 89 | 88:12 |
| 9 | G | Bz | NaOt-Bu (10) | THF | 88 | 93:7 |
| 10 | C | Bz | NaOt-Bu (10) | DCM | 51 | 92:8 |
| 11 | C | Bz | NaOt-Bu (10) | PhMe | 68 | 80:20 |
| 12 | C | Bz | NaOt-Bu (10) | DCE | 86 | 93:7 |
| 13 | C | Bz | KOt-Bu | THF | 88 | 94:6 |
| 14 | C | Bz | LiOt-Bu | THF | 82 | 95:5 |
| 15 | C | Bz | NaOs-amyl | THF | 74 | 79:21 |
| 16 | C | Boc | NaOt-Bu (10) | THF | 52 | 96:4 |
| 17 ^b | C | Bz | NaOt-Bu (10) | THF | 69 | 97:3 |
| 18 ^c | C | Bz | NaOt-Bu (10) | THF | 74 | 94:6 |
| 19 ^d | C | Bz | NaOt-Bu (10) | THF | 85 | 97:3 |

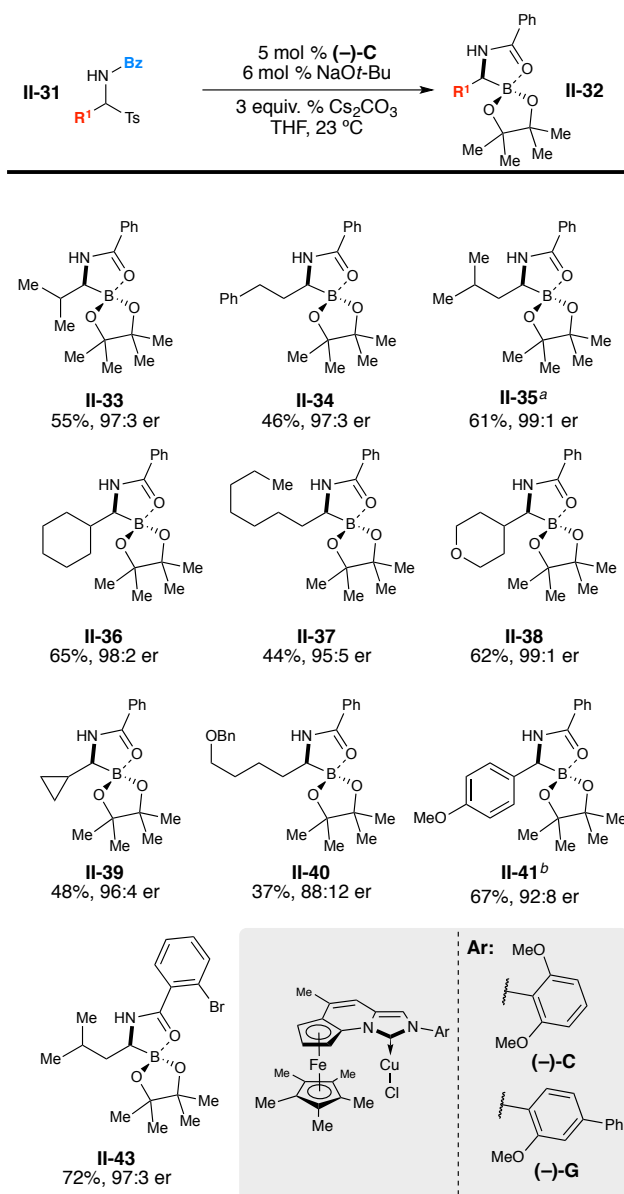


^aYields determined by ¹H NMR of the unpurified product integrated against an internal standard. ^bRun at 0 °C. ^c3.0 equiv. K₂CO₃ instead of Cs₂CO₃. ^d2.0 equiv. Cs₂CO₃.

Enantioselectivity typically was observed above 95:5 er for a range of substrates bearing alkyl and heteroalkyl substitution (**Table 2-3**). A notable exception to this trend was isobutyl analog **II-35**, which could only be obtained in 85:15 er with catalyst **C**. This result was of particular concern due to the widespread presence of this motif in therapeutic substances as an

isoleucine analog.¹⁴⁰ Screening of other catalyst derivatives bearing bulkier substitution along the wingtip aryl ring revealed reduced selectivity, however, use of derivative **G** completely rescued er. We additionally observed that analog **II-43** bearing a 2-bromobenzamide group also could be obtained in high er with catalyst **C**.

Table 2–3. Substrate scope.



^aCatalyst **G** used in place of **C**. Catalyst **C** provided 85:15 er. ^bRun in MTBE instead of THF.

2.2.3 Isolation via precipitation of BF_3K salts

Despite having identified ideal reaction conditions for selectivity, we nevertheless desired an improved isolation protocol that could avoid purity and yield issues associated with SiO_2 -promoted protodeborylation. Potassium trifluoroborate salts typically exhibit markedly improved stability in relation to their acid and ester analogs as well as diminished solubility in organic solvents, which often allows their isolation to be conducted via simple precipitation.^{157,163-164} To our disappointment, initial attempts at conversion of crude pinacol ester **II-44** to the corresponding salts via exposure to an aqueous solution of KHF_2 only afforded trifluoroborate **II-45** in extremely low yields (**Scheme 2-5**).¹⁶⁵⁻¹⁶⁶ However, use of milder conditions developed by Lennox allowed for the isolation of **II-48** in considerably improved yield.¹⁶⁷⁻¹⁶⁸ The application of this protocol to a selection of our substrate scope revealed considerably improved yield in all cases (**Table 2-4**).

Scheme 2-5. Product isolation via precipitation as BF_3K salt.

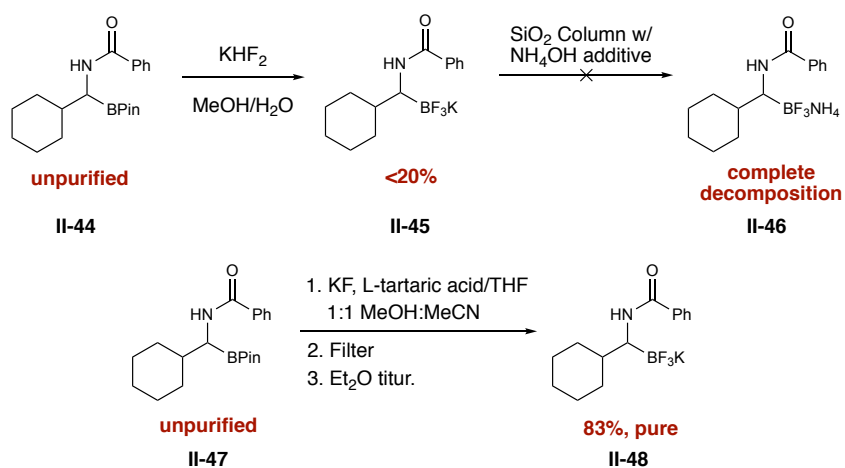
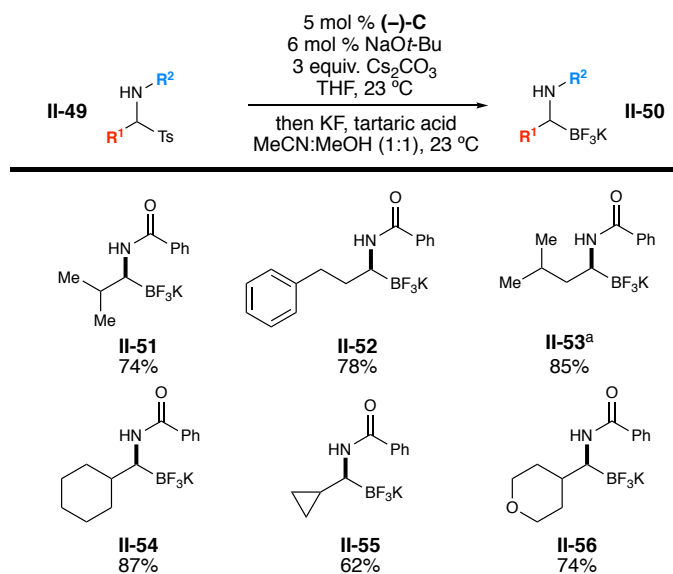


Table 2–4. Products isolated via precipitation.

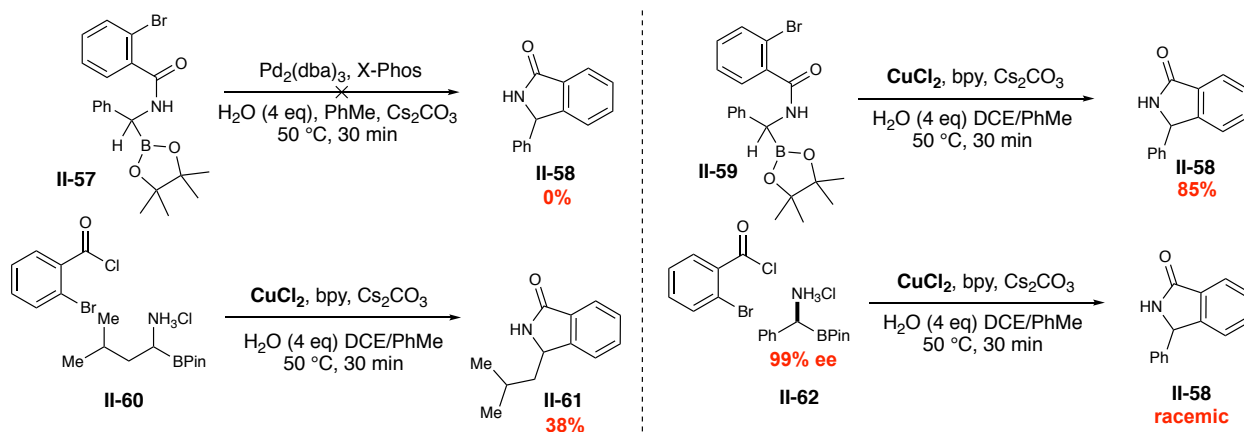
^aCatalyst **G** used in place of **C**.

2.3 Intramolecular Suzuki coupling of α -benzamidoboronates

α -Aminoboronates have also been employed as coupling partners in transition metal catalyzed reactions. The palladium-catalyzed Suzuki coupling of α -(acylamino)benzylboronic esters was first reported by Suginome in 2009,¹⁶⁹ who later reported stereospecific variants in 2010 and 2011.¹⁷⁰⁻¹⁷¹ Here, it was demonstrated that benzoyl and pivoyl α -aminoboronic esters could undergo highly enantioselective coupling with a variety of aryl halides with inversion of configuration. Later, Dumas and coworkers reported a copper-catalyzed intramolecular coupling of *N*-(2-bromo)benzoyl α -aminoboronates, where it was found that Cu(I/II) source was necessary to promote the Suzuki reaction (**Scheme 2-6**).¹⁷² Surprisingly, palladium was completely ineffective for this transformation, despite the authors' employment of conditions similar to those used by Suginome. Disappointingly, the authors observed that when

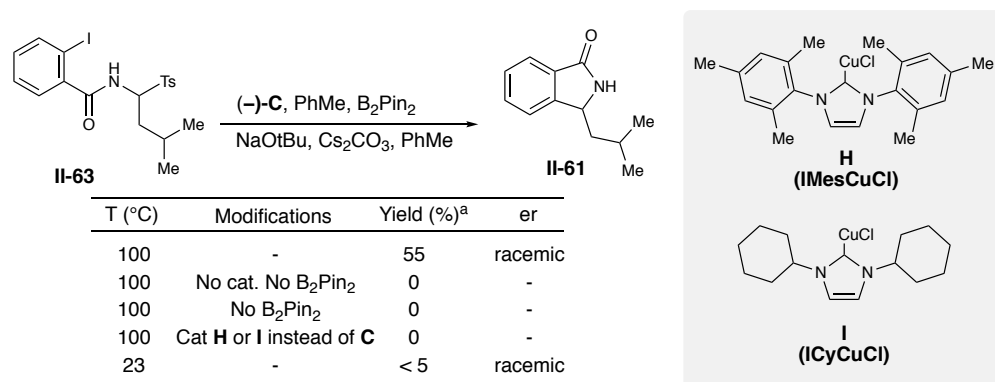
enantioenriched boronic ester **II-62** was subjected to their optimized conditions, only racemic isoindolinone was obtained.

Scheme 2-6. Inter- and intramolecular Cu(I) catalyzed Suzuki reactions disclosed by Dumas.



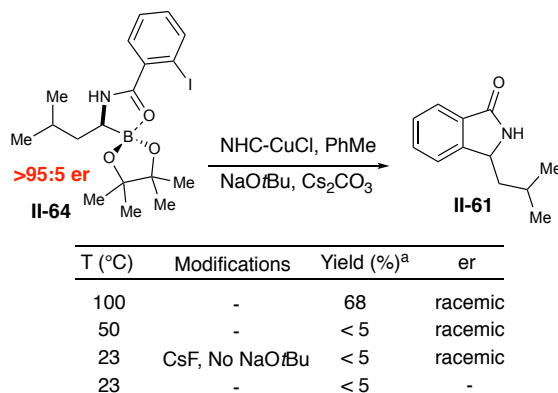
2.3.1 NHC-Cu(I)-mediated tandem borylation-Suzuki coupling

Despite the lack of any demonstrated diastereoselectivity in Dumas' related transformation,¹⁷² we reasoned that our conditions differed in several key respects that might allow us to promote an enantioselective reaction, namely (1) our use of a chiral Cu(I) ligand rather than an achiral bipy/CuCl system; (2) the exclusion of water from our reaction; and (3) our use of milder temperatures. During the borylation of substrate **II-63** with catalyst **C**, a small amount of **II-61** could be observed via GCMS after 16 hours. Unfortunately, this was accompanied by significant protodeborylation and protodehalogenation.

Table 2–5. Control studies on One-pot Borylation-Suzuki coupling sequence

^aYields determined by ¹H NMR of the crude product integrated against an internal standard.

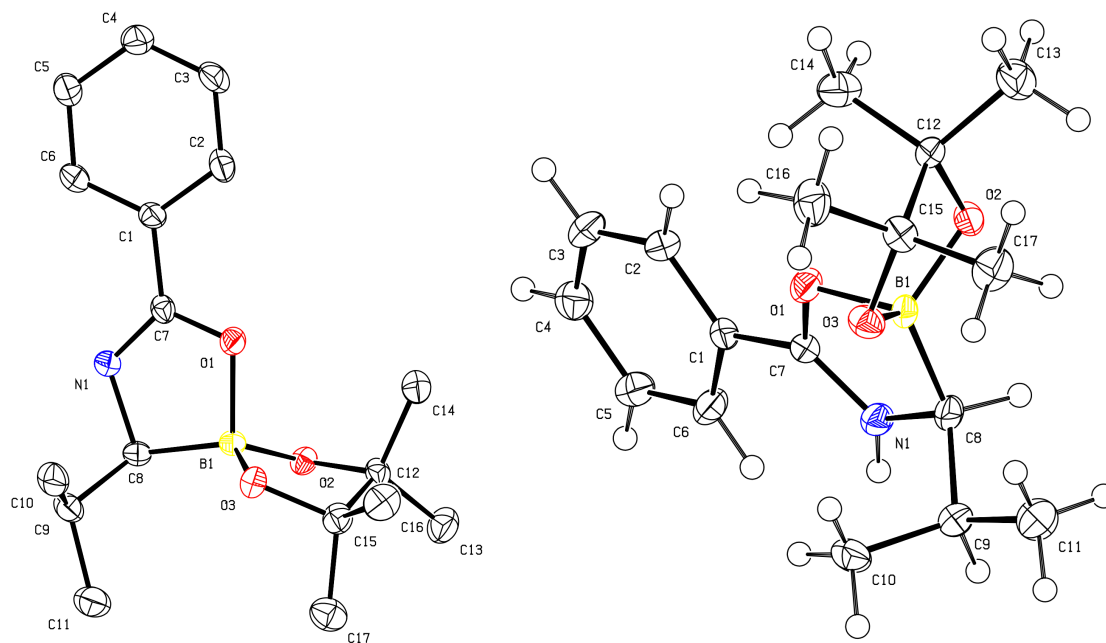
We then reasoned that use of more reactive iodide **II-63** might allow the desired transformation to outpace the formation of side products. Complete consumption of **II-63** and its borylated adduct after 12 hours of heating at 100 °C was observed, although the product was isolated as the racemate (**Table 2-5**). Conducting the reaction at room temperature significantly decreased yield and did not improve selectivity. To confirm that the coupling required the activation of a C-B bond (as opposed to the direct hydroarylation of the aldimine), B₂pin₂ was omitted from the reaction, whereupon no isoindolinone could be detected at a range of temperatures. Interestingly, achiral catalysts **IMesCuCl** and **ICyCuCl** promoted borylation, although no further reaction of the boronate was observed. Isolation of the boronate **II-64** (obtained in 99:1 er when borylated at room temperature) and reexposure to catalyst **C** at a range of temperatures also failed to reveal any enantioenriched isoindolinone (**Table 2-6**). These results suggest a profound configurational instability of putative intermediate of the intermediate α -aminocuprate. Despite this disappointing result, this is the first instance of a single-catalyst Cu(I)-mediated borylation-Suzuki coupling cascade that we are aware of.

Table 2–6. Direct Suzuki coupling of the isolated enantioenriched boronate.

^aYields determined by ¹H NMR of the crude product integrated against an internal standard.

2.4 Determination of absolute stereochemistry

To determine the absolute stereochemistry of the borylated adducts obtained with use of catalyst (–)-**C**, compound **II-33** was crystallized and submitted for characterization via X-ray diffraction. Upon slow evaporation of a THF solution of unpurified **II-33** in open atmosphere, the product was obtained as a cocrystal with the aminal condensation product of benzamide and isobuteraldehyde (see experimental section for complete x-ray data). Bijvoet pair analysis revealed that product was obtained as the *S*-enantiomer (**Figure 2-8**). Significant donation of the carbonyl lone pair into the empty p-orbital of boron was observed with significant paramidylation, imparting a B-centered 5,5-spiroboronate configuration. Although such a configuration may suggest the presence of a boron-centered negative formal charge (i.e. from a deprotonated amide), the presence of a counterion could be reliably excluded from the diffraction data.



Thermal ellipsoids are shown at the 50% probability level. Hydrogens are omitted for clarity in left view.

Figure 2-8. Crystal structure of compound **II-33**.

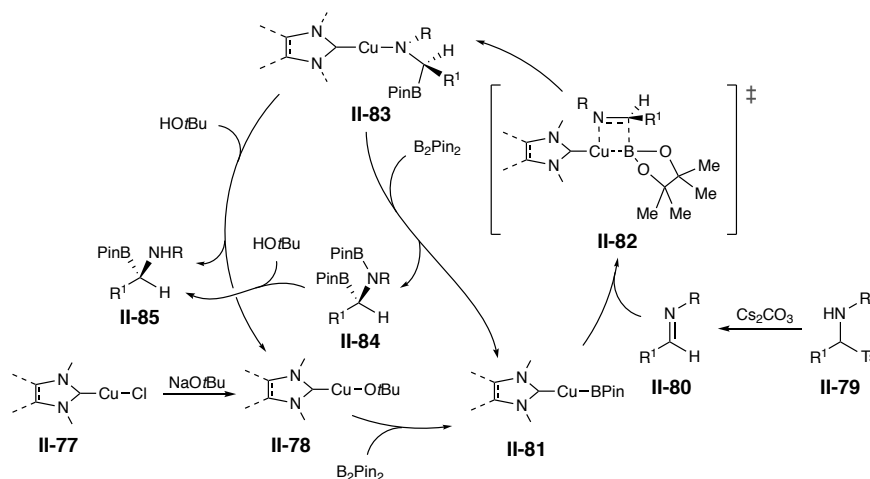
2.5 Mechanism and proposed DFT computational studies

To better understand the mechanism of stereoselection promoted by our catalysts, we plan to use DFT-based computational methods to estimate the relative energies of several putative pathways. Our proposed mechanism (**Scheme 2-7**) is largely informed by the extensive computational and empirical work devoted to characterizing the analogous borylation of aldehydes,¹⁶¹⁻¹⁶² as well as the absolute stereochemistry of our catalysts and products as determined by X-ray crystallography (**Figure 2-8**). We propose that in the course of the reaction, copper(I) chloride precatalyst **II-77** is first converted to active alkoxide **II-78**, which then can undergo σ -bond metathesis with B_2Pin_2 , to yield copper boryl species **II-81**. After deprotonation of sulfinyl species **II-79**, the resultant imine (**II-80**) can undergo σ -bond metathesis as depicted in transition state **II-82**. Amine (**II-83**) can then undergo protonolysis with *tert*-butanol to yield

the product (**II-85**), or exchange with an additional equivalent of B_2Pin_2 to afford bis(boronate)

II-84. **II-84** can then undergo protonolysis to yield the product.

Scheme 2-7. Postulated catalytic cycle



2.5.1 Proposed stereoinduction model

Analysis of the crystal structure of catalyst (-)-**C**, as well as buried volume calculations (**Figure 2-9**, bottom right) reveal a clearly discernable “open” NW quadrant. Therefore, our proposed major transition state (**II-87**) depicts an approach of the E-aldimine via the face of the NHC opposite to the ferrocene. In this arrangement, the benzoyl group occupies the open quadrant, minimizing interaction with the out-of-plane N-aryl ring while possibly participating in π -stacking with the ferrocene and its adjacent ring (**II-86**, **II-87**). The identity of the operative minor pathways is less clear. The reversal of the orientation of the E-imine (**II-96**), as well as borylation of the Z isomer of the imine (**II-94**, **II-95**) must be considered. We also note that computational studies concerning the borylation of aldehydes by Lin *et al.* have suggested that the reversal of the connectivity of the four-membered intermediate (**II-91**) serves as a minor pathway which would lead to intermediate **II-92** (**Figure 2-9**).¹⁶² As strongly implied by our

studies (section 2.3.1) and previous work by Dumas,¹⁷² this intermediate is a possible source of racemization due to configurational instability of the α -aminocuprate. We propose that identification of the relative energies of transition states **II-87**, **II-91**, **II-94**, and **II-96** with catalyst **C** via DFT will provide a useful basis for comparative computations with catalyst analogs.

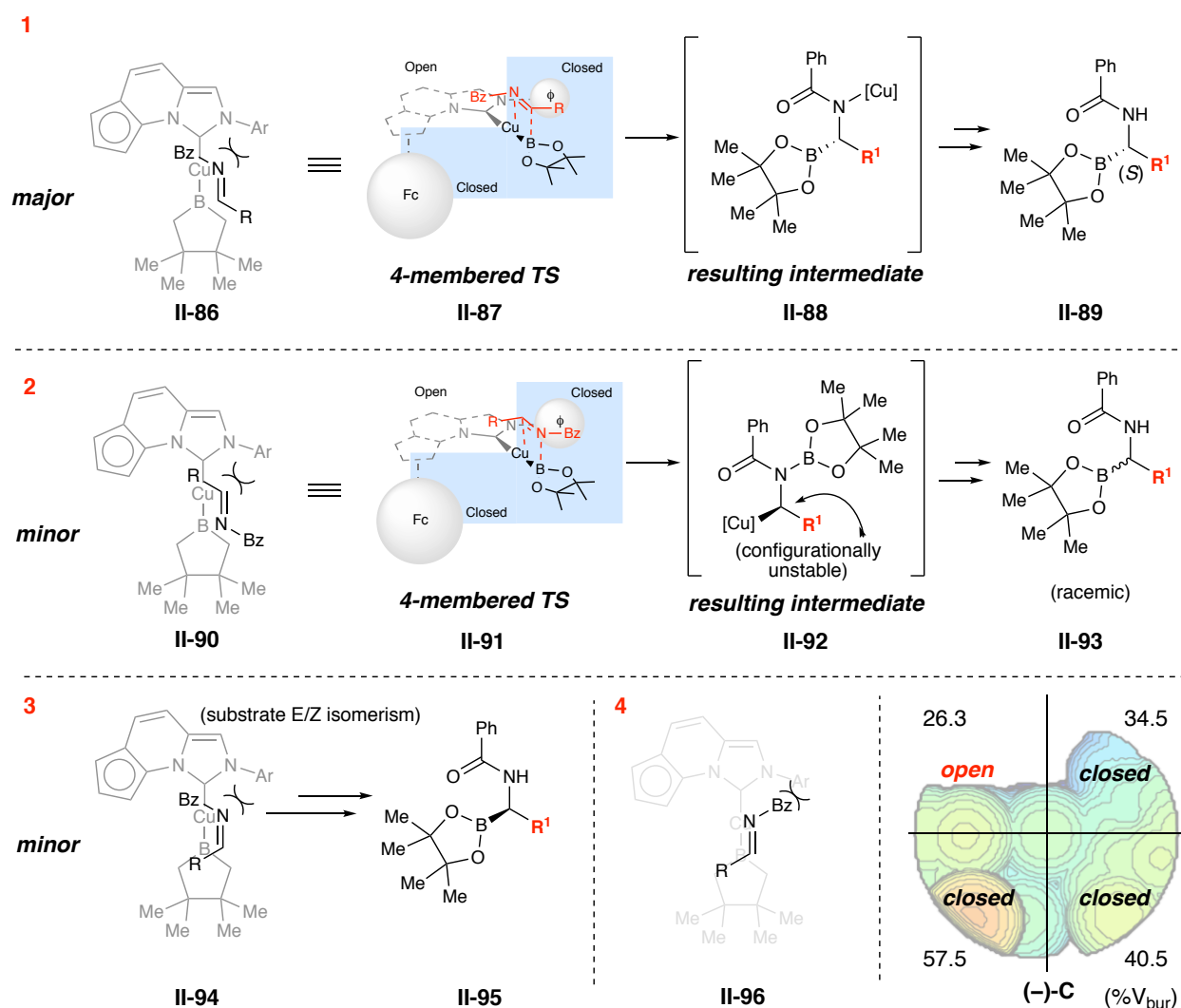


Figure 2-9. Proposed major and minor pathways.

2.6 Conclusion

The first highly efficient catalytic enantioselective synthesis of α,α -alkylaminoboronates has been undertaken, utilizing a new family of planar chiral imidazopyridinium NHC ligands. Additionally, the search for an improved process for isolation of these sensitive products has led to the development of a chromatography-free protocol for their construction starting from commercially-available aldehydes. Crystallographic analysis of the products and catalysts used in this methodology should serve as useful input for computational work on the mechanism of enantioinduction, which we anticipate will provide partial insight into the impact of small changes in catalyst structure and further inform future modifications to this catalyst class. Provided adequate catalyst availability and supply, it is anticipated that the high selectivity and operational simplicity of this protocol for aminoboronate synthesis can contribute towards a viable strategy for researchers interested in quick access to an array of these important products.

2.7 Experimental Section

General Information

All reactions were carried out under a nitrogen atmosphere in oven-dried glassware with magnetic stirring. THF, toluene, and DMF were purified by passage through a bed of activated alumina.¹²¹ Reagents were purified prior to use unless otherwise stated following the guidelines of Perrin and Armarego.¹²² Bis(pinacolato)diboron was recrystallized from hexanes. Silicycle SiliaFlash P60 silica gel 60 (230-400 mesh) was used for column chromatography. Analytical thin layer chromatography was performed on EM Reagent 0.25 mm silica gel 60-F plates. Visualization was accomplished with UV light. Infrared spectra were recorded on a Bruker Tensor 37 FT-IR spectrometer. ¹H NMR spectra were recorded on AVANCE III 500 MHz w/ direct cryoprobe (500 MHz) spectrometer and are reported in ppm using solvent as an internal standard (CDCl₃ at 7.26 ppm, (CD₃)₂SO at 2.50 ppm). Data are reported as (ap = apparent, s = singlet, d = doublet, t = apparent triplet, q = quartet, m = multiplet, b = broad; coupling constant(s) in Hz; integration.) Proton-decoupled ¹³C NMR spectra were recorded on an AVANCE III 500 MHz w/ direct cryoprobe (125 MHz) spectrometer and are reported in ppm using solvent as an internal standard (CDCl₃ at 77.16 ppm, (CD₃)₂SO at 39.52 ppm). ¹⁹F and ¹¹B NMR spectra were acquired at 26 °C on a 400 MHz Agilent 400MR-DD2 spectrometer equipped with a OneNMR probe and a 7600AS autosampler; this system was funded by NSF CRIF grant CHE-104873. Optical rotations were measured on a Perkin Elmer Model 341 Polarimeter with a sodium lamp. Mass spectra were obtained on a WATERS Acquity-H UPLC-MS with a single quad detector (ESI) or an Agilent 7890 gas chromatograph equipped with a 5975C single quadrupole EI-MS. Accurate masses were obtained using an Agilent 6120A LC-TOF MS.

Standardization of ^{11}B and ^{19}F Spectra

Standardization of all heteronuclear spectra was conducted using the IUPAC unified scale according to eqn. (1), as described in *Pure Appl. Chem.* **2008**, *80*, 59-84.

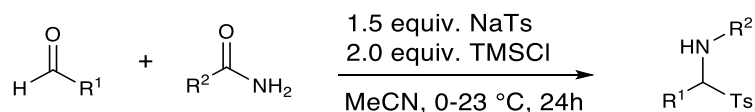
$$(1) \quad \mathcal{E}_x = 100 \times (\nu_x / \nu_o)$$

where ν_o = the absolute ^1H frequency of 0.00 ppm (δ_{TMS}) for experiments conducted in CDCl_3 , $\delta_{\text{TMS}} + 0.062$ ppm for DMSO, and $\delta_{\text{TMS}} - 0.160$ for acetone- d_6 , taken consecutively with heteronuclear experiments.

and $\mathcal{E}_{^{19}\text{F}} = 94.094011$ and $\mathcal{E}_{^{11}\text{B}} = 32.083974$.

and ν_x = absolute frequency of the 0 ppm position for isotope x .

2.7.1 General Procedure for the Synthesis of α -tosyl Benzamides

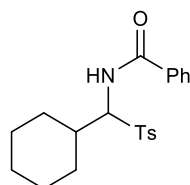


Method A¹⁷³: To a mixture of aldehyde (16.5 mmol 1.0 equiv.), sodium p-toluenesulfinate (4.41 g, 27.8 mmol, 1.5 equiv.), and amide (24.8 mmol, 1.5 equiv.) in MeCN (500 mL, 0.03 M) at 0 °C was added TMSCl (4.22 mL, 33.0 mmol, 2 equiv.) dropwise. Upon completion of addition the reaction was allowed to warm to room temperature and stirred for 24 hours. 500 mL water was then added and the reaction was stirred for 30 minutes. The resulting precipitate was isolated by filtration, washed with water (3 x 50 mL), and dried under vacuum at 50 °C for 16 hours to yield the product as a white solid.

Method B: Procedure followed that of **Method A** except that the reaction was immediately concentrated *in vacuo* after the reaction was deemed complete. 50 mL of diethyl ether was then added to the concentrate and the resulting suspension was stirred for 15 minutes. The solid impurities were removed by filtration, the filtrate was concentrated *in vacuo*, and the product was then purified via flash column chromatography on silica gel.

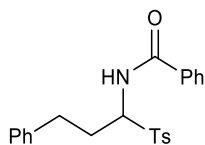
Method C: To a mixture of amide (1.0 g, 8.5 mmol, 1 equiv.), sodium p-toluenesulfinate (3.80 g, 21.3 mmol, 2.5 equiv.) in a 2:1 methanol/water mixture (0.3 M, 19 mL:9.5 mL) was added aldehyde (17.1 mmol, 2 equiv.) and formic acid (0.655 mL, 17.1 mL, 2 equiv). The reaction was

stirred at room temperature for 24 hours, and resulting precipitate was isolated by filtration, washed with water (2 x 50 mL) and diethyl ether (25 mL), and dried in under vacuum at 50 °C for 16 h to yield the product as a white solid.



***N*-(cyclohexyl(tosyl)methyl)benzamide (II-65)**

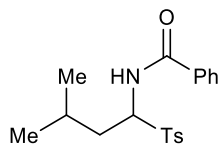
Prepared according to **Method A** using cyclohexane carboxaldehyde (1.85 g, 16.46 mmol, 1 equiv.) and benzamide (3.0 g, 24.8 mmol, 1.5 equiv.) to afford *N*-(cyclohexyl(tosyl)methyl)benzamide (5.29 g, 14.24 mmol, 87%). ¹H NMR (500 MHz, CDCl₃) δ 7.73 (d, *J* = 8.1 Hz, 2H), 7.62 (d, *J* = 7.2 Hz, 2H), 7.53 (t, *J* = 7.4 Hz, 1H), 7.44 (t, *J* = 7.6 Hz, 2H), 7.23 (d, *J* = 7.9 Hz, 2H), 6.61 (d, *J* = 10.8 Hz, 1H), 5.30 (dd, *J* = 10.8, 3.8 Hz, 1H), 2.57 (tq, *J* = 11.6, 3.5 Hz, 1H), 2.37 (s, 3H), 2.21 (dt, *J* = 12.4, 3.4 Hz, 1H), 1.89 (dt, *J* = 12.7, 3.4 Hz, 1H), 1.79 (tt, *J* = 12.7, 3.9 Hz, 2H), 1.73 – 1.58 (m, 2H), 1.39 (dtt, *J* = 17.0, 12.8, 3.6 Hz, 2H), 1.32 – 1.05 (m, 3H).



***N*-(3-phenyl-1-tosylpropyl)benzamide (II-66)**

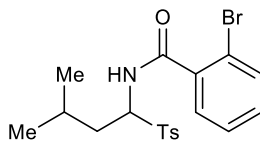
Prepared according to **Method A** using hydrocinnamaldehyde (tech. grade 90% w/w, 2.42 mL, 16.5 mmol, 1 equiv.) and benzamide (3.0 g, 24.8 mmol, 1.5 equiv.) to afford *N*-(3-phenyl-1-tosylpropyl)benzamide (5.12 g, 14.0 mmol, 85%) as a white solid. Analytical data: ¹H NMR

(500 MHz, CDCl₃) δ 7.73 (d, J = 8.0 Hz, 2H), 7.57 – 7.48 (m, 3H), 7.40 (t, J = 7.6 Hz, 2H), 7.35 – 7.21 (m, 4H), 7.21 – 7.11 (m, 3H), 6.46 (d, J = 10.4 Hz, 1H), 5.47 (ddd, J = 10.7, 10.4, 3.3 Hz, 1H), 2.83 (dd, J = 8.9, 7.2 Hz, 2H), 2.69 (dddd, J = 14.2, 8.9, 7.2, 3.3 Hz, 1H), 2.38 (s, 3H), 2.26 (ddt, J = 14.2, 10.7, 7.2 Hz, 1H); ¹³C NMR (126 MHz, CDCl₃) δ 166.50, 145.39, 140.03, 133.71, 132.96, 132.40, 129.97, 129.18, 128.83, 128.54, 127.05, 126.59, 69.05, 31.81, 28.63, 21.85. LRMS (ESI): Mass calcd. for C₂₃H₂₄NO₃S [M+H]⁺: 394; found 394.



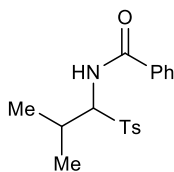
***N*-(3-methyl-1-tosylbutyl)benzamide (II-67)**

Prepared according to **Method A** using isovaleraldehyde (2.0 mL, 18.23 mmol, 1 equiv.) and benzamide (3.31 g, 27.3 mmol, 1.5 equiv.) to afford *N*-(3-methyl-1-tosylbutyl)benzamide (5.32 g, 15.4 mmol, 84%) as a white solid. Analytical data: ¹H NMR (500 MHz, CDCl₃) δ 7.76 (d, J = 7.9 Hz, 2H), 7.61 (t, J = 8.0 Hz, 2H), 7.56 – 7.45 (m, 1H), 7.45 – 7.32 (m, 2H), 7.25 (d, J = 7.9 Hz, 2H), 6.95 – 6.43 (m, 1H), 5.71 – 5.33 (m, 1H), 2.38 (s, 3H), 2.21 – 2.03 (m, 1H), 2.03 – 1.84 (m, 1H), 1.82 – 1.65 (m, 1H), 0.97 (m, 6H). ¹³C NMR (126 MHz, CDCl₃) δ 166.54, 166.44, 145.28, 133.78, 133.05, 132.34, 132.30, 132.28, 129.92, 129.21, 128.84, 128.79, 128.77, 127.15, 127.07, 68.29, 68.16, 35.11, 35.02, 25.05, 23.45, 21.84, 21.43.



2-bromo-*N*-(3-methyl-1-tosylbutyl)benzamide (II-68)

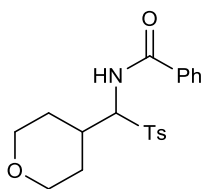
Prepared according to **Method A** using isovaleraldehyde (0.730 mL, 6.7 mmol, 1 equiv.) and 2-bromobenzamide (2.0 g, 10.0 mmol, 1.5 equiv.) to afford 2-bromo-*N*-(3-methyl-1-tosylbutyl)benzamide (2.31 g, 5.4 mmol, 82%) as a white solid. Analytical data: ^1H NMR (500 MHz, CDCl_3) δ 7.83 (d, $J = 7.9$ Hz, 2H), 7.55 (d, $J = 7.6$ Hz, 1H), 7.34 (d, $J = 8.0$ Hz, 2H), 7.34 – 7.23 (m, 2H), 7.12 (dd, $J = 7.3, 2.0$ Hz, 1H), 6.35 (d, $J = 10.4$ Hz, 1H), 5.51 (ddd, $J = 11.0, 10.4, 3.1$ Hz, 1H), 2.44 (s, 3H), 2.09 (ddd, $J = 14.2, 11.0, 2.8$ Hz, 1H), 1.98 – 1.77 (m, 2H), 1.03 (d, $J = 6.4$ Hz, 3H), 0.99 (d, $J = 6.4$ Hz, 3H). ^{13}C NMR (126 MHz, CDCl_3) δ 166.40, 145.39, 136.21, 133.92, 133.77, 132.01, 129.98, 129.61, 129.35, 127.62, 119.16, 67.88, 35.13, 24.97, 23.58, 21.90, 21.28.



N-(2-methyl-1-tosylpropyl)benzamide (II-69)

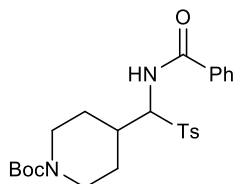
Prepared according to **Method B** using isobutyraldehyde (1.0 mL, 10.96 mmol, 1 equiv.) and benzamide (2.0 g, 16.4 mmol, 1.5 equiv.) and purified by flash column chromatography (10-40% EtOAc/hex; TLC 40% EtOAc/hex, UV, CAM or KMnO_4 , R_f 0.57) to afford *N*-(2-methyl-1-tosylpropyl)benzamide (3.21 g, 9.7 mmol, 88%) as a white solid. Analytical data: ^1H NMR (500 MHz, CDCl_3) δ 7.74 (d, $J = 8.0$ Hz, 2H), 7.62 (d, $J = 6.9$ Hz, 1H), 7.54 (t, $J = 7.3$ Hz, 1H), 7.44

(t, $J = 7.5$ Hz, 2H), 7.25 (d, $J = 7.7$ Hz, 3H), 6.57 (d, $J = 10.8$ Hz, 1H), 5.32 (dd, $J = 10.8, 3.7$ Hz, 1H), 2.89 (dhept, $J = 6.7, 3.7$ Hz, 1H), 2.38 (s, 3H), 1.22 (d, $J = 6.7$ Hz, 3H), 1.12 (d, $J = 6.7$ Hz, 3H). ^{13}C NMR (126 MHz, CDCl_3) δ 166.77, 145.18, 134.97, 133.20, 132.40, 129.96, 128.94, 128.80, 127.03, 72.71, 27.48, 21.82, 20.87, 17.31. LRMS (ESI): Mass calcd. for $\text{C}_{18}\text{H}_{22}\text{NO}_3\text{S}$ $[\text{M}+\text{H}]^+$: 332; found 332.



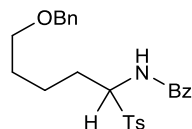
***N*-((tetrahydropyran-4-yl)(tosyl)methyl)benzamide (II-70)**

Prepared according to **Method B** using tetrahydropyran-4-carbaldehyde (1.0 g, 8.76 mmol, 1 equiv.) and benzamide (1.59 g, 13.14 mmol, 2 equiv.) and purified by flash column chromatography (40-80% EtOAc/hex; TLC 40% EtOAc/hex, UV, R_f 0.25) to afford *N*-((tetrahydropyran-4-yl)(tosyl)methyl)benzamide (2.15 g, 5.76 mmol, 66%) as a white solid. Analytical data: ^1H NMR (500 MHz, CDCl_3) δ 7.73 (d, $J = 8.0$ Hz, 2H), 7.60 (d, $J = 7.5$ Hz, 2H), 7.55 (t, $J = 7.4$ Hz, 1H), 7.44 (t, $J = 7.5$ Hz, 2H), 7.25 (d, $J = 8.0$ Hz, 1H), 6.60 (d, $J = 10.4$ Hz, 1H), 5.33 (dd, $J = 10.8, 4.3$ Hz, 1H), 4.01 (ddd, $J = 15.7, 11.8, 4.2$ Hz, 2H), 3.50 (ddd, $J = 11.9, 11.8, 6.2$ Hz, 2H), 2.97 – 2.66 (m, 1H), 2.38 (s, 2H), 2.05 (d, $J = 13.0$ Hz, 1H), 1.79 (d, $J = 13.2$ Hz, 1H), 1.73 – 1.48 (m, 2H). ^{13}C NMR (126 MHz, CDCl_3) δ 166.72, 145.46, 134.58, 132.91, 132.57, 130.04, 128.99, 128.81, 127.01, 71.71, 67.63, 67.32, 34.46, 30.20, 27.83, 21.85. LRMS (ESI): Mass calcd. for $\text{C}_{20}\text{H}_{24}\text{NO}_4\text{S}$ $[\text{M}+\text{H}]^+$: 374; found 374.



***tert*-butyl 4-(benzamido(tosyl)methyl)piperidine-1-carboxylate (II-71)**

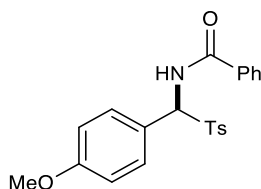
Prepared according to **Method B** using 1-boc-piperidine-4-carboxaldehyde (1.0 g, 4.69 mmol, 1 equiv.) and benzamide (0.852 g, 7.03 mmol, 1.5 equiv.) and purified via flash column chromatography (30-70% EtOAc/hex; TLC 40% EtOAc/hex, UV, R_f 0.31) to afford *tert*-butyl 4-(benzamido(tosyl)methyl)piperidine-1-carboxylate (1.58 g, 3.34 mmol, 71%) as a white solid. Analytical data: ^1H NMR (500 MHz, CDCl_3) δ 7.74 (d, $J = 7.9$ Hz, 2H), 7.61 (d, $J = 7.6$ Hz, 2H), 7.54 (t, $J = 7.5$ Hz, 1H), 7.44 (t, $J = 7.6$ Hz, 2H), 7.36 – 7.18 (m, 3H), 6.64 (d, $J = 10.8$ Hz, 1H), 5.36 (dd, $J = 10.8, 4.1$ Hz, 1H), 4.18 (br, 2H), 3.01 – 2.57 (m, 3H), 2.38 (s, 3H), 2.14 (d, $J = 12.8$ Hz, 1H), 1.87 (d, $J = 13.2$ Hz, 1H), 1.44 (m, 11H). ^{13}C NMR (126 MHz, CDCl_3) δ 166.65, 154.71, 145.45, 134.53, 132.82, 132.55, 130.02, 128.95, 128.79, 127.04, 79.80, 71.72, 35.47, 29.73, 28.53, 27.01, 21.82.



***N*-(5-(benzyloxy)-1-tosylpentyl)benzamide (II-72)**

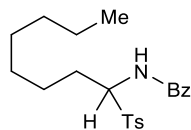
Prepared according to **Method B** using 5-(benzyloxy)pentanal (400 mg, 2.08 mmol, 1 equiv.) and benzamide (378 mg, 3.12 mmol, 1.5 equiv.) and purified via flash column chromatography to afford *N*-(5-(benzyloxy)-1-tosylpentyl)benzamide (640 mg, 1.42 mmol, 68%) as a white solid.

Analytical data: ^1H NMR (500 MHz, CDCl_3) δ 7.75 (d, $J = 8.3$ Hz, 2H), 7.57 (d, $J = 7.4$ Hz, 2H), 7.51 (t, $J = 7.5$ Hz, 1H), 7.40 (t, $J = 7.7$ Hz, 2H), 7.34 – 7.28 (m, 4H), 7.30 – 7.20 (m, 3H), 6.78 – 6.28 (m, 1H), 5.44 (td, $J = 10.7, 3.2$ Hz, 1H), 4.46 (d, $J = 2.9$ Hz, 2H), 3.56 – 3.32 (m, 2H), 2.38 (m, 4H), 2.03 – 1.88 (m, 1H), 1.78 – 1.46 (m, 4H). ^{13}C NMR (126 MHz, CDCl_3) δ 166.65, 145.32, 138.48, 133.81, 133.04, 132.34, 129.94, 129.18, 128.84, 128.52, 127.84, 127.72, 127.09, 73.09, 69.84, 69.34, 29.14, 26.49, 22.62, 21.85. LRMS (ESI): Mass calcd. for $\text{C}_{26}\text{H}_{30}\text{NO}_4\text{S}$ $[\text{M}+\text{H}]^+$: 452; found 452.



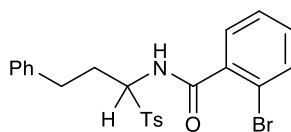
***N*-((4-methoxyphenyl)(tosyl)methyl)benzamide (II-97)**

Prepared according to **Method A** using 4-methoxybenzaldehyde (2.00 mL, 16.4 mmol, 1 equiv.) and benzamide (3.00 g, 24.6 mmol, 1.5 equiv.) to afford *N*-((4-methoxyphenyl)(tosyl)methyl)benzamide: (5.42 g, 16.4 mmol, 83%) as a white solid. Analytical data: ^1H NMR (500 MHz, CDCl_3) δ 7.76 (d, $J = 8.3$ Hz, 2H), 7.66 (dd, $J = 8.4, 1.4$ Hz, 2H), 7.53 (tt, $J = 7.5, 1.9$ Hz, 1H), 7.49 – 7.34 (m, 4H), 7.27 (d, $J = 7.3$ Hz, 2H), 7.08 (d, $J = 10.3$ Hz, 1H), 6.94 (d, $J = 8.7$ Hz, 2H), 6.40 (d, $J = 10.3$ Hz, 1H), 3.83 (s, 3H), 2.40 (s, 3H). ^{13}C NMR (126 MHz, CDCl_3) δ 166.27, 161.13, 145.51, 134.01, 133.32, 132.56, 130.47, 130.05, 129.47, 129.03, 127.29, 122.26, 114.64, 72.15, 55.63, 21.98.



***N*-(1-tosylpropyl)benzamide (II-73)**

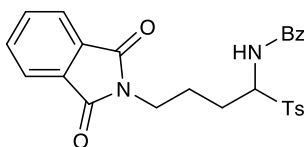
Prepared according to **Method B** using *n*-octanal (1.0 mL, 6.43 mmol, 1 equiv.) and benzamide (1.20 g, 9.65 mmol, 1.5 equiv.) and purified via flash column chromatography to afford *N*-(1-tosylpropyl)benzamide (1.88 g, 4.85 mmol, 75%) as a clear viscous oil that gradually solidified to a white solid under high vacuum. Analytical data: ^1H NMR (500 MHz, CDCl_3) δ 7.75 (d, $J = 7.9$ Hz, 2H), 7.64 (d, $J = 7.5$ Hz, 2H), 7.47 (t, $J = 7.4$ Hz, 1H), 7.36 (t, $J = 7.6$ Hz, 2H), 7.24 (d, $J = 7.9$ Hz, 2H), 7.02 (d, $J = 10.3$ Hz, 1H), 5.46 (td, $J = 10.8, 3.3$ Hz, 1H), 2.37 (s, 3H), 2.31 (dddd, $J = 13.4, 9.8, 6.4, 3.3$ Hz, 1H), 2.09 – 1.77 (m, 1H), 1.67 – 1.01 (m, 10H), 0.84 (t, $J = 6.6$ Hz, 3H). ^{13}C NMR (126 MHz, CDCl_3) δ 166.80, 145.17, 133.85, 132.98, 132.17, 129.83, 129.10, 128.65, 127.19, 69.55, 31.71, 29.08, 28.99, 26.60, 25.50, 22.61, 21.76, 14.11. LRMS (ESI): Mass calcd. for $\text{C}_{22}\text{H}_{30}\text{NO}_3\text{S}$ $[\text{M}+\text{H}]^+$: 388; found 388.



2-bromo-*N*-(3-phenyl-1-tosylpropyl)benzamide (II-74)

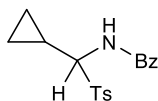
Prepared according to **Method A** using hydrocinnamaldehyde (tech. grade 90% w/w, 2.42 mL, 16.5 mmol, 1 equiv) and 2-bromobenzamide (4.95 g, 24.75 mmol, 1.5 equiv) to afford 2-bromo-*N*-(3-phenyl-1-tosylpropyl)benzamide (4.83 g, 10.87 mmol, 66%) as a white solid. Analytical data: ^1H NMR (500 MHz, CDCl_3) δ 7.78 (t, $J = 7.0$ Hz, 2H), 7.57 (t, $J = 6.7$ Hz, 1H), 7.46 – 7.24 (m, 6H), 7.21 (t, $J = 7.1$ Hz, 3H), 7.08 (dd, $J = 6.8, 2.4$ Hz, 1H), 6.70 – 6.36 (m, 1H), 5.46 (td, J

= 10.7, 3.1 Hz, 1H), 2.98 (ddd, $J = 14.4, 9.5, 5.1$ Hz, 1H), 2.83 (dt, $J = 13.6, 8.3$ Hz, 1H), 2.74 – 2.59 (m, 1H), 2.44 (s, 3H), 2.20 (dtd, $J = 14.4, 9.8, 5.0$ Hz, 1H). ^{13}C NMR (126 MHz, CDCl_3) δ 166.61, 145.46, 139.91, 136.18, 133.78, 133.73, 132.08, 132.03, 130.00, 129.72, 129.67, 129.28, 128.81, 128.60, 127.67, 127.64, 126.63, 119.18, 68.71, 31.68, 28.82, 21.88.



***N*-(4-(1,3-dioxoisindolin-2-yl)-1-tosylbutyl)benzamide (II-75)**

Prepared according to **Method A** using 4-(1,3-dioxoisindolin-2-yl)butanal (1.0 g, 4.60 mmol, 1 equiv.) and benzamide (0.837 g, 6.91 mmol, 1.5 equiv.) to afford *N*-(4-(1,3-dioxoisindolin-2-yl)-1-tosylbutyl)benzamide (1.40 g, 2.94 mmol, 64%) as a pale yellow solid. Analytical data: ^1H NMR (500 MHz, CDCl_3) δ 7.96 – 7.74 (m, 4H), 7.74 – 7.58 (m, 4H), 7.48 (t, $J = 7.1$ Hz, 1H), 7.37 (t, $J = 7.6$ Hz, 2H), 7.32 – 7.16 (m, 3H), 5.58 (td, $J = 10.7, 3.4$ Hz, 1H), 3.87 – 3.60 (m, 2H), 2.56 – 2.20 (m, 4H), 2.12 – 1.96 (m, 1H), 1.96 – 1.81 (m, 2H). ^{13}C NMR (126 MHz, CDCl_3) δ 168.40, 166.83, 145.21, 134.07, 133.60, 132.82, 132.18, 131.94, 129.85, 129.16, 128.62, 127.25, 123.34, 69.16, 37.16, 24.92, 23.60, 21.74.

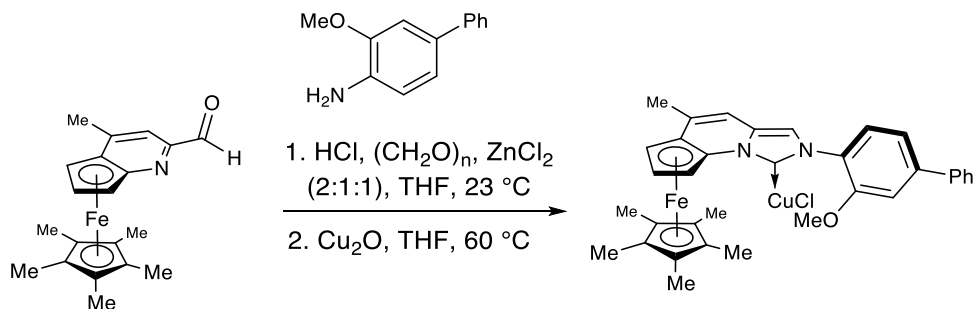


***N*-(cyclopropyl(tosyl)methyl)benzamide (II-76)**

Prepared according to **Method B** using cyclopropane carbaldehyde (2.0 mL, 26.8 mmol, 1 equiv.) and benzamide (4.86 g, 40.1 mmol, 1.5 equiv.) and purified via flash column

chromatography (30-70% EtOAc/hex; TLC 40% EtOAc/hex, UV, R_f 0.48) to afford *N*-(cyclopropyl(tosyl)methyl)benzamide (6.78 g, 20.58 mmol, 77%) as a white solid. Analytical data: Analytical data: ^1H NMR (500 MHz, CDCl_3) δ 7.79 (d, $J = 8.0$ Hz, 2H), 7.66 (d, $J = 7.7$ Hz, 2H), 7.52 (t, $J = 7.7$ Hz, 1H), 7.42 (t, $J = 7.5$ Hz, 2H), 7.27 (d, $J = 7.6$ Hz, 3H), 6.99 – 6.64 (m, 1H), 4.90 (t, $J = 9.7$ Hz, 1H), 2.39 (s, 3H), 1.47 (ddq, $J = 13.0, 8.6, 4.8$ Hz, 1H), 0.91 – 0.76 (m, 1H), 0.76 – 0.55 (m, 2H), 0.47 (dp, $J = 6.0, 4.8$ Hz, 1H). ^{13}C NMR (126 MHz, CDCl_3) δ 166.45, 145.28, 134.37, 133.07, 132.39, 129.91, 129.23, 128.86, 127.19, 73.24, 21.84, 9.65, 5.31, 2.60. LRMS (ESI): Mass calcd. for $\text{C}_{18}\text{H}_{20}\text{NO}_3\text{S}$ $[\text{M}+\text{H}]^+$: 330; found 330.

2.7.2 Synthesis of Catalyst (–)-G



To a solution of 3-methoxy-[1,1'-biphenyl]-2-amine (28 mg, 0.143 mmol, 1.0 equiv.) and (–)-pentamethyl- η^5 -cyclopentadienyl (1-methyl- η^5 -cyclopenta[b]pyridinyl-3-carbaldehyde)iron (50 mg, 0.143 mmol, 1.0 equiv.) in THF (1.4 mL, 0.1 M) was added dropwise a solution of paraformaldehyde (5.2 mg, 0.172 mmol, 1.2 equiv.) and ZnCl_2 (23.4 mg, 0.172 mmol, 1.2 equiv.) in concentrated HCl (27.4 μL , 38% w/w, 2.4 equiv.). The dark-green solution was stirred at room temperature for 30 minutes, whereupon the reaction changed to a red-orange color and a small amount of precipitate was observed. The solvent was then removed *in vacuo* and the

residue was redissolved in 1.0 mL dichloromethane. The resulting homogeneous solution was directly loaded on a plug of neutral alumina and impurities were eluted using additional dichloromethane. The azolium salt was then eluted as a bright-orange band using CH₂Cl₂:EtOH (5:1), concentrated *in vacuo*, and redissolved in 1.4 mL THF (0.1 M) in a 1 dram vial under dry nitrogen atmosphere. To this solution was added Cu₂O (19 mg, 0.13 mmol) and the mixture was heated at 60 °C for 16 hours. The solution was then concentrated and the residue was purified by column chromatography on silica gel (CH₂Cl₂, R_f~0.4) to provide the complex as an orange solid (60 mg, 0.094 mmol, 72% yield). X-ray quality crystals were obtained by vapor diffusion (DCM/pentane, -30 °C) (36 mg, 0.065 mmol, 90% yield). ¹H NMR (500 MHz, CDCl₃) δ 7.65 – 7.61 (m, 2H), 7.60 (d, *J* = 8.0 Hz, 1H), 7.53 – 7.46 (m, 2H), 7.42 (tt, *J* = 7.4, 1.8 Hz, 1H), 7.30 (dd, *J* = 8.0, 1.8 Hz, 1H), 7.29 (s, 1H), 7.25 (s, 1H), 6.74 (q, *J* = 1.3 Hz, 1H), 5.59 (dd, *J* = 2.7, 1.1 Hz, 1H), 4.02 (dd, *J* = 2.7, 1.2 Hz, 1H), 3.92 (s, 3H), 3.85 (t, *J* = 2.6 Hz, 1H), 2.27 (d, *J* = 1.4 Hz, 3H), 1.67 (s, 15H). ¹³C NMR (126 MHz, CDCl₃) δ 180.37, 153.71, 144.01, 136.01, 130.53, 129.09, 128.68, 128.42, 128.17, 128.11, 127.49, 120.17, 115.45, 111.58, 107.52, 81.08, 71.51, 65.24, 62.99, 56.13, 19.26, 10.00. LCMS (ESI⁺) mass calcd. for C₃₄H₃₄CuFeN₂O [M-Cl]⁺, 605.1; found 605.3.

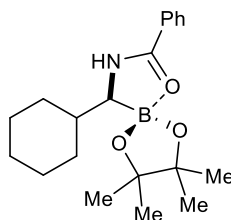
2.7.3 General Procedure for the Enantioselective Synthesis of α -amidoboronates

Inside a glovebox, to a 2-dram vial was added catalyst **C** (0.03 equiv.), sodium *tert*-butoxide (0.04 equiv.), and THF (0.17 M). The vial was capped with a teflon septum, and the resulting orange solution was stirred for 15 minutes at room temperature. To a separate 2-dram vial was added tosyl benzamide (1 equiv.), cesium carbonate (2.0 equiv.), B₂Pin₂ (1.2 equiv.) and a teflon

stirbar. The orange solution in the first vial was then transferred to the other vial via syringe and stirred vigorously at room temperature for 12 hours, or until the reaction was deemed complete via GCMS. The crude mixture was then eluted through a short plug of deactivated silica gel (35% w/w H₂O), washing with 5-10 mL EtOAc. The crude material was then dry loaded on celite and purified via flash column chromatography on deactivated silica gel (35% w/w H₂O).

General Procedure for the Enantioselective Synthesis of potassium α -amidotrifluoroborates¹⁶⁷

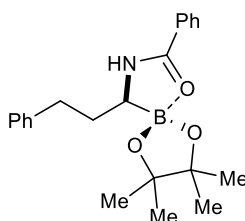
Procedure follows BPin adduct synthesis (see previous section) throughout elution of crude reaction mixture through a pad of celite. The filtered solution was concentrated *in vacuo*, and then redissolved in a 1:1 mixture of MeCN:MeOH (0.25 M). Aqueous KF was then added to the mixture dropwise (4.0 eq, 10 M), and the reaction was stirred for a further 5 minutes or until complete dissolution is observed. L-(+)-tartaric acid in THF (2.05 equiv., 1.33 M) was then added dropwise over a period of 5 minutes, whereupon the reaction was diluted 1x with MeCN and any precipitate was broken up with a spatula. After stirring for a further 3-5 minutes, the reaction was again diluted 1x with MeCN, and filtered over a fritted funnel. The filter cake is washed thoroughly with MeCN, and the filtrate was concentrated *in vacuo*. The residue was titrated with Et₂O, and the resulting white precipitate was collected via filtration and washed with hot acetone to yield the pure trifluoroborate salt.



(S)-N-(cyclohexyl(4,4,5,5-tetramethyl-1,3,2-dioxaborolan-2-yl)methyl)benzamide (II-36)

Prepared according to the general procedure using 200 mg **II-65** (0.538 mmol) to afford (S)-N-(cyclohexyl(4,4,5,5-tetramethyl-1,3,2-dioxaborolan-2-yl)methyl)benzamide (120 mg, 65% yield).

Analytical data: ^1H NMR (500 MHz, CDCl_3) δ 7.80 (d, $J = 7.8$ Hz, 2H), 7.52 (tt, $J = 8.2, 7.4, 1.0$ Hz, 1H), 7.43 (dd, $J = 8.4, 7.0$ Hz, 2H), 6.92 (s, 1H), 3.01 (dd, $J = 6.2, 4.1$ Hz, 1H), 1.95 – 1.79 (m, 2H), 1.79 – 1.49 (m, 4H), 1.28 (d, $J = 3.0$ Hz, 13H), 1.26 – 1.18 (m, 2H), 1.18 – 1.01 (m, 2H). ^{13}C NMR (126 MHz, CDCl_3) δ 169.63, 132.45, 131.16, 128.76, 127.62, 82.32, 39.79, 31.39, 30.44, 26.63, 26.46, 25.40, 25.37. LRMS (EI) m/z : $[\text{M}-\text{H}]^+$ Calcd. for $\text{C}_{20}\text{H}_{29}\text{BNO}_3$ 342.2; Found 342.3. HRMS (ESI/TOF): $[\text{M}+\text{H}]^+$ Calcd. For $\text{C}_{20}\text{H}_{31}\text{BNO}_3$ 344.2392; Found 344.2390. Enantiomeric ratio was measured by chiral phase HPLC (Regis Whelk-O 1 (#1-786515-300), 5% *i*-PrOH/Hexanes, 1.0 mL/min, 210 nm) R_t (major) = 5.5 min, R_t (minor) = 4.9 min; er = 98:2.

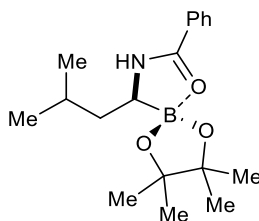


(S)-N-(3-phenyl-1-(4,4,5,5-tetramethyl-1,3,2-dioxaborolan-2-yl)propyl)benzamide (II-34)

Prepared according to the general procedure using 200 mg **II-66** (0.508 mmol) to afford (S)-N-(3-phenyl-1-(4,4,5,5-tetramethyl-1,3,2-dioxaborolan-2-yl)propyl)benzamide (85 mg, 46% yield).

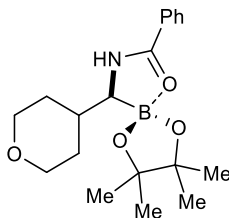
Analytical data: ^1H NMR (500 MHz, CDCl_3) δ 7.57 – 7.47 (m, 4H), 7.43 – 7.36 (m, 2H), 7.36 –

7.30 (m, 2H), 7.30 – 7.22 (m, 2H), 6.50 (s, 1H), 2.96 (ddd, $J = 12.9, 7.3, 5.0$ Hz, 1H), 2.91 (ddd, $J = 9.8, 4.2, 2.3$ Hz, 1H), 2.70 (ddd, $J = 13.6, 8.8, 7.3$ Hz, 1H), 2.19 – 2.09 (m, 1H), 1.96 – 1.83 (m, 1H), 1.27 (d, $J = 4.7$ Hz, 12H). LRMS (EI) m/z : $[M-H]^+$ Calcd. for $C_{22}H_{27}BNO_3$ 364.2; found 364.2. HRMS (ESI/TOF) m/z : $[M+Na]^+$ Calcd. for $C_{22}H_{29}BNO_3Na$ 388.2058; Found 388.2069. Enantiomeric ratio was measured by chiral phase SFC (Chiracel IA-3 (#80524), 15% MeOH/CO₂, 3.0 mL/min, 250 nm) R_t (major) = 1.3 min, R_t (minor) = 1.1 min; er = 97:3.



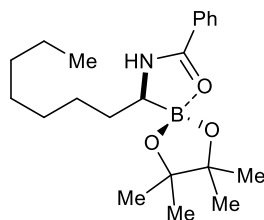
(S)-N-(3-methyl-1-(4,4,5,5-tetramethyl-1,3,2-dioxaborolan-2-yl)butyl)benzamide (II-35)

Note: Used catalyst **G**. Prepared otherwise according to the general procedure using 100 mg **II-67** (0.289 mmol) to afford (S)-N-(3-methyl-1-(4,4,5,5-tetramethyl-1,3,2-dioxaborolan-2-yl)butyl)benzamide (56 mg, 61% yield). Analytical data: ¹H NMR (500 MHz, CDCl₃) δ 7.79 (dd, $J = 8.2, 1.2$ Hz, 2H), 7.54 (tt, $J = 7.4, 1.3$ Hz, 1H), 7.42 (t, $J = 7.8$ Hz, 2H), 7.27 (br, 1H), 2.95 (td, $J = 7.5, 2.5$ Hz, 1H), 1.70 (dh, $J = 13.4, 6.9$ Hz, 1H), 1.51 (t, $J = 7.3$ Hz, 2H), 1.27 (s, 5H), 1.26 (s, 7H), 0.96 (d, $J = 2.5$ Hz, 3H), 0.94 (d, $J = 2.5$ Hz, 3H). ¹³C NMR (126 MHz, CDCl₃) δ 170.79, 133.16, 128.82, 128.76, 127.93, 81.19, 40.47, 26.32, 25.39, 25.24, 23.60, 22.09. LRMS (EI) m/z : $[M-H]^+$ Calcd. for $C_{18}H_{27}BNO_3$ 316.2; Found 316.2. HRMS (ESI/TOF) m/z : $[M+H]^+$ Calcd. for $C_{18}H_{29}BNO_3$ 318.2238; Found 318.2251. Enantiomeric ratio was measured by chiral phase SFC (Chiracel IA-3 (#80524), 5% *i*-PrOH/CO₂, 3.0 mL/min, 250 nm) R_t (major) = 7.4 min, R_t (minor) = 10.0 min; er = >99:1.



(S)-N-((tetrahydro-2H-pyran-4-yl)(4,4,5,5-tetramethyl-1,3,2-dioxaborolan-2-yl)methyl)benzamide (II-38)

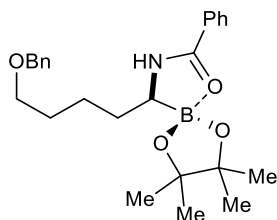
Prepared according to the general procedure using 115 mg **II-70** (0.308 mmol) to (S)-N-((tetrahydro-2H-pyran-4-yl)(4,4,5,5-tetramethyl-1,3,2-dioxaborolan-2-yl)methyl)benzamide (66 mg, 62% yield). Analytical data: ^1H NMR (500 MHz, CDCl_3) δ 7.82 – 7.72 (m, 2H), 7.57 – 7.49 (m, 1H), 7.43 (dd, $J = 8.3, 7.1$ Hz, 2H), 6.97 (s, 1H), 3.95 (ddd, $J = 11.2, 5.0, 1.8$ Hz, 2H), 3.47 – 3.28 (m, 2H), 2.93 (dd, $J = 6.2, 3.7$ Hz, 1H), 1.94 (tdd, $J = 10.7, 8.0, 5.4$ Hz, 1H), 1.74 (dddd, $J = 28.8, 12.9, 4.0, 2.1$ Hz, 2H), 1.53 – 1.38 (m, 1H), 1.26 (s, 8H). ^{13}C NMR (126 MHz, CDCl_3) δ 170.30, 132.91, 128.91, 127.67, 82.19, 68.21, 68.18, 37.01, 31.32, 30.17, 25.49, 25.36. LRMS (EI) m/z : $[\text{M}-\text{H}]^+$ Calcd. for $\text{C}_{19}\text{H}_{27}\text{BNO}_4$ 344.2; Found 344.2. HRMS (ESI/TOF) m/z : $[\text{M}+\text{Na}]^+$ Calcd. for $\text{C}_{19}\text{H}_{28}\text{BNO}_4\text{Na}$ 368.2007; Found 368.2013. Enantiomeric ratio was measured by chiral phase HPLC (Chiracel OD-H (#14325), 2% *i*-PrOH/Hexanes, 1.0 mL/min, 250 nm) R_t (major) = 7.8 min, R_t (minor) = 8.9 min; er = >99:1.



(S)-N-(1-(4,4,5,5-tetramethyl-1,3,2-dioxaborolan-2-yl)octyl)benzamide (II-37)

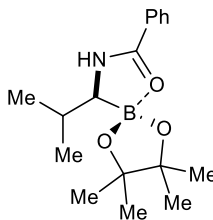
Prepared according to the general procedure using 100 mg **II-73** (0.258 mmol) to afford (*S*)-*N*-(1-(4,4,5,5-tetramethyl-1,3,2-dioxaborolan-2-yl)octyl)benzamide (41 mg, 44% yield).

Analytical data: ^1H NMR (500 MHz, CDCl_3) δ 8.09 (s, 1H), 7.79 (d, $J = 7.6$ Hz, 2H), 7.48 (t, $J = 7.5$ Hz, 1H), 7.35 (t, $J = 7.7$ Hz, 2H), 2.93 – 2.67 (m, 1H), 1.70 (ddt, $J = 13.3, 9.5, 6.2$ Hz, 1H), 1.56 (tdd, $J = 13.5, 8.7, 5.6$ Hz, 1H), 1.51 – 1.35 (m, 2H), 1.35 – 1.07 (m, 20H), 0.87 (t, $J = 6.6$ Hz, 3H). ^{13}C NMR (126 MHz, CDCl_3) δ 170.78, 133.05, 128.63, 128.14, 81.13, 32.02, 31.39, 29.90, 29.40, 28.04, 25.45, 25.28, 22.82, 14.25. LRMS (EI) m/z : $[\text{M}-\text{H}]^+$ Calcd. for $\text{C}_{21}\text{H}_{33}\text{BNO}_3$ 358.3; Found 358.3. HRMS (ESI/TOF) m/z : $[\text{M}+\text{H}]^+$ Calcd. for $\text{C}_{21}\text{H}_{35}\text{BNO}_3$ 360.2708; Found 360.2718. Enantiomeric ratio was measured by chiral phase SFC (Chiracel IG-3 (#87524), gradient: 5-10% *i*-PrOH/ CO_2 0-7 mins, hold: 7-10 min 10% *i*-PrOH/ CO_2 , 3.0 mL/min, 250 nm) R_t (major) = 6.4 min, R_t (minor) = 8.5 min; er = 95:5.



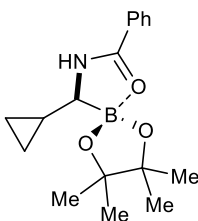
(S)-N-(5-(benzyloxy)-1-(4,4,5,5-tetramethyl-1,3,2-dioxaborolan-2-yl)pentyl)benzamide (II-40)

Prepared according to the general procedure using 95 mg **II-72** (0.211 mmol) to afford (S)-N-(5-(benzyloxy)-1-(4,4,5,5-tetramethyl-1,3,2-dioxaborolan-2-yl)pentyl)benzamide (31 mg, 37% yield). Analytical data: ^1H NMR (500 MHz, CDCl_3) δ 7.75 (d, $J = 7.2$ Hz, 2H), 7.62 – 7.49 (m, 2H), 7.42 – 7.36 (m, 2H), 7.32 (d, $J = 4.4$ Hz, 4H), 7.31 – 7.23 (m, 1H), 4.50 (s, 2H), 3.52 (t, $J = 6.2$ Hz, 2H), 2.93 – 2.82 (m, 1H), 1.77 – 1.49 (m, 5H), 1.26 (d, $J = 2.7$ Hz, 13H). ^{13}C NMR (126 MHz, CDCl_3) δ 170.88, 138.56, 133.15, 128.79, 128.54, 127.96, 127.84, 127.75, 81.09, 73.13, 70.56, 30.89, 29.56, 25.45, 25.23, 24.67. LRMS (EI) m/z : $[\text{M}-\text{H}]^+$ Calcd. for $\text{C}_{25}\text{H}_{33}\text{BNO}_4$, 422.3; Found 422.2. HRMS (ESI/TOF) m/z : $[\text{M}+\text{Na}]^+$ Calcd. for $\text{C}_{25}\text{H}_{33}\text{BNO}_4\text{Na}$ 446.2478; Found 446.2481. Enantiomeric ratio was measured by chiral phase SFC (Chiracel ID-3 (#84524), 10% *i*-PrOH/ CO_2 , 3.0 mL/min, 250 nm) R_t (major) = 5.3 min, R_t (minor) = 6.2 min; er = 88:12.



(S)-N-(2-methyl-1-(4,4,5,5-tetramethyl-1,3,2-dioxaborolan-2-yl)propyl)benzamide (II-33)

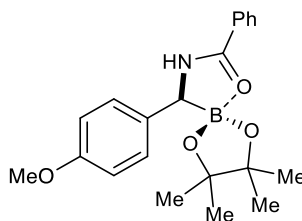
Prepared according to the general procedure using 200 mg **II-69** (0.603 mmol) to afford (*S*)-*N*-(2-methyl-1-(4,4,5,5-tetramethyl-1,3,2-dioxaborolan-2-yl)propyl)benzamide (100 mg, 55% yield). Analytical data: ^1H NMR (500 MHz, CDCl_3) δ 7.80 (d, $J = 8.6$ Hz, 1H), 7.54 (td, $J = 7.3, 1.3$ Hz, 1H), 7.48 – 7.42 (m, 2H), 6.65 (d, $J = 14.1$ Hz, 1H), 3.02 (dd, $J = 6.2, 4.1$ Hz, 1H), 2.13 – 1.96 (m, 1H), 1.36 – 1.13 (m, 18H). ^{13}C NMR (126 MHz, CDCl_3) δ 169.82, 132.52, 131.01, 128.77, 127.62, 82.21, 30.02, 25.44, 25.38, 20.91, 20.07. LRMS (EI) m/z : $[\text{M}-\text{H}]^+$ Calcd. for $\text{C}_{17}\text{H}_{25}\text{BNO}_3$ 302.2; Found 302.2. HRMS (ESI/TOF) m/z : $[\text{M}+\text{H}]^+$ Calcd. for $\text{C}_{17}\text{H}_{27}\text{BNO}_3$ 304.2082; Found 304.2093. Enantiomeric ratio was measured by chiral phase SFC (Chiracel ID-3 (#84524), 5% *i*-MeOH/ CO_2 , 3.0 mL/min, 250 nm) Rt (major) = 1.9 min, Rt (minor) = 2.9 min; er = 97:3.



(S)-N-(cyclopropyl(4,4,5,5-tetramethyl-1,3,2-dioxaborolan-2-yl)methyl)benzamide (II-39)

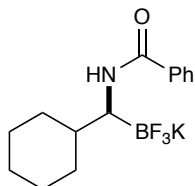
Prepared according to the general procedure using 100 mg **II-76** (0.304 mmol) to afford (*S*)-*N*-(2-methyl-1-(4,4,5,5-tetramethyl-1,3,2-dioxaborolan-2-yl)propyl)benzamide (44 mg, 48% yield). Analytical data: ^1H NMR (500 MHz, CDCl_3) δ 7.93 – 7.78 (m, 2H), 7.58 (td, $J = 7.3, 1.3$ Hz,

1H), 7.47 (t, $J = 7.8$ Hz, 2H), 7.04 (d, $J = 9.9$ Hz, 1H), 2.08 (d, $J = 10.4$ Hz, 1H), 1.29 (m, 12H), 1.15 – 1.03 (m, 1H), 0.61 (tdd, $J = 8.6, 5.5, 4.4$ Hz, 1H), 0.51 (dddd, $J = 9.2, 7.4, 5.5, 3.9$ Hz, 1H), 0.32 (dq, $J = 9.7, 4.8$ Hz, 1H), 0.19 (dtd, $J = 10.3, 5.2, 4.0$ Hz, 1H). LRMS (EI) m/z : $[M-H]^+$ Calcd. for $C_{17}H_{23}BNO_3$ 300.2; Found 300.2. HRMS (ESI/TOF) m/z : $[M+Na]^+$ Calcd. for $C_{17}H_{24}BNO_3Na$ 324.1745; Found 324.1742. Enantiomeric ratio was measured by chiral phase SFC (Chiracel IG-3 (#87524), 15% *i*-PrOH/ CO_2 , 3.0 mL/min, 250 nm) R_t (major) = 2.0 min, R_t (minor) = 2.9 min; er = 96:4.



**(*S*)-*N*-((4-methoxyphenyl)(4,4,5,5-tetramethyl-1,3,2-dioxaborolan-2-yl)methyl)benzamide
(II-41)**

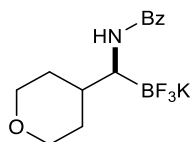
Note: Used MTBE instead of THF. Otherwise, prepared according to the general procedure using 100 mg **II-97** (0.253 mmol) to afford (*S*)-*N*-((4-methoxyphenyl)(4,4,5,5-tetramethyl-1,3,2-dioxaborolan-2-yl)methyl)benzamide (62 mg, 67% yield). 1H NMR (500 MHz, $CDCl_3$) δ 8.32 (br, 1H), 7.89 (d, $J = 7.2$ Hz, 2H), 7.63 – 7.51 (m, 1H), 7.50 – 7.35 (m, 2H), 7.21 – 7.05 (m, 2H), 6.82 (d, $J = 8.8$ Hz, 2H), 3.93 (s, 1H), 3.78 (s, 2H), 1.09 (s, 6H), 1.00 (s, 6H). ^{13}C NMR (126 MHz, $CDCl_3$) δ 171.71, 158.14, 133.73, 132.92, 128.89, 128.58, 128.41, 128.39, 113.69, 81.10, 77.38, 55.41, 24.99, 24.63. HRMS (ESI/TOF) m/z : $[M+H]^+$ Calcd. for $C_{21}H_{27}BNO_4$ 368.2031; Found 368.2044. Enantiomeric ratio was measured by chiral phase SFC (Chiracel IB-3 (#81524), 15% *i*-MeOH/ CO_2 , 3.0 mL/min, 250 nm) R_t (major) = 1.2 min, R_t (minor) = 1.4 min; er = 92:8.



Potassium (*S*)-(benzamido(cyclohexyl)methyl)trifluoroborate (II-54)

Prepared according to the general trifluoroborate synthesis using 200 mg **II-36** (0.539 mmol) to afford Potassium (*S*)-(benzamido(cyclohexyl)methyl)trifluoroborate (152 mg, 87% yield).

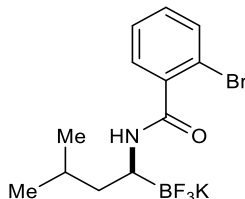
Analytical data for N: ^1H NMR (500 MHz, DMSO- d_6) δ 7.69 (d, $J = 6.6$ Hz, 2H), 7.57 – 7.24 (m, 3H), 6.44 (d, $J = 9.2$ Hz, 1H), 2.82 (dt, $J = 9.3, 4.7$ Hz, 1H), 1.78 – 1.49 (m, 6H), 1.42 (tt, $J = 11.8, 4.3$ Hz, 1H), 1.18 – 0.96 (m, 5H). ^{13}C NMR (126 MHz, DMSO- d_6) δ 198.16, 165.54, 136.55, 130.15, 128.22, 126.49, 40.66, 31.42, 29.57, 26.64, 26.55. HRMS (ESI/TOF) m/z : [M-KHF] $^-$ Calcd. for $\text{C}_{14}\text{H}_{17}\text{BF}_2\text{NO}^-$ 264.1377; Found 264.1384.



Potassium (*S*)-(benzamido(tetrahydro-2*H*-pyran-4-yl)methyl)trifluoroborate (II-56)

Prepared according to the general trifluoroborate synthesis using 115 mg **II-70** (0.308 mmol) to afford Potassium (*S*)-(benzamido(tetrahydro-2*H*-pyran-4-yl)methyl)trifluoroborate (74 mg, 74% yield). Analytical data: ^1H NMR (500 MHz, DMSO- d_6) δ 7.83 – 7.68 (m, 2H), 7.54 – 7.39 (m, 3H), 6.52 (d, $J = 9.3$ Hz, 1H), 3.77 (td, $J = 10.6, 3.5$ Hz, 2H), 3.17 (ddt, $J = 12.5, 11.1, 2.1$ Hz, 2H), 2.86 (dt, $J = 9.6, 4.8$ Hz, 1H), 1.69 – 1.60 (m, 1H), 1.53 (t, $J = 14.2$ Hz, 2H), 1.40 – 1.23 (m, 2H). ^{13}C NMR (126 MHz, DMSO- d_6) δ 165.78, 136.37, 130.21, 128.19, 126.58, 67.87,

67.71, 37.90, 31.54, 29.99. The resonance pertaining to the carbon bound to boron was not observed due to quadrupolar relaxation of the ^{11}B nucleus. HRMS (ESI/TOF) m/z : $[\text{M-KHF}]^-$
Calcd. for $\text{C}_{13}\text{H}_{15}\text{BF}_2\text{NO}_2^-$ 266.1169; Found 266.1171.

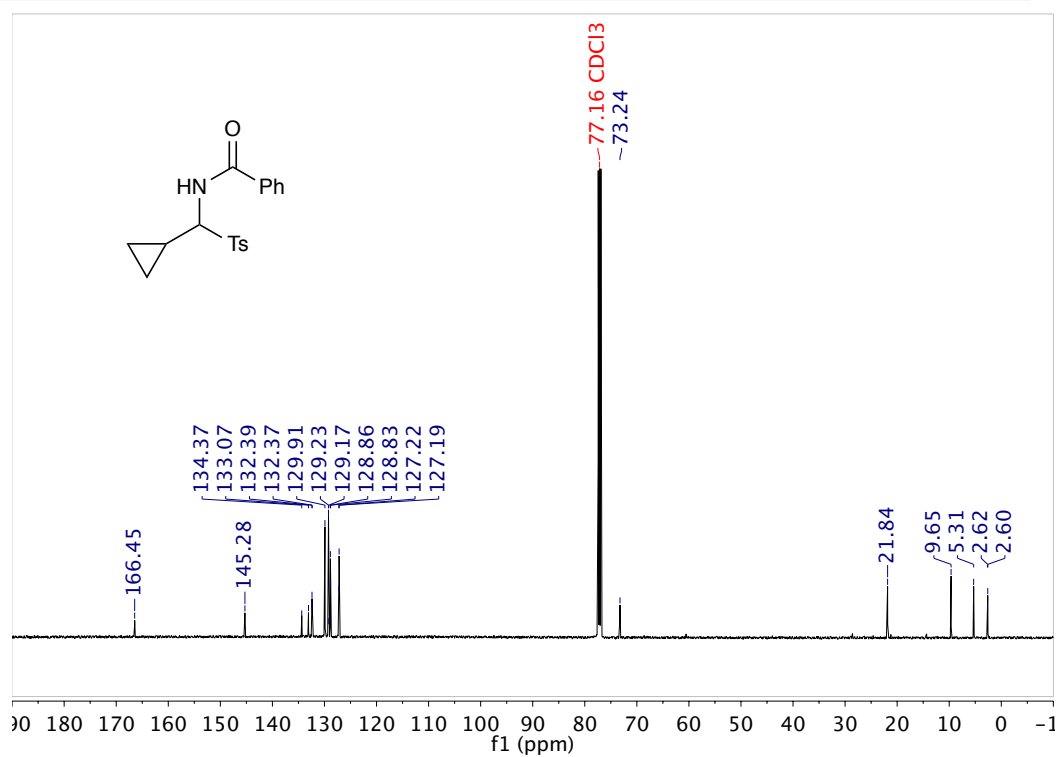
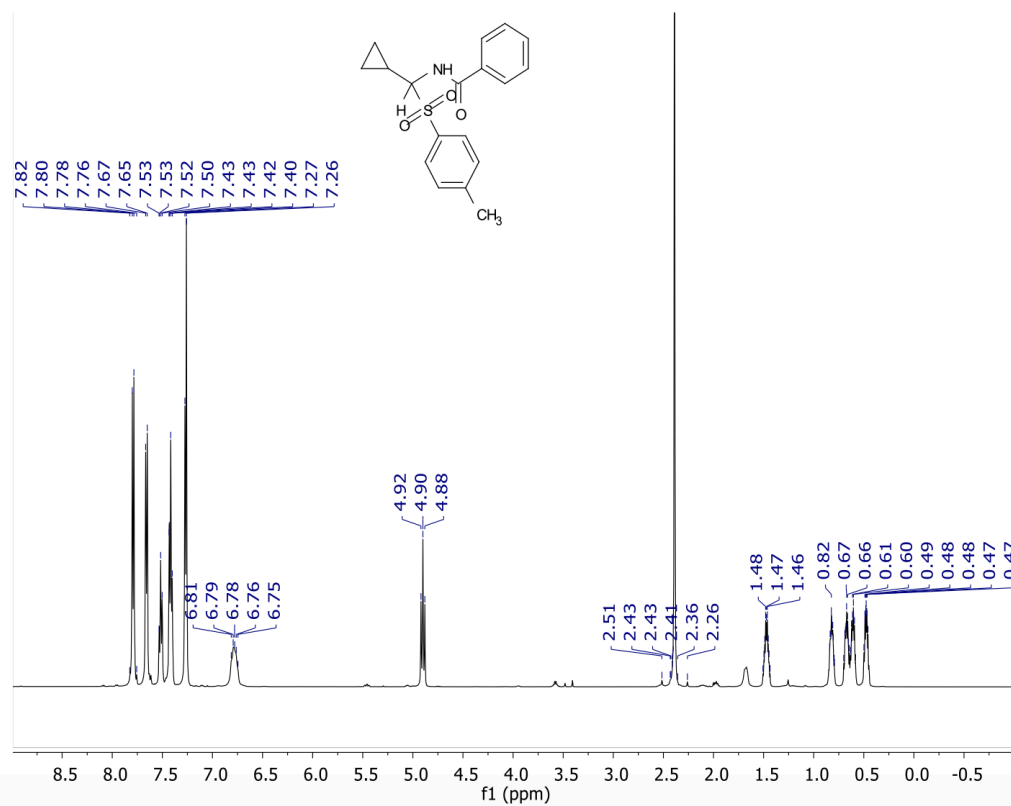


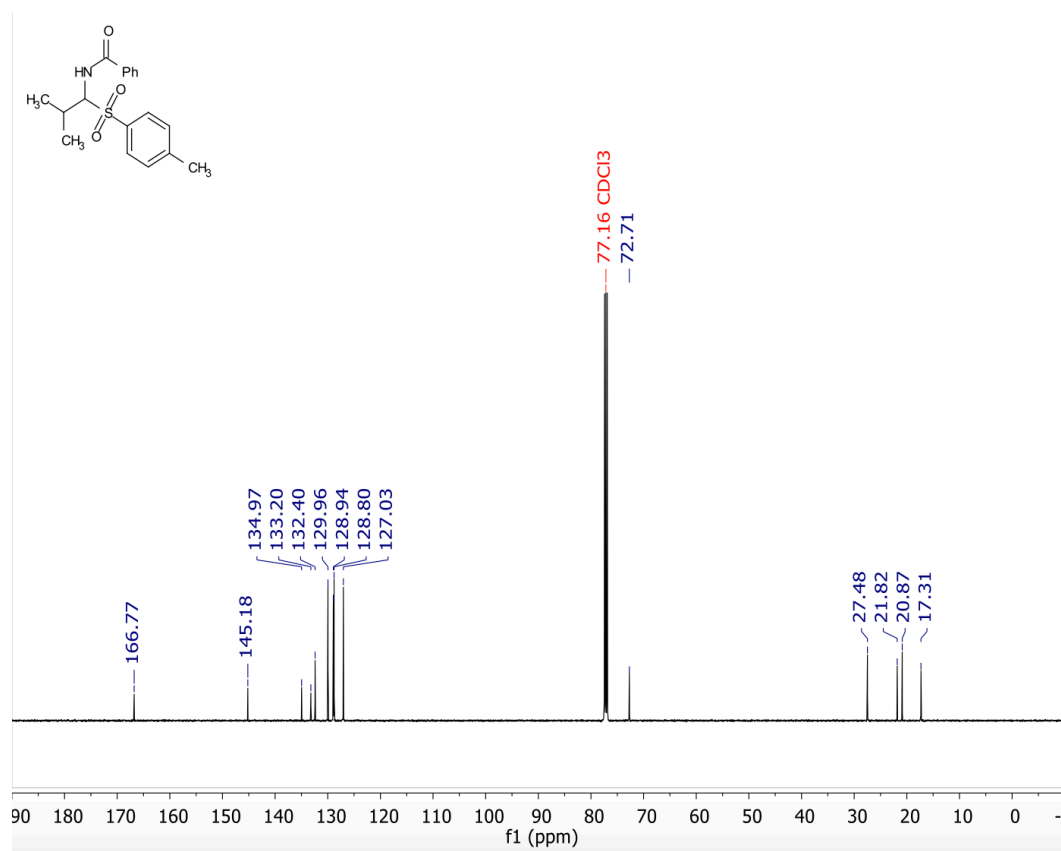
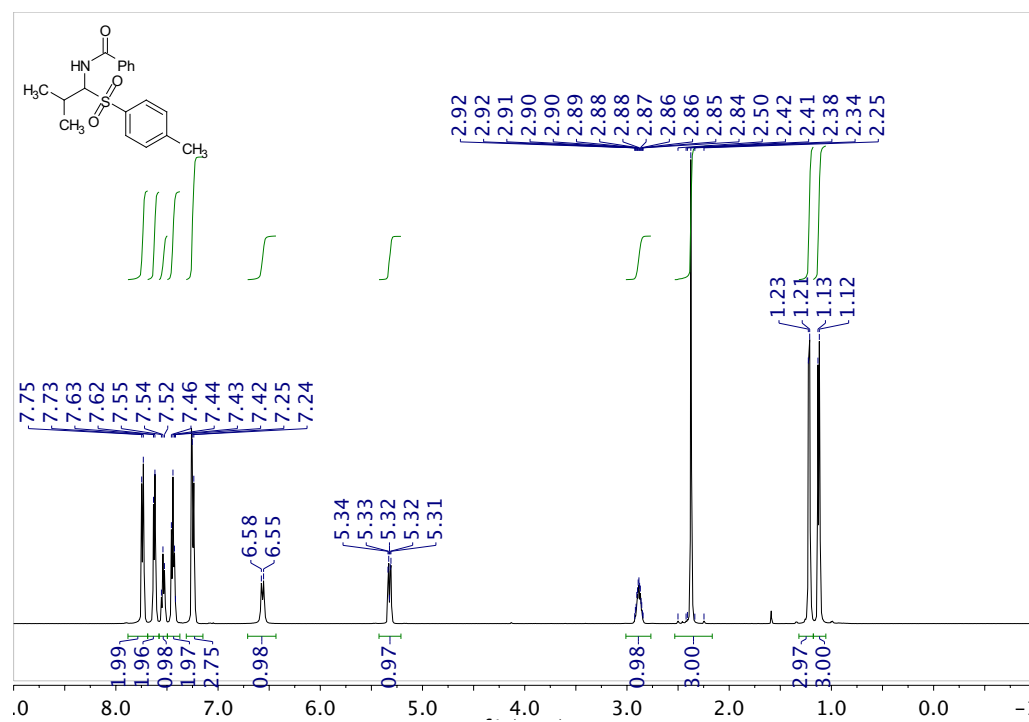
Potassium (*S*)-(1-(2-bromobenzamido)-3-methylbutyl)trifluoroborate

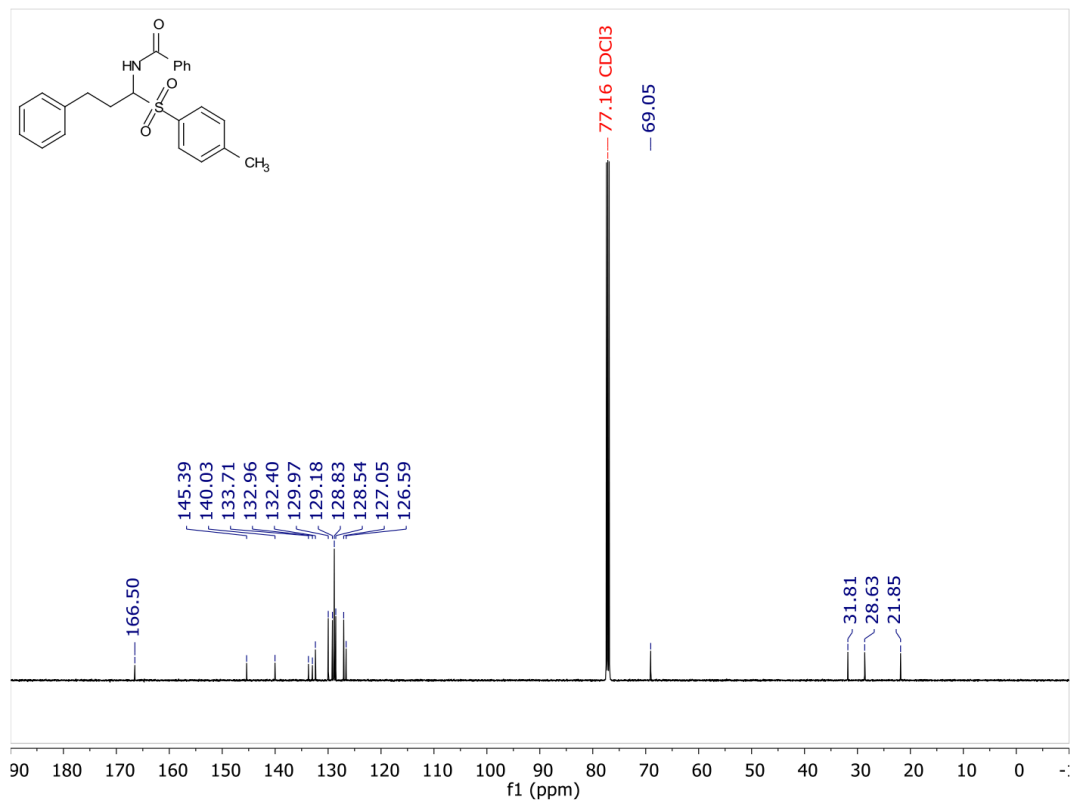
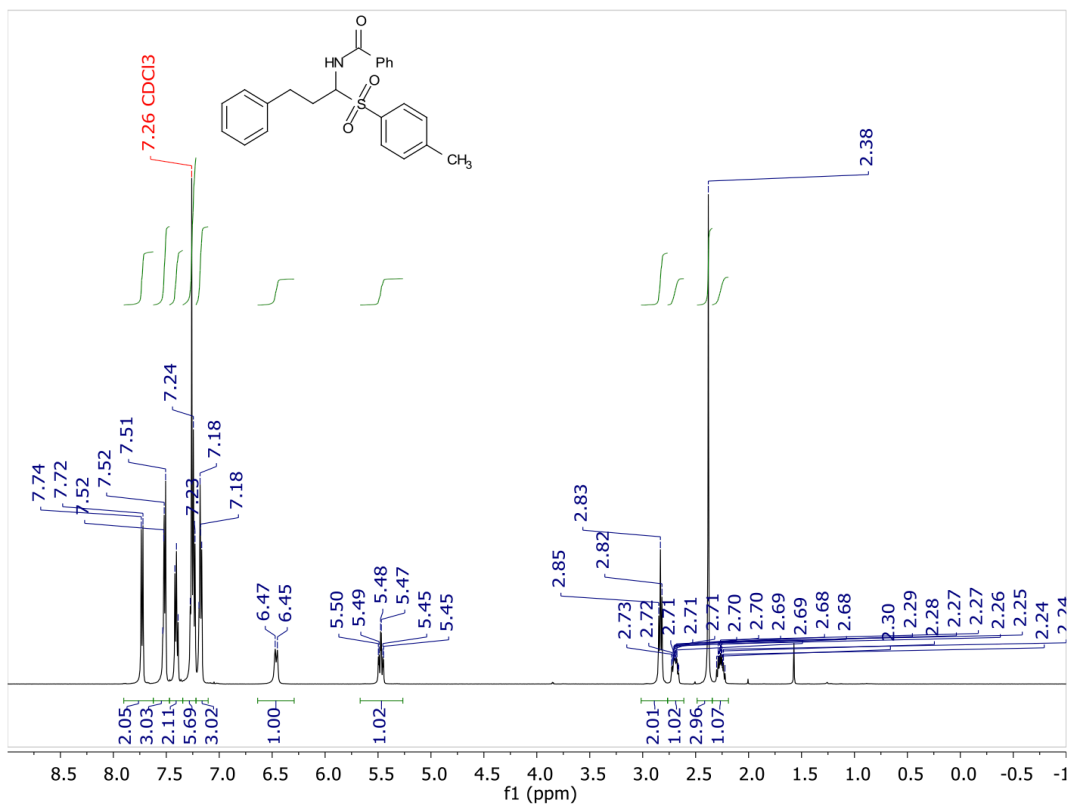
Prepared according to the general trifluoroborate synthesis using 100 mg **II-68** (0.236 mmol) to afford Potassium (*S*)-(1-(2-bromobenzamido)-3-methylbutyl)trifluoroborate (58 mg, 83% yield).

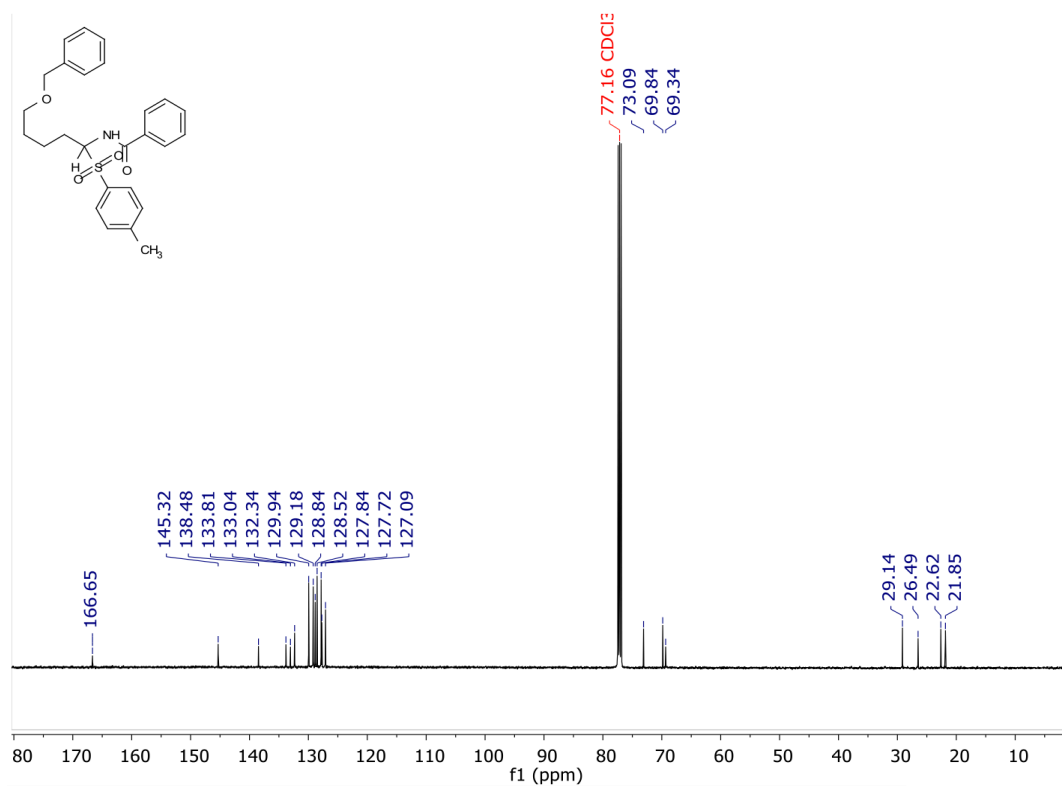
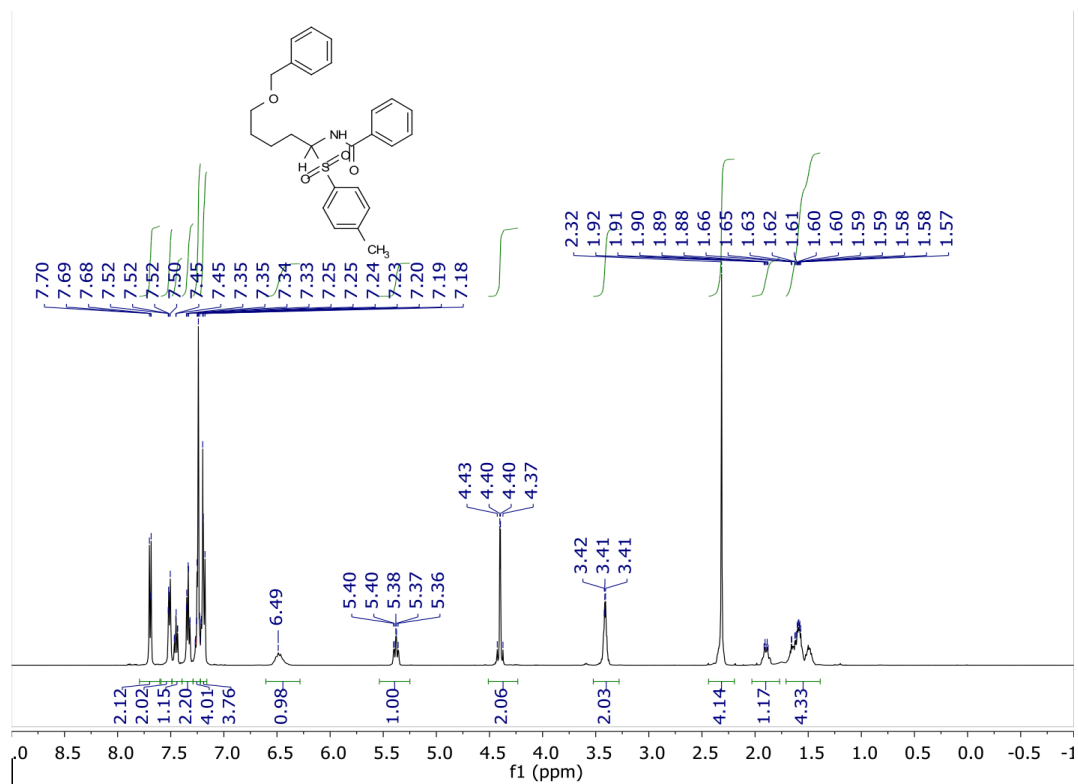
Analytical data: ^1H NMR (500 MHz, $\text{DMSO-}d_6$) δ 7.12 (d, $J = 7.9$ Hz, 1H), 6.92 (t, $J = 7.6$ Hz, 1H), 6.83 (dd, $J = 14.3, 7.3$ Hz, 2H), 5.89 (d, $J = 9.4$ Hz, 1H), 2.54 (tt, $J = 9.9, 4.6$ Hz, 1H), 1.27 (p, $J = 6.8$ Hz, 1H), 0.80 (ddd, $J = 14.8, 10.4, 4.7$ Hz, 1H), 0.69 (ddd, $J = 13.6, 9.2, 4.4$ Hz, 1H), 0.42 (d, $J = 6.5$ Hz, 3H), 0.38 (d, $J = 6.7$ Hz, 3H). ^{13}C NMR (126 MHz, $\text{DMSO-}d_6$) δ 165.97, 140.52, 132.63, 130.10, 128.98, 127.36, 118.76, 41.80, 24.85, 24.03, 22.47.

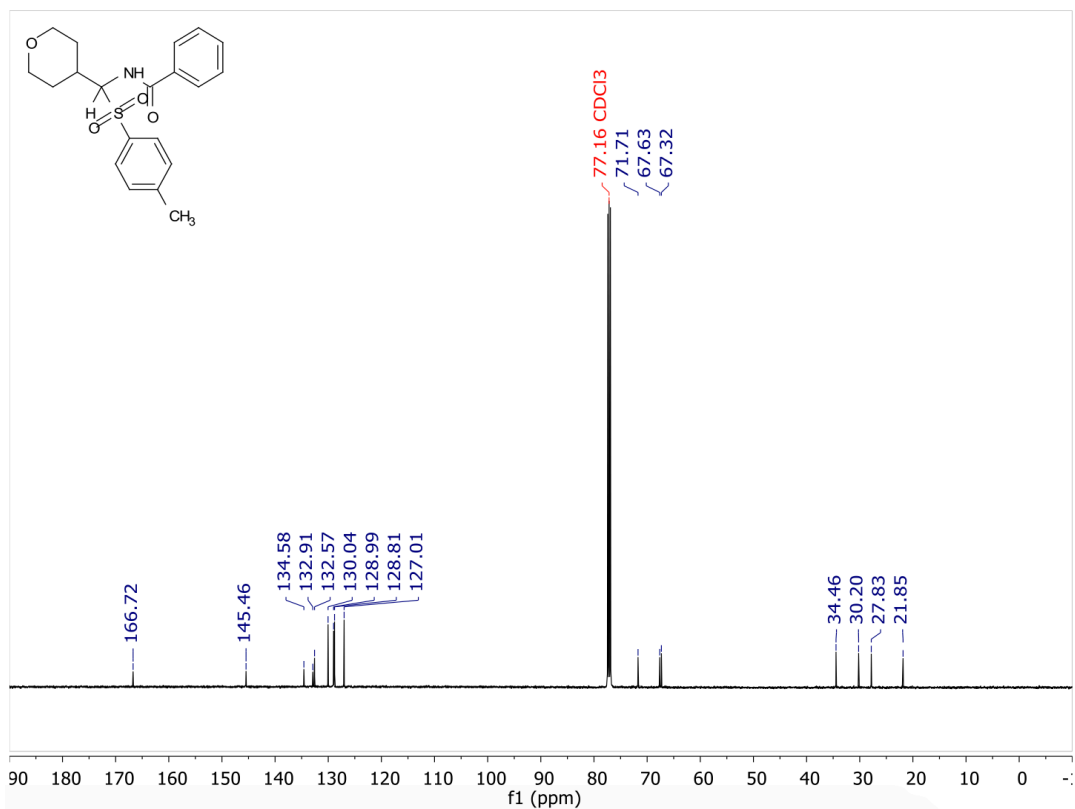
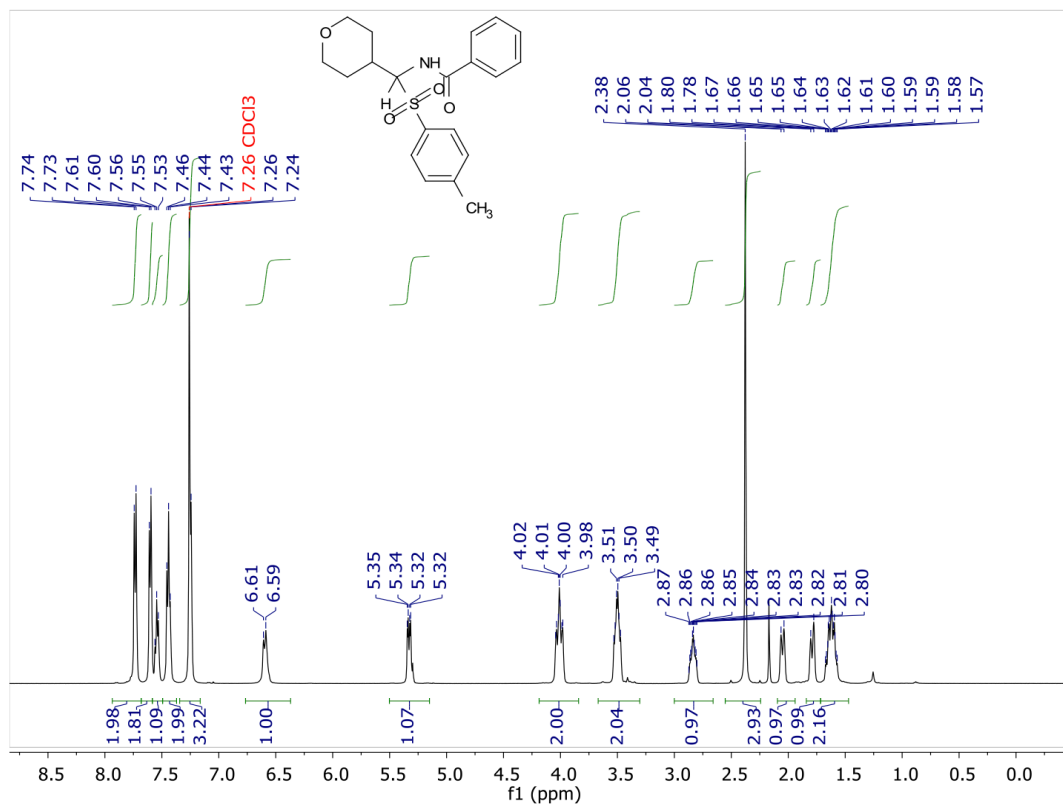
2.7.4 Selected NMR Spectra

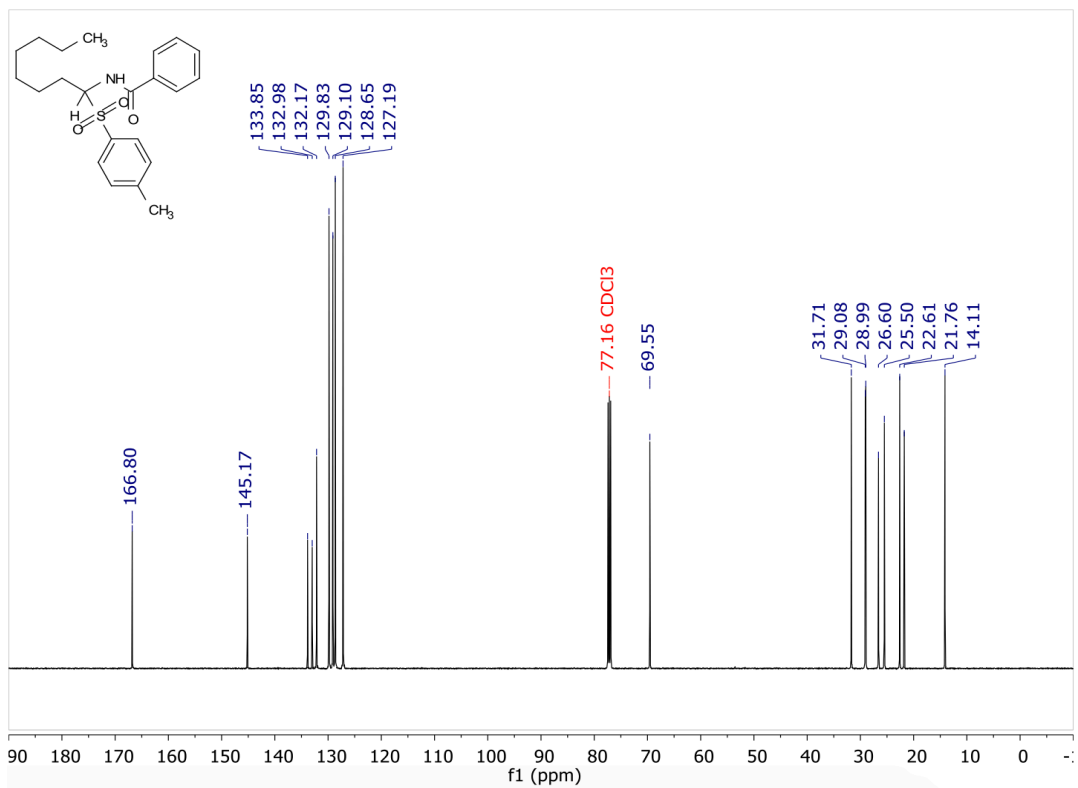
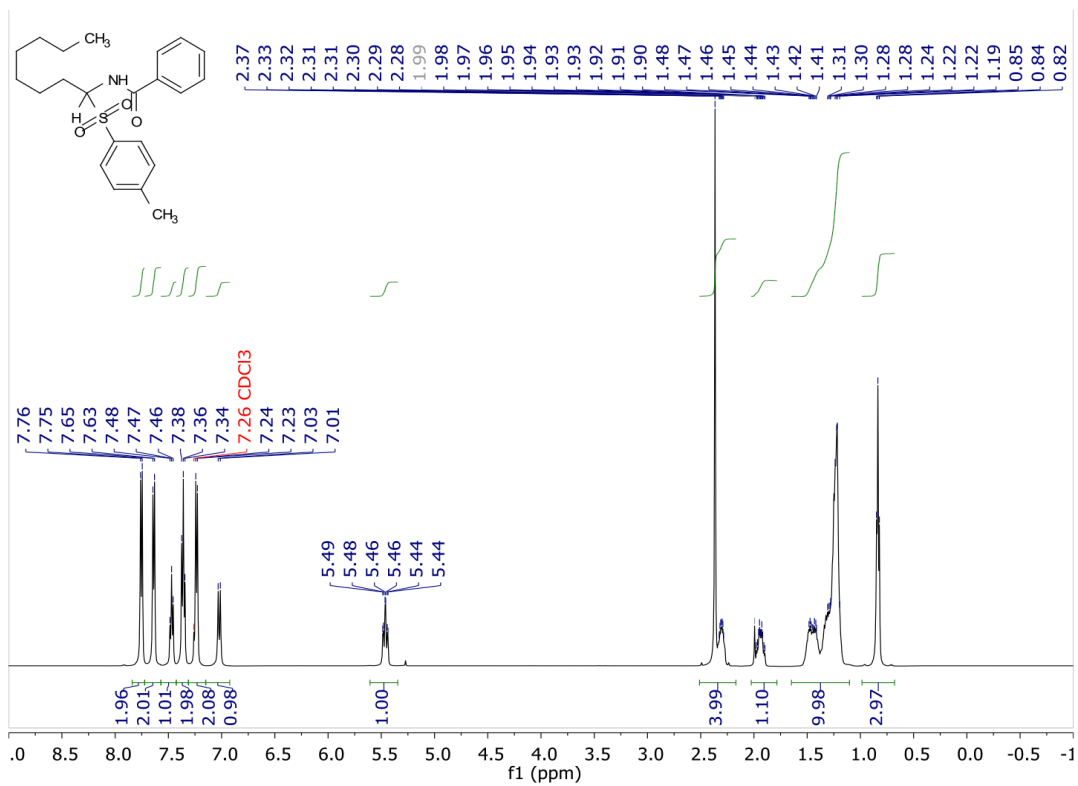


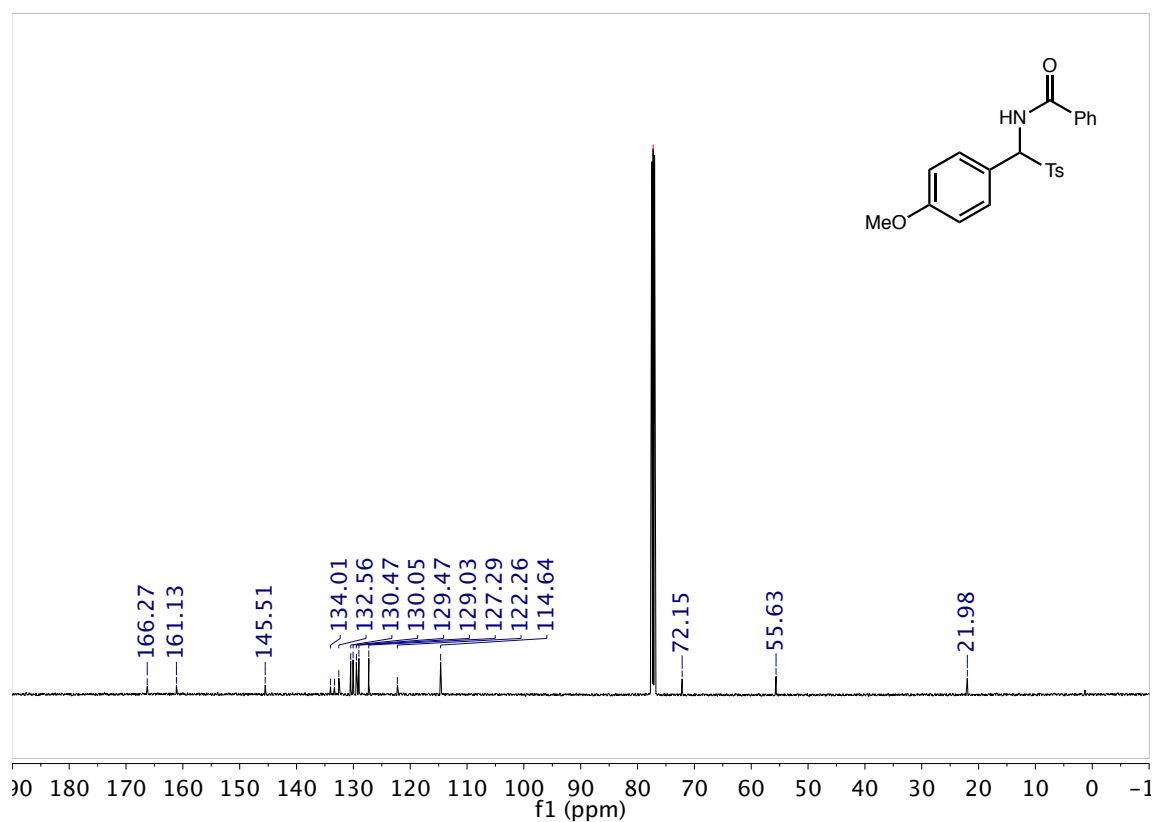
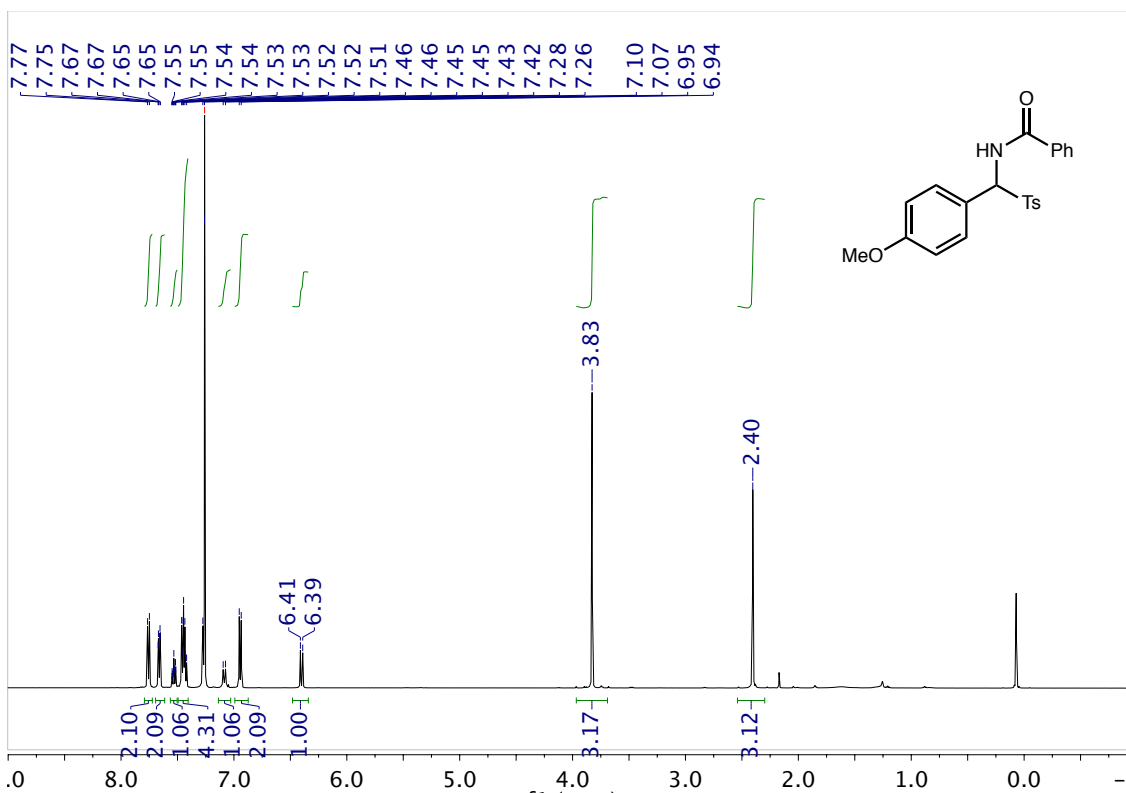


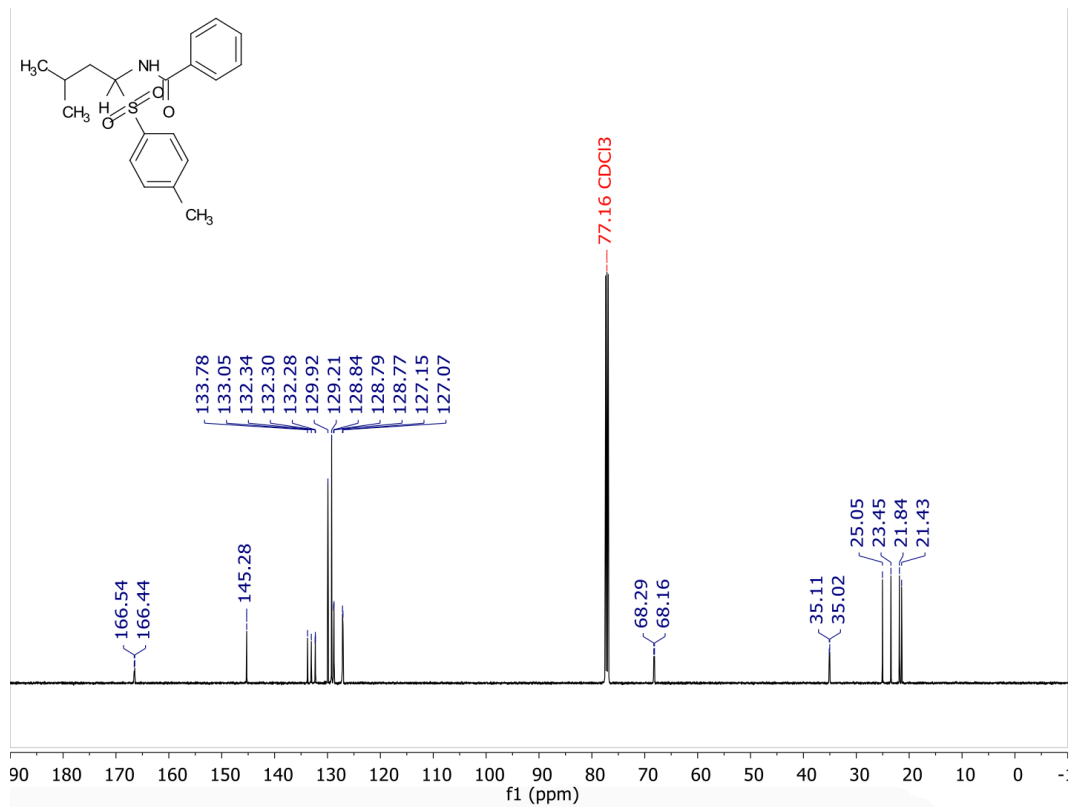
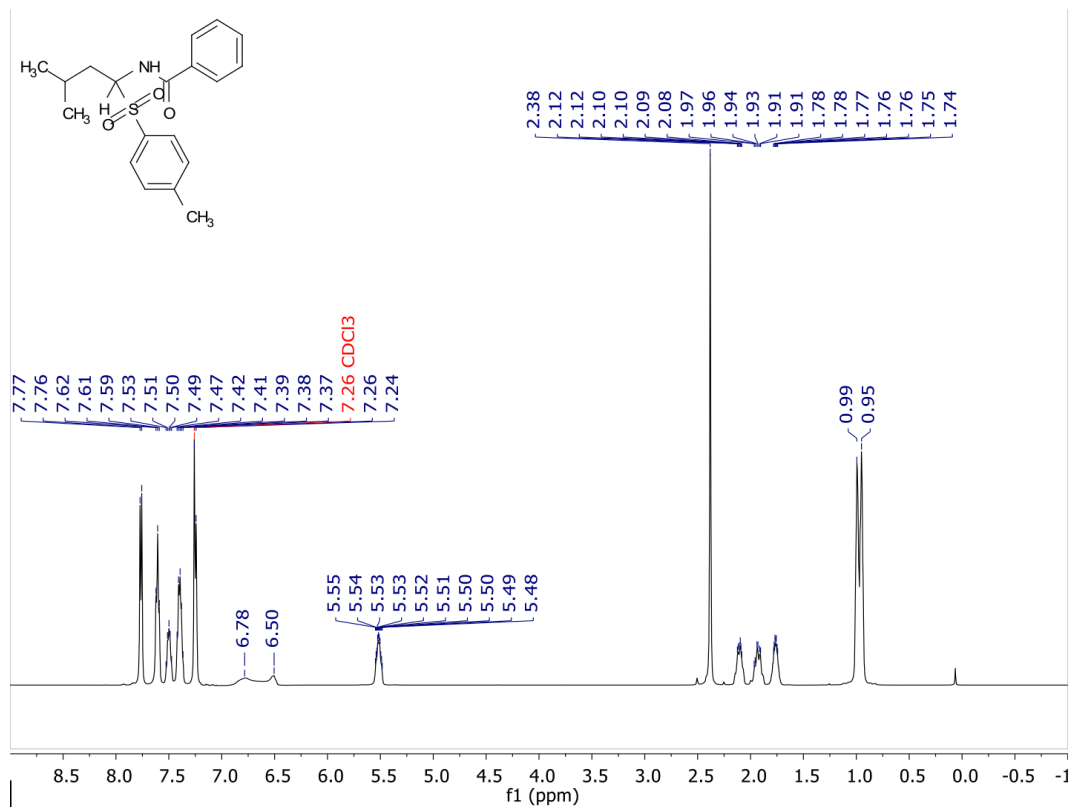


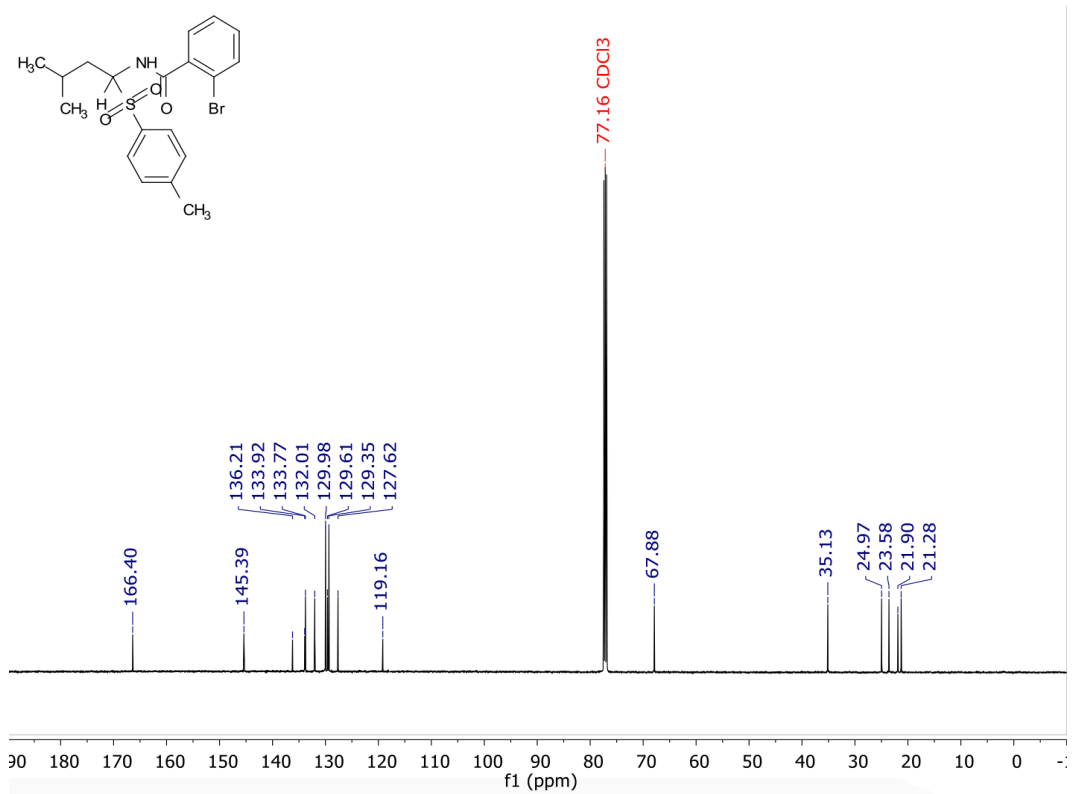
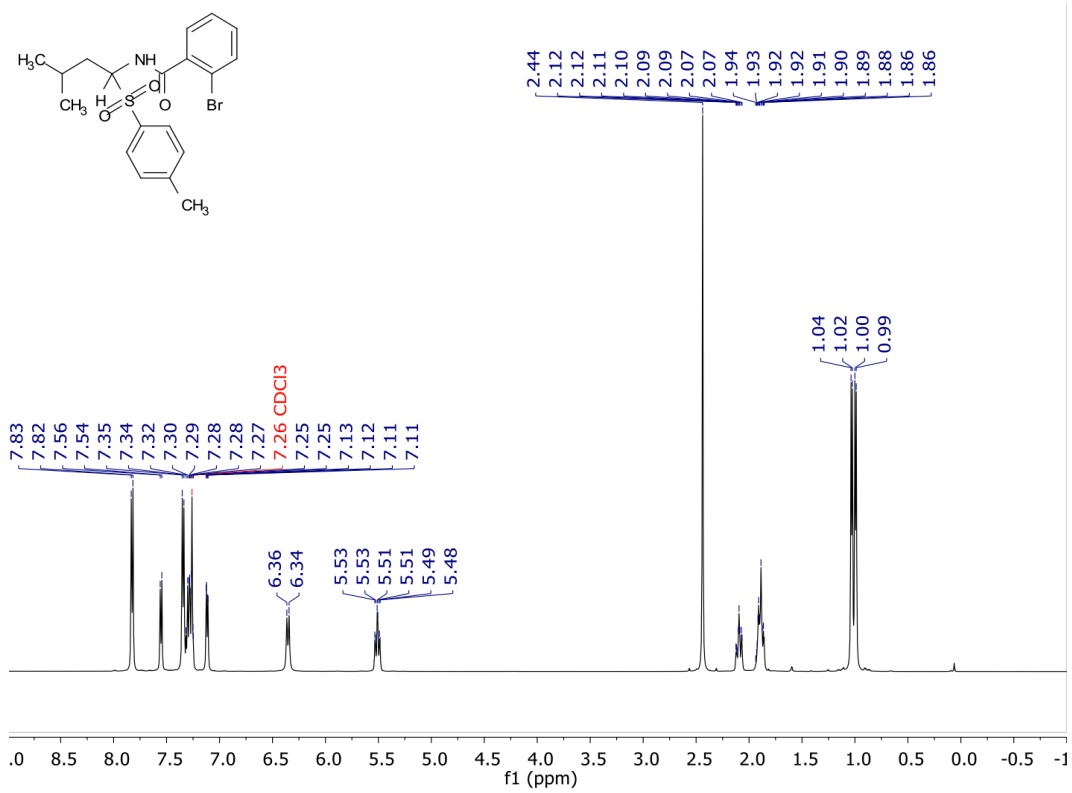


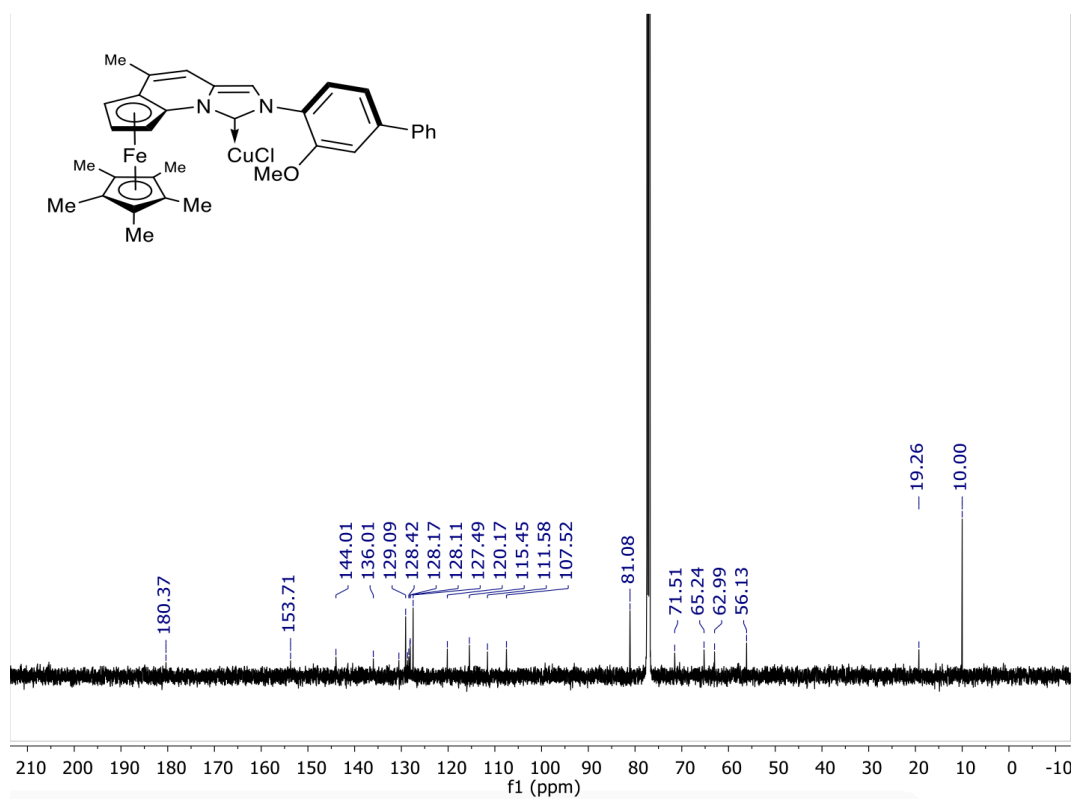
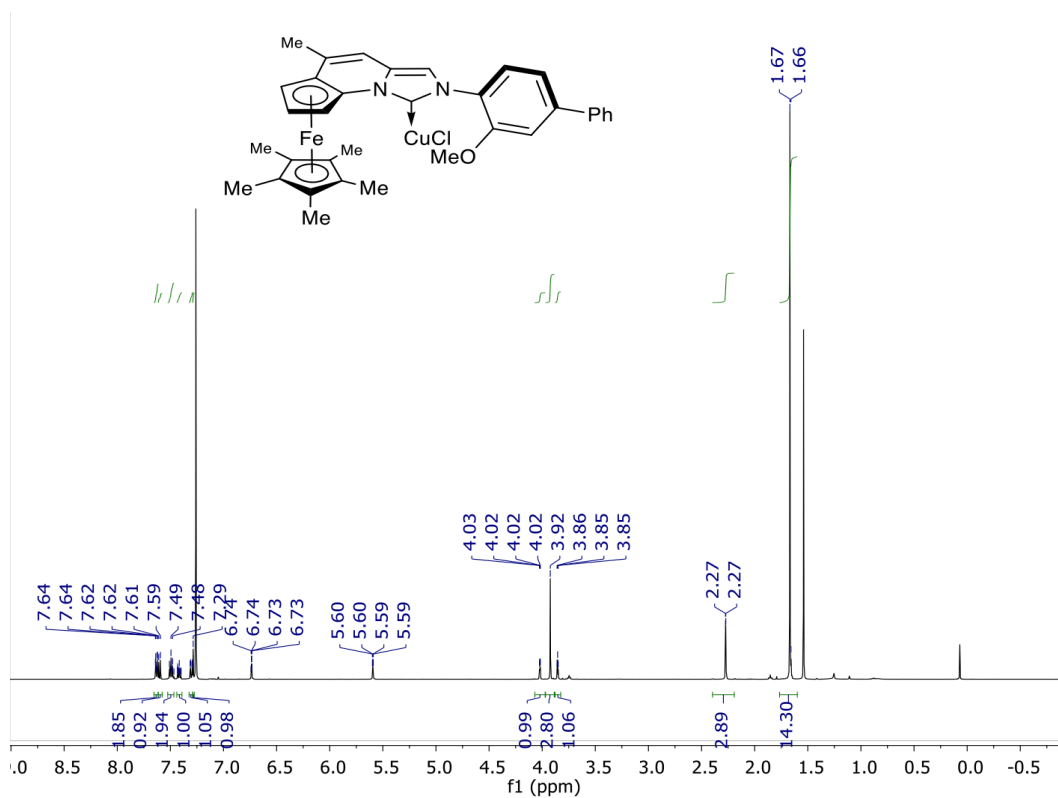


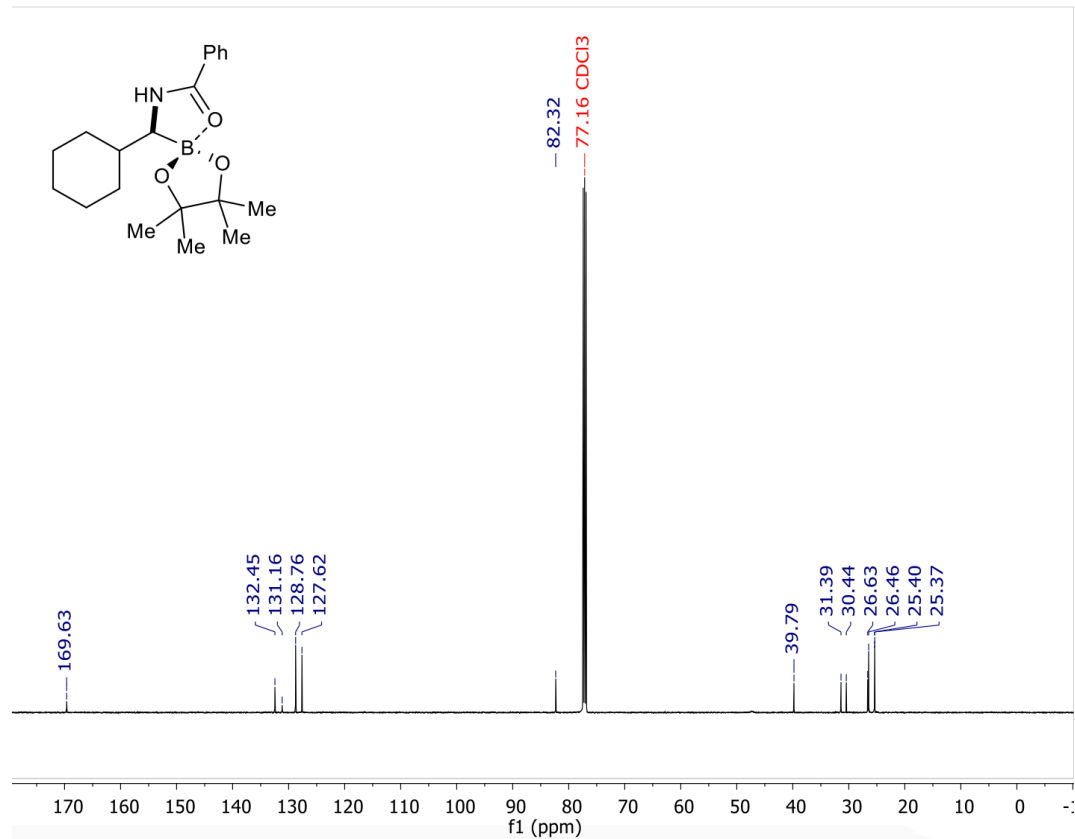
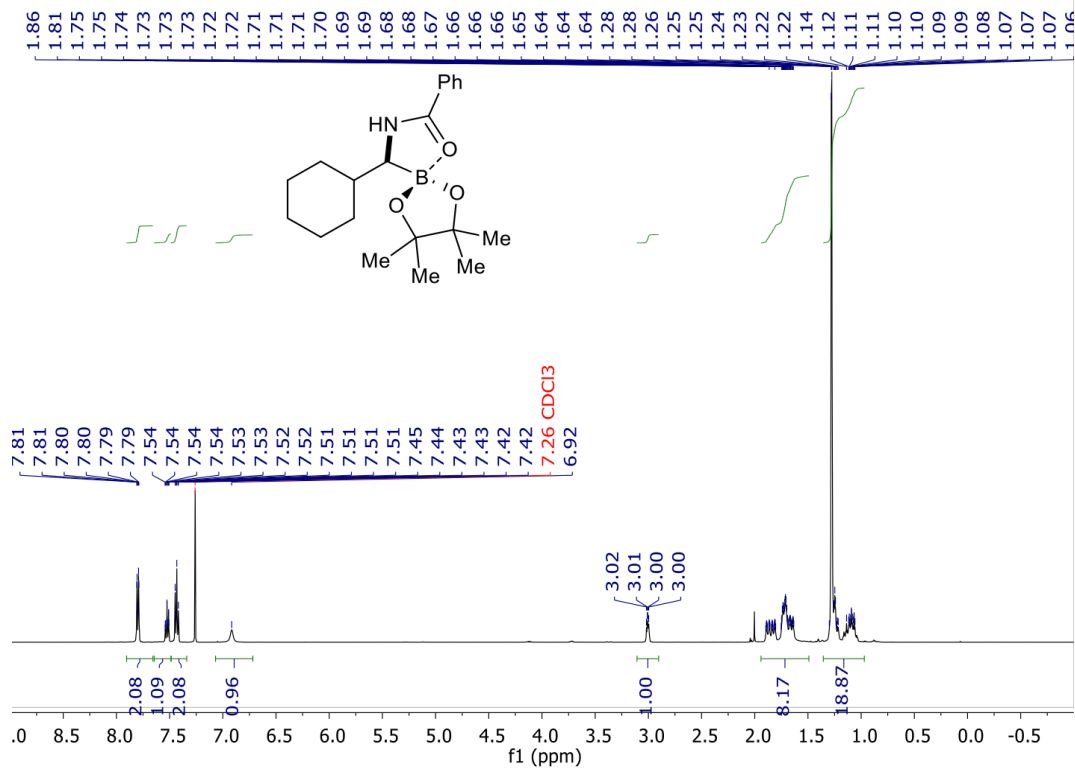


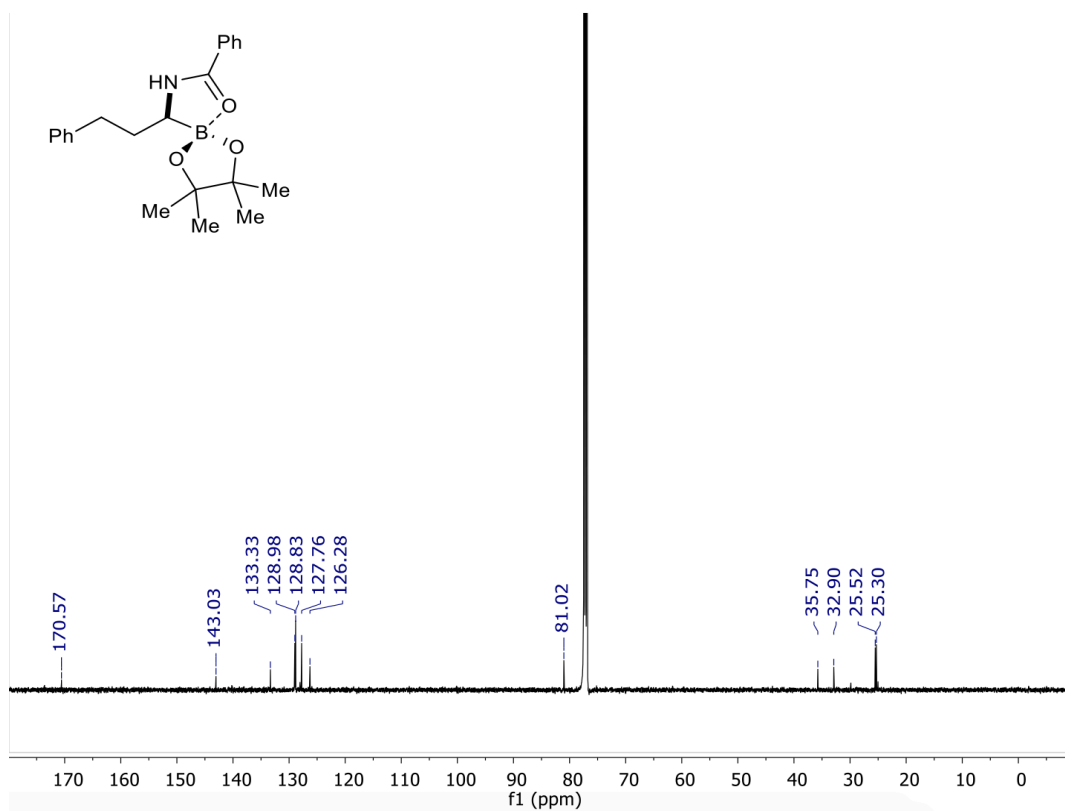
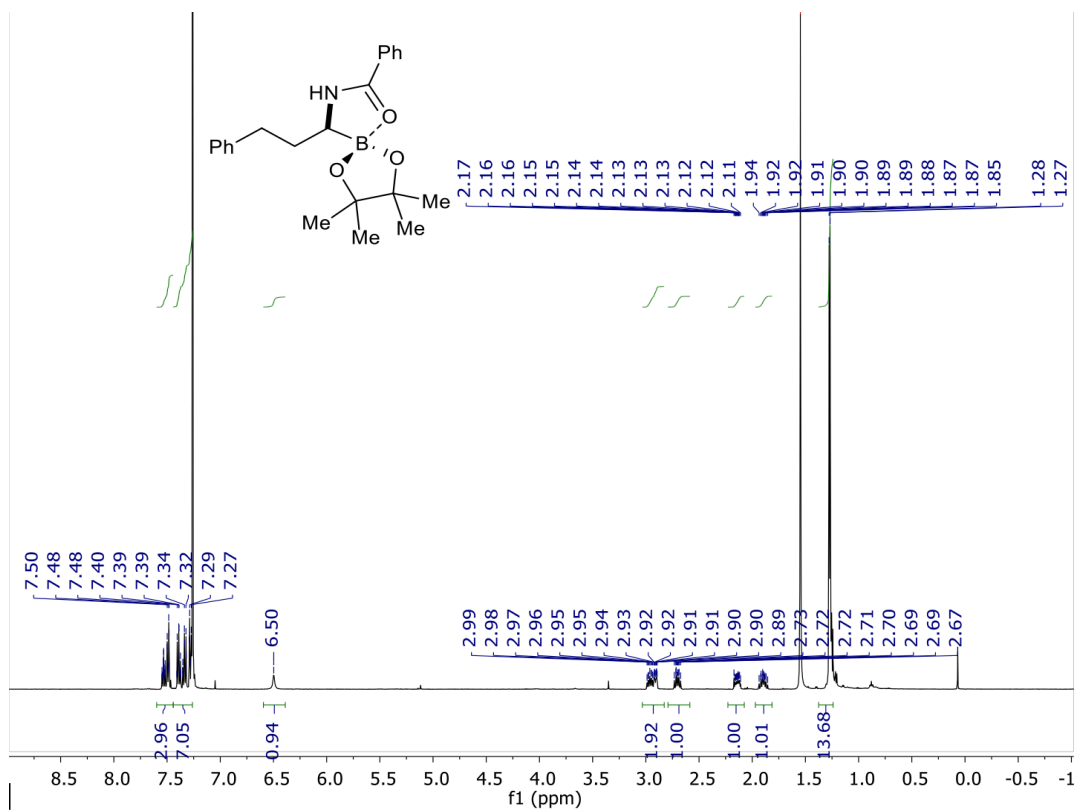


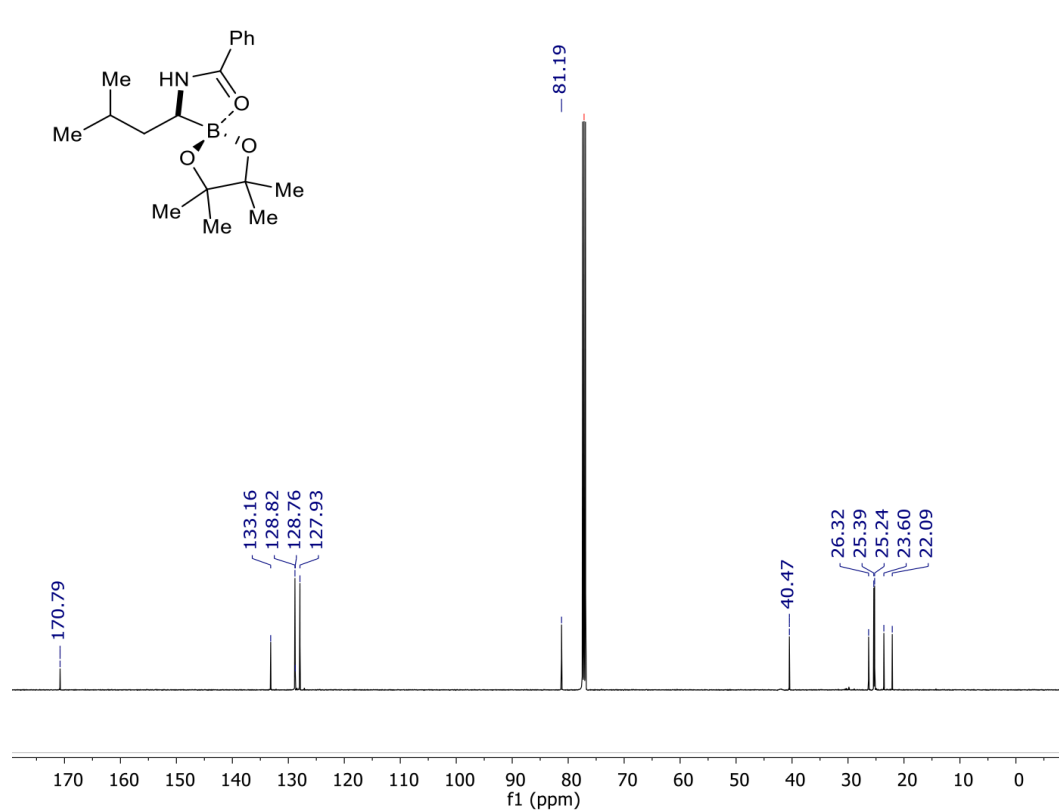
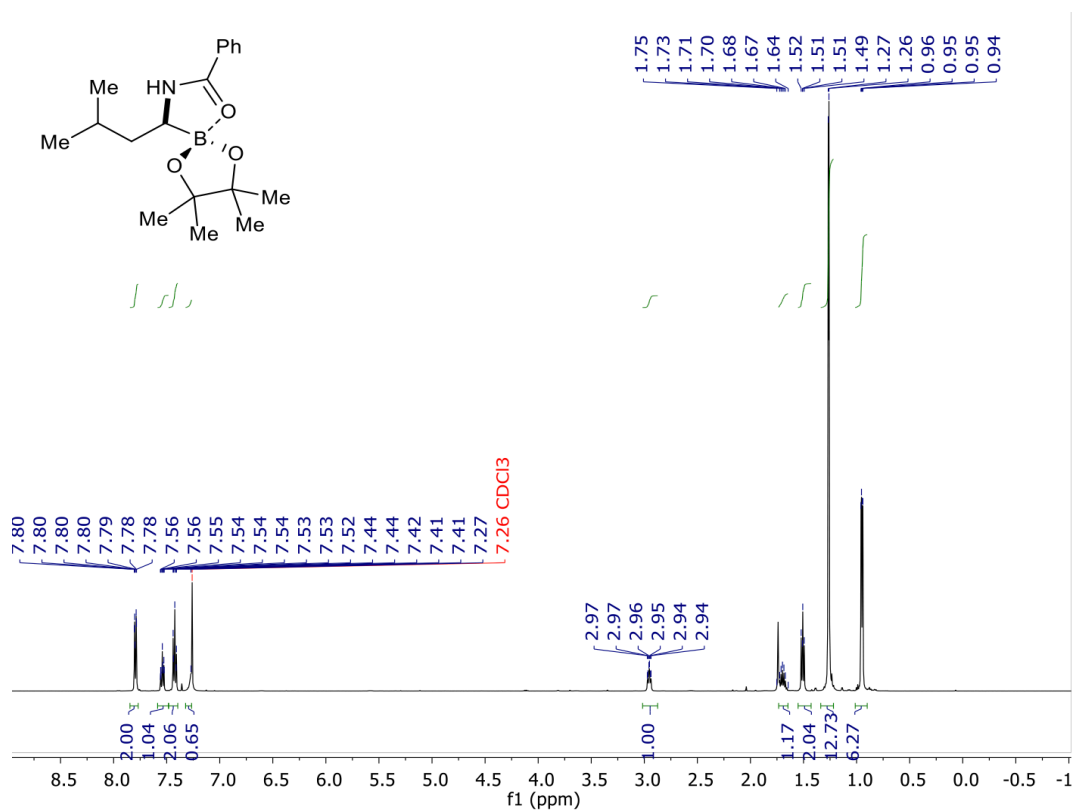


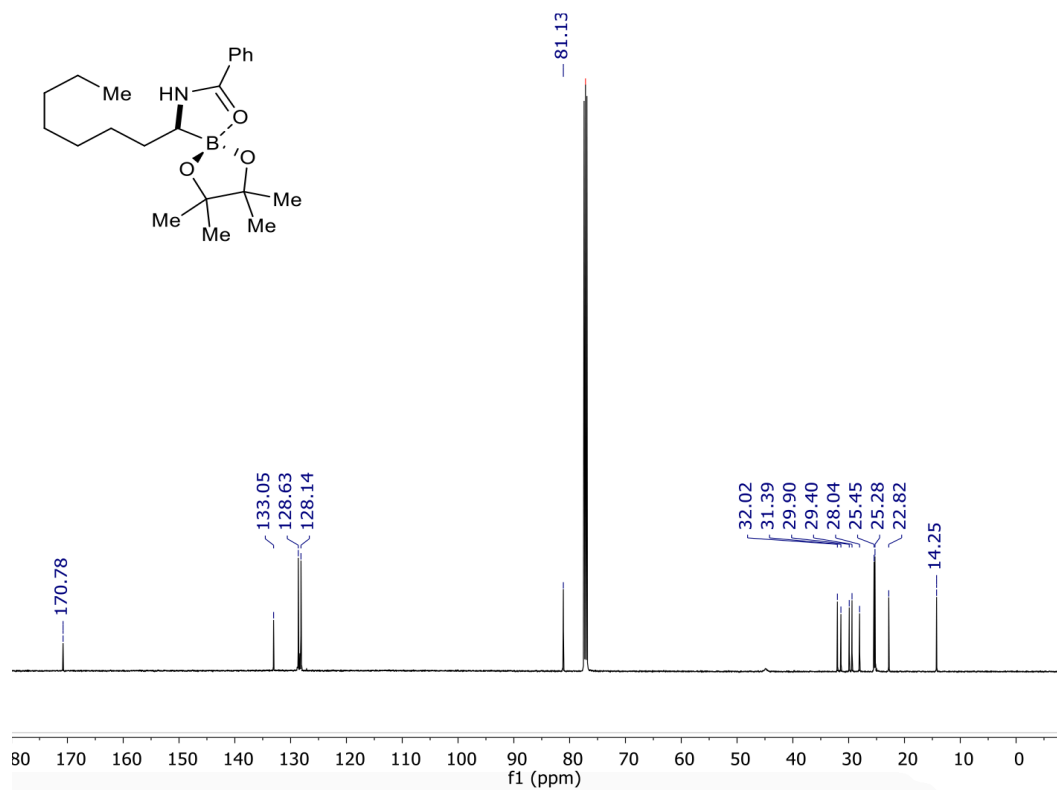
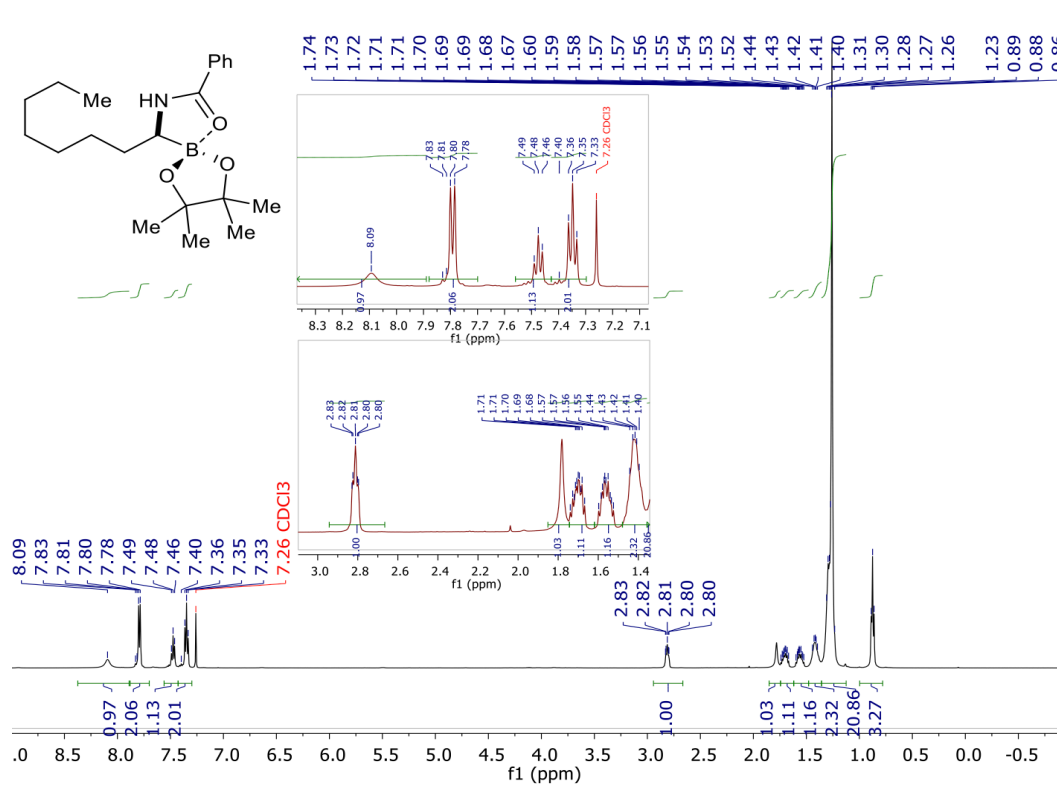


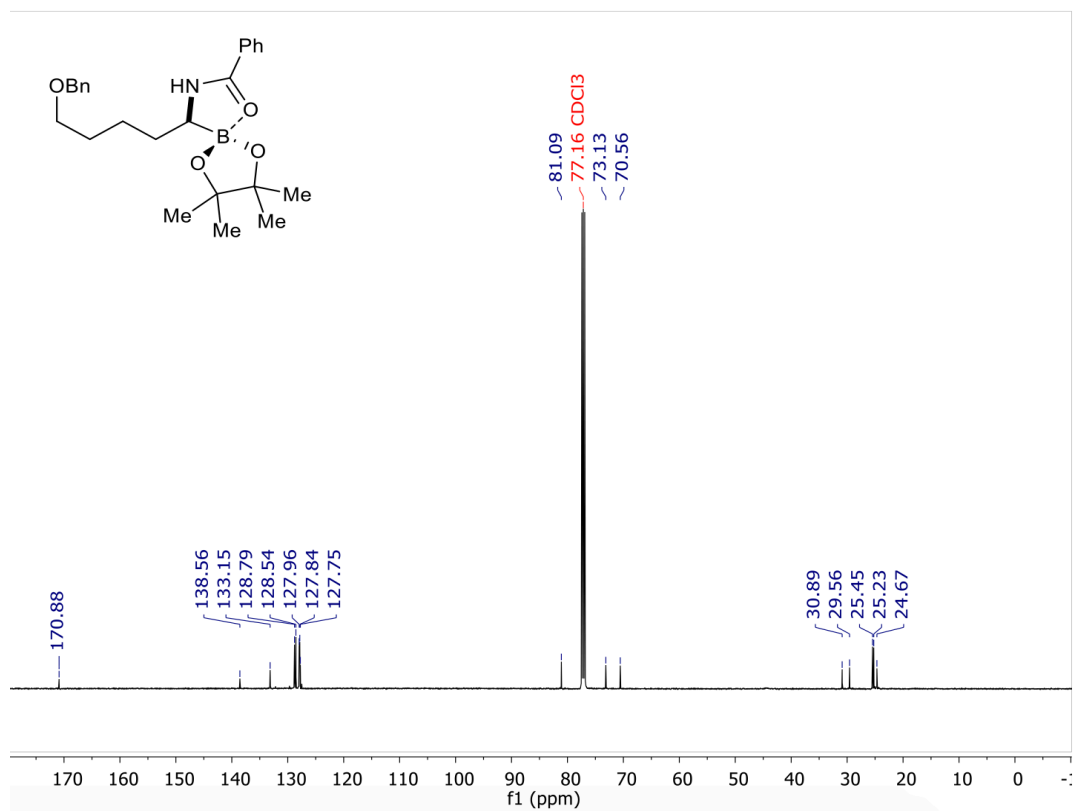
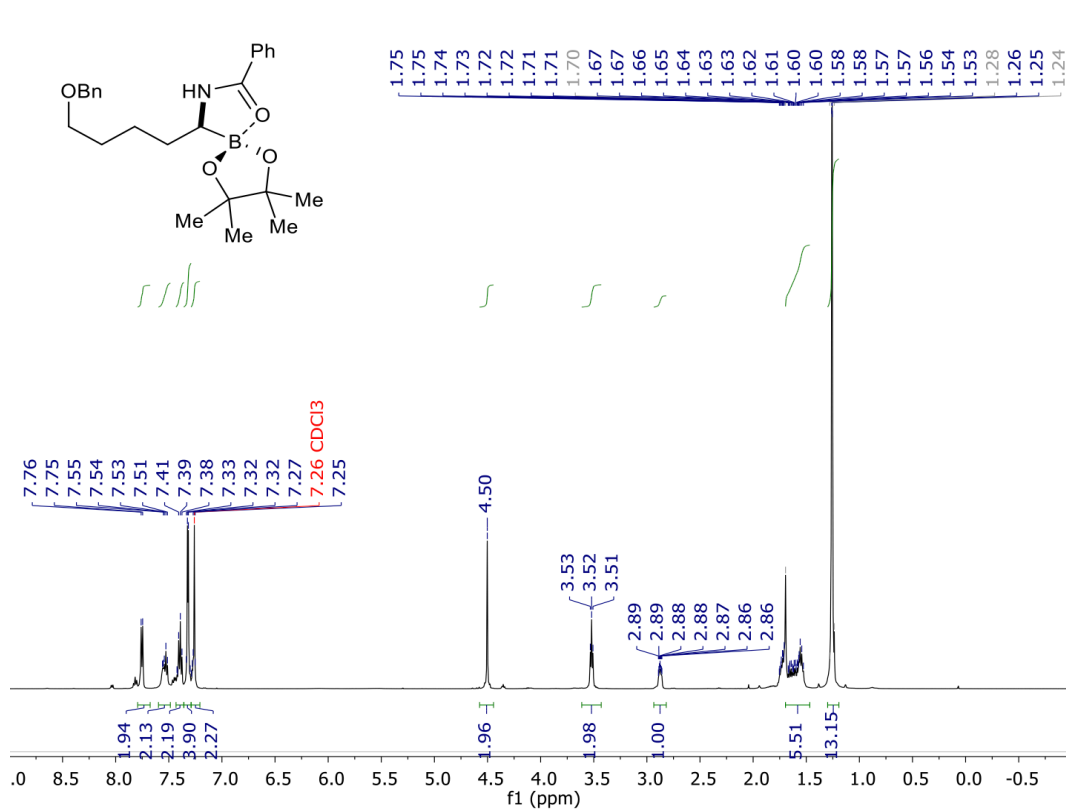


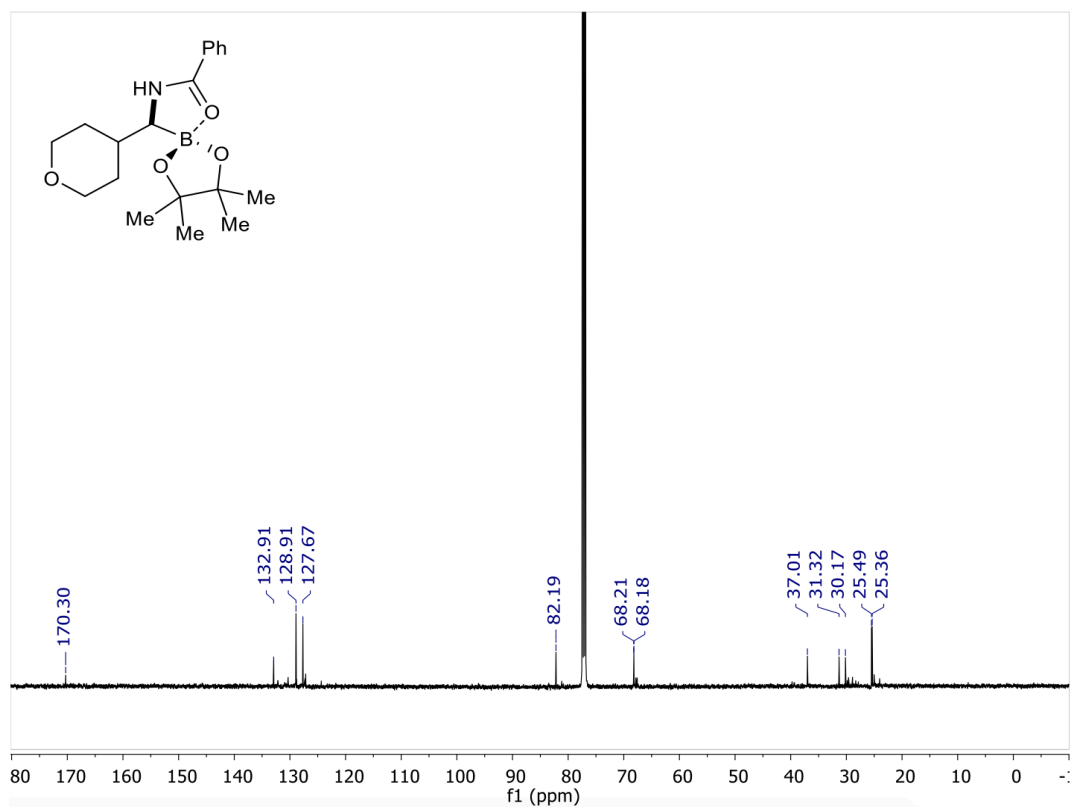
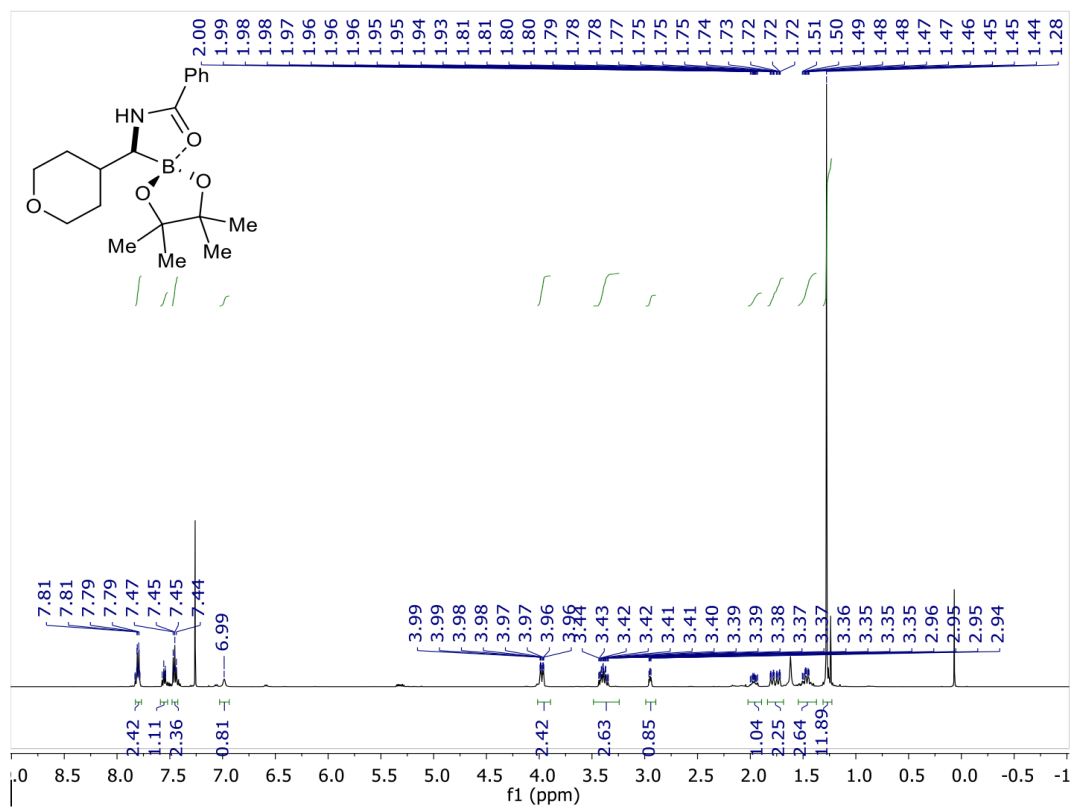


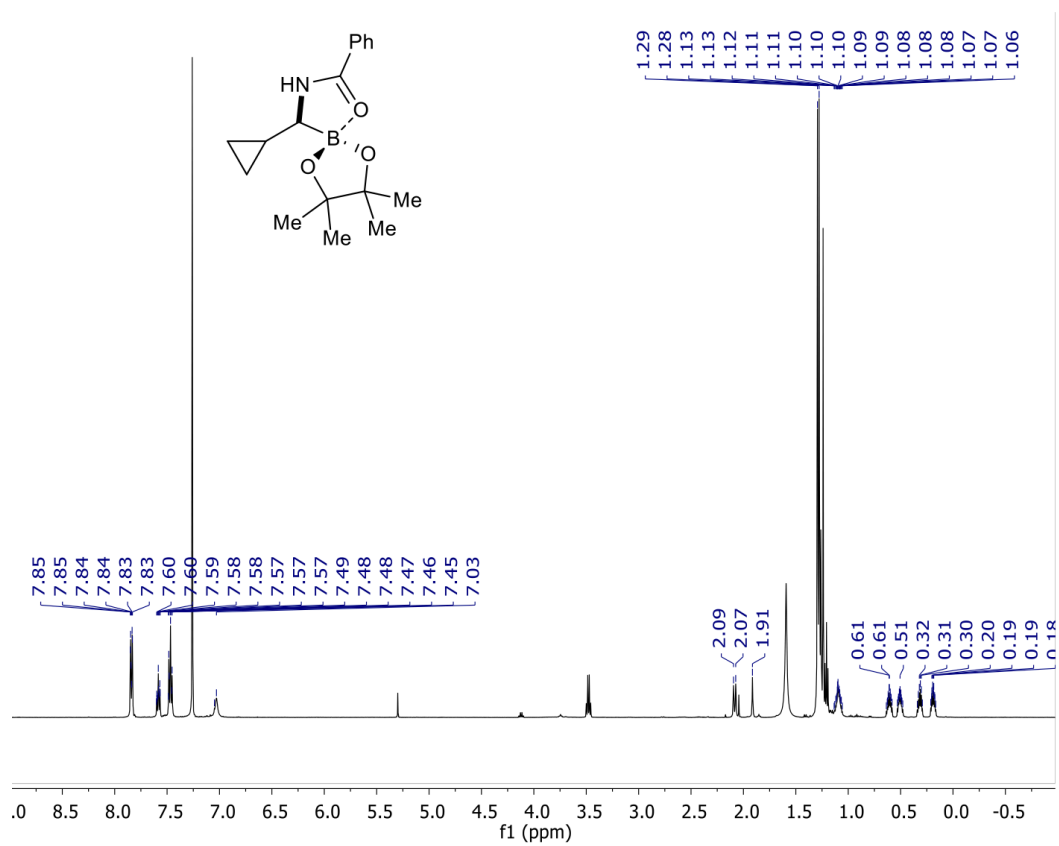


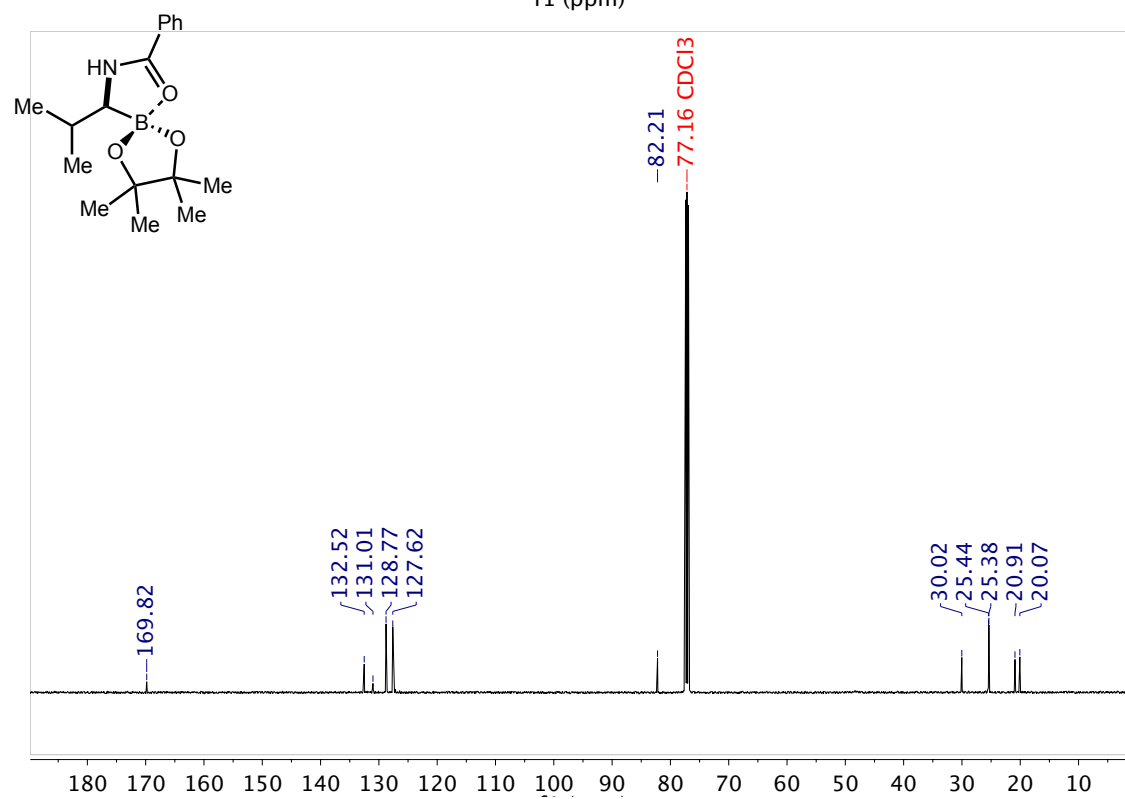
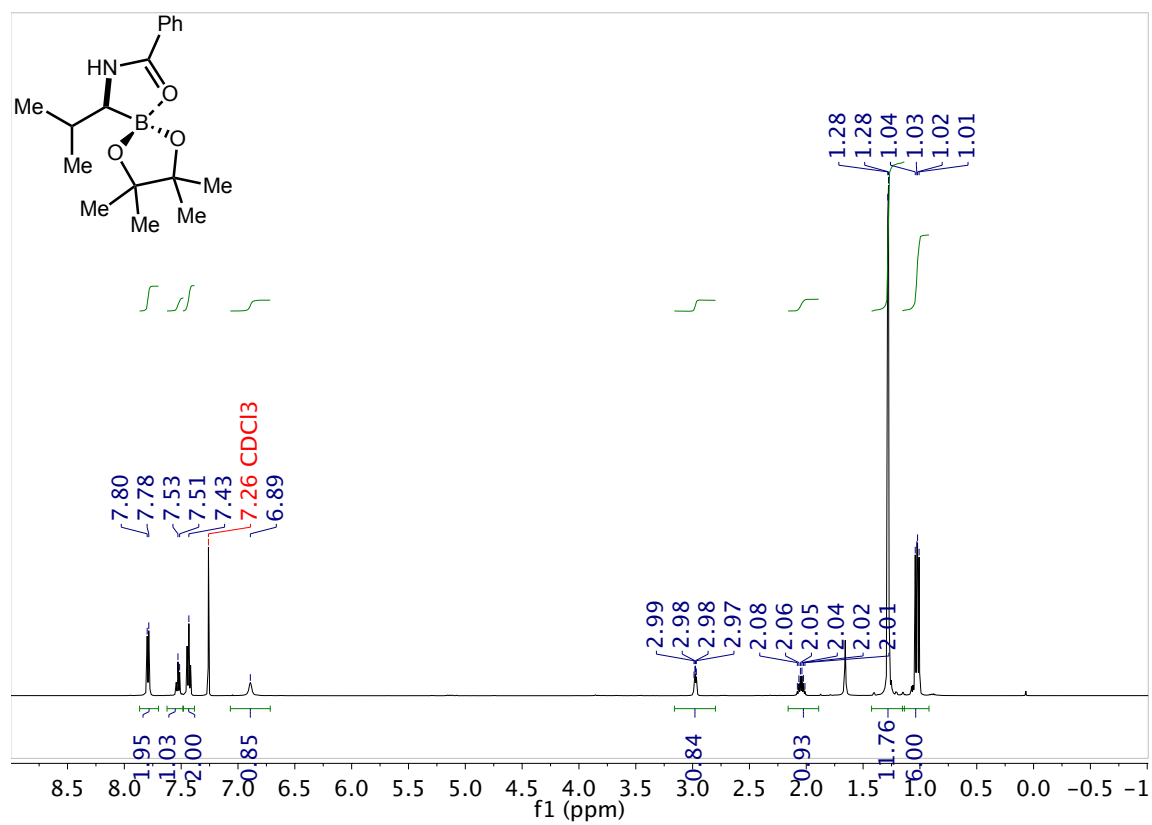


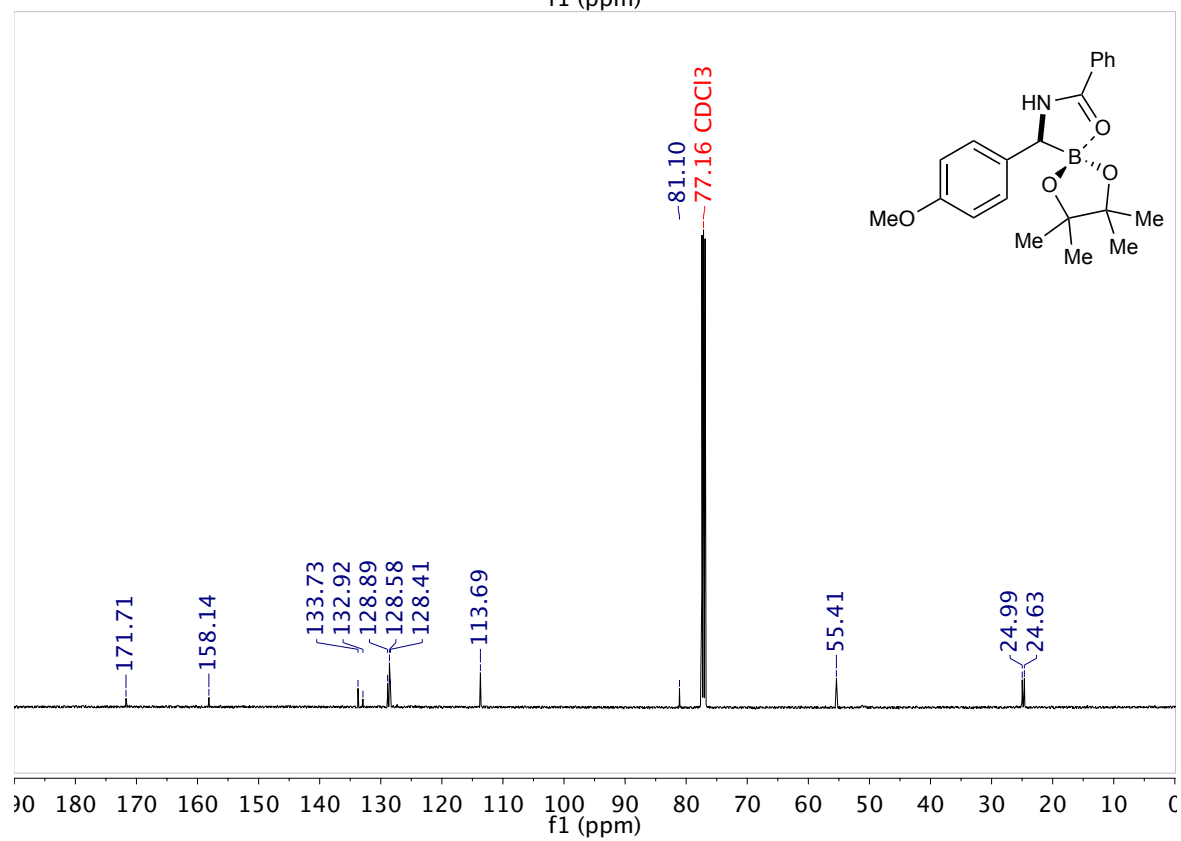
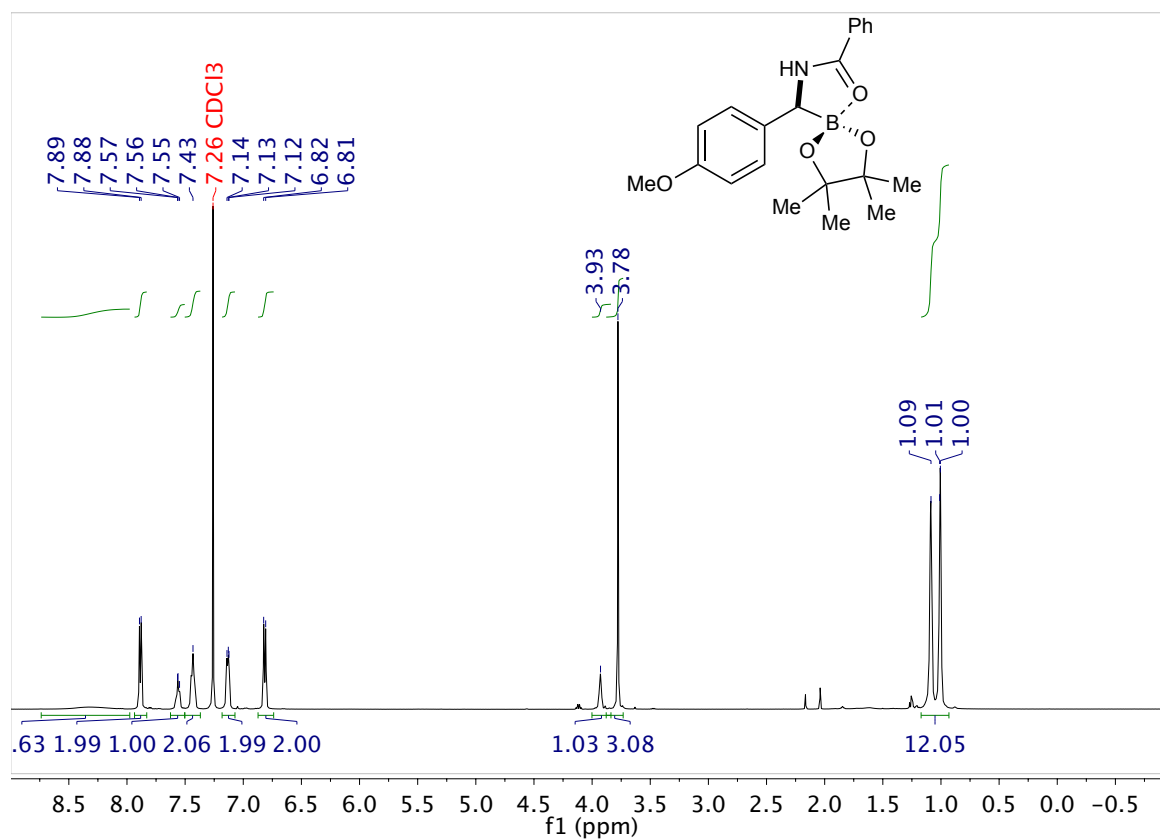


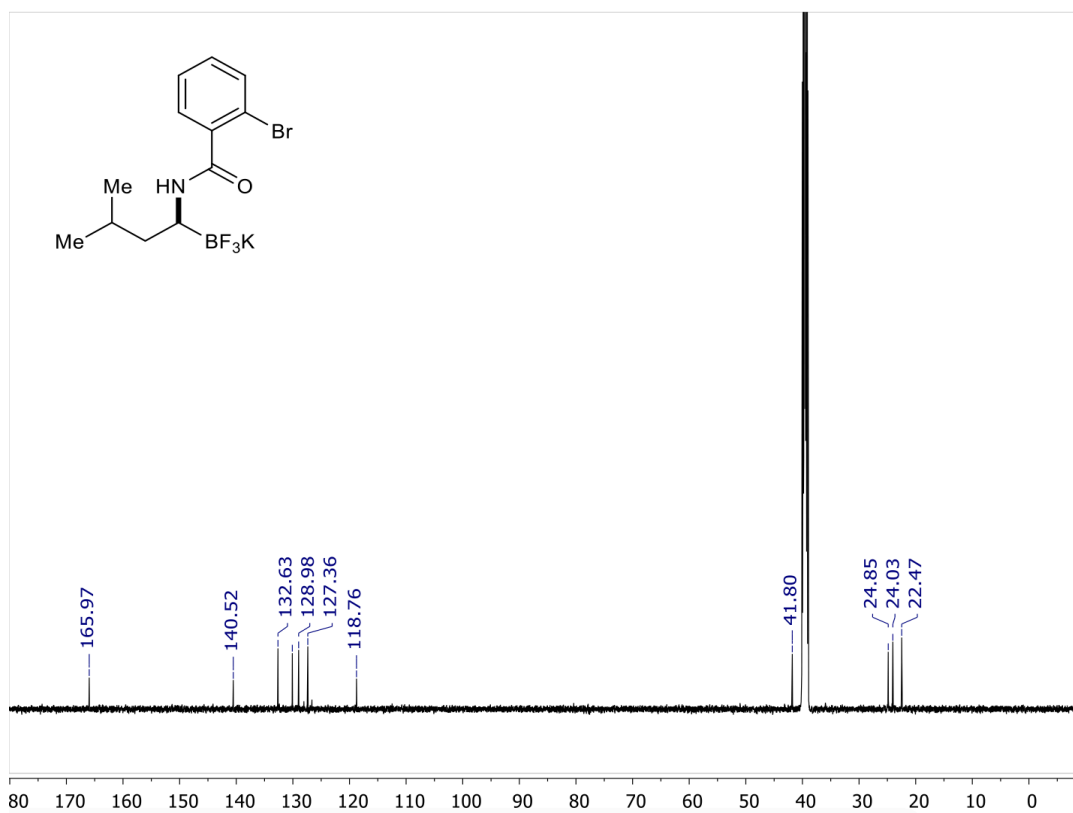
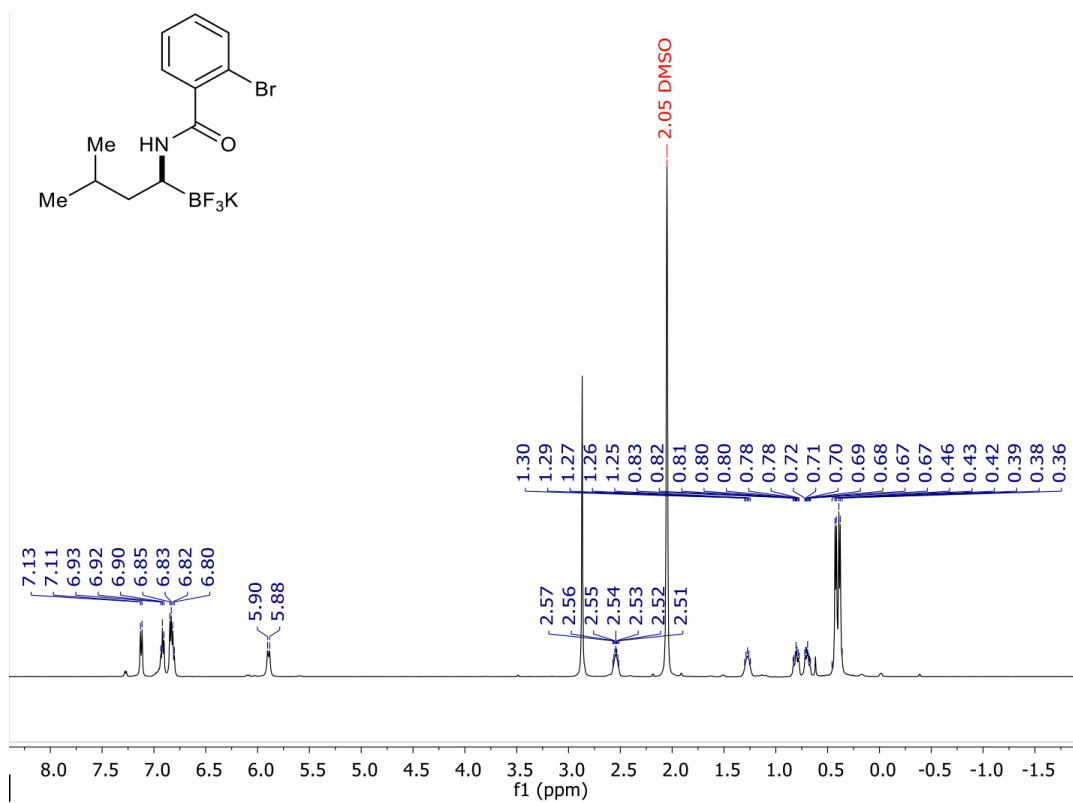


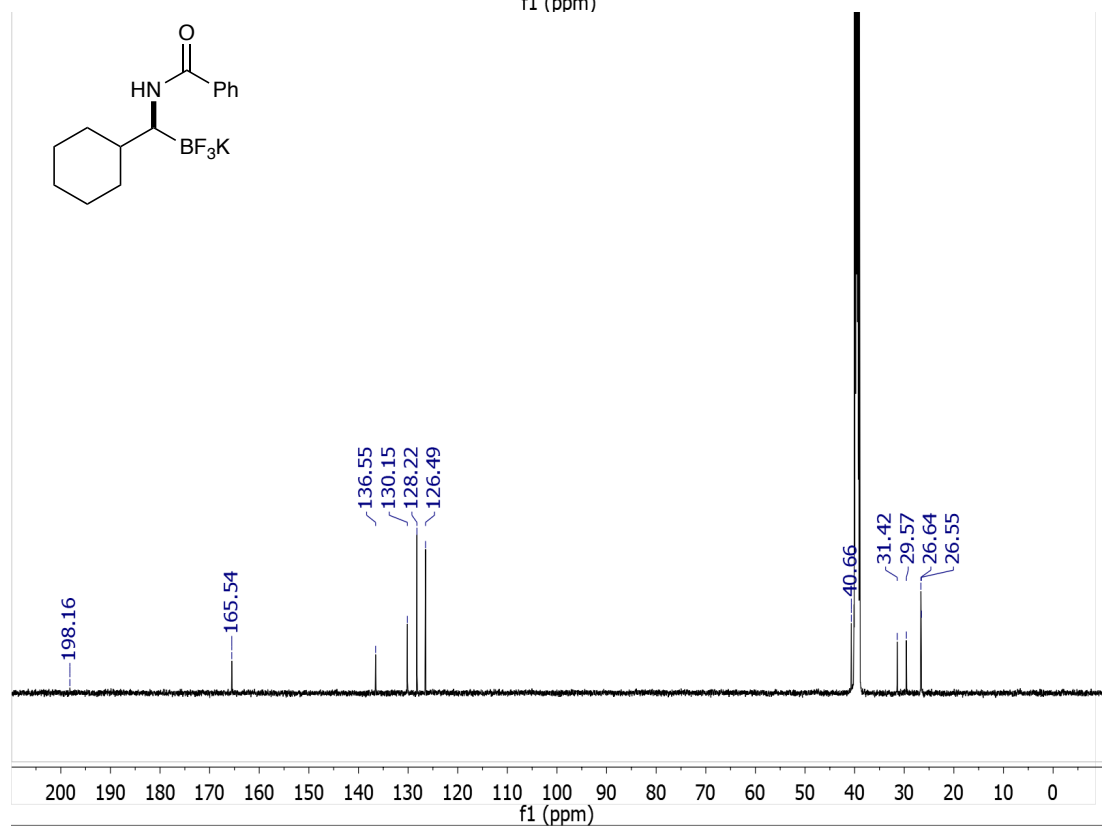
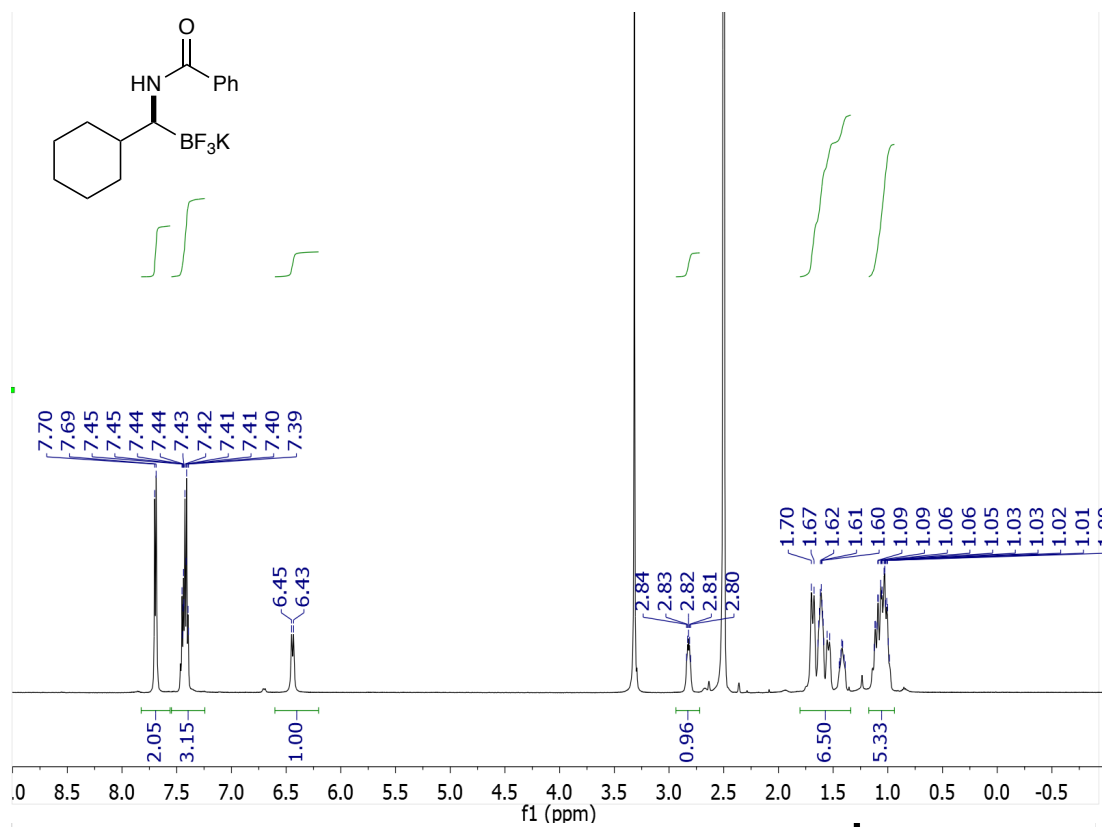


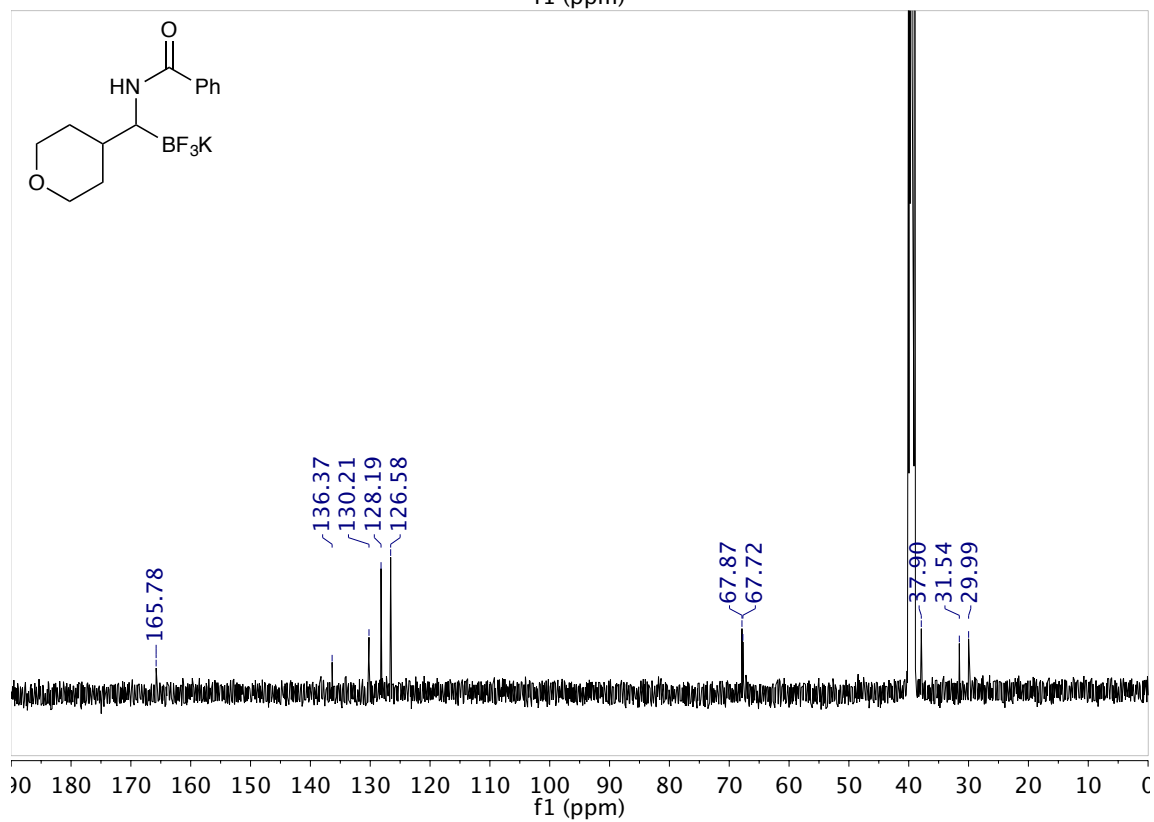
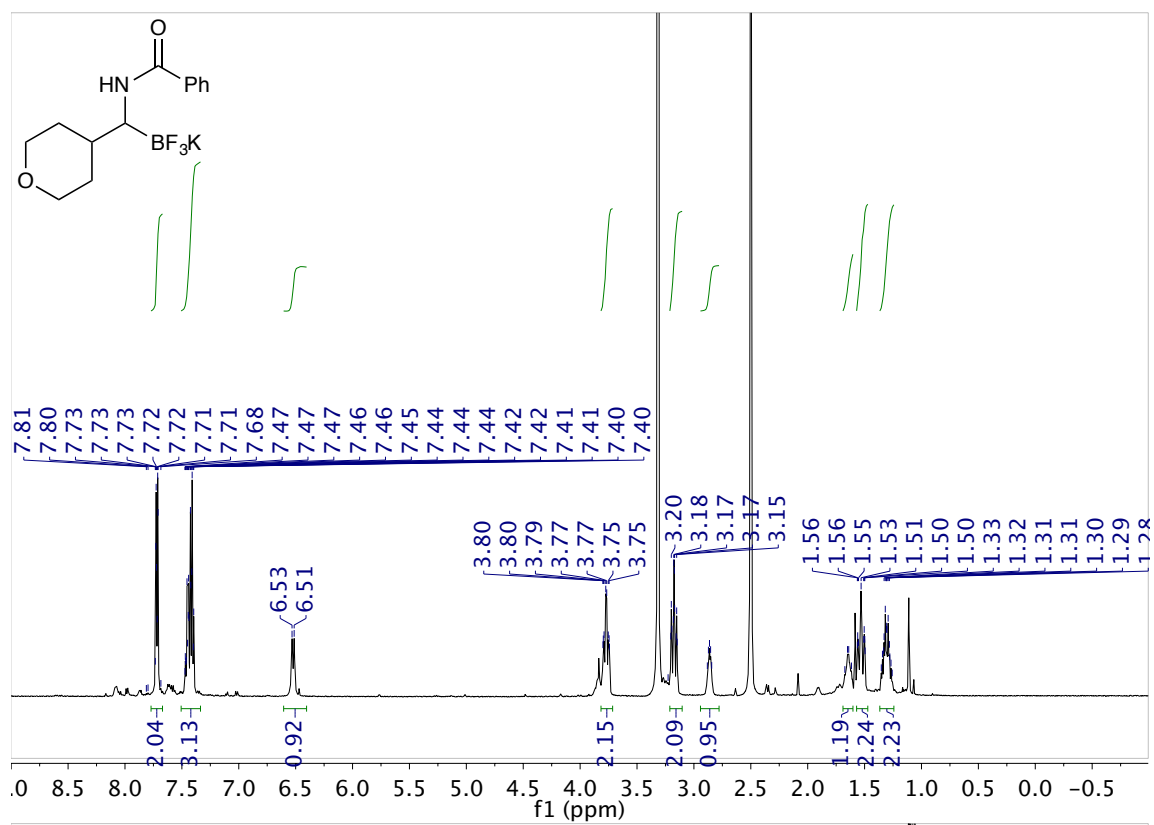




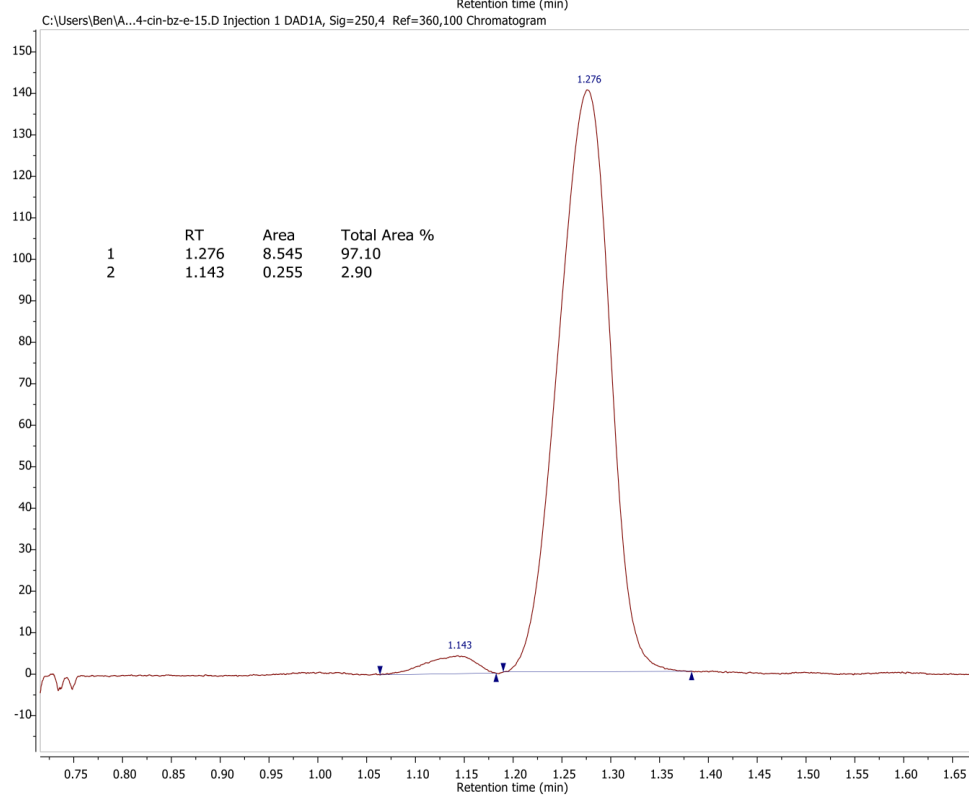
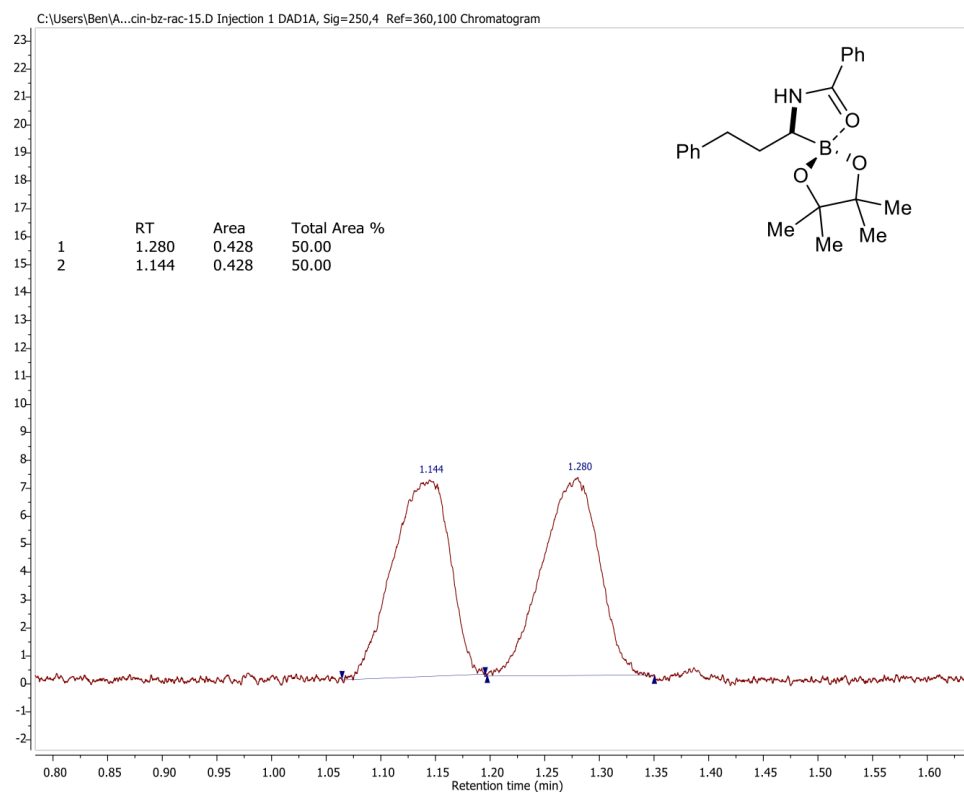


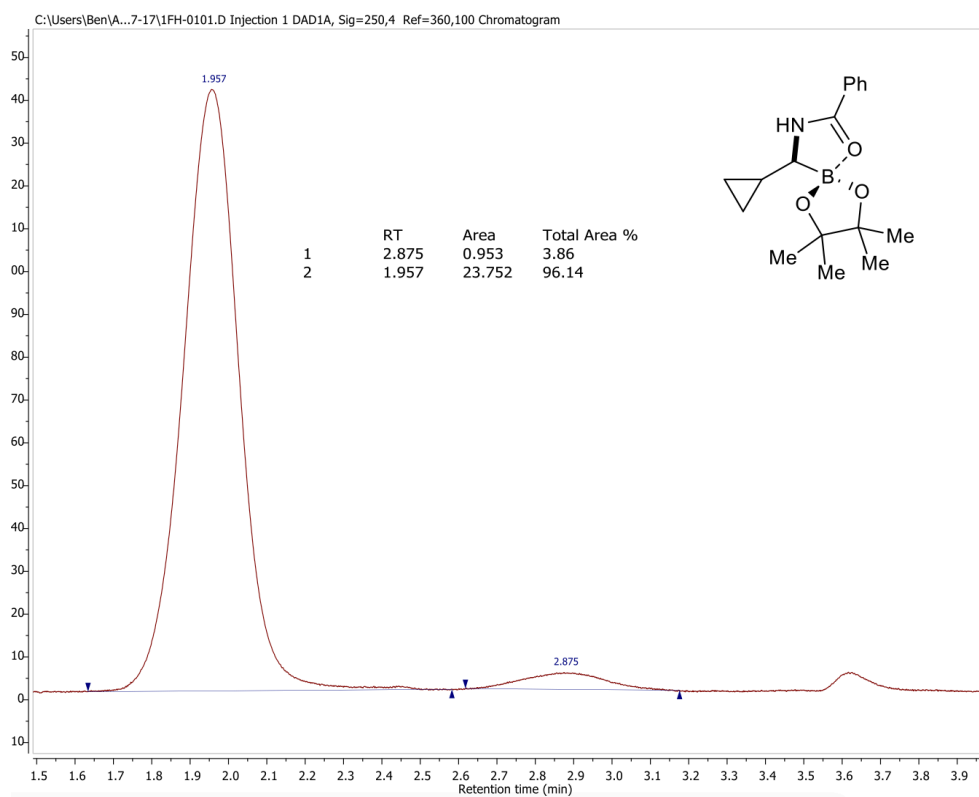
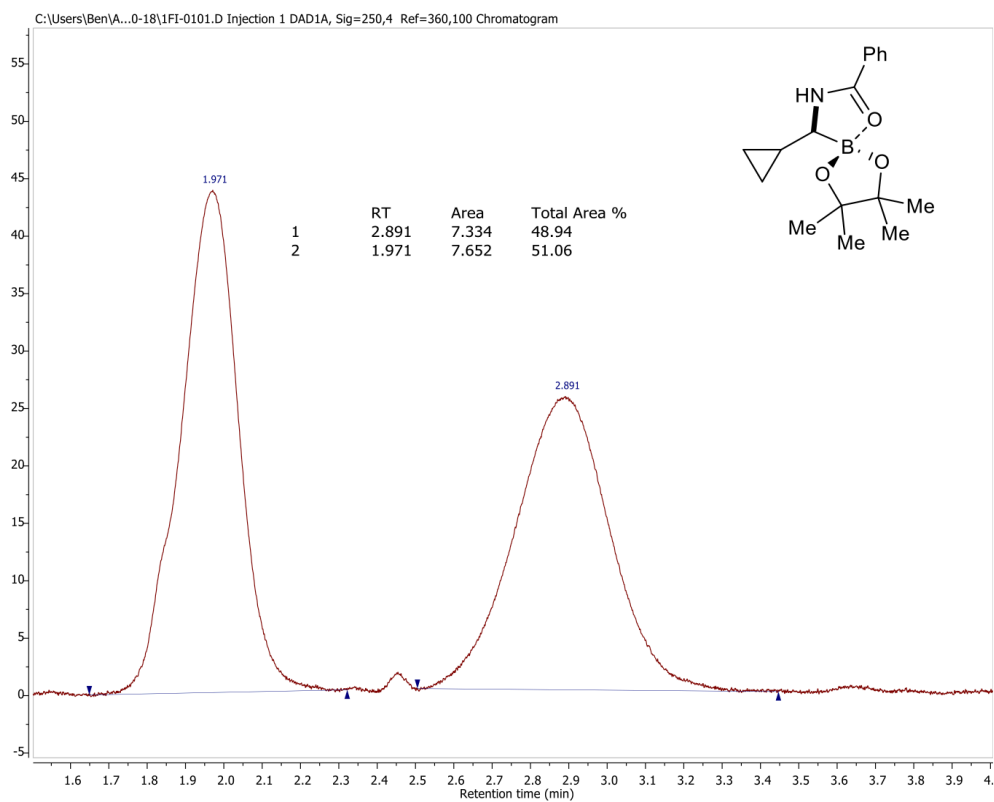


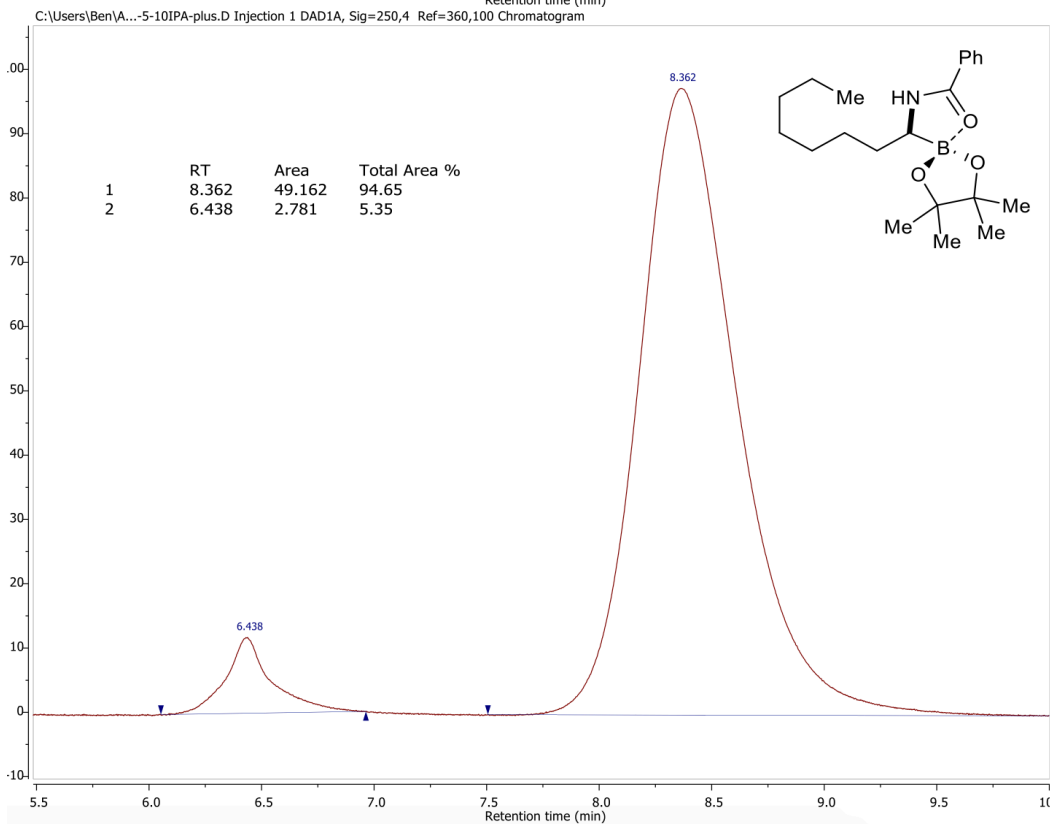
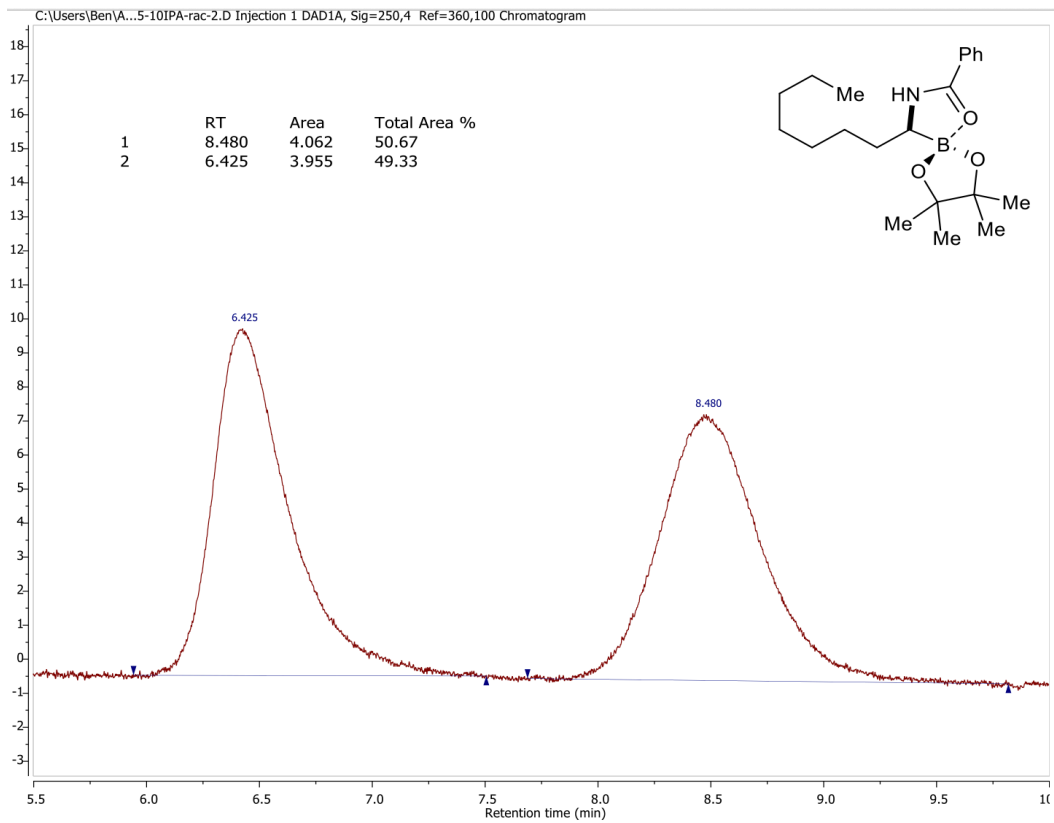


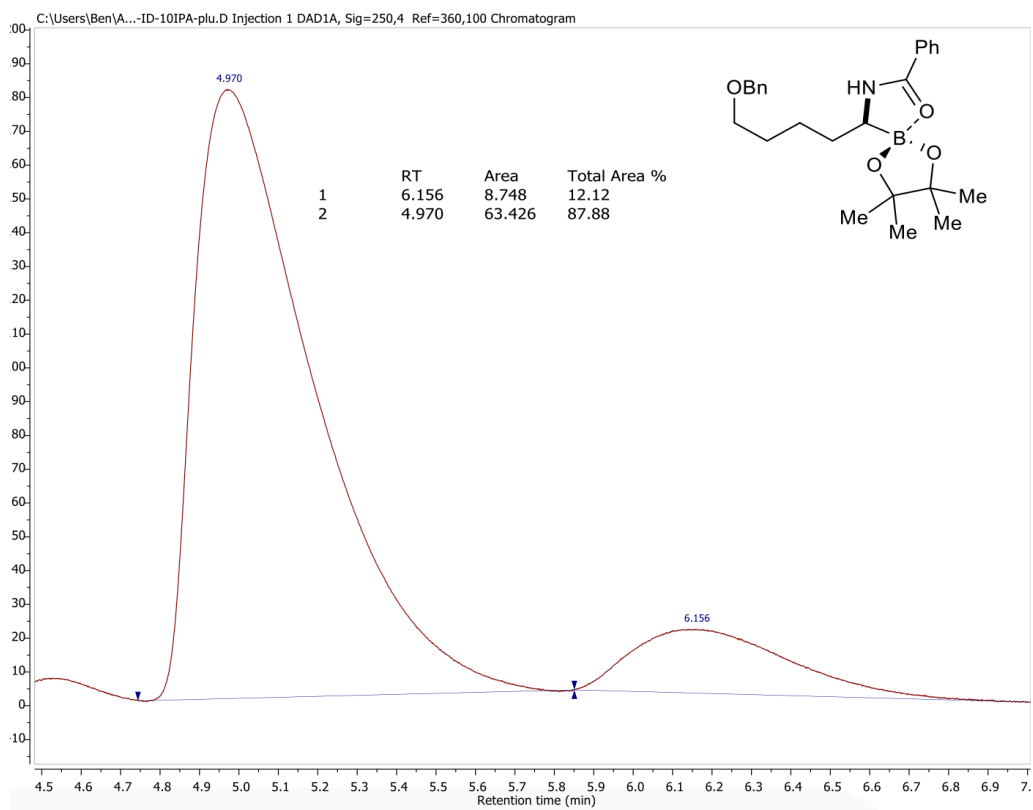
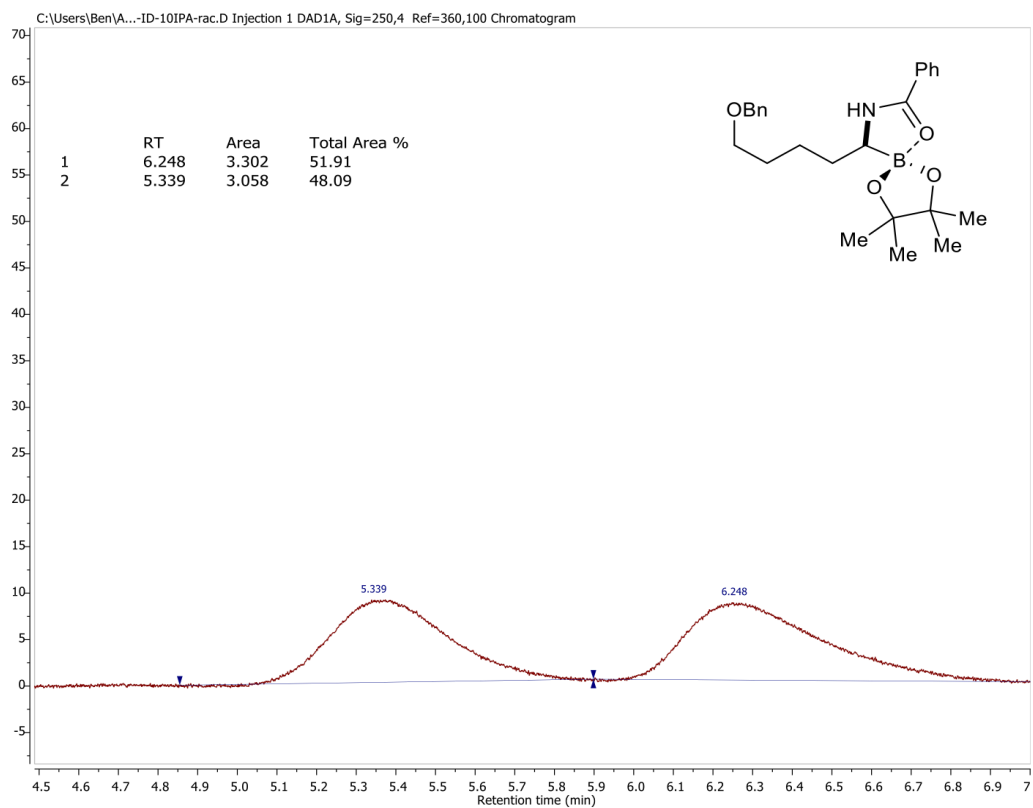


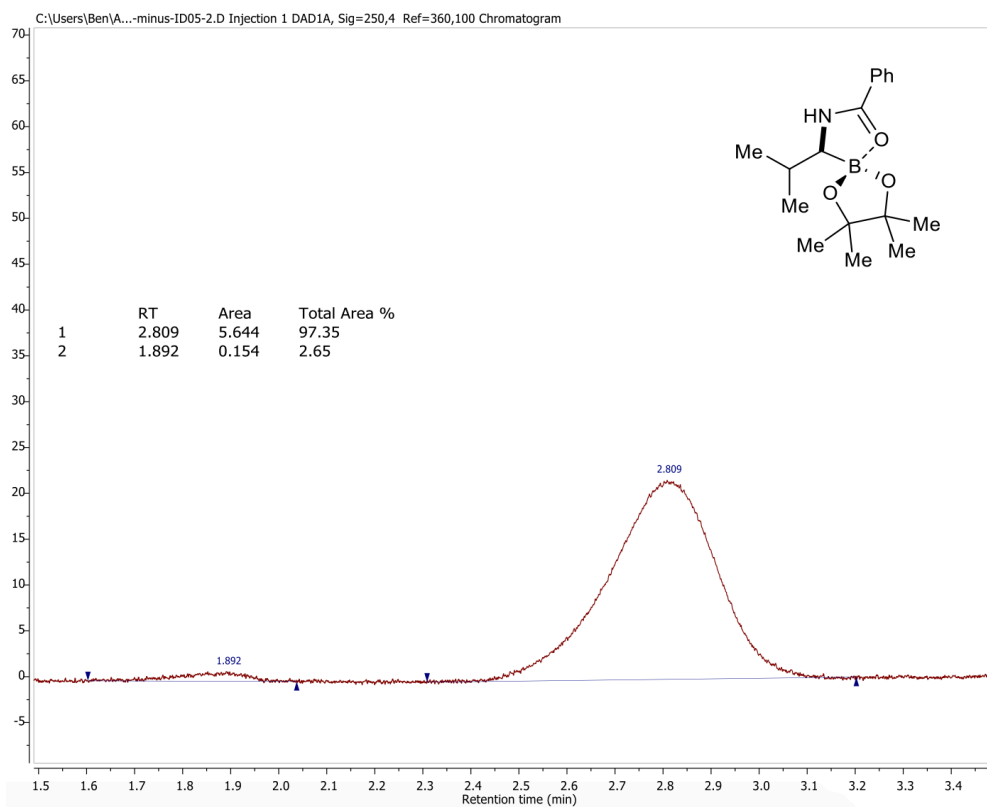
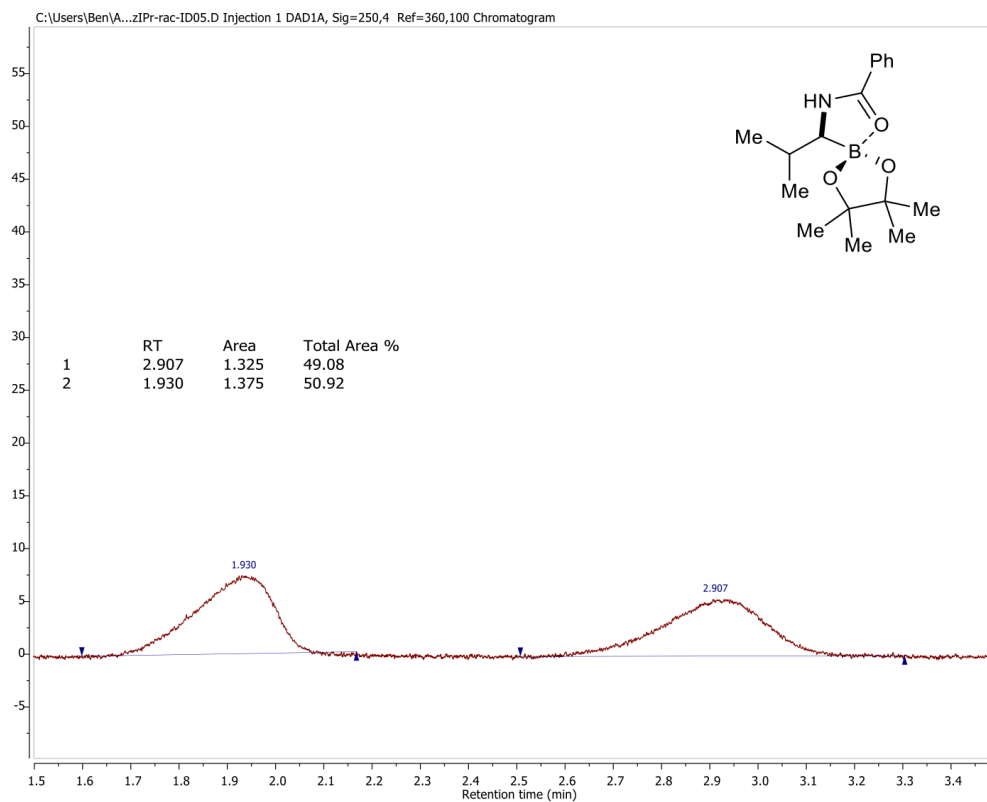
2.7.5 HPLC and SFC Traces of Racemic and Enantioenriched Compounds

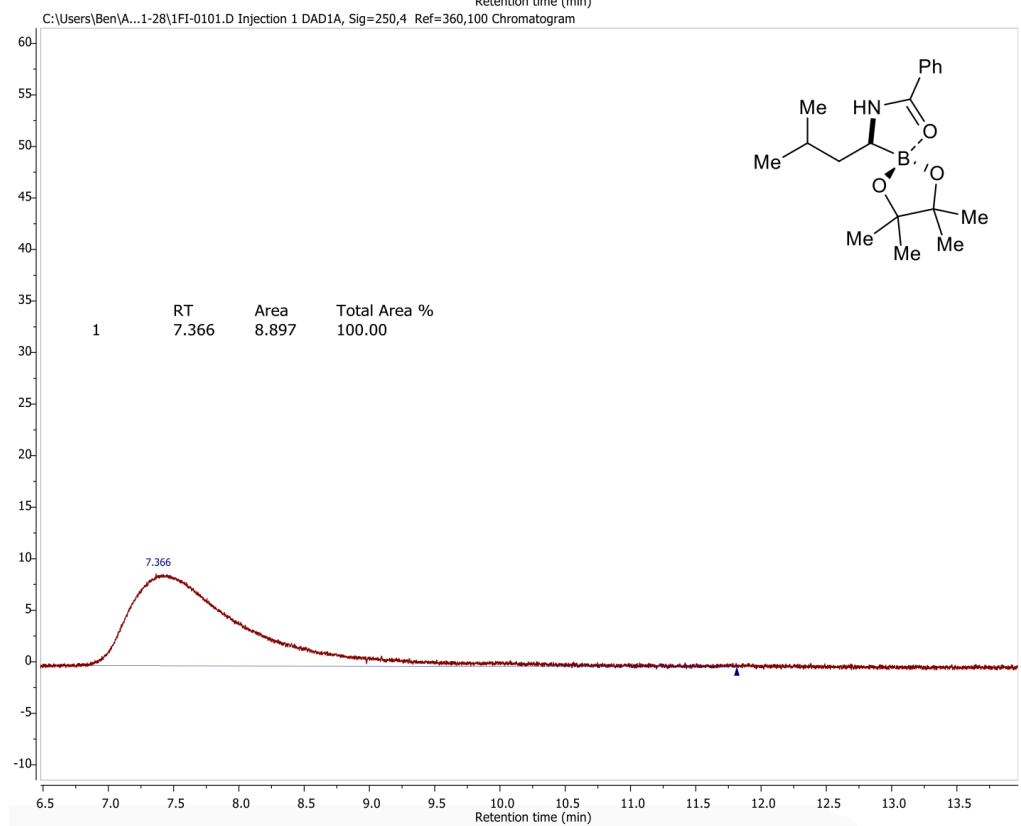
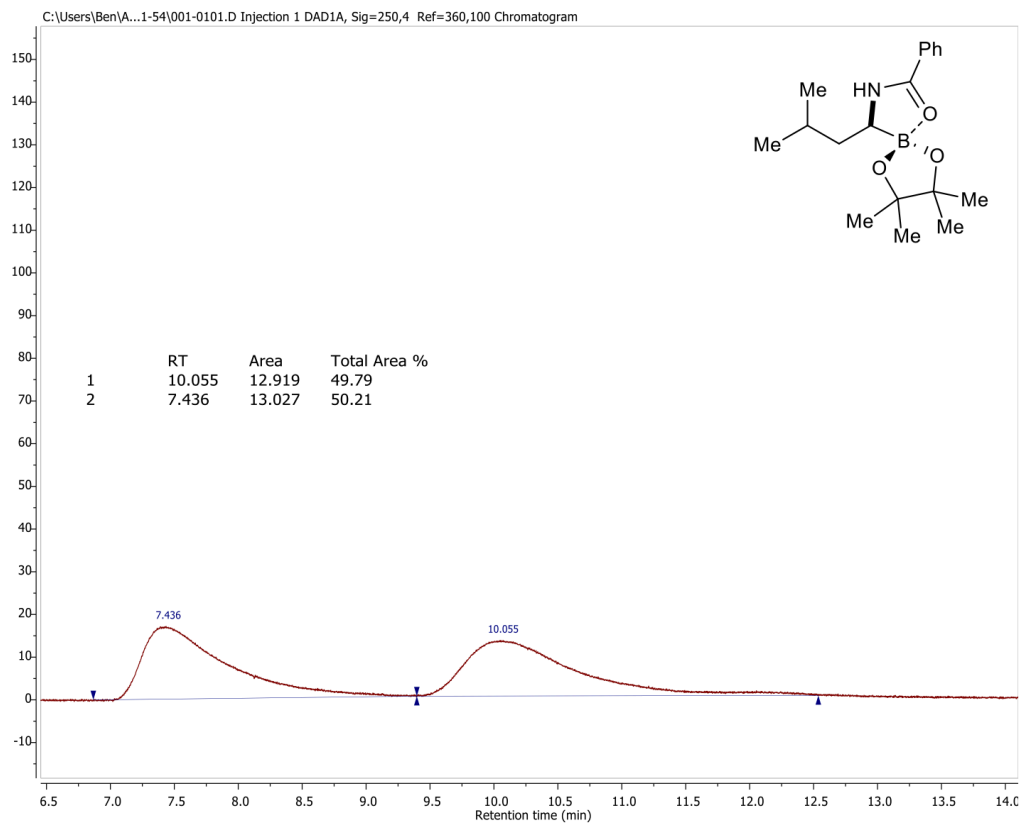


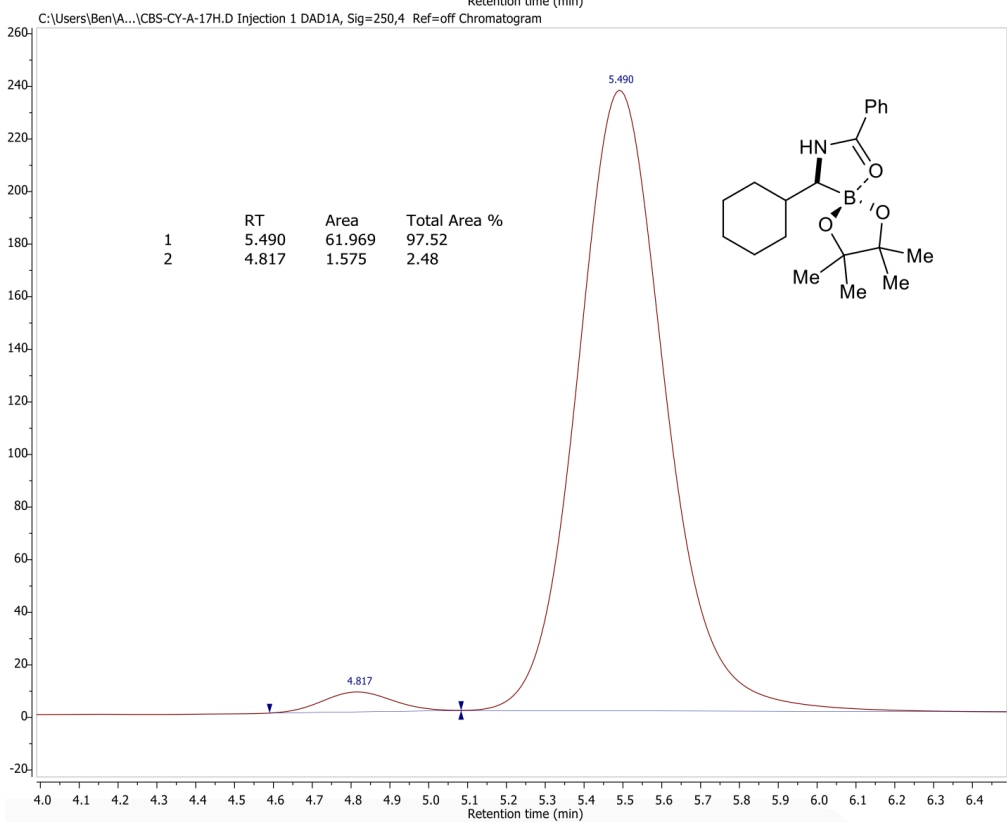
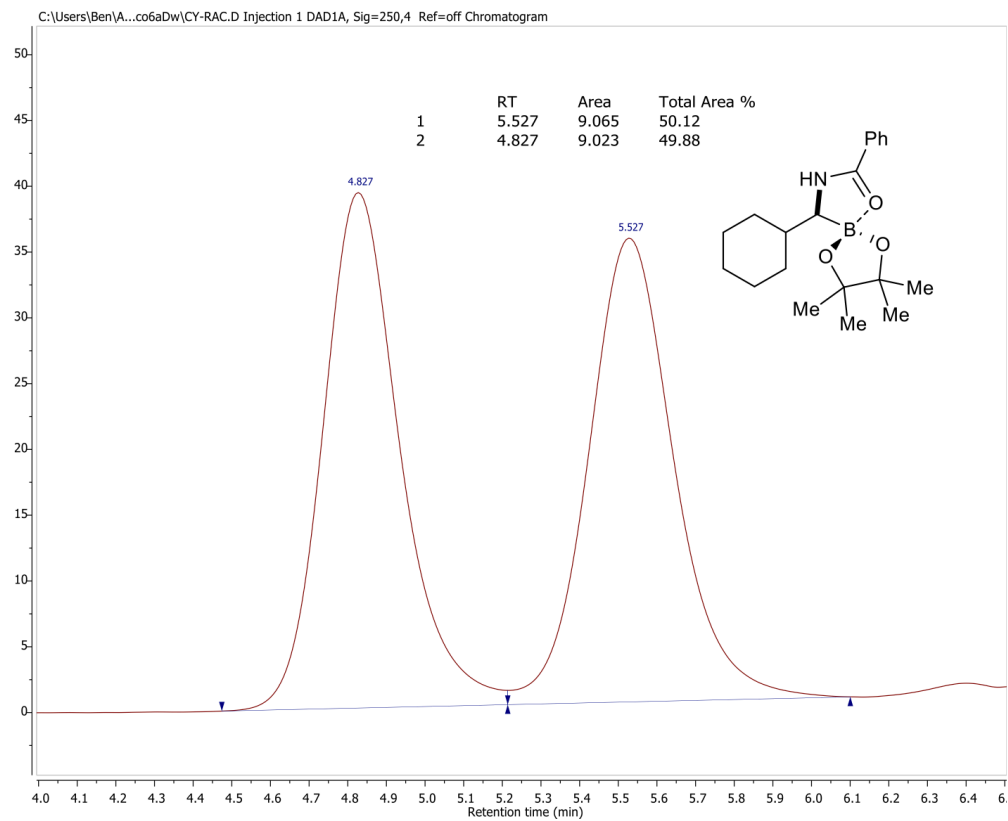










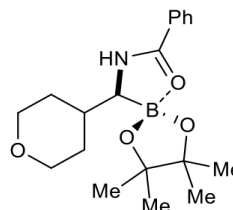
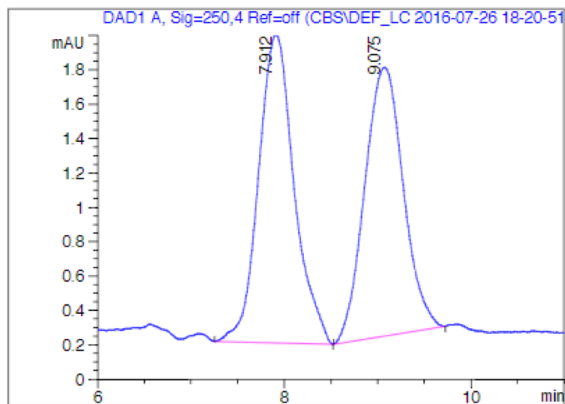


Sample Name: CBS-THP-rac-iso-adh

1

Injection Date : Tue, 26. Jul. 2016
 Sample Name : CBS-THP-rac-iso-adh
 Acq Operator : CBS
 ODH, 2% IPA, 1 ml/min

Inj. Vol. : 10 µl



Signal 1: DAD1 A, Sig=250,4 Ref=off

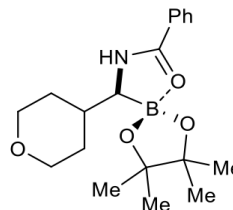
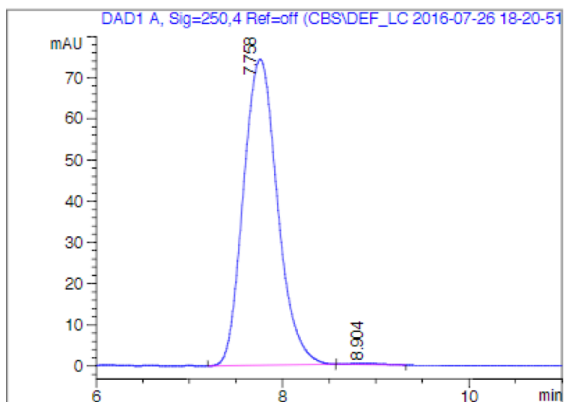
| Peak # | RT [min] | Type | Width [min] | Area | Area % | Name |
|--------|----------|------|-------------|--------|--------|------|
| 1 | 7.912 | BB | 0.395 | 47.523 | 51.399 | |
| 2 | 9.075 | BB | 0.435 | 44.936 | 48.601 | |

Sample Name: THP-v91

1

Injection Date : Tue, 26. Jul. 2016
 Sample Name : THP-v91
 Acq Operator : CBS
 ODH, 2% IPA, 1 ml/min

Inj. Vol. : 10 µl



Signal 1: DAD1 A, Sig=250,4 Ref=off

| Peak # | RT [min] | Type | Width [min] | Area | Area % | Name |
|--------|----------|------|-------------|----------|--------|------|
| 1 | 7.758 | BB | 0.401 | 1890.386 | 99.675 | |
| 2 | 8.904 | MM | 0.409 | 6.169 | 0.325 | |

Sample Name: CBS-valbr-5h-whk3-rac

1

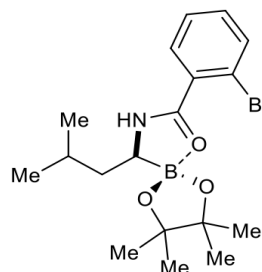
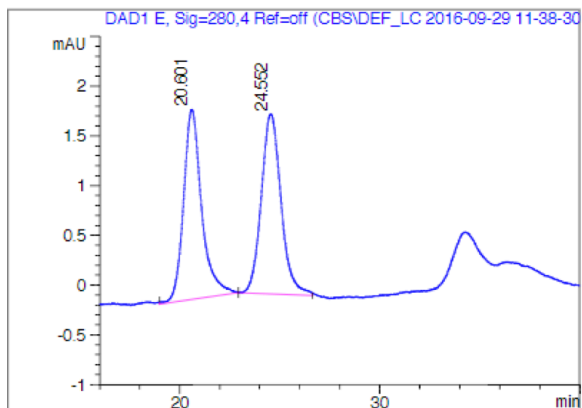
Injection Date : Thu, 29. Sep. 2016

Sample Name : CBS-valbr-5h-whk3-rac

Inj. Vol. : 10 µl

Acq Operator : CBS

ODH, 2% IPA, 1 ml/min



Signal 1: DAD1 E, Sig=280,4 Ref=off

| Peak # | RT [min] | Type | Width [min] | Area | Area % | Name |
|--------|----------|------|-------------|---------|--------|------|
| 1 | 20.601 | MM | 1.048 | 120.252 | 49.256 | |
| 2 | 24.552 | MM | 1.140 | 123.883 | 50.744 | |

Sample Name: valbr-e23-4d

1

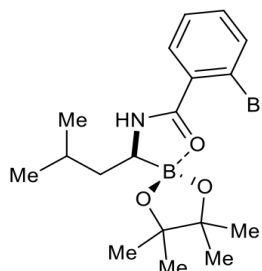
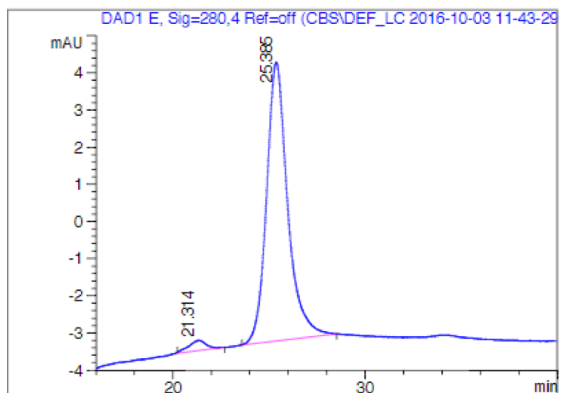
Injection Date : Mon, 3. Oct. 2016

Sample Name : valbr-e23-4d

Inj. Vol. : 10 µl

Acq Operator : CBS

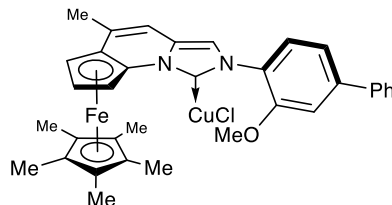
ODH, 2% IPA, 1 ml/min



Signal 1: DAD1 E, Sig=280,4 Ref=off

| Peak # | RT [min] | Type | Width [min] | Area | Area % | Name |
|--------|----------|------|-------------|---------|--------|------|
| 1 | 21.314 | MM | 1.054 | 17.373 | 2.953 | |
| 2 | 25.385 | BB | 1.015 | 571.006 | 97.047 | |

2.7.6 X-Ray Structure Data



Determination of Structure of (-)-Ferrocenyl Methoxy Biphenyl Imidazo[1,5-a]pyridine Copper Chloride Complex (Catalyst G)

Single crystals of $C_{34}H_{34}N_2OCIFeCu$ were supplied. A suitable crystal was selected and the crystal was mounted on a MITIGEN holder in Paratone oil on a Kappa Apex 2 diffractometer. The crystal was kept at 249.99 K during data collection. Using Olex2, the structure was solved with the ShelXT structure solution program using Intrinsic Phasing and refined with the ShelXL refinement package using Least Squares minimisation.

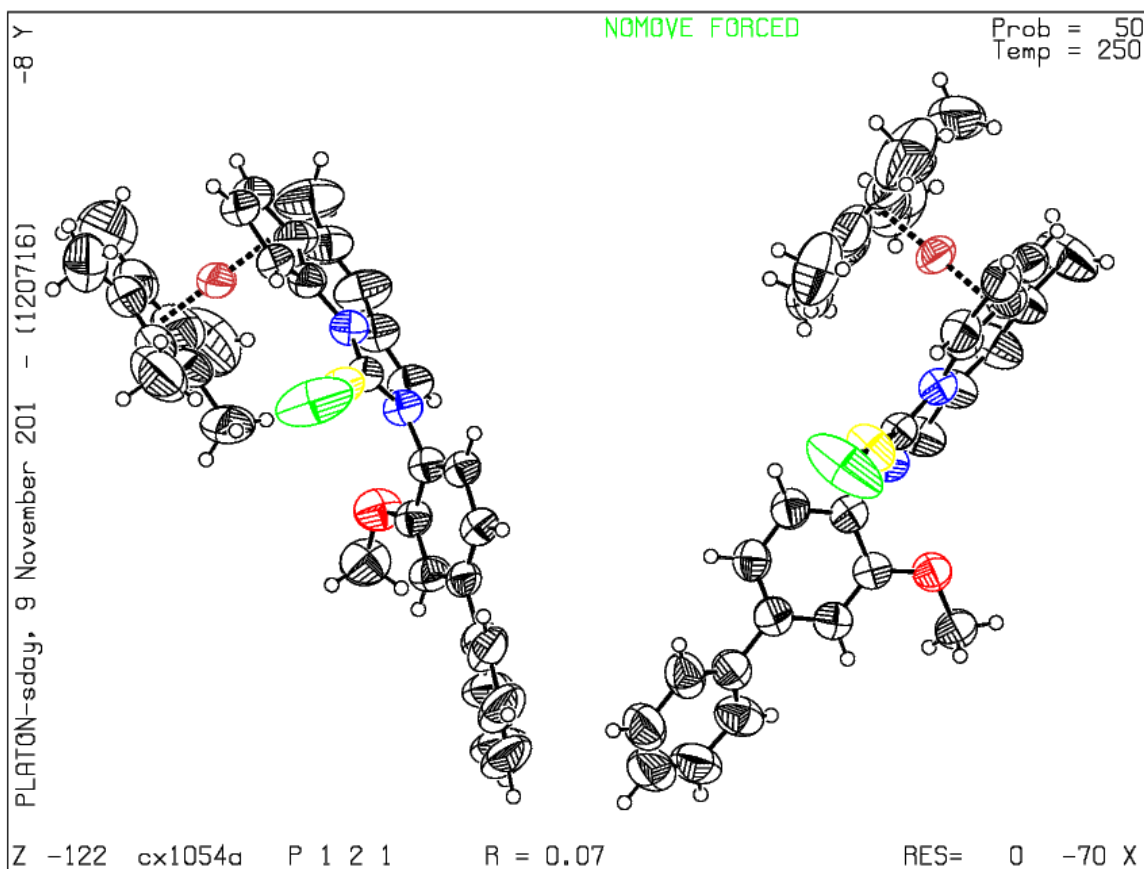
Crystal structure determination of catalyst G

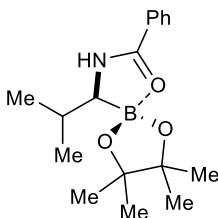
Crystal Data for $C_{34}H_{34}N_2OCIFeCu$ ($M=641.47$): monoclinic, space group P2 (no. 3), $a = 18.3929(16)$ Å, $b = 9.5949(8)$ Å, $c = 18.9878(17)$ Å, $\beta = 96.359(5)^\circ$, $V = 3330.3(5)$ Å³, $Z = 4$, $T = 249.99$ K, $\mu(\text{CuK}\alpha) = 5.217$ mm⁻¹, $D_{\text{calc}} = 1.279$ g/mm³, 22492 reflections measured ($4.682 \leq 2\theta \leq 130.154$), 11142 unique ($R_{\text{int}} = 0.0685$, $R_{\text{sigma}} = 0.0974$) which were used in all calculations. The final R_1 was 0.0691 ($I > 2\sigma(I)$) and wR_2 was 0.2034 (all data).

Refinement Details. The enhanced rigid-bond restraint (SHELX keyword RIGU) was applied globally. (Acta Cryst. A68 (2012) 448-451)

Solvent Treatment Details. The solvent masking procedure as implemented in Olex2 was used to remove the electronic contribution of solvent molecules from the refinement. As the

exact solvent content is not known, only the atoms used in the refinement model are reported in the formula here. Total solvent accessible volume / cell = 440.2 Å³ [13.2%] Total electron count / cell = 67.4





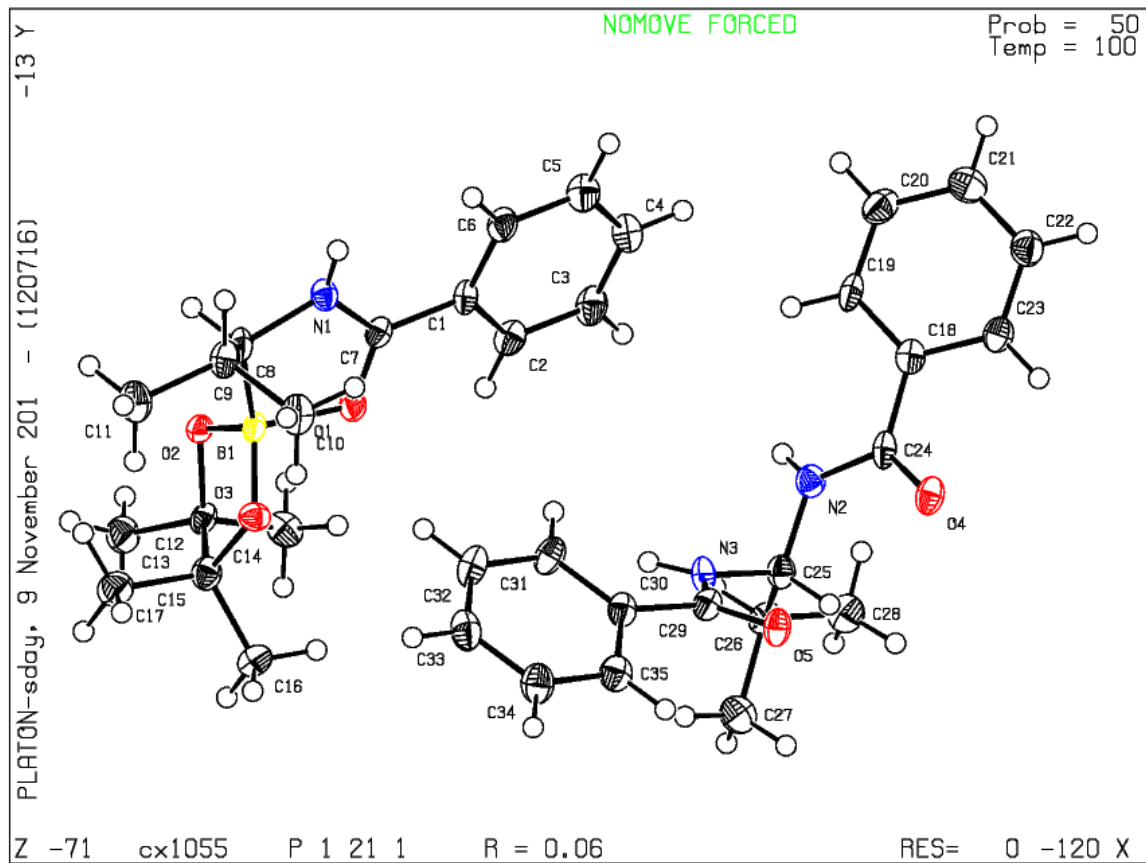
Determination of Structure of (*S*)-*N*-(2-methyl-1-(4,4,5,5-tetramethyl-1,3,2-dioxaborolan-2-yl)propyl)benzamide (II-33)

Single crystals of $C_{35}H_{46}BN_3O_5$ [cx1055] were supplied. A suitable crystal was selected and the crystal was mounted on a MITIGEN holder in Paratone oil on a Kappa Apex 2 diffractometer. The crystal was kept at 100.01 K during data collection. Using Olex2 [1], the structure was solved with the ShelXT [2] structure solution program using Intrinsic Phasing and refined with the ShelXL [3] refinement package using Least Squares minimisation. The absolute structure parameter y (Hooft, Straver & Spek, 2008) was calculated using PLATON (Spek, 2010). The resulting value was $y = -0.1(3)$ indicating that the absolute structure has probably been determined correctly. Structure contained cocrystal of impurity.

Crystal structure determination of [cx1055]

Crystal Data for $C_{35}H_{46}BN_3O_5$ ($M = 599.56$): monoclinic, space group $P2_1$ (no. 4), $a = 10.9592(17)$ Å, $b = 9.3307(12)$ Å, $c = 16.2386(19)$ Å, $\beta = 91.805(11)^\circ$, $V = 1659.7(4)$ Å³, $Z = 2$, $T = 100.01$ K, $\mu(\text{CuK}\alpha) = 0.634$ mm⁻¹, $D_{\text{calc}} = 1.200$ g/mm³, 12226 reflections measured ($5.444 \leq 2\theta \leq 30.16$), 5335 unique ($R_{\text{int}} = 0.0970$, $R_{\text{sigma}} = 0.1119$) which were used in all calculations. The final R_1 was 0.0574 ($I > 2\sigma(I)$) and wR_2 was 0.1361 (all data).

Refinement Details. No special refinement necessary.



Chapter 3: Modular Synthesis of Amido Azoles

3.1 Introduction

Since the first characterization of a stable diamino carbene by Arduengo in 1991,¹⁷⁴ N-heterocyclic carbenes which contain alkyl or aryl substitution on the vicinal wingtip nitrogen atoms have featured prominently in the fields of chemical catalysis and coordination chemistry.^{6,9,175-180} However, despite ample evidence regarding dramatic alterations in carbene behavior observed with the modification of wingtip substituents,¹⁸¹⁻¹⁸³ there has been little effort devoted to the systematic exploration of non-carbon groups in this crucial position.¹⁸⁴⁻¹⁹¹ Given that the structural variety of NHCs has largely been constrained to the N-alkyl or N-aryl motif, the design and development of new carbenes of this nature would serve as a much needed, highly divergent expansion of the NHC repertoire and offer new opportunities for the characterization of carbene behavior associated with atypical wingtip substitution.

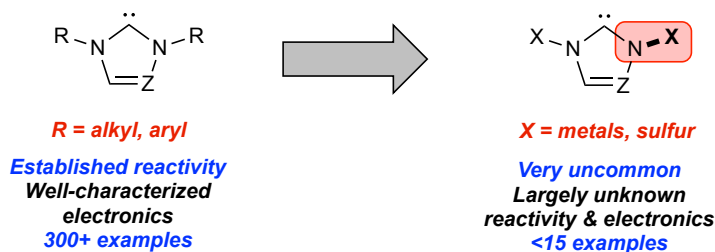


Figure 3-1. Arduengo carbene wingtip substituents

3.2 Metal-amido azoles and N-heterocyclic carbenes

While N-metallated imidazoliums and triazoliums are not unprecedented structures as carbene precursors, the design and characterization of such a metallo-carbene species (which could be used as a ligand for a heterobimetallic catalytic system or as an organocatalyst) has not been realized (**Figure 3-1**).^{184,187,192} Given the ample precedent regarding the highly variable reactivity associated with changes to an NHC nitrogen substituent,¹⁸¹ synthesis of a structure of

this nature would provide useful information regarding the largely unknown effects of a metal-nitrogen bond vicinal to a persistent carbene or carbene-metal bond. Moreover, this system may advantageously permit use of the remarkably diverse repertoire of metal-coordinating ligands as a means of imparting chirality and altering catalyst electronics. Consequently, generation of these structures could be approached from a modular standpoint, whereby many possible catalyst structures can be envisioned from a single NHC-metal chelate and a range of known privileged metal ligands (**Figure 3-2**).

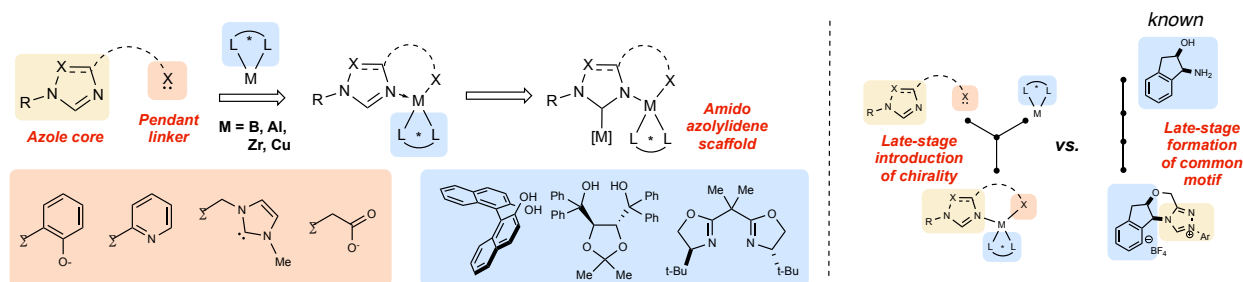
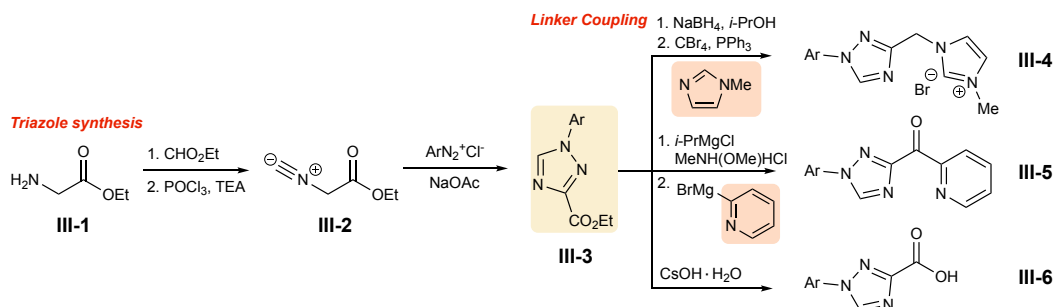


Figure 3-2. General approach towards modular ligand diversification

Our initial approach towards realization of such a structure envisioned a metal chelated to a N-aryl triazole via a pendant carboxylate. Synthesis of this ligand was carried out beginning from the glycine ester **III-I**, which could be converted to isocyanate **III-2** by formylation and subsequent dehydration with POCl_3 (**Scheme 3-1**). This was then mixed with the diazonium salt of 2,4,6-trimethylaniline to yield the 1,2,4-triazole, which could then be saponified to yield the desired triazole. Alternatively, ester **III-3** could be reduced to the corresponding alcohol, converted to the primary bromide via an Appel reaction and exposed to N-methylimidazole to yield triazoloimidazolium **III-4**. Finally, nicotonyl triazole **N** was constructed via addition of pyridylmagnesium bromide to the Weinreb amide of **III-3**.

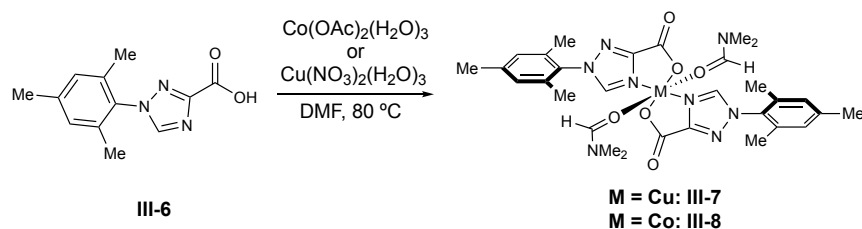
Scheme 3-1. Azole ligand synthesis

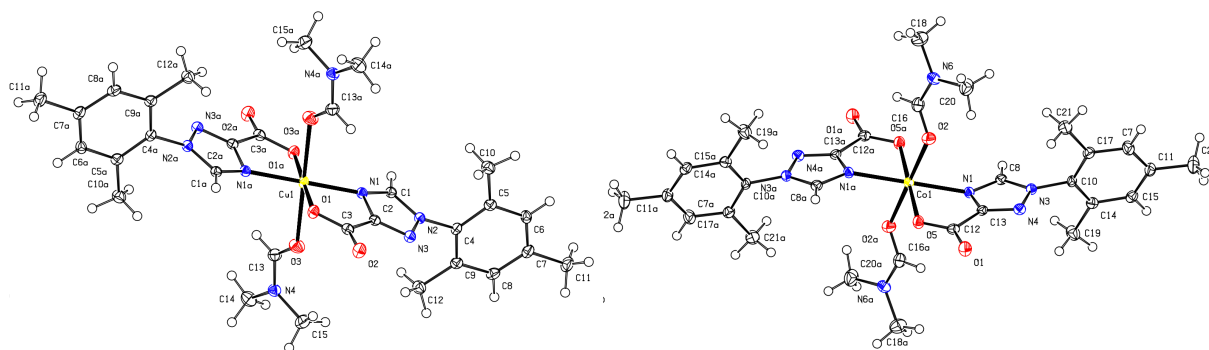


3.3 Square planar complexes of Cu(II) and Co(II)

A simple square planar structures of Cu(II) and Co(II) could be isolated via mixing a DMF solution of acid **III-6** with either $\text{Cu}(\text{NO}_3)_2(\text{H}_2\text{O})_3$ or $\text{Co}(\text{OAc})_2(\text{H}_2\text{O})_3$. Unfortunately, efforts to deprotonate the coordinated imidazole at the 2-position failed to deliver any rearranged or coordinated compounds. **III-7** and **III-8** demonstrated limited solubility in highly polar solvents such as DMF and DMA, and efforts to use alkyl lithium bases to promote deprotonation produced a complex mixture of products at room temperature and did not proceed at lower temperatures due to poor solubility of the complexes.

Scheme 3-2. Synthesis of Cu(II) and Co(II) triazolylcarboxylate complexes.





Thermal ellipsoids shown at 50% probability. Selected bond distances (Å) and angles (°). **III-7**: Cu1-N1 2.0018(13), Cu1-O3 2.4119(13), Cu1-O1 1.9739(11), N1-C1-N2 108.60(13). **III-8**: Co1-N1 2.138(2) Co1-O2 2.1391(18) Co1-O5 2.0579(15) N1-C8-N3 109.3(2).

Figure 3-3. X-ray structures of compounds **III-7** (left) and **III-8** (right).

3.4 Zn(II) coordination polymers

We also sought to characterize coordination behavior of Zn(II) with acid **III-6**. Exposure of acid **III-6** to Zn(OAc)₂ under identical conditions did not deliver any analogous compounds to **III-7/8**, but rather a mixture of two species of closely related coordination polymers which were isolated as irregular blocks or colorless rhombohedral prisms. Overall resolution of the solution structures was poor, but qualitative observations can be easily made. The two polymers both share a Zn-O-N-Zn bridging pattern and identical stoichiometry, although only **III-9** features tetrahedral Zn(II), which is common for this ion. While **III-10** includes all connectivity found in **III-9**, alternating “links” in its chain-like structure have been effectively pinched to give rise to a four-membered arrangement of zinc and oxygen. Here, Zn(II) is found in a highly distorted

square pyramidal geometry and two of every three carboxylate residues shares their negative charge with two metal centers in a μ_2 arrangement.

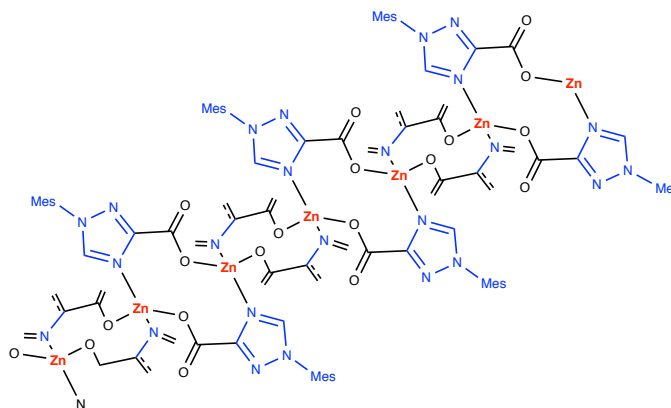


Figure 3-4. X-ray structure of coordination polymer of tetrahedral Zn(II) (**III-9**).

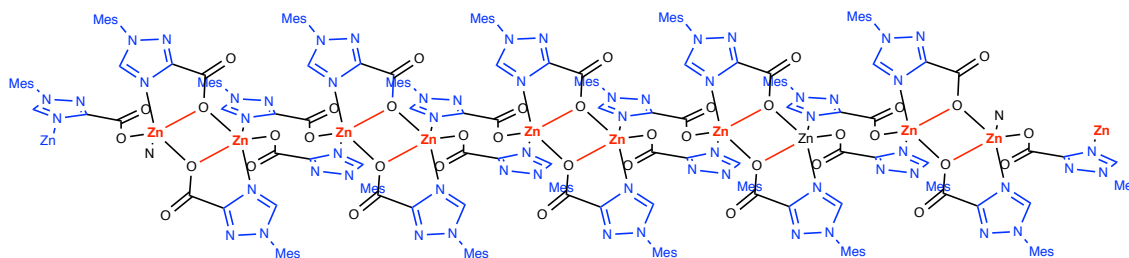


Figure 3-5. X-ray structure of coordination polymer of pentacoordinate Zn(II) (**III-10**).

3.5 Cu-Cu bimetallic coordination polymer

An unusual coordination polymer of copper (**III-11**) was also obtained and characterized via X-ray diffraction. Unfortunately, this unique structure was only able to be grown on one occasion, where it appeared as yellow rods interspersed amongst a batch of aqua-blue crystals of **III-7**. The crystal structure reveals a repeating pattern of two uniquely coordinated instances of copper, alternating between linear N-Cu-N and O-Cu-O (**Figures 3-5, 3-6**). Interestingly, the overall structure features two polymer layers spaced 2.77 Å apart. The two strands appear to be

connected via a Cu-Cu interaction, although the distance is also likely affected by the bulky mesityl rings rotated out of the plane of each strand.

Although the polymer was grown from a Cu(II) source, the oxidation state of each metal center is not immediately clear. While the oxygen-bridging copper could easily be assigned as Cu(II) without consideration of the other metal center, this oxidation state would necessitate that it is paired with Cu(0), which is extremely unlikely for an organic complex of a first row transition metal. As the presence of a counterion was soundly ruled out upon thorough analysis of X-ray data, it is likely that the polymer solely consists of Cu(I). In this configuration, the overall net negative charge created from the coordination of two carboxylate residues to a Cu(I) center would be countered by the positive charge propagated by the coordination of two neutral nitrogen lone-pair donors. This arrangement would imply the presence of an unknown Cu(I)-containing impurity during synthesis, or a redox process between Cu(II) and a reducing impurity such as metallic copper or another metal in a low oxidation state. To our disappointment, efforts to grow this structure directly from Cu(I) sources such as Cu₂O, CuCl, and CuOTf have failed. It is of note that **III-11**, first isolated as yellow rod-shaped crystals, was observed to turn in color to a blue-green shade. Although this could be interpreted as a phase-change, a chemical reaction such as a redox process cannot be ruled out. A reproducible synthesis of this structure would be highly desirable, as the interchangeability of the pendant aryl ring in the synthesis of triazole **III-6** (**Scheme 3-1**) may allow for construction of closely related polymers where the inter-strand Cu-Cu gap is controlled as a function of the bulk of the aryl ring.

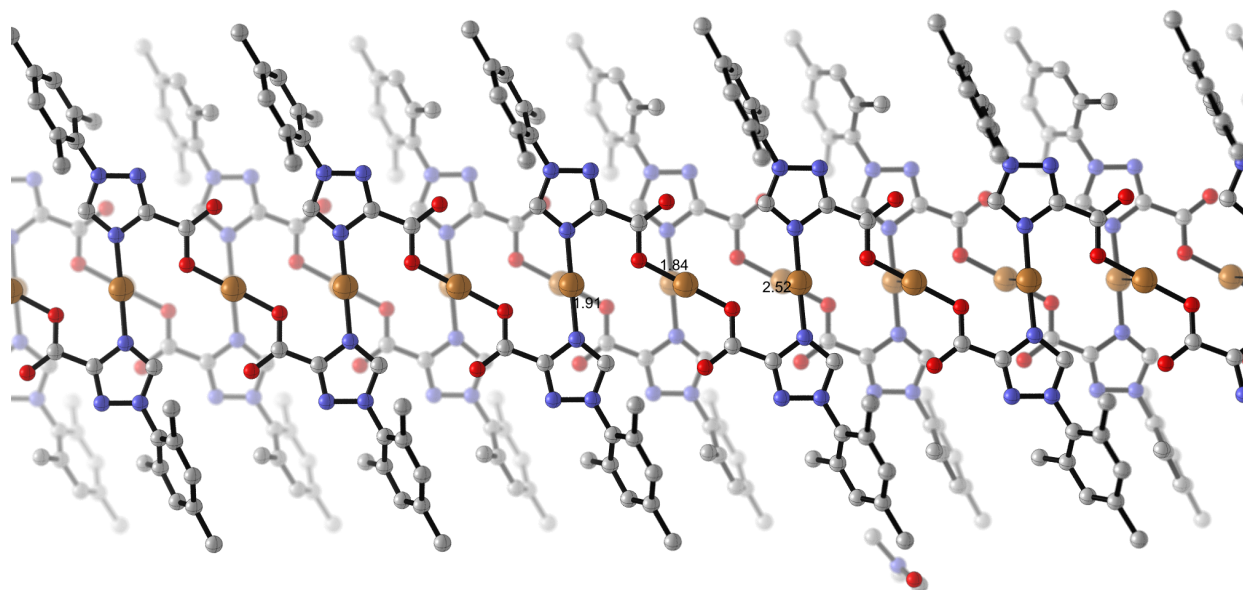


Figure 3-6. Coordination polymer III-11.

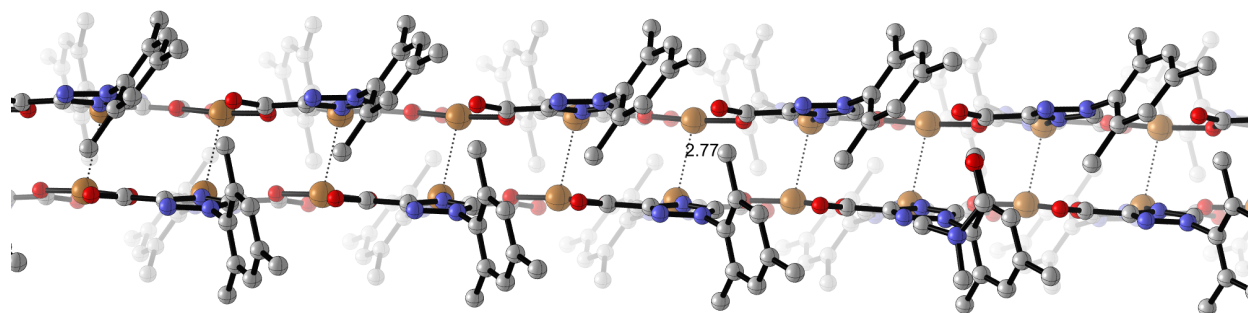
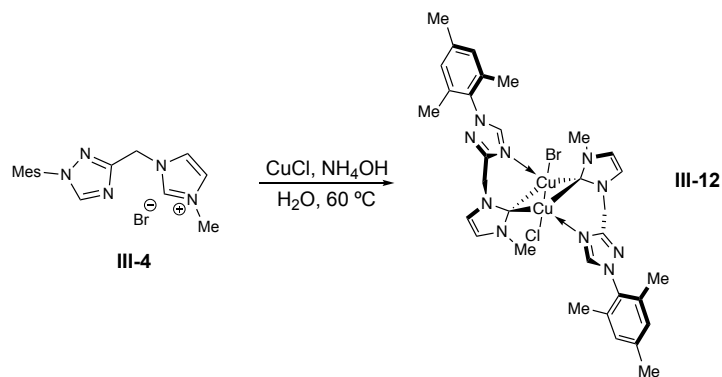


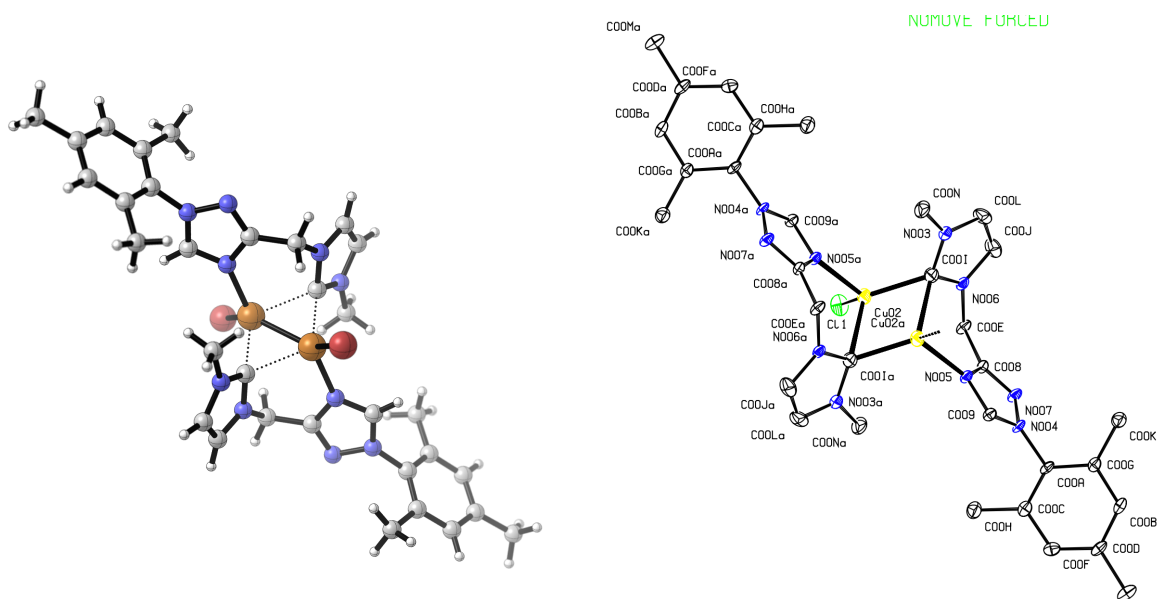
Figure 3-7. Coordination polymer III-11, rotated 90° about long axis relative to figure 3-5.

3.6 η_2 -bound Cu(I) imidazolylidene complex

Scheme 3-3. Synthesis of dinuclear Cu(I) complex **III-12**



The coordination behavior of triazoloimidazolium **III-4** with copper was also explored. Exposure of **III-4** to a suspension of CuCl in an aqueous solution of ammonia delivered complex **III-12** which were obtained as pale green crystals (**Scheme 3-3**).¹⁹³ X-ray diffraction of this compound reveals an unusual mode of coordination between the imidazolylidene motif and the bimetallic Cu(I) cluster. Here, the carbene lone pair bonds the η_2 mode to the Cu-Cu bond, creating a rhombohedral arrangement of Cu(I) and carbon (**Figure 3-8**). This type of coordination has been previously observed in a small amount of N-heteroaromatic bidentate Cu(I) complexes, although the Cu-Cu distance of 2.363(3) Å is dramatically shorter than any known examples featuring a η_2 -bound Arduengo carbene.¹⁹³⁻¹⁹⁵



Thermal ellipsoids are shown at 50% probability. Selected bond distances (Å) and angles (°): Cu02-C001 2.033(3)
 Cu02a-C001 2.276(4) Cu02-Cu02a 2.3627(8) Cu02-N005a 2.050(3) N006-C001-N003 103.3(3) N005-C009-N004
 110.0(3)

Figure 3-8. X-ray structure of compound **III-12**.

3.7 Conclusion

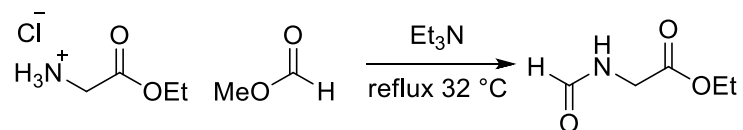
Several novel azole-Cu(I), Cu(II), Zn(II), and Co(II) compounds have been synthesized and characterized via X-ray diffraction. Although this initial set of results is small and no metal amido-NHC structure has been isolated, the unusual complexes detailed in this chapter serve as useful synthetic framework for the further exploration of this goal. Coordination polymer III-11 remains an especially intriguing target for reasons beyond realizing a N-metallated NHC due to its highly unique dual-stranded structure, likely stabilized by both a Cu(I)-Cu(I) interaction and electrostatic forces. Reliable reproduction of the synthesis of III-11 should immediately be followed by verification of the oxidation state of copper via EPR or cyclic voltammetry, whereupon attempts to control the Cu-Cu distance through modification of N-aryl steric and electronic parameters can be made.

3.8 Experimental Section

General Information

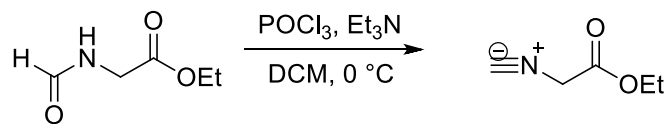
All reactions were carried out under a nitrogen atmosphere in oven-dried glassware with magnetic stirring. THF, toluene, and DMF were purified by passage through a bed of activated alumina.¹²¹ Reagents were purified prior to use unless otherwise stated following the guidelines of Perrin and Armarego.¹²² Silica gel used in flash chromatography using Silicycle SiliaFlash P60 silica gel 60 (230-400 mesh). Analytical thin layer chromatography was performed on EM Reagent 0.25 mm silica gel 60-F plates. Visualization was accomplished with UV light and ceric ammonium nitrate stain or potassium permanganate stain followed by heating. Infrared spectra were recorded on a Bruker Tensor 37 FT-IR spectrometer. ¹H NMR spectra were recorded on AVANCE III 500 MHz w/ direct cryoprobe (500 MHz) spectrometer and are reported in ppm using solvent as an internal standard (CDCl₃ at 7.26 ppm, (CD₃)₂SO at 2.50 ppm). Data are reported as (ap = apparent, s = singlet, d = doublet, t = apparent triplet, q = quartet, m = multiplet, b = broad; coupling constant(s) in Hz; integration.) Proton-decoupled ¹³C NMR spectra were recorded on an AVANCE III 500 MHz w/ direct cryoprobe (125 MHz) spectrometer and are reported in ppm using solvent as an internal standard (CDCl₃ at 77.16 ppm, (CD₃)₂SO at 39.52 ppm).. Mass spectra were obtained on a WATERS Acquity-H UPLC-MS with a single quad detector (ESI) or an Agilent 7890 gas chromatograph equipped with a 5975C single quadrupole EI-MS detector.

3.8.1 Experimental Procedures



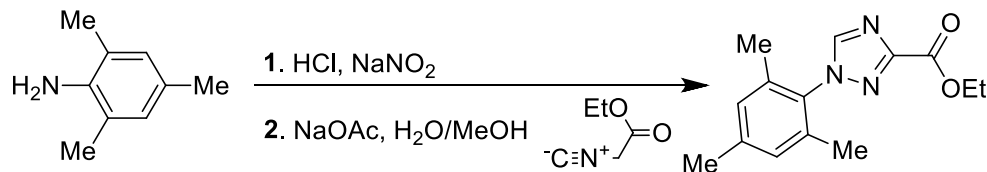
Ethyl 2-formamidoacetate

Synthesized according to literature procedure.¹⁹⁶ A 1-l., three-necked, round-bottomed flask fitted with a mechanical stirrer, a pressure-equalizing dropping funnel, and a reflux condenser bearing a calcium chloride drying tube is charged with mole) of 2-ethoxy-2-oxoethanaminium chloride (10 g, 71.6 mmol) and methyl formate (36.2 ml, 590 mmol). The suspension is stirred and heated at reflux while triethylamine (10.98 ml, 79 mmol) is added. The resulting mixture is stirred and heated under reflux for 20 hours, cooled to room temperature, and filtered through a Büchner funnel, removing triethylamine hydrochloride. The filtrate is concentrated on a rotary evaporator, and the remaining orange oil is distilled under reduced pressure, yielding ethyl 2-formamidoacetate (6 g, 45.8 mmol, 63.9 % yield), b.p. $94\text{--}97^\circ$ (0.05 mm.) as a clear oil. ^1H NMR spectrum matched literature data.



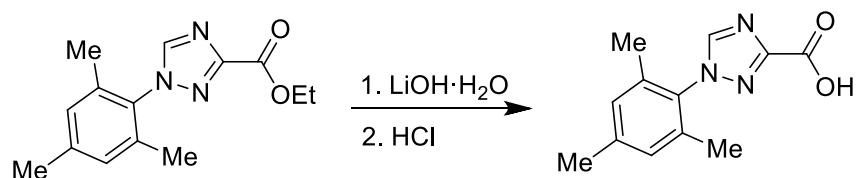
Ethyl isocyanoacetate

Synthesized according to literature procedure.¹⁹⁶ A 3-l., three-necked, round-bottomed flask equipped with a thermometer, a mechanical stirrer, and a pressure-equalizing dropping funnel bearing a nitrogen inlet is charged with ethyl 2-formamidoacetate (25 g, 191 mmol), triethylamine (65.7 ml, 471 mmol) and dichloromethane (Volume: 191 ml), and the apparatus is flushed with nitrogen. The resulting solution is stirred and cooled to 0° to -2° in an ice-salt bath, and POCl₃ (17.77 ml, 191 mmol) (Note 3) is added dropwise over 15-20 minutes while the temperature is kept at 0°. The mixture becomes reddish brown as it is stirred and cooled at 0° for an additional 1 hour. The ice-salt bath is removed and replaced by an ice-water bath. Stirring is continued as a solution of 38.2 g sodium carbonate in 153 ml of water is added dropwise at a rate such that the temperature of the mixture is maintained at 25-30° (Note 4). The two-phase mixture is stirred for another 30 minutes, after which water is added until the volume of the aqueous layer is brought to 1 l. The aqueous layer is separated and extracted with two portions of dichloromethane (95 ml, 1483 mmol). The dichloromethane solutions are combined, washed with saturated sodium chloride solution, and dried over anhydrous potassium carbonate. Evaporation of the solvent under reduced pressure and distillation of the remaining brown oil afford ethyl 2-isocyanoacetate, b.p. 89-91° (11 mm.) as a clear oil (17 g, 150 mmol, 79% yield). *Note: Glassware is freed of odor by rinsing in 5% methanolic sulfuric acid solution.* ¹H NMR spectrum matched literature data.



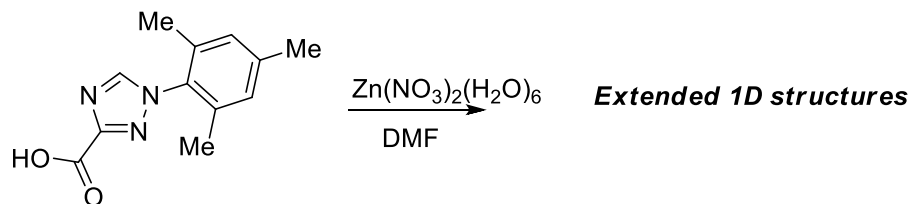
Ethyl 1-mesityl-1H-1,2,4-triazole-3-carboxylate (III-3)

Synthesized according to a modified literature procedure.¹⁹⁷ A three-necked 50 mL round-bottom flask was equipped with a thermometer, nitrogen inlet, and septum and purged with N₂ gas for 15 minutes. To this flask was added 2,4,6-trimethylaniline (9.5 g, 70.3 mmol) dissolved in a mixture of 37.6 ml water and hydrochloric acid (20.68 ml, 680 mmol, conc. 38%) whereupon the stirring solution was cooled down to 0°C in an ice/salt bath. A solution of sodium nitrite (4.85 g, 70.3 mmol) in 3.76 ml of water was added to the solution of 2,4,6-trimethylaniline dropwise maintaining temperature of the solution in 0 - 5 °C range. After addition was complete, the mixture was stirred for 5 min at 0 °C. The solution of diazonium salt was added dropwise to the mixture of sodium acetate trihydrate (61.7 g, 451 mmol) and ethyl 2-isocyanoacetate (7.14 g, 63.1 mmol) in a MeOH/H₂O mixture (75 ml:7.51 ml). The temperature of the reaction mixture was maintained between 0 °C and 5 °C. After addition of a final portion of the diazonium solution, reaction mixture was stirred at 0°C for 30 min, warmed up to ambient temperature, and stirred for additional 3 hours. After formation of significant amount of red precipitate, the mixture was transferred to a round bottom flask and most of methanol was removed in vacuo. The remaining suspension of 1,2,4-triazole in water was filtered and remaining solid precipitate was washed with cold water. Titration with diethyl ether and recrystallization of the remaining solid in benzene afforded ethyl 1-mesityl-1H-1,2,4-triazole-3-carboxylate (9.1 g, 35.1 mmol, 55.6 % yield). Analytical data: ¹H NMR (500 MHz, CDCl₃) δ 8.18 (s, 1H), 6.98 (s, 2H), 4.52 (q, J = 7.1 Hz, 2H), 2.34 (s, 3H), 1.98 (s, 6H), 1.46 (t, J = 7.1 Hz, 3H).



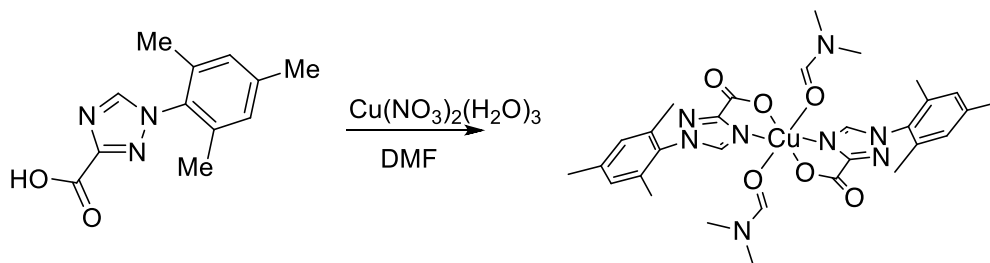
1-mesityl-1H-1,2,4-triazole-3-carboxylic acid (III-4)

A mixture of ethyl 1-mesityl-1H-1,2,4-triazole-3-carboxylate (2 g, 7.71 mmol) and lithium hydroxide monohydrate (0.377 g, 7.71 mmol) in MeOH (Ratio: 3) and water (Ratio: 1.000) was stirred at room temperature overnight. The reaction was concentrated under reduced pressure. Upon acidification with conc. HCl to ~pH 1, a pink ppt was formed. The ppt was isolated by filtration and washed with Et₂O (4 x 10 mL). Yield = 0.659 g (85%). ¹H NMR (500 MHz, DMSO-*d*₆) δ 13.50 (s, 1H), 8.89 (s, 1H), 7.11 (s, 2H), 2.33 (s, 3H), 1.92 (s, 6H). ¹³C NMR (126 MHz, DMSO-*d*₆) δ 160.81, 155.47, 147.32, 139.71, 134.77, 132.81, 128.91, 20.62, 16.84. LCMS (ESI) *m/z* = 463.40 [2M+1]⁺.



Extended 1D Zn(II) Structures

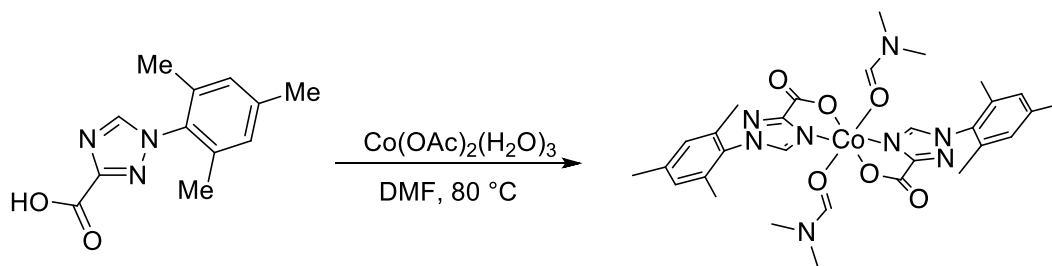
As a solution in 0.5 mL DMF, 1-mesityl-1*H*-1,2,4-triazole-3-carboxylic acid (135 mg, 0.584 mmol) was added to bis(nitroxy)zinc hexahydrate (83 mg, 0.278 mmol) in 0.5 mL DMF while stirring at 23 °C. No precipitate was immediately observed. The static solution was placed in an oven at 80 °C. After 48 hours, two types of crystals were found inside the reaction vial and were analyzed by XRD. Both are poorly soluble 1-D structures in solid state. The coordination environment around the Zn centres are similar, but distinct. The structures could not be refined to a publishable quality but do display valid connectivity data.



Cu(II) Triazole-carboxylate complex and Cu(I) 2D Polymer (III-7) (III-11)

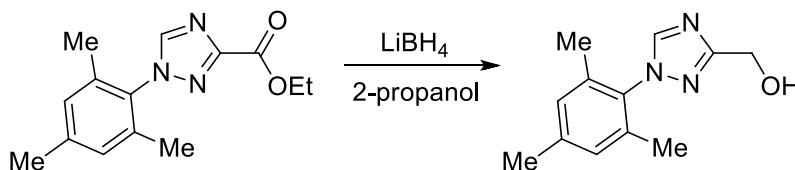
As a solution in 0.5 mL DMF, 1-mesityl-1*H*-1,2,4-triazole-3-carboxylic acid (135 mg, 0.584 mmol) was added to bis(nitroxy)copper trihydrate (67.2 mg, 0.278 mmol) in 0.5 mL DMF while stirring at 23 °C. No precipitate was immediately observed. The static solution was placed in an oven at 80 °C. After 48 hours, two types of crystals were found inside the reaction vial and

were analyzed by XRD. 28 are aqua-blue plates. 28a originally appeared as yellow rods, but changed color to appear as blue-green rods. They are composed of extended 1D structures.



Co(II) Triazole-carboxylate complex (III-8)

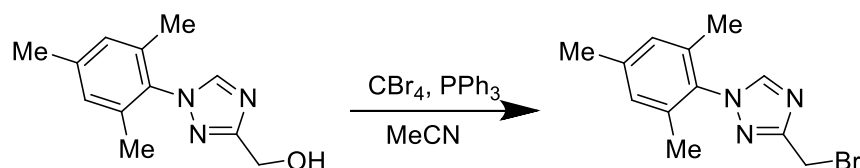
As a solution in 0.5 mL DMF, 1-mesityl-1H-1,2,4-triazole-3-carboxylic acid (135 mg, 0.584 mmol) was added to diacetoxycobalt trihydrate (64.2 mg, 0.278 mmol) in 0.5 mL DMF while stirring at 23 °C. No precipitate was immediately observed, however solution immediately changed from the violet color characteristic of cobalt acetate trihydrate to a deep blue color. The static solution was placed in an oven at 80 °C. After one day, the formation of tan crystals was observed, and an XRD structure was obtained.



(1-mesityl-1H-1,2,4-triazol-3-yl)methanol

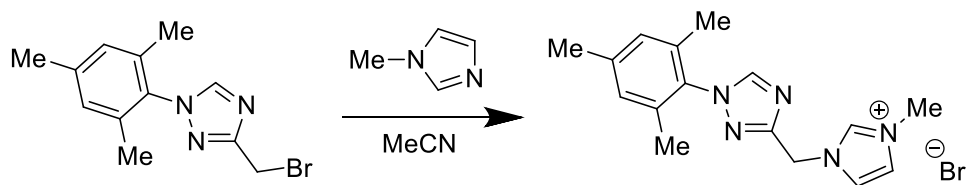
A mixture of LiBH_4 (0.422 g, 19.36 mmol) in 2-propanol (Volume: 38.7 ml) under N_2 was treated with ethyl 1-mesityl-1H-1,2,4-triazole-3-carboxylate (2.51 g, 9.68 mmol) at room temperature. The reaction was stirred at room temperature overnight. The mixture was treated

with 30 mL of water and stirred to decompose the excess LiBH_4 . The residuals were suspended in $\text{CH}_3\text{OH}/\text{H}_2\text{O}$ and adsorbed onto silica gel at reduced pressure. The material was chromatographed with silica gel packed with $\text{CHCl}_3\text{-CH}_3\text{OH}$ (92:8) and eluted with increasing CH_3OH gradient to 12% to obtain product. Titration with Et_2O gave (1-mesityl-1H-1,2,4-triazol-3-yl)methanol (1.0 g, 4.60 mmol, 47.5 % yield). ^1H NMR (500 MHz, CDCl_3) δ 8.08 (s, 1H), 6.98 (s, 2H), 4.87 (d, $J = 6.1$ Hz, 2H), 2.34 (s, 3H), 1.99 (s, 6H).



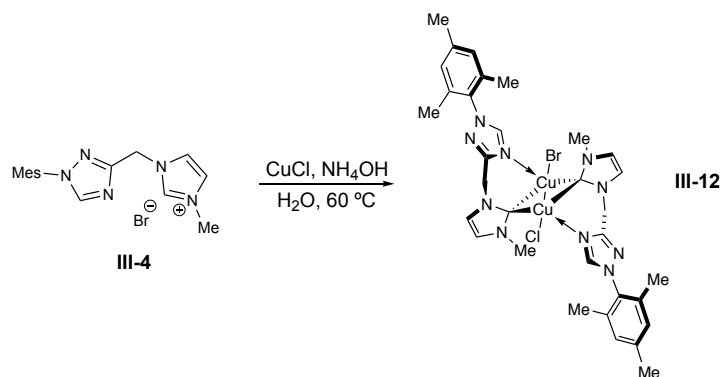
3-(bromomethyl)-1-mesityl-1H-1,2,4-triazole

To a stirring solution of (1-mesityl-1H-1,2,4-triazol-3-yl)methanol (0.52 g, 2.393 mmol) and TRIPHENYLPHOSPHINE (0.753 g, 2.87 mmol) in acetonitrile (Volume: 7.27 ml) at 0°C under nitrogen atmosphere was added CARBON TETRABROMIDE (0.952 g, 2.87 mmol) portionwise. The mixture was stirred at 23°C for 12 hours, concentrated in vacuo, and purified by flash chromatography on silica gel (4:6 ethyl acetate:hexanes) to yield 3-(bromomethyl)-1-mesityl-1H-1,2,4-triazole (0.502 g, 1.792 mmol, 74.9 % yield) as an oil which crystallized as a tan white solid upon drying under high vacuum. ^1H NMR (500 MHz, CDCl_3) δ 8.07 (s, 1H), 6.97 (s, 2H), 4.58 (s, 2H), 2.34 (s, 3H), 1.99 (s, 6H). ^{13}C NMR (126 MHz, CDCl_3) δ 161.55, 145.70, 140.26, 135.56, 132.98, 129.27, 23.19, 21.26, 17.50. LCMS (ESI) $m/z = 280, 282$ $[\text{M}+1]^+$.



1-((1-mesityl-1H-1,2,4-triazol-3-yl)methyl)-3-methyl-1H-imidazol-3-ium bromide (III-6)

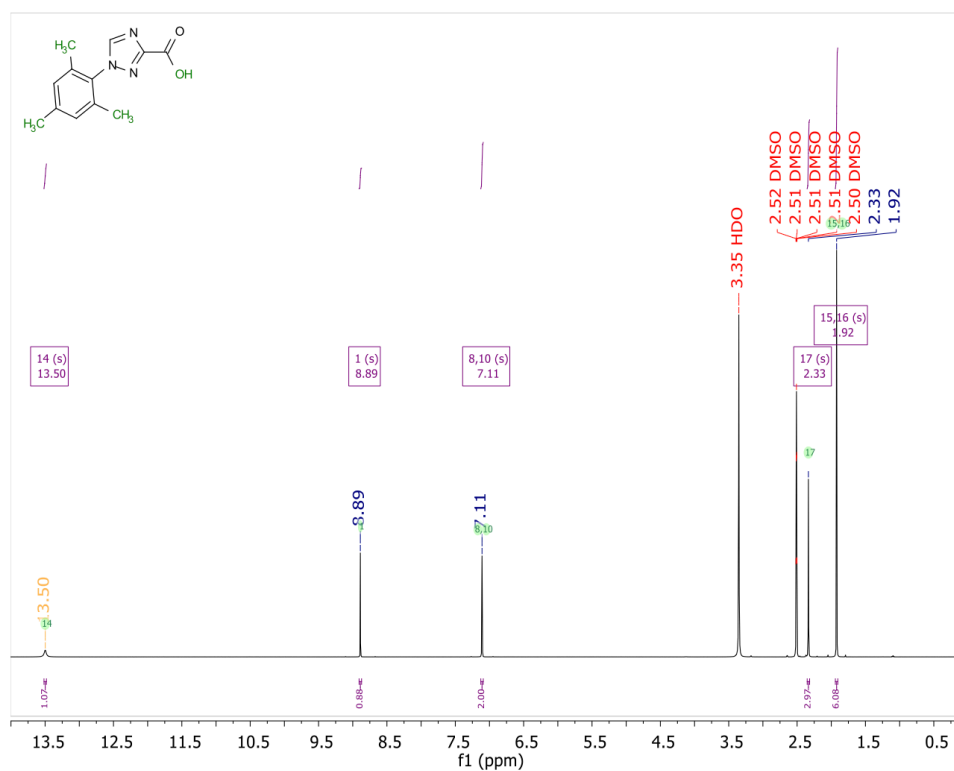
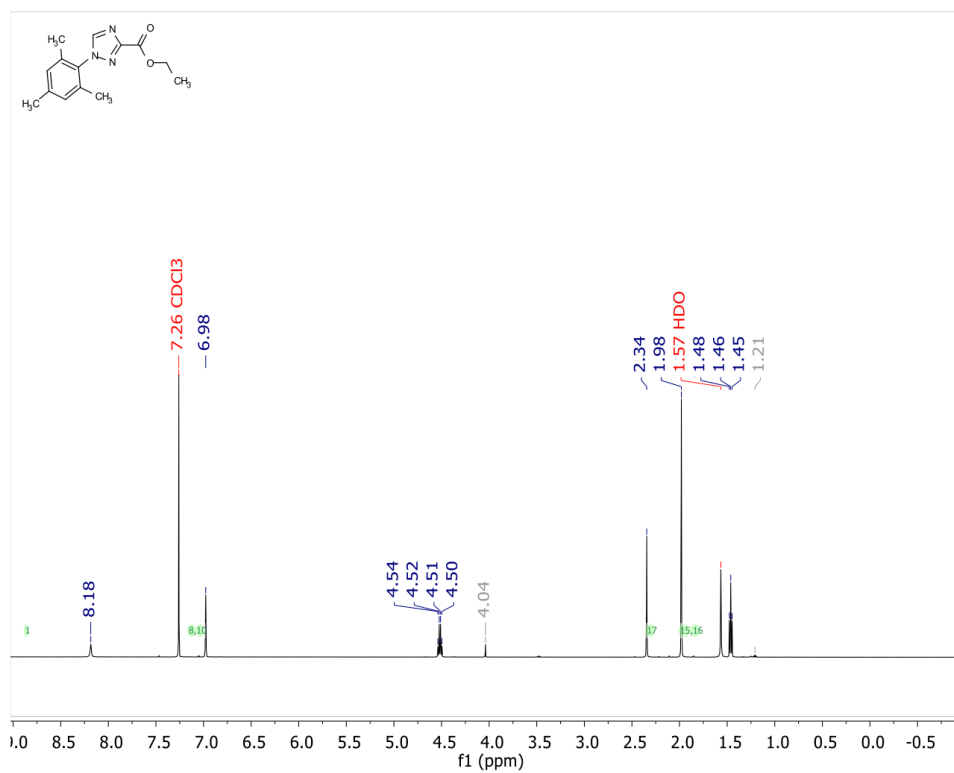
To a stirring solution of 3-(bromomethyl)-1-mesityl-1H-1,2,4-triazole (.5 g, 1.785 mmol) in MeCN (Volume: 2.231 ml) was added 1-methylimidazole (0.142 ml, 1.785 mmol) under nitrogen. The mixture was refluxed for 1 h, whereupon a white solid was observed to precipitate. After cooling to room temperature, the precipitate was collected via filtration and washed with cold diethyl ether to yield 1-((1-mesityl-1H-1,2,4-triazol-3-yl)methyl)-3-methyl-1H-imidazol-3-ium bromide (244 mg, 0.674 mmol, 37.7 % yield) as a pure white solid. An additional amount of precipitate may be collected upon letting the filtrate stand in a -30 °C freezer overnight. Analytical data: ^1H NMR (500 MHz, CDCl_3) δ 10.62 (s, 1H), 8.11 (s, 1H), 7.65 – 7.49 (m, 1H), 7.45 (s, 1H), 6.96 (s, 2H), 5.76 (s, 2H), 4.15 (s, 3H), 2.33 (s, 3H), 1.94 (s, 6H). ^{13}C NMR (126 MHz, CDCl_3) δ 157.69, 146.26, 140.60, 138.50, 135.33, 132.61, 129.40, 123.79, 122.21, 47.12, 37.11, 21.23, 17.60. LCMS (ESI) $m/z = 282$ $[\text{M}]^+$.

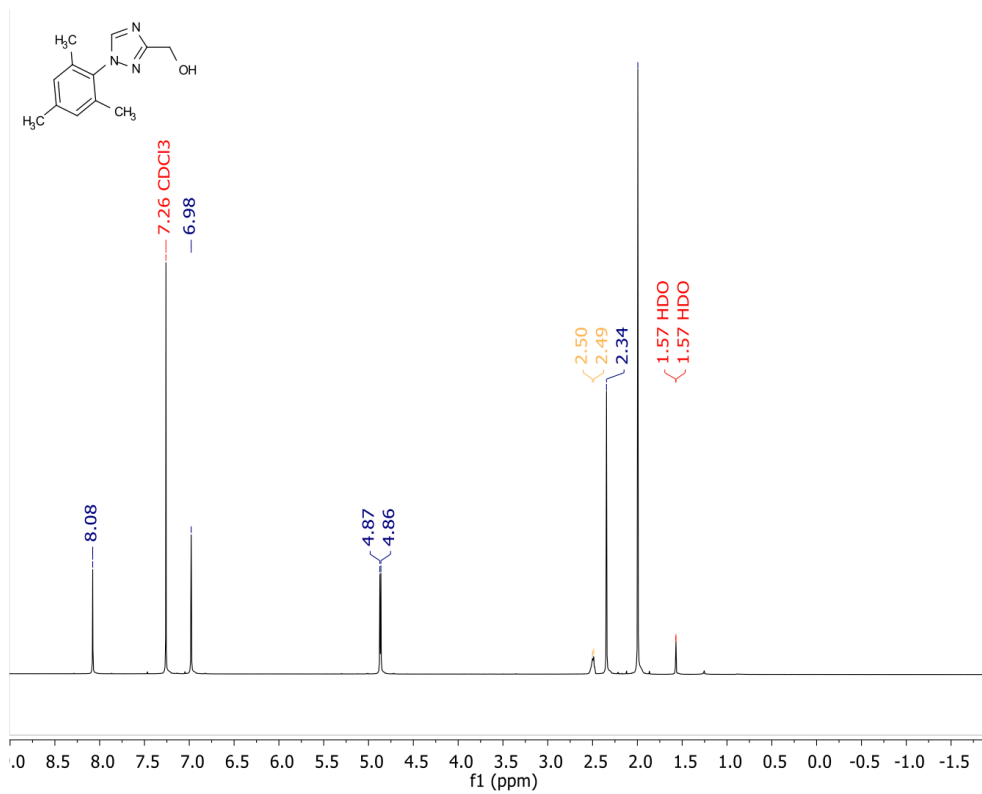
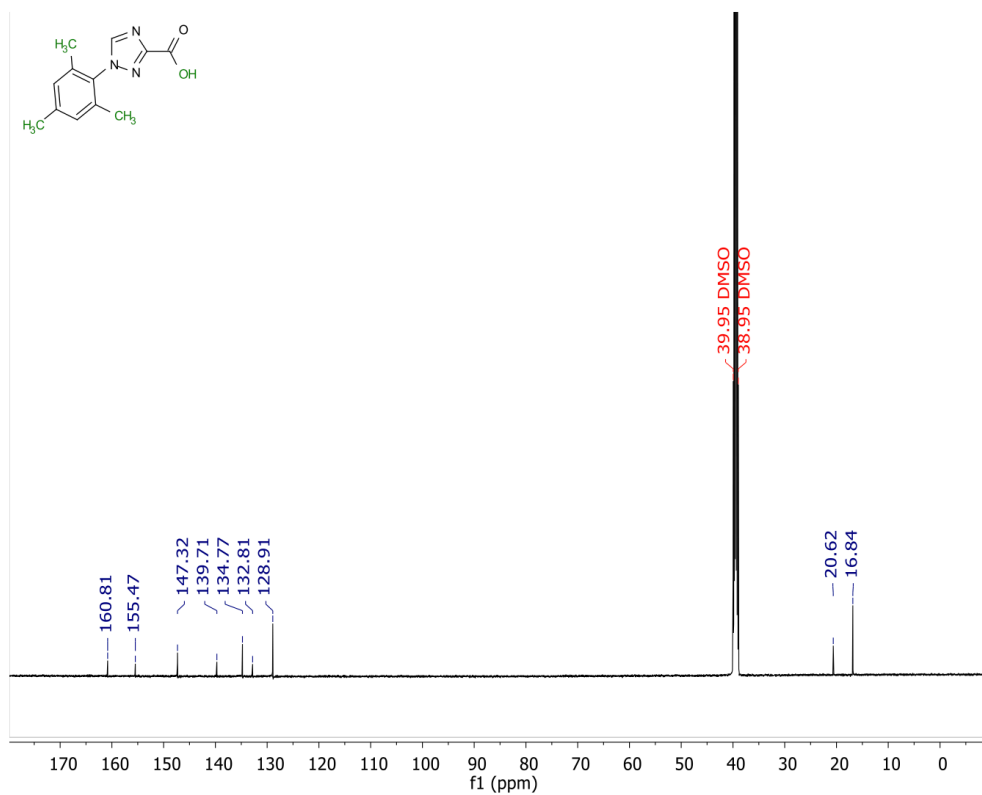


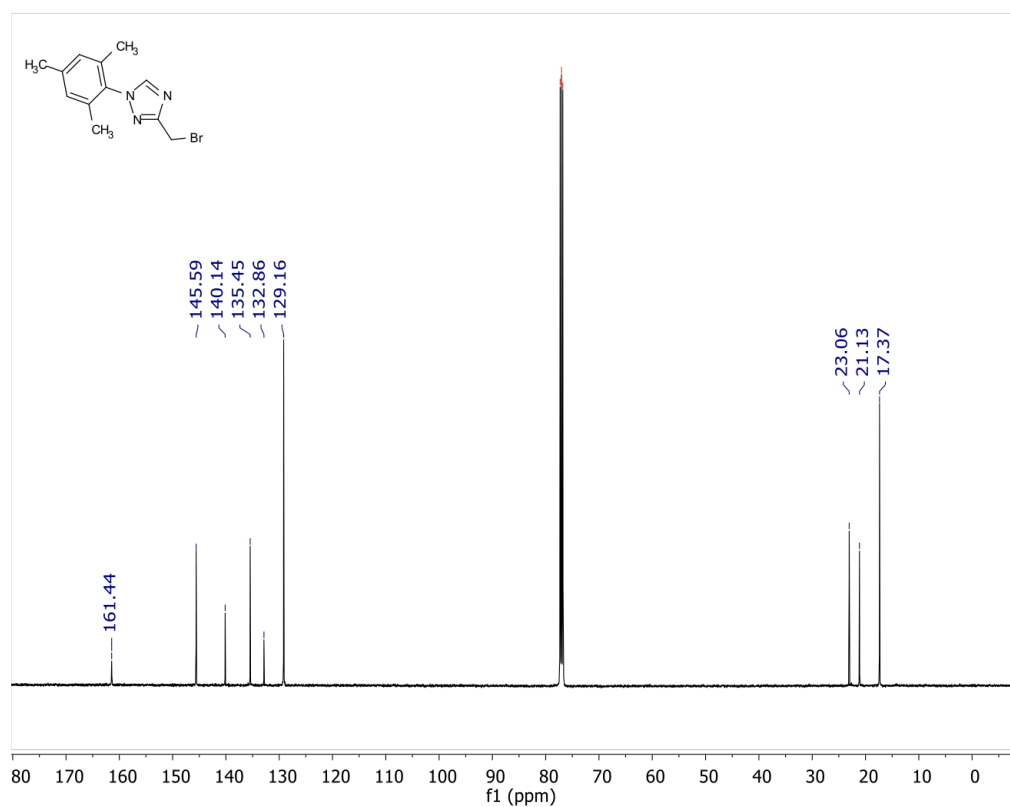
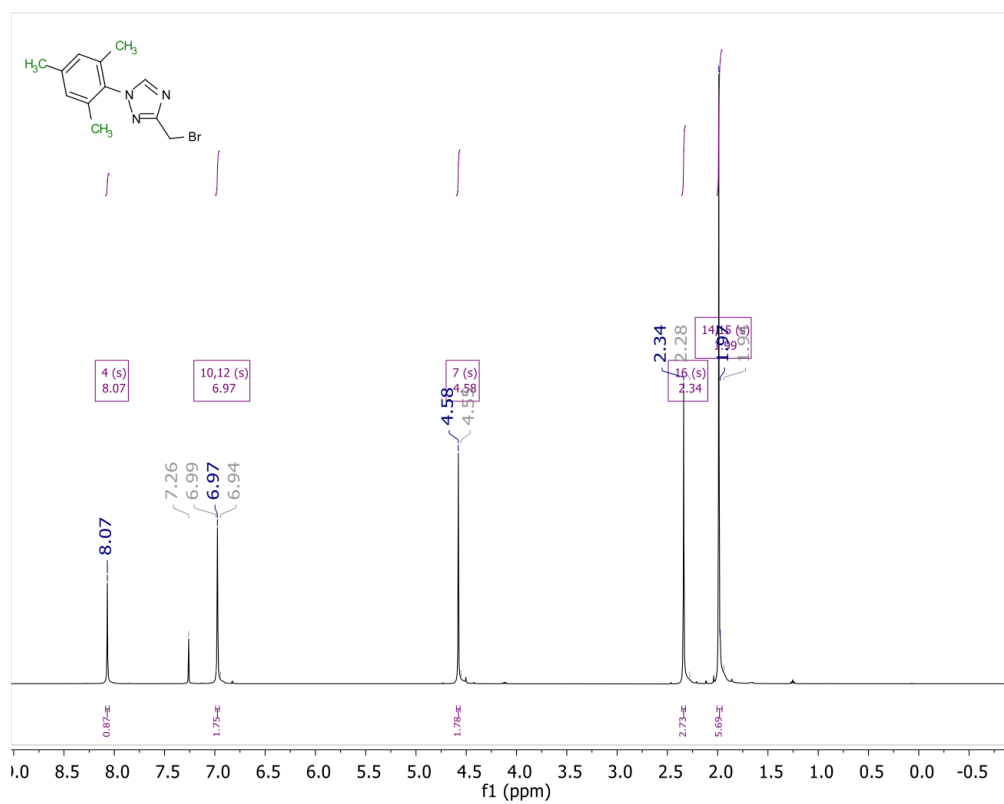
Dinuclear Cu(I) complex III-12

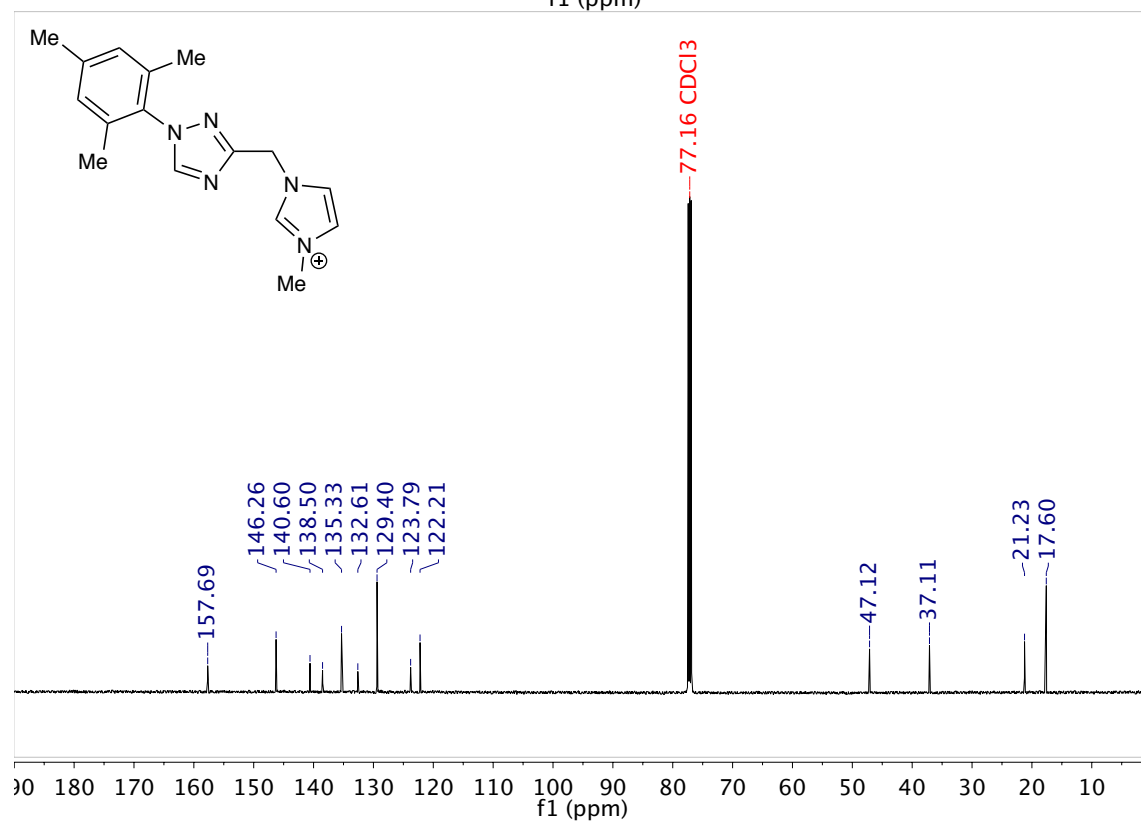
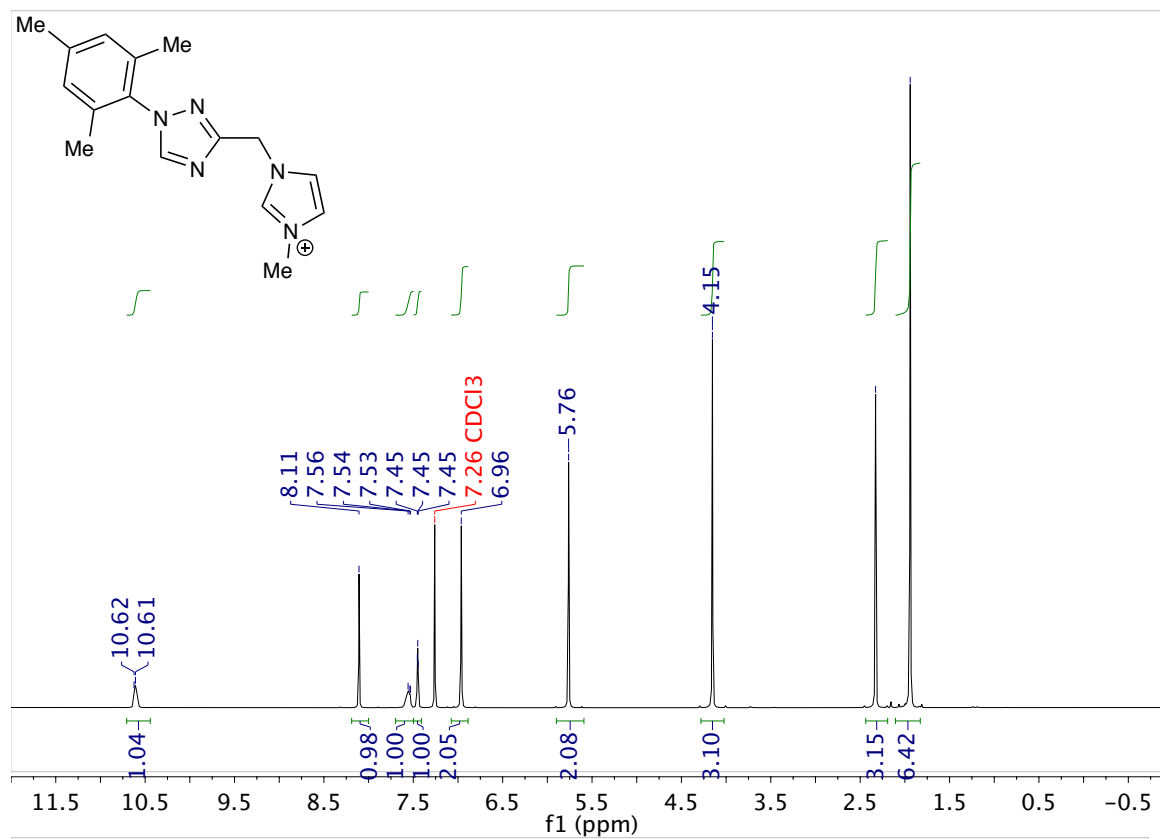
Synthesized according to literature procedure.¹⁹³ The imidazolium bromide (1 mmol) was suspended in 10 mL of water. The corresponding copper halide (1.5 mmol, 1.5 equiv) was added, and the flask was stoppered and degassed by bubbling argon for 5 min. Then, 382 μL of aqueous ammonia (15.7 mol L⁻¹, 6 equiv) was added with a syringe through the stopper, and the reaction vessel was degassed for 1 more minute. The mixture was stirred vigorously for 1 h at 60 °C. The reaction mixture was transferred to a separating funnel containing 10 mL of dichloromethane. Extraction was performed three times (while extracting, the aqueous layer assumed the deep blue color characteristic of Cu(II)-ammine complexes). The combined organic phases were dried (K₂CO₃, this agent also absorbing traces of Cu(II) and evaporated. Small, pale green crystals were collected for analysis via X-ray diffraction.

3.8.2 Selected NMR Spectra







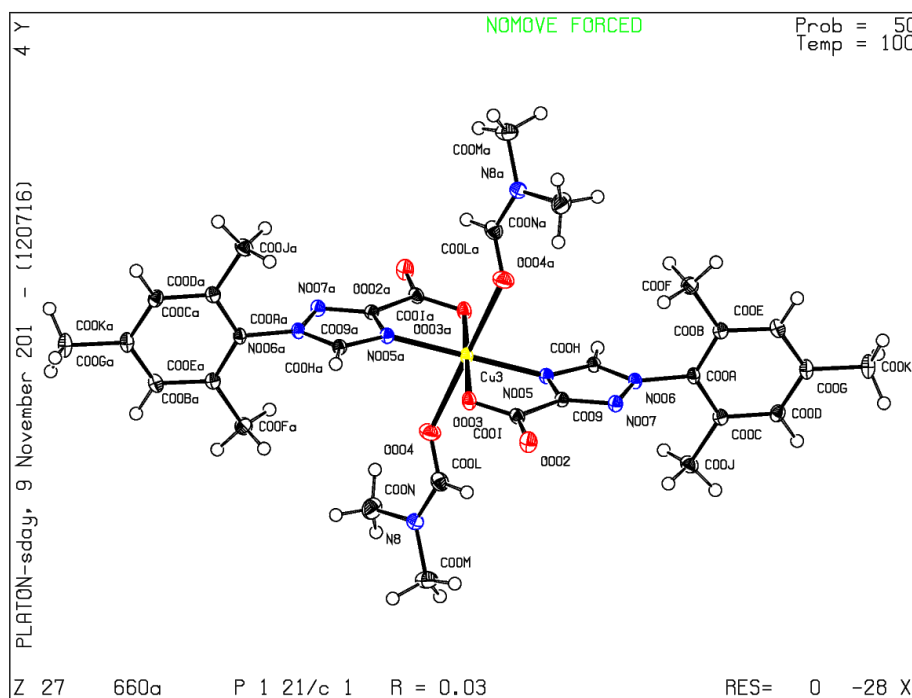


3.8.3 X-ray Crystal Structure Data

Cu(II) Triazole-carboxylate complex (III-7)

Single crystals of $C_{30}H_{38}CuN_8O_6$ were supplied. A suitable crystal was selected and mounted in inert oil and transferred to the cold gas stream of a Bruker APEX-II CCD diffractometer. The crystal was kept at 99.99 K during data collection. Using Olex2 [1], the structure was solved with the ShelXT [2] structure solution program using Direct Methods and refined with the ShelXL [3] refinement package using Least Squares minimisation.

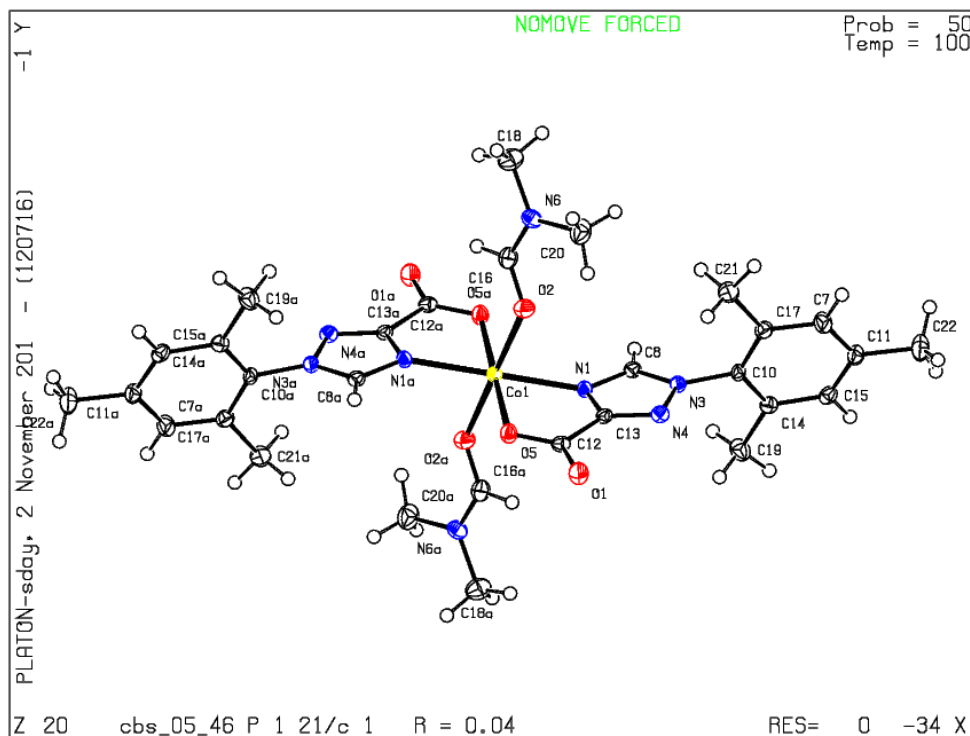
Crystal Data for $C_{30}H_{38}CuN_8O_6$ ($M=670.22$): monoclinic, space group $P2_1/c$ (no. 14), $a = 13.0633(4)$ Å, $b = 15.8109(5)$ Å, $c = 7.6182(3)$ Å, $\beta = 96.478(2)^\circ$, $V = 1563.44(9)$ Å³, $Z = 2$, $T = 99.99$ K, $\mu(\text{MoK}\alpha) = 0.755$ mm⁻¹, $D_{\text{calc}} = 1.424$ g/mm³, 41602 reflections measured ($3.138 \leq 2\theta \leq 61.16$), 4793 unique ($R_{\text{int}} = 0.0365$, $R_{\text{sigma}} = 0.0206$) which were used in all calculations. The final R_1 was 0.0308 ($I > 2\sigma(I)$) and wR_2 was 0.0987 (all data).



Co(II) Triazole-carboxylate complex (III-8)

Single crystals of $C_{30}H_{38}CoN_8O_6$ were supplied. A suitable crystal was selected and mounted in inert oil and transferred to the cold gas stream of a 'Bruker APEX-II CCD' diffractometer. The crystal was kept at 100.07 K during data collection. Using Olex2 [1], the structure was solved with the ShelXT [2] structure solution program using Intrinsic Phasing and refined with the ShelXL [3] refinement package using Least Squares minimisation.

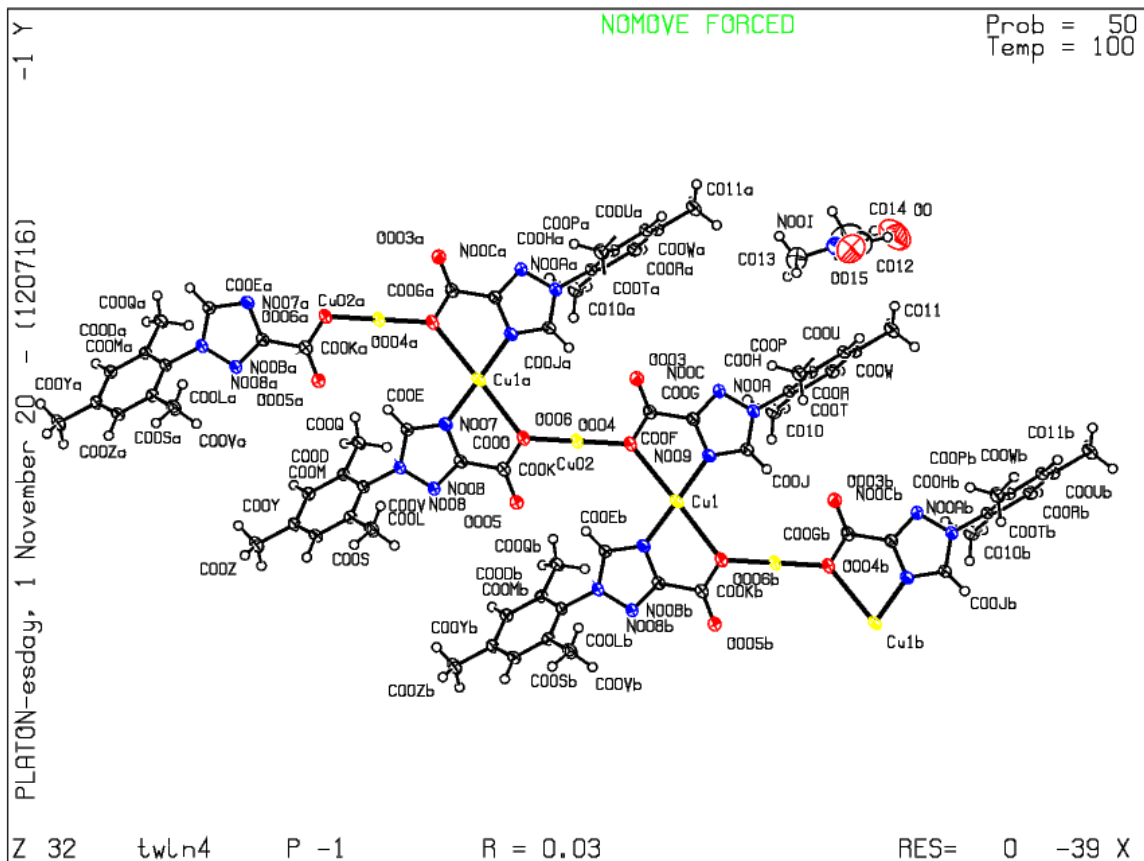
Crystal Data for $C_{30}H_{38}CoN_8O_6$ ($M=665.61$): monoclinic, space group $P2_1/c$ (no. 14), $a = 13.4769(6)$ Å, $b = 15.4027(8)$ Å, $c = 7.5918(3)$ Å, $\beta = 97.518(2)^\circ$, $V = 1562.36(12)$ Å³, $Z = 2$, $T = 100.07$ K, $\mu(\text{CuK}\alpha) = 4.779$ mm⁻¹, $D_{\text{calc}} = 1.415$ g/mm³, 10196 reflections measured ($6.616 \leq 2\theta \leq 130.148$), 2649 unique ($R_{\text{int}} = 0.0577$, $R_{\text{sigma}} = 0.0363$) which were used in all calculations. The final R_1 was 0.0430 ($I > 2\sigma(I)$) and wR_2 was 0.1177 (all data).



Cu(I) 2D Polymer (III-11)

Single crystals of $C_{27}H_{31}Cu_2N_7O_5$ polymer III-11 were supplied. A suitable crystal was selected and mounted in inert oil and transferred to the cold gas stream of a 'Bruker APEX-II CCD' diffractometer. The crystal was kept at 100.02 K during data collection. Using Olex2 [1], the structure was solved with the ShelXT [2] structure solution program using Intrinsic Phasing and refined with the XL [3] refinement package using Least Squares minimisation.

Crystal Data for $C_{27}H_{31}Cu_2N_7O_5$ ($M=745.23$): triclinic, space group P-1 (no. 2), $a = 7.9479(8)$ Å, $b = 13.5728(14)$ Å, $c = 13.7744(15)$ Å, $\alpha = 99.854(2)^\circ$, $\beta = 100.725(2)^\circ$, $\gamma = 100.537(2)^\circ$, $V = 1402.6(3)$ Å³, $Z = 2$, $T = 100.02$ K, $\mu(\text{CuK}\alpha) = 11.101$ mm⁻¹, $D_{\text{calc}} = 1.765$ g/mm³, 4736 reflections measured ($8.45 \leq 2\Theta \leq 130.184$), 4736 unique ($R_{\text{int}} = ?$, $R_{\text{sigma}} = 0.0197$) which were used in all calculations. The final R_1 was 0.0334 ($I > 2\sigma(I)$) and wR_2 was 0.0926 (all data).

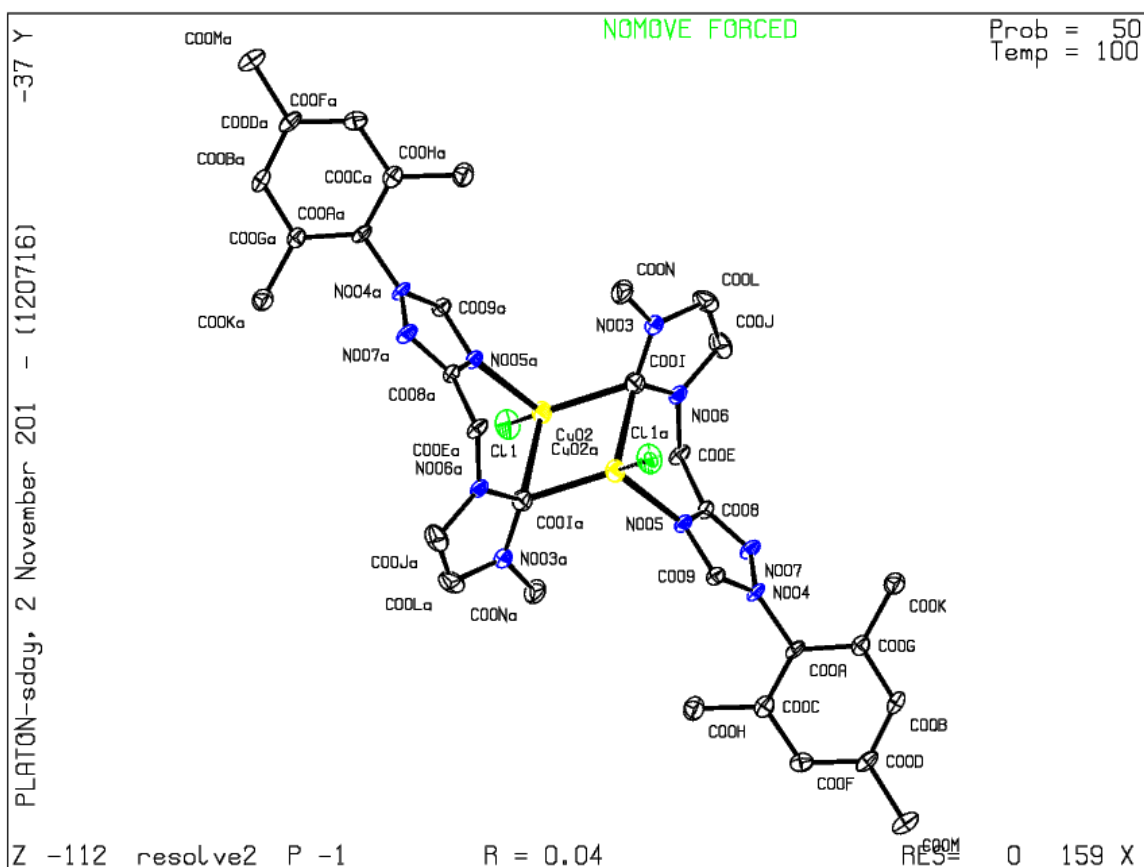


Dinuclear Cu(I) complex III-12

Single crystals of $C_{32}H_{38}Br_{1.06}Cl_{0.94}Cu_2N_{10}$ were supplied. A suitable crystal was selected and mounted in inert oil and transferred to the cold gas stream of a 'Bruker APEX-II CCD' diffractometer. The crystal was kept at 99.98 K during data collection. Using Olex2 [1], the

structure was solved with the ShelXT [2] structure solution program using Intrinsic Phasing and refined with the ShelXL [3] refinement package using Least Squares minimisation.

Crystal Data for $C_{32}H_{38}Br_{1.06}Cl_{0.94}Cu_2N_{10}$ ($M=805.16$): triclinic, space group P-1 (no. 2), $a = 7.6421(2)$ Å, $b = 10.1781(3)$ Å, $c = 11.4955(3)$ Å, $\alpha = 74.967(2)^\circ$, $\beta = 71.140(2)^\circ$, $\gamma = 81.977(2)^\circ$, $V = 815.66(4)$ Å³, $Z = 1$, $T = 99.98$ K, $\mu(\text{CuK}\alpha) = 4.121$ mm⁻¹, $D_{\text{calc}} = 1.639$ g/mm³, 7040 reflections measured ($8.348 \leq 2\theta \leq 129.792$), 2734 unique ($R_{\text{int}} = 0.0167$, $R_{\text{sigma}} = 0.0194$) which were used in all calculations. The final R_1 was 0.0369 ($I > 2\sigma(I)$) and wR_2 was 0.0820 (all data).



References:

1. Wang, F.; Liu, L.-j.; Wang, W.; Li, S.; Shi, M. *Coord. Chem. Rev.* **2012**, *256*, 804–853.
2. Hock, S. J.; Schaper, L.-A.; Herrmann, W. A.; Kuhn, F. E. *Chem. Soc. Rev.* **2013**, *42*, 5073–5089.
3. Bellemin-Laponnaz, S.; Dagorne, S. *Chem. Rev.* **2014**, *114*, 8747–8774.
4. Wang, Z.; Jiang, L.; Mohamed, D. K. B.; Zhao, J.; Hor, T. S. A. *Coord. Chem. Rev.* **2015**, *293–294*, 292–326.
5. Zhang, D.; Zi, G. *Chem. Soc. Rev.* **2015**, *44*, 1898–1921.
6. Bugaut, X.; Glorius, F. *Chem. Soc. Rev.* **2012**, *41*, 3511–3522.
7. Grossmann, A.; Enders, D. *Angew. Chem. Int. Ed.* **2012**, *51*, 314–325.
8. Ryan, S. J.; Candish, L.; Lupton, D. W. *Chem. Soc. Rev.* **2013**, *42*, 4906–4917.
9. Hopkinson, M. N.; Richter, C.; Schedler, M.; Glorius, F. *Nature* **2014**, *510*, 485–496.
10. Flanigan, D. M.; Romanov-Michailidis, F.; White, N. A.; Rovis, T. *Chem. Rev.* **2015**, *115*, 9307–9387.
11. Bhunia, A.; Thorat, S.; Gonnade, R. G.; Biju, A. T. *Chem. Commun.* **2015**, *51*, 13690–13693.
12. Du, G.-F.; Guo, H.; Wang, Y.; Li, W.-J.; Shi, W.-J.; Dai, B. *Journal of Saudi Chemical Society* **2015**, *19*, 112–115.
13. Furfari, S. K.; Gyton, M. R.; Twycross, D.; Cole, M. L. *Chem. Commun.* **2015**, *51*, 74–76.
14. Lummiss, J. A. M.; Higman, C. S.; Fyson, D. L.; McDonald, R.; Fogg, D. E. *Chem. Sci.* **2015**, *6*, 6739–6746.

15. Naumann, S.; Dove, A. P. *Polymer Chemistry* **2015**, *6*, 3185–3200.
16. Snider, B. B. *J. Chem. Educ.* **2015**, *92*, 1394–1397.
17. Ungureanu, A.; Levens, A.; Candish, L.; Lupton, D. W. *Angew. Chem.* **2015**, *127*, 11946–11950.
18. Cramer, D. L.; Bera, S.; Studer, A. *Chem. - Eur. J.* **2016**, *22*, 7403–7407.
19. Di Marco, L.; Hans, M.; Delaude, L.; Monbaliu, J.-C. M. *Chem. - Eur. J.* **2016**, *22*, 4508–4514.
20. Naumann, S.; Dove, A. P. *Polym. Int.* **2016**, *65*, 16–27.
21. Gade, L. H.; Bellemin-Laponnaz, S. Chiral N-Heterocyclic Carbenes as Stereodirecting Ligands in Asymmetric Catalysis. In *N-Heterocyclic Carbenes in Transition Metal Catalysis*; Springer Berlin Heidelberg: Berlin, Heidelberg, 2007; pp 117–157.
22. Wagschal, S.; Mercier, A.; Kündig, E. P. *Organometallics* **2013**, *32*, 7133–7140.
23. Deng, R.; Huang, Y.; Ma, X.; Li, G.; Zhu, R.; Wang, B.; Kang, Y.-B.; Gu, Z. *J. Am. Chem. Soc.* **2014**, *136*, 4472–4475.
24. Akagawa, K.; Akiyama, M.; Kudo, K. *Eur. J. Org. Chem.* **2015**, *2015*, 3894–3898.
25. Arae, S.; Nakajima, K.; Takahashi, T.; Ogasawara, M. *Organometallics* **2015**, *34*, 1197–1202.
26. Arae, S.; Ogasawara, M. *Tetrahedron Lett.* **2015**, *56*, 1751–1761.
27. Cassar, D. J.; Roghzai, H.; Villemin, D.; Horton, P. N.; Coles, S. J.; Richards, C. J. *Organometallics* **2015**, *34*, 2953–2961.
28. Chen, J.; Murillo Parra, D. A.; Lalancette, R. A.; Jäkle, F. *Angew. Chem. Int. Ed.* **2015**, *54*, 10202–10205.

29. Gao, D.-W.; Gu, Q.; You, S.-L. *J. Am. Chem. Soc.* **2016**, *138*, 2544–2547.
30. Colacot, T. *J. Chem. Rev.* **2003**, *103*, 3101–3118.
31. Atkinson, R. C. J.; Gibson, V. C.; Long, N. J. *Chem. Soc. Rev.* **2004**, *33*, 313–328.
32. Gómez Arrayás, R.; Adrio, J.; Carretero, J. C. *Angew. Chem. Int. Ed.* **2006**, *45*, 7674–7715.
33. *Chiral Ferrocenes in Asymmetric Catalysis: Synthesis and Applications*; Dai, L.-X.; Hou, X.-L., Eds.; Chiral Ferrocenes in Asymmetric Catalysis: Synthesis and Applications; Wiley-VCH: Weinheim, Germany, Wiley-VCH: Weinheim, Germany.
34. Drusan, M.; Šebesta, R. *Tetrahedron* **2014**, *70*, 759–786.
35. Ogasawara, M.; Tseng, Y.-Y.; Arae, S.; Morita, T.; Nakaya, T.; Wu, W.-Y.; Takahashi, T.; Kamikawa, K. *J. Am. Chem. Soc.* **2014**, *136*, 9377–9384.
36. Schaarschmidt, D.; Grumbt, M.; Hildebrandt, A.; Lang, H. *Eur. J. Org. Chem.* **2014**, *2014*, 6676–6685.
37. Zhang, X.; Ma, P.; Zhang, D.; Lei, Y.; Zhang, S.; Jiang, R.; Chen, W. *Org. Biomol. Chem.* **2014**, *12*, 2423–2426.
38. Biosca, M.; Coll, M.; Lagarde, F.; Brémond, E.; Routaboul, L.; Manoury, E.; Pàmies, O.; Poli, R.; Diéguez, M. *Tetrahedron* **2015**.
39. Han, F.-Z.; Yu, S.-B.; Zhang, C.; Hu, X.-P. *Tetrahedron* **2015**.
40. Lee, T.; Wilson, T. W.; Berg, R.; Ryberg, P.; Hartwig, J. F. *J. Am. Chem. Soc.* **2015**, *137*, 6742–6745.
41. Schrapel, C.; Peters, R. *Angew. Chem. Int. Ed.* **2015**, *54*, 10289–10293.

42. Sorádová, Z.; Máziková, J.; Mečiarová, M.; Šebesta, R. *Tetrahedron: Asymmetry* **2015**, *26*, 271–275.
43. Bauer, J. M.; Frey, W.; Peters, R. *Chem. - Eur. J.* **2016**, n/a–n/a.
44. Kumar, D.; Deb, M.; Singh, J.; Singh, N.; Keshav, K.; Elias, A. J. *Coord. Chem. Rev.* **2016**, *306, Part 1*, 115–170.
45. Weiss, M.; Holz, J.; Peters, R. *Eur. J. Org. Chem.* **2016**, *2016*, 210–227.
46. Wu, Z.; Retailleau, P.; Gandon, V.; Voituriez, A.; Marinetti, A. *Eur. J. Org. Chem.* **2016**, *2016*, 70–75.
47. Butler, I. R. η -C₅H₅-and η -arene substituted transition metal complexes. In *Organometallic Chemistry: Volume 26*; Green, M., Ed.; The Royal Society of Chemistry: Cambridge, UK, 1998; pp 453–519.
48. Long, N. J. *Metallocenes: An Introduction to Sandwich Complexes*; Wiley-Blackwell: Oxford, 1998.
49. *Metallocenes: Synthesis - Reactivity - Applications*; Tongi, A.; Halterman, R. L., Eds.; *Metallocenes: Synthesis - Reactivity - Applications*; Wiley-VCH: Weinheim, Germany, Wiley-VCH: Weinheim, Germany.
50. Maslowsky Jr, E. *Coord. Chem. Rev.* **2011**, *255*, 2746–2763.
51. Edelmann, F. T. *Coord. Chem. Rev.* **2013**, *257*, 1122–1231.
52. Blaser, H.-U.; Chen, W.; Camponovo, F.; Togni, A. Synthesis and Catalytic Use of Planar Chiral and Polydentate Ferrocene Donors. In *Ferrocenes: Ligands, Materials and Biomolecules*; Stepnicka, P., Ed.; John Wiley & Sons, Inc.: Hoboken, NJ, 2008; pp 237–278.

53. Štěpnička, P. The Chemistry of Organoiron Compounds. Marek, I., Rappoport, Z., Eds.; PATAI'S Chemistry of Functional Groups; John Wiley & Sons, Ltd: Hoboken, NJ, 2009; pp 103–154.
54. Manoury, E.; Poli, R. Phosphorus Compounds. In 37; Peruzzini, M., Poli, R., Eds.; Catalysis by Metal Complexes; Springer: New York, 2011; pp 121–149.
55. Toma, S.; Csizmadiova, J.; Meciarova, M.; Sebesta, R. *Dalton Trans.* **2014**, *43*, 16557–16579.
56. Valdés, H.; Poyatos, M.; Peris, E. *Organometallics* **2014**, *33*, 394–401.
57. Forcher, G.; Silvanus, A.; de Frémont, P.; Jacques, B.; Pearson-Long, M. S. M.; Boeda, F.; Bertus, P. *J. Organomet. Chem.* **2015**, *797*, 1–7.
58. John, J.; Wilson-Konderka, C.; Metallinos, C. *Adv. Synth. Catal.* **2015**, *357*, 2071–2081.
59. Blaser, H.-U.; Lotz, M.; Platonov, A. Y. R)-1-[(1R)-1-(Dicyclohexylphosphino) ethyl]-2-(diphenylphosphino)-ferrocene and (2S)-1-[(1R)-1-(Dicyclohexylphosphino) ethyl]-2-(diphenylphosphino)-ferrocene (Josiphos). In *Encyclopedia of Reagents for Organic Synthesis*; Fuchs, P. L., Ed.; John Wiley & Sons, Ltd: Hoboken, NJ, 2001.
60. Blaser, H.-U.; Brieden, W.; Pugin, B.; Spindler, F.; Studer, M.; Togni, A. *Top. Catal.* **2002**, *19*, 3–16.
61. Tang, W.; Zhang, X. *Chem. Rev.* **2003**, *103*, 3029–3070.
62. A query for publications containing the term "josiphos" via Google Scholar yields over 3500 results.
63. Togni, A.; Breutel, C.; Schnyder, A.; Spindler, F.; Landert, H.; Tijani, A. *J. Am. Chem. Soc.* **1994**, *116*, 4062–4066.

64. Bolm, C.; Kesselgruber, M.; Raabe, G. *Organometallics* **2002**, *21*, 707–710.
65. Cesar, V.; Bellemin-Lapponnaz, S.; Gade, L. H. *Chem. Soc. Rev.* **2004**, *33*, 619–636.
66. Check, C. T.; Jang, K. P.; Schwamb, C. B.; Wong, A. S.; Wang, M. H.; Scheidt, K. A. *Angew. Chem. Int. Ed.* **2015**, *54*, 4264–4268.
67. L. Knight, R.; J. Leeper, F. *J. Chem. Soc., Perkin Trans. I* **1998**, 1891–1894.
68. Kerr, M. S.; Read de Alaniz, J.; Rovis, T. *J. Am. Chem. Soc.* **2002**, *124*, 10298–10299.
69. Struble, J. R.; Bode, J. W. *Org. Synth.* **2010**, *87*, 362.
70. Rios, R.; Liang, J.; Lo, M. M. C.; Fu, G. C. *Chem. Commun.* **2000**, 377–378.
71. Fu, G. C. *Acc. Chem. Res.* **2004**, *37*, 542–547.
72. Fu, G. C. *Acc. Chem. Res.* **2006**, *39*, 853–860.
73. Hu, B.; Meng, M.; Wang, Z.; Du, W.; Fossey, J. S.; Hu, X.; Deng, W.-P. *J. Am. Chem. Soc.* **2010**, *132*, 17041–17044.
74. Shi, Y.-H.; Wang, Z.; Hu, B.; Wang, M.; Fossey, J. S.; Deng, W.-P. *Org. Lett.* **2011**, *13*, 6010–6013.
75. Treichel, P. M.; Johnson, J. W. *J. Organomet. Chem.* **1975**, *88*, 207–214.
76. Johnson, J. W.; Treichel, P. M. *J. Chem. Soc., Chem. Commun.* **1976**, 688–689.
77. Johnson, J. W.; Treichel, P. M. *J. Am. Chem. Soc.* **1977**, *99*, 1427–1436.
78. Rigby, S. S.; Decken, A.; Bain, A. D.; McGlinchey, M. J. *J. Organomet. Chem.* **2001**, *637–639*, 372–381.
79. Pammer, F.; Sun, Y.; May, C.; Wolmershäuser, G.; Kelm, H.; Krüger, H.-J.; Thiel, W. R. *Angew. Chem. Int. Ed.* **2007**, *46*, 1270–1273.

80. Kirillov, E.; Kahlal, S.; Roisnel, T.; Georgelin, T.; Saillard, J.-Y.; Carpentier, J.-F. *Organometallics* **2008**, *27*, 387–393.
81. Hutt, J. T.; Aron, Z. D. *Org. Lett.* **2011**, *13*, 5256–5259.
82. Brennführer, A.; Neumann, H.; Beller, M. *Angew. Chem. Int. Ed.* **2009**, *48*, 4114–4133.
83. Gadge, S. T.; Bhanage, B. M. *RSC Adv.* **2014**, *4*, 10367–10389.
84. Evans, D. A.; Bartroli, J.; Shih, T. L. *J. Am. Chem. Soc.* **1981**, *103*, 2127–2129.
85. Ho, G.-J.; Mathre, D. J. *J. Org. Chem.* **1995**, *60*, 2271–2273.
86. Myers, A. G.; Yang, B. H.; Chen, H.; McKinstry, L.; Kopecky, D. J.; Gleason, J. L. *J. Am. Chem. Soc.* **1997**, *119*, 6496–6511.
87. White, J. M.; Tunoori, A. R.; Georg, G. I. *J. Am. Chem. Soc.* **2000**, *122*, 11995–11996.
88. Leighty, M. W.; Spletstoser, J. T.; Umihara, H.; Fukuyama, T.; Georg, G. I. *Org. Synth.* **2011**, *88*, 427–437.
89. Berthon-Gelloz, G.; Siegler, M. A.; Spek, A. L.; Tinant, B.; Reek, J. N. H.; Marko, I. E. *Dalton Trans.* **2010**, *39*, 1444–1446.
90. Wakatsuki, Y.; Yamazaki, H.; Lindner, E.; Bosamle, A. (1, 3-Butadiene-1, 4-Diyl)(η^5 -Cyclopentadienyl)-(Triphenylphosphine)Cobalt with Various Substituents. In *Inorganic Syntheses 26*; Kaesz, H. D., Ed.; John Wiley & Sons, Inc.: Hoboken, NJ, 2007; pp 189–200.
91. Bertrand, G.; Tortech, L.; Fichou, D.; Malacria, M.; Aubert, C.; Gandon, V. *Organometallics* **2012**, *31*, 126–132.
92. Singh, N.; Elias, A. J. *Organometallics* **2012**, *31*, 2059–2065.
93. Singh, J.; Kumar, D.; Singh, N.; Elias, A. J. *Organometallics* **2014**, *33*, 1044–1052.

94. Singh, J.; Deb, M.; Elias, A. J. *Organometallics* **2015**, *34*, 4946–4951.
95. Piper, T. S.; Cotton, F. A.; Wilkinson, G. J. *Inorg. Nucl. Chem.* **1955**, *1*, 165–174.
96. Frith, S. A.; Spencer, J. L.; Geiger, W. E.; Edwin, J. (η^5 -Pentamethylcyclopentadienyl)Cobalt Complexes. In *Inorg. Synth.*; John Wiley & Sons, Inc.: Hoboken, NJ, 2007; pp 15–21.
97. Mistryukov, E. A. *Mendeleev Commun.* **2006**, *16*, 258–259.
98. Briggs, A. J. *Synth. Commun.* **2013**, *43*, 3258–3261.
99. Citadelle, C. A.; Nouy, E. L.; Bisaro, F.; Slawin, A. M. Z.; Cazin, C. S. J. *Dalton Trans.* **2010**, *39*, 4489–4491.
100. Tolman, C. A. *Chem. Rev.* **1977**, *77*, 313–348.
101. Dorta, R.; Stevens, E. D.; Scott, N. M.; Costabile, C.; Cavallo, L.; Hoff, C. D.; Nolan, S. P. *J. Am. Chem. Soc.* **2005**, *127*, 2485–2495.
102. Nelson, D. J.; Nolan, S. P. *Chem. Soc. Rev.* **2013**, *42*, 6723–6753.
103. Back, O.; Henry-Ellinger, M.; Martin, C. D.; Martin, D.; Bertrand, G. *Angew. Chem. Int. Ed.* **2013**, *52*, 2939–2943.
104. Liske, A.; Verlinden, K.; Buhl, H.; Schaper, K.; Ganter, C. *Organometallics* **2013**, *32*, 5269–5272.
105. Verlinden, K.; Buhl, H.; Frank, W.; Ganter, C. *Eur. J. Inorg. Chem.* **2015**, *2015*, 2416–2425.
106. Vummaleti, S. V. C.; Nelson, D. J.; Poater, A.; Gomez-Suarez, A.; Cordes, D. B.; Slawin, A. M. Z.; Nolan, S. P.; Cavallo, L. *Chem. Sci.* **2015**, *6*, 1895–1904.
107. Woitellier, S.; Launay, J. P.; Joachim, C. *Chem. Phys.* **1989**, *131*, 481–488.

108. Venkataraman, L.; Klare, J. E.; Nuckolls, C.; Hybertsen, M. S.; Steigerwald, M. L. *Nature* **2006**, *442*, 904-907.
109. Solomon, G. C.; Andrews, D. Q.; Van Duyne, R. P.; Ratner, M. A. *ChemPhysChem* **2009**, *10*, 257-264.
110. Arnold, P. L. *Heteroat. Chem* **2002**, *13*, 534-539.
111. Poater, A.; Cosenza, B.; Correa, A.; Giudice, S.; Ragone, F.; Scarano, V.; Cavallo, L. *Eur. J. Inorg. Chem.* **2009**, *2009*, 1759-1766.
112. Clavier, H.; Nolan, S. P. *Chem. Commun.* **2010**, *46*, 841-861.
113. Dorta, R.; Stevens, E. D.; Scott, N. M.; Costabile, C.; Cavallo, L.; Hoff, C. D.; Nolan, S. *P. J. Am. Chem. Soc.* **2005**, *127*, 2485-2495.
114. Falivene, L.; Cavallo, L.; Talarico, G. *ACS Catal.* **2015**, *5*, 6815-6822.
115. Kendall, A. J.; Zakharov, L. N.; Tyler, D. R. *Inorg. Chem.* **2016**, *55*, 3079-3090.
116. Würtz, S.; Lohre, C.; Fröhlich, R.; Bergander, K.; Glorius, F. *J. Am. Chem. Soc.* **2009**, *131*, 8344-8345.
117. Burstein, C.; Lehmann, C. W.; Glorius, F. *Tetrahedron* **2005**, *61*, 6207-6217.
118. Alcarazo, M.; Stork, T.; Anoop, A.; Thiel, W.; Fürstner, A. *Angew. Chem. Int. Ed.* **2010**, *49*, 2542-2546.
119. Burstein, C.; Tschan, S.; Xie, X.; Glorius, F. *Synthesis* **2006**, *2006*, 2418-2439.
120. Li, Y.; Zhao, Z.-A.; He, H.; You, S.-L. *Adv. Synth. Catal.* **2008**, *350*, 1885-1890.
121. Pangborn, A. B.; Giardello, M. A.; Grubbs, R. H.; Rosen, R. K.; Timmers, F. J. *Organometallics* **1996**, *15*, 1518-1520.

122. Perrin, D. D.; Armarego, W. L. F. *Purification of Laboratory Chemicals*; 3rd ed.; Pergamon Press: Oxford, 1988.
123. Falivene, L.; Credendino, R.; Poater, A.; Petta, A.; Serra, L.; Oliva, R.; Scarano, V.; Cavallo, L. *Organometallics* **2016**, *35*, 2286-2293.
124. Bondi, A. *The Journal of Physical Chemistry* **1964**, *68*, 441-451.
125. Cardillo, G.; Gentilucci, L.; Tolomelli, A. *Mini-Rev. Med. Chem.* **2006**, *6*, 293-304.
126. Wang, L.; Xie, J.; Schultz, P. G. *Annu. Rev. Biophys. Biomol. Struct.* **2006**, *35*, 225-249.
127. Liu, C. C.; Schultz, P. G. *Annu. Rev. Biochem* **2010**, *79*, 413-444.
128. Danilewicz, J. C.; Abel, S. M.; Brown, A. D.; Fish, P. V.; Hawkeswood, E.; Holland, S. J.; James, K.; McElroy, A. B.; Overington, J.; Powling, M. J.; Rance, D. J. *J. Med. Chem.* **2002**, *45*, 2432-2453.
129. Figueiredo, A. C.; Clement, C. C.; Zakia, S.; Gingold, J.; Philipp, M.; Pereira, P. J. B. *PLoS One* **2012**, *7*, e34354.
130. Yang, W.; Gao, X.; Wang, B. *Med. Res. Rev.* **2003**, *23*, 346-368.
131. Trippier, P. C.; McGuigan, C. *MedChemComm* **2010**, *1*, 183-198.
132. Ni, N.; Wang, B. Applications of Boronic Acids in Chemical Biology and Medicinal Chemistry. In *Boronic Acids*; Hall, D. G., Ed.; Wiley-VCH Verlag GmbH & Co. KGaA: 2011; pp 591-620.
133. Das, B. C.; Thapa, P.; Karki, R.; Schinke, C.; Das, S.; Kambhampati, S.; Banerjee, S. K.; Van Veldhuizen, P.; Verma, A.; Weiss, L. M.; Evans, T. *Future Med. Chem.* **2013**, *5*, 653-676.
134. Leśnikowski, Z. J. *Expert Opin. Drug Discovery* **2016**, *11*, 569-578.

135. Philipp, M.; Bender, M. L. *Proc. Nat. Acad. Sci.* **1971**, *68*, 478–480.
136. Valery, M. D.; Abed Al Aziz, Q.; Morris, S. *Mini-Rev. Med. Chem.* **2004**, *4*, 1001–1018.
137. Matteson, D. S. *Med. Res. Rev.* **2008**, *28*, 233–246.
138. Milo, L. J.; Lai, J. H.; Wu, W.; Liu, Y.; Maw, H.; Li, Y.; Jin, Z.; Shu, Y.; Poplawski, S. E.; Wu, Y.; Sanford, D. G.; Sudmeier, J. L.; Bachovchin, W. W. *J. Med. Chem.* **2011**, *54*, 4365–4377.
139. Touchet, S.; Carreaux, F.; Carboni, B.; Bouillon, A.; Boucher, J.-L. *Chem. Soc. Rev.* **2011**, *40*, 3895–3914.
140. Micale, N.; Scarbaci, K.; Troiano, V.; Ettari, R.; Grasso, S.; Zappalà, M. *Med. Res. Rev.* **2014**, *34*, 1001–1069.
141. Kane, R. C.; Bross, P. F.; Farrell, A. T.; Pazdur, R. *The Oncologist* **2003**, *8*, 508–513.
142. Al-Salama, Z. T.; Garnock-Jones, K. P.; Scott, L. J. *Targeted Oncology* **2017**, *12*, 535–542.
143. Voelker, R. *JAMA* **2017**, *318*, 1432–1432.
144. Ballatore, C.; Huryn, D. M.; Smith, A. B. *ChemMedChem* **2013**, *8*, 385–395.
145. Dembitsky, V. M.; Srebnik, M. Chemistry of α -Aminoboronic Acids and their Derivatives. In *Amino Acids, Peptides and Proteins in Organic Chemistry*; Wiley-VCH Verlag GmbH & Co. KGaA: 2009; pp 145–187.
146. Andrés, P.; Ballano, G.; Calaza, M. I. *Chem. Soc. Rev.* **2016**, *45*, 2291.
147. Beenen, M. A.; An, C.; Ellman, J. A. *J. Am. Chem. Soc.* **2008**, *130*, 6910–6911.
148. Xie, J.-b.; Luo, J.; Winn, T. R.; Cordes, D. B.; Li, G. *Beilstein J. Org. Chem.* **2014**, *10*, 746–751.

149. Sole, C.; Gulyas, H.; Fernandez, E. *Chem. Commun.* **2012**, *48*, 3769-3771.
150. Zhang, S.-S.; Zhao, Y.-S.; Tian, P.; Lin, G.-Q. *Synlett* **2013**, *24*, 437-442.
151. Wang, D.; Cao, P.; Wang, B.; Jia, T.; Lou, Y.; Wang, M.; Liao, J. *Org. Lett.* **2015**, *17*, 2420-2423.
152. Hong, K.; Morken, J. P. *J. Am. Chem. Soc.* **2013**, *135*, 9252-9254.
153. Hu, N.; Zhao, G.; Zhang, Y.; Liu, X.; Li, G.; Tang, W. *J. Am. Chem. Soc.* **2015**, *137*, 6746-6749.
154. Nishikawa, D.; Hirano, K.; Miura, M. *J. Am. Chem. Soc.* **2015**, *137*, 15620.
155. López, A.; Clark, T. B.; Parra, A.; Tortosa, M. *Org. Lett.* **2017**.
156. Chen, L.; Zou, X.; Zhao, H.; Xu, S. *Org. Lett.* **2017**, *19*, 3676-3679.
157. Molander, G. A.; Wisniewski, S. R. *J. Am. Chem. Soc.* **2012**, *134*, 16856-16868.
158. Kubota, K.; Yamamoto, E.; Ito, H. *J. Am. Chem. Soc.* **2015**, *137*, 420-424.
159. Kubota, K. Copper(I)-Catalyzed Enantioselective Nucleophilic Borylation of Aldehydes. In *Synthesis of Functionalized Organoboron Compounds Through Copper(I) Catalysis*; Springer Singapore: Singapore, 2017; pp 99-127.
160. Kubota, K.; Osaki, S.; Jin, M.; Ito, H. *Angew. Chem. Int. Ed.* **2017**, *56*, 6646-6650.
161. Kubota, K.; Jin, M.; Ito, H. *Organometallics* **2016**, *35*, 1376-1383.
162. Zhao, H.; Dang, L.; Marder, T. B.; Lin, Z. *J. Am. Chem. Soc.* **2008**, *130*, 5586-5594.
163. Molander, G. A. *J. Org. Chem.* **2015**, *80*, 7837-7848.
164. Molloy, J. J.; Watson, A. J. B. B-Protected Boronic Acids: Methodology Development and Strategic Application. In *Boron Reagents in Synthesis*; Coca, A., Ed.; ACS Symposium Series; American Chemical Society: Washington, DC, 2016; pp 379-413.

165. Vedejs, E.; Chapman, R. W.; Fields, S. C.; Lin, S.; Schrimpf, M. R. *J. Org. Chem.* **1995**, *60*, 3020–3027.
166. Buesking, A. W.; Ellman, J. A. *Chem. Sci.* **2014**, *5*, 1983–1987.
167. Lennox, A. J. J. Organotrifluoroborate Preparation. In *Organotrifluoroborate Preparation, Coupling and Hydrolysis*; Springer Theses; Springer International Publishing: Cham, 2013; pp 11–36.
168. Lennox, A. J. J.; Lloyd-Jones, G. C. *Angew. Chem. Int. Ed.* **2012**, *51*, 9385–9388.
169. Toshimichi, O.; Tomotsugu, A.; Michinori, S. *Chem. Lett.* **2009**, *38*, 664–665.
170. Ohmura, T.; Awano, T.; Suginome, M. *J. Am. Chem. Soc.* **2010**, *132*, 13191–13193.
171. Awano, T.; Ohmura, T.; Suginome, M. *J. Am. Chem. Soc.* **2011**, *133*, 20738–20741.
172. Dumas, A. M.; Sieradzki, A. J.; Donnelly, L. J. *Org. Lett.* **2016**, *18*, 1848–1851.
173. Murry, J. A.; Frantz, D. E.; Soheili, A.; Tillyer, R.; Grabowski, E. J.; Reider, P. J. *J. Am. Chem. Soc.* **2001**, *123*, 9696–9697.
174. Arduengo, A. J.; Harlow, R. L.; Kline, M. *J. Am. Chem. Soc.* **1991**, *113*, 361–363.
175. Enders, D.; Niemeier, O.; Henseler, A. *Chem. Rev.* **2007**, *107*, 5606–5655.
176. Hahn, F. E.; Jahnke, M. C. *Angew. Chem. Int. Ed.* **2008**, *47*, 3122–3172.
177. Díez-González, S.; Marion, N.; Nolan, S. P. *Chem. Rev.* **2009**, *109*, 3612–3676.
178. Nair, V.; Menon, R. S.; Biju, A. T.; Sinu, C. R.; Paul, R. R.; Jose, A.; Sreekumar, V. *Chem. Soc. Rev.* **2011**, *40*, 5336–5346.
179. Berkessel, A.; Elfert, S.; Yatham, V. R.; Neudörfl, J.-M.; Schlörer, N. E.; Teles, J. H. *Angew. Chem. Int. Ed.* **2012**, *51*, 12370–12374.
180. Nelson, D. J.; Nolan, S. P. *Chemical Society Reviews* **2013**, *42*, 6723–6753.

181. Mahatthananchai, J.; Bode, J. W. *Chem. Sci.* **2012**, *3*, 192–197.
182. Collett, C. J.; Massey, R. S.; Maguire, O. R.; Batsanov, A. S.; O'Donoghue, A. C.; Smith, A. D. *Chem. Sci.* **2013**, *4*, 1514-1522.
183. Mahatthananchai, J.; Bode, J. W. *Accounts of Chemical Research* **2014**, *47*, 696-707.
184. Ruiz, J.; Perandones, B. F. *J. Am. Chem. Soc.* **2007**, *129*, 9298–9299.
185. Brill, M.; Díaz, J.; Huertos, M. A.; López, R.; Pérez, J.; Riera, L. *Chemistry – A European Journal* **2011**, *17*, 8584-8595.
186. Miranda-Soto, V.; Grotjahn, D. B.; Cooksy, A. L.; Golen, J. A.; Moore, C. E.; Rheingold, A. L. *Angew. Chem. Int. Ed.* **2011**, *50*, 631-635.
187. Xiang, L.; Xiao, J.; Deng, L. *Organometallics* **2011**, *30*, 2018–2025.
188. Karagiari, O.; Lalonde, M. B.; Bury, W.; Sarjeant, A. A.; Farha, O. K.; Hupp, J. T. *J. Am. Chem. Soc.* **2012**, *134*, 18790-18796.
189. Lalonde, M. B.; Farha, O. K.; Scheidt, K. A.; Hupp, J. T. *ACS Catalysis* **2012**, *2*, 1550-1554.
190. Schettini, M. F.; Wu, G.; Hayton, T. W. *Chem. Commun.* **2012**, *48*, 1484-1486.
191. Flowers, S. E.; Cossairt, B. M. *Organometallics* **2014**, *33*, 4341-4344.
192. Ruiz, J.; Berros, A.; Perandones, B. F.; Vivanco, M. *Dalton Trans.* **2009**, 6999–7007.
193. Gibard, C.; Ibrahim, H.; Gautier, A.; Cisnetti, F. *Organometallics* **2013**, *32*, 4279-4283.
194. Cisnetti, F.; Lemoine, P.; El-Ghozzi, M.; Avignant, D.; Gautier, A. *Tetrahedron Lett.* **2010**, *51*, 5226-5229.
195. Liu, B.; Chen, C.; Zhang, Y.; Liu, X.; Chen, W. *Organometallics* **2013**, *32*, 5451-5460.
196. Hartman, G. D.; Weinstock, L. M. *Org. Synth.* **1988**, *50-9*, 620-624.

197. Zibinsky, M.; Fokin, V. V. *Org. Lett.* **2011**, *13*, 4870-4872.